Advancing surgical guidance: from (hybrid) molecule to man and beyond

Berg, N.S. van den

ADVANCING SURGICAL GUIDANCE: FROM (HYBRID) MOLECULE TO MAN AND BEYOND

NYNKE S. VAN DEN BERG

Cover design Seçkin Yilmaz
Design and lay-out Studio GroenLicht, www.groenlicht.eu, Leiden, The Netherlands
Printed by GVO, Enschede, The Netherlands
ISBN/EAN 978-94-6332-092-4

The research described in this thesis was carried out at the Leiden University Medical Center (Leiden) and the Netherlands Cancer Institute-Antoni van Leeuwenhoek Hospital (Amsterdam).

The studies described in this thesis were financially supported by a Eurostars grant (grant no. E! 7555), an NWO-STW-VIDI grant (grant no. STW BGT11272), a KWF translational research award (grant no. PGF 2009-4344), a European Research Council under the European Union's Seventh Framework Program (FP7/2007-2013) grant (grant no. 2012-306890), and the Leiden University Fund / Den Dulk-Moermans.

Financial support from the Van den Berg family, Chipsoft, EUROMEDICAL Instruments, EURORAD S.A., Hamamatsu Photonics K.K., IDB Holland B.V., Intuitive Surgical Inc., KARL STORZ Endoscopie Nederland B.V., Medi-Radiopharma Co., Ltd, Mermaid Medical, ONCOVISION, PI Medical Diagnostic Equipment B.V., and SurgicEye GmbH for the printing of this thesis is gratefully acknowledged.

ADVANCING SURGICAL GUIDANCE: FROM (HYBRID) MOLECULE TO MAN AND BEYOND

Proefschrift

ter verkrijging van
de graad van Doctor aan de Universiteit Leiden,
op gezag van Rector Magnificus prof. mr. C.J.J.M. Stolker,
volgens besluit van het College voor Promoties
te verdedigen op donderdag 10 november 2016
klokke 13.45 uur

door

Nynke Sjoerdtje van den Berg
geboren te Harlingen
in 1986

Promotor:	Prof. dr. J.L. Bloem
Co-promotores:	Dr. F.W.B. van Leeuwen Dr. R.A. Valdés Olmos
Leden promotiecommissie:	Prof. dr. H.J. Tanke Prof. dr. A.J.M. Balm (Nederlands Kanker Instituut-Antoni van Leeuwenhoek ziekenhuis en Universiteit van Amsterdam) Prof. dr. M.A. de Jong (Erasmus MC) Dr. A.R. van Erkel Dr. H.G. van der Poel (Nederlands Kanker Instituut-Antoni van Leeuwenhoek ziekenhuis)

Foar heit en mem

TABLE OF CONTENTS

CHAPTER 1

GENERAL INTRODUCTION, OUTLINE OF THIS THESIS

GENERAL INTRODUCTION

Radiotracers, in combination with positron emission tomography imaging (PET), or single photon emission computed tomography (SPECT) imaging, provide a very sensitive technique for the localization of cancer [1, 2]. Combined with anatomical imaging techniques (such as computed tomography (CT) or magnetic resonance imaging (MRI)), nuclear medicine has become important for the non-invasive identification of various cancers and detection of metastasis. More and more the combined technique of SPECT/CT, PET/CT, and PET/MRI is also used to guide interventions, for example treatment response measurements and surgical procedures [3, 4].

Surgery, often combined with (neo-adjuvant) chemo-, hormonal- or radiotherapy, can be considered the main pillar in the management of cancer. However, when approaching the tumor or lymph nodes that possibly contain metastases, during the surgical procedure it is not always clear what has to be removed. Here interventional molecular imaging technologies may provide outcome. Using radio- or fluorescence-guidance, or a combination of both, may direct the surgeon more accurately to the lesion(s) of interest.

Ideally, a combination of a radiotracer and a fluorescence tracer is used in order to allow accurate pre- and intraoperative lesion identification [5, 6]. In this thesis, a hybrid approach for surgical guidance, based on the clinical use of the hybrid tracer indocyanine green (ICG)-technetium-99m (^{99m}Tc)-nanocolloid, is presented. Next to the clinical validation of the technique, extensions towards the use of multispectral imaging, hybrid modalities and navigation technologies have been exploited.

OUTLINE OF THIS THESIS

Part one of this thesis introduces the reader into the concept of image-guided surgery and the evolution from fluorescence-based surgical guidance into the hybrid approach for surgical guidance. Chapter 2 provides the reader with the basics of fluorescence imaging, after which clinically available tracers for fluorescence imaging in the field of urology as well as fluorescence imaging hardware requirements are discussed. In chapter 3 the clinically available radiotracers, blue dyes, fluorescence tracers and hybrid tracers for sentinel node biopsy are presented.

Part two of this thesis focuses on the clinical evaluation of the hybrid tracer ICG-^{99m}Tc-nanocolloid for sentinel node biopsy of different malignancies. In chapter 4, in patients that were to undergo sentinel node biopsy for oral cavity carcinoma (n=14), the value of the fluorescent component of the hybrid tracer was evaluated and compared to the conventional radioguided approach. In chapter 5 the hybrid tracer was evaluated in a large cohort of 65 patients with penile cancer. Here optical sentinel node identification via blue dye was compared to optical sentinel node identification via the fluorescent signature of the hybrid tracer. In chapter 6, in 104 patients with melanoma (head-and-neck, trunk or on an extremity) with drainage to amongst others the neck, axilla and groin, we evaluated

the value of the hybrid tracer for sentinel node identification. In all cases findings were compared to the conventional radioguided- and blue dye-based approach.

While the clinical value of the hybrid tracer is evaluated in part two of this thesis, in **part three** the main aim was to study if the hybrid approach for surgical guidance could be further extended via technical improvements made on the hardware side. As a first step herein, chapter 7 describes the use of a prototype fluorescence camera for open surgery procedures, (head-and-neck) melanoma oral cavity, and penile carcinoma; n=27) that, in contrast to many other cameras, works under ambient light conditions and thereby allows for real-time fluorescence imaging-assisted surgical guidance. In chapter 8, in 40 patients with prostate cancer that were to undergo robot-assisted laparoscopic sentinel node biopsy optimization of the hybrid tracer formulation and improvements on the fluorescence laparoscopic camera were studied. In doing so, the surgical guidance process was further refined. In chapter 9, we extended the functionalities of the fluorescence laparoscope in order to allow for the intraoperative detection of multiple fluorescence signatures (ICG-^{99m}Tc-nanocolloid and fluorescein), so-called multispectral imaging.

Next to refining individual modalities, their integration was also explored. In chapter 10 the feasibility and accuracy of 3D navigation of conventional surgical tools to the lesion(s) of interest is presented in patients with melanoma or Merkel cell carcinoma (n=5). Alternatively hybrid surgical imaging modalities were explored. In chapter 11 we describe the evaluation of the first prototype opto-nuclear probe, an imaging modality that allows for conventional gamma tracing as well as fluorescence tracing (head-and-neck malignancies and penile caranoma; n=9).

In chapter 12, the **outlook** of this thesis, steps are described that can extend the hybrid surgical guidance concept on both the tracer and hardware side.

REFERENCES

1. Mariani G, Bruselli L, Kuwert T, Kim EE, Flotats A, Israel O, et al. A review on the clinical uses of SPECT/CT. Eur J Nucl Med Mol Imaging. 2010;37:1959-85.
2. Wechalekar K, Sharma B, Cook G. PET/CT in oncology-a major advance. Clin Radiol. 2005;60:1143-55.
3. Fraum TJ, Fowler KJ, McConathy J. PET/MRI: Emerging Clinical Applications in Oncology. Acad Radiol. 2016;23:220-36.
4. Histed SN, Lindenberg ML, Mena E, Turkbey B, Choyke PL, Kurdziel KA. Review of functional/anatomical imaging in oncology. Nucl Med Comm. 2012;33:349-61.
5. van der Poel HG, Buckle T, Brouwer OR, Valdes Olmos RA, van Leeuwen FW. Intraoperative laparoscopic fluorescence guidance to the sentinel lymph node in prostate cancer patients: clinical proof of concept of an integrated functional imaging approach using a multimodal tracer. Eur Urol. 2011;60:826-33.
6. Phillips E, Penate-Medina O, Zanzonico PB, Carvajal RD, Mohan P, Ye Y, et al. Clinical translation of an ultrasmall inorganic optical-PET imaging nanoparticle probe. Sci Transl Med. 2014;6:260ra149.

PART ONE

CHAPTER 2

FLUORESCENCE GUIDANCE IN UROLOGIC SURGERY

Adapted from: van den Berg NS, van Leeuwen FWB and van der Poel HG. Curr Opin Urol. 2012;22:109-20.

ABSTRACT

Fluorescent tracers can provide anatomical and functional information without altering the visual surgical field. Despite the advances that are being made in tracer development, only a few fluorescent tracers are available for urological interventions. Protoporphyrin IX, hypericin, fluorescein, and indocyanine green were shown to facilitate surgical resection in various ways. Hybrid imaging agents, combining radio- and fluorescent labels, have shown improved integration between preoperative and intraoperative imaging. With the rise of surgical fluorescence guidance, various camera systems have been developed that are tailored for optimal detection of the fluorochromes of interest. In this review, the basics of fluorescence-guided surgery, including tracer and hardware requirements are discussed.

INTRODUCTION

Surgical performance is partly dependent on functional preoperative imaging, such as single photon emission computed tomography combined with computed tomography (SPECT/CT) or positron emission tomography (PET), to identify local areas of interest. Preoperative imaging may reveal anatomical details on organ orientation, and in some cases tumor location, but is often poorly translated into the surgical field. Intraoperative guidance so far is mainly limited to visual anatomical landmarks such as vessels and bones. Functional imaging information would therefore be a useful addition during surgical procedures. Intraoperatively, the gamma-ray detection probe (hereafter referred to as gamma probe) allows for radiotracer detection in for example sentinel nodes (SNs) based on acoustic tracing, but suffers from a background signal emitted from the injection site [1]. Moreover, depth perception is hampered due to collimation issues [1]. As such this technology alone does not allow for detection with a high spatial resolution. Ideally, functional information would be integrated into a visual image during surgery. Fluorescent tracers possess several properties that make them interesting candidates for functional imaging; most importantly they can be imaged in real-time within the surgical field without contaminating this field. To date, several approaches have been explored to achieve intraoperative fluorescence guidance. However, the clinical introduction of fluorescent tracers, and in particular for urological applications, is still in its infancy, though rapidly emerging. In this review, the basics of fluorescence-guided surgery, including tracer development and hardware requirements are discussed focusing on the field of urology.

EXOGENOUS FLUORESCENT TRACERS

Fluorescence imaging differs markedly from the visual detection of the more common vital dyes such as methylene blue and patent blue. Blue dye visualization is a result of light absorbance, which is maximal in the visual range (400-650 nm) and minimal in the near-infrared range (700-1000 nm), whereas fluorescence is based on light emission by fluorochromes. For more in-depth information regarding the basics of fluorescence, please see supporting information. Despite the advances that are being made in tracer development, only a few exogenous fluorescent tracers are available for urologic interventions. Currently only protoporphyrin IX (PpIX) precursors 5-aminolevulinic acid (5-ALA) and hexylaminolevulinate (HAL), fluorescein and indocyanine green (ICG) have received approval for clinical use by the Food and Drug Administration (FDA; Table 1, Figure 1). Several newly developed fluorescent tracers, though not FDA approved yet, have already been studied in a urological setting, such as hypericin and the hybrid tracer ICG-^{99m}Tc-nanocolloid (Table 1, Figure 1).

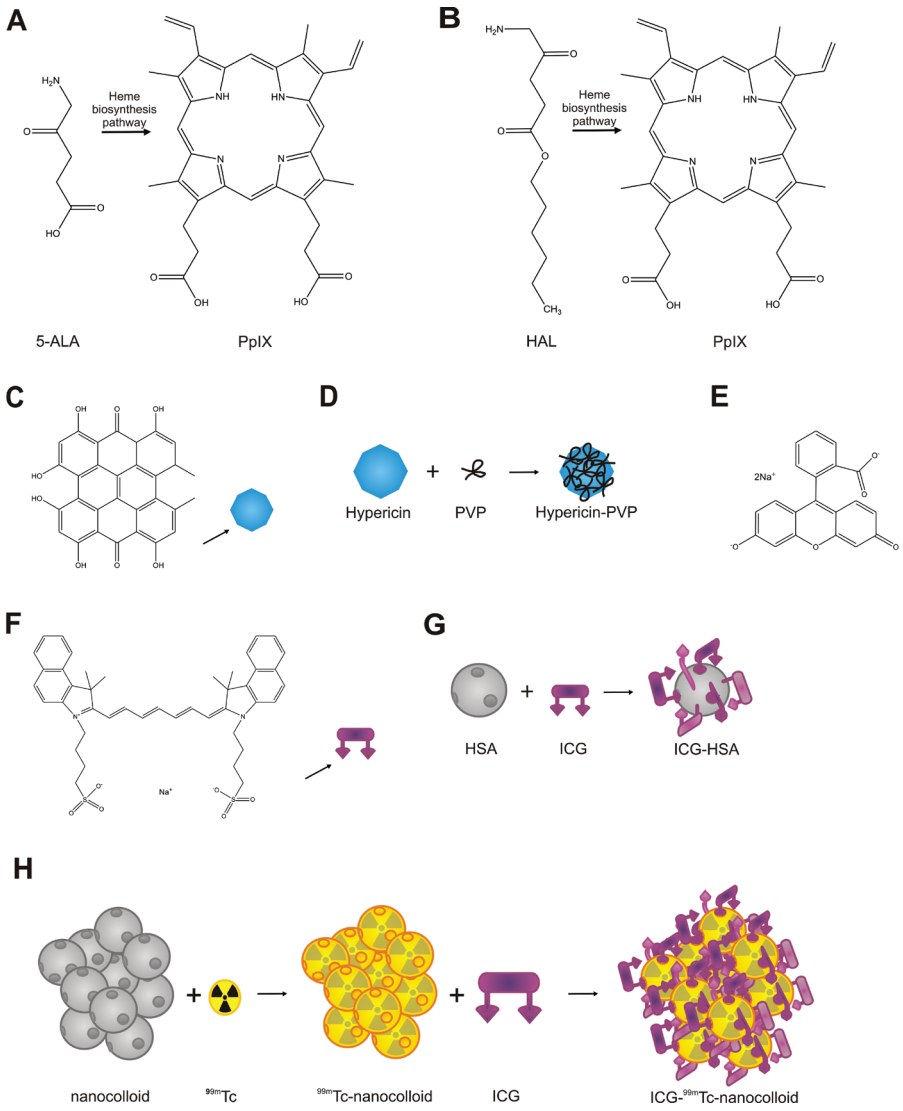

Figure 1. Structures of clinically available fluorescent tracers. A) 5-ALA and B) HAL are metabolically converted in the red fluorescing protoporphyrin IX (PpIX) during the initial steps of the heme biosynthesis pathway; C) Hypericin; D) Mixing hypericin with PVP results in water-soluble hypericin-PVP; E) Fluorescein; F) ICG; G) Formation of ICG-HSA; and H) Schematic overview of the assembly of the hybrid tracer ICG-^{99m}Tc-nanocolloid. Nanocolloid (HSA aggregate) and ^{99m}Tc covalently bind, thereby forming ^{99m}Tc-nanocolloid. Via non-covalent self-assembly, ICG-^{99m}Tc-nanocolloid is formed when mixing ^{99m}Tc-nanocolloid and ICG. 5-ALA = 5-aminolevulinic acid; HAL = hexylamino-levulinate; HSA = human serum albumin; ICG = indocyanine green; PpIX = protoporphyrin IX; PVP = polyvinylpyrrolidone; Na = sodium; Tc = technetium.

Table 1. Clinically available exogenous fluorescence tracers

Tracer	*Excitation and emission peaks*	*QY*	*Target*	*Urological imaging application*
Clinically approved				
PpIX	$\lambda_{ex\ max}$ 450 nm; $\lambda_{em\ max}$ 635 nm	0.011	Heme biosynthesis pathway; accumulation in tumor cells (mainly used for PDD and PDT)	Detection of bladder [2-6,7-11], prostate [12-15], and penile lesions [16,17]
Fluorescein	$\lambda_{ex\ max}$ 488 nm; $\lambda_{em\ max}$ 530 nm	0.76	Accumulation near/around tumor cells	Bladder carcinoma [18,19] and renal vasculature and tumor [20] detection
ICG	$\lambda_{ex\ max}$ 780 nm; $\lambda_{em\ max}$ 820-830 nm	0.0028	Lymphatic and vascular system and urinary tract	Ureter [21] and vasculature [22] visualization
Clinically evaluated				
Hypericin	$\lambda_{ex\ max}$ 598 nm; $\lambda_{em\ max}$ 649 nm	<0.02	Tumor cell accumulation	Detection of bladder carcinoma [23-25]
Hypericin-PVP	$\lambda_{ex\ max}$ 595 nm; $\lambda_{em\ max}$ 651 nm	-	Tumor cell accumulation	Detection of bladder carcinoma [26]
ICG-^{99m}Tc-nanocolloid	$\lambda_{ex\ max}$ 807 nm; $\lambda_{em\ max}$ 822 nm	-	Lymph nodes	SN biopsy procedure prostate cancer [1,2]

QY = quantum yield; $\lambda_{ex\ max}$ = excitation maximum; $\lambda_{em\ max}$ = emission maximum; PpIX = protoporphyrin IX; PDD = photodynamic diagnosis; PDT = photodynamic therapy; ICG = indocyanine green; Tc = technetium; NADH = nicotinamide adenine dinucleotide hydrogen; PVP = polyvinylpyrrolidone; SN = sentinel node.

PROTOPORPHYRIN IX

5-ALA (LEVULAN, DUSA Pharmaceuticals Inc., Wilmington, Massachusetts, USA; Figure 1A), a non-fluorescent prodrug, is the first compound in the heme biosynthesis pathway and is enzymatically converted into the fluorescent PpIX (Figure 1A) and finally into heme in the mitochondria. After 5-ALA administration, the abundantly produced PpIX cannot be rapidly converted into heme and will therefore accumulate intracellularly, leading to a higher signal intensity in proliferative (tumor) tissue [28]. Decreased activity of the enzyme ferrochelatase, which is responsible for the conversion of PpIX into heme and limited availability of iron have been shown to contribute to increased PpIX accumulation in tumor cells [28]. Porphyrins, such as PpIX, have been well studied for their application as photosensitizers for photodynamic diagnosis and -therapy (PDD and PDT, respectively) of cancer [29]. When excited with ultraviolet light, PpIX had a visual red fluorescence emission ($\lambda_{ex\ max}$: 450 nm; $\lambda_{em\ max}$: 635 nm; quantum yield 0.011 in water [29, 30]), which does not necessarily give the best contrast during urological applications; the tissue background is generally also reddish. However, on a white background, such as bladder mucosa, this red fluorescence may provide sufficient contrast for surgical guidance.

5-ALA can be administered orally, intravenously or can be intravesically instilled into the bladder. In a prospective randomized comparison of intravesical 5-ALA instillation for the early detection of small bladder tumors by cystoscopy, Stenzl et al. [10] showed that although slightly more patients in the 5-ALA arm were diagnosed with bladder lesions, the recurrence-free and progression-free survival at 12 months did not significantly differ from the placebo group. These findings are contradictory to earlier data from other groups [2-5] who reported a benefit of PpIX-guided cystoscopy for bladder cancer detection. Inexperience with fluoroscopy, a low number of carcinoma in situ patients, and more meticulous inspection in the placebo group were put forward as explanations for a lack of benefit for fluorescence-guided cystoscopy found in their study [10].

Additionally, 5-ALA has also been used for the detection of penile (Figure 2A) and prostate cancer. Local application of 5-ALA provided fluorescence guidance for the identification and resection of penile carcinoma [16,17]. Zaak et al. [15] showed accumulation of PpIX in prostate cancer tumor cells in 16 out of 16 patients following oral administration of 5-ALA. Moreover, two small multi-institutional phase II nonrandomized studies (n=24 and n=39) showed that oral 5-ALA administration (20 mg/kg), 3 h prior to surgery, might be useful for the intraoperative detection of a positive surgical margin during prostatectomy [12,14]. In a Japanese study (n=16), the specificity and sensitivity for detecting a positive margin during prostatectomy were 82 and 69%, respectively [13].

Both the cellular uptake of 5-ALA and the fluorescence quantum yield of PpIX are limited, which has led to the development of a great number of alternative structures based on the same principle [29]. Already clinically approved and used is HAL (HEXVIX; Photocure, Oslo, Norway; Figure 1B), which was obtained by addition of a lipophilic hexyl moiety to 5-ALA. HAL is considered to be superior to 5-ALA with respect to fluorescence intensity (a 2-4 times higher intensity was reported using a lower dose and a shorter incubation time), pharmacokinetic properties, and ease of preparation [11,29]. Recent studies found a benefit for fluorescence cystoscopy after bladder instillation of HAL over white light cystoscopy, in detecting carcinoma in situ of the bladder (87 vs. 75%) following bladder instilled HAL [7], but also for the management of multifocal recurrent non-muscle invasive bladder cancer [9]. Moreover, Ray et al. [8] showed improved bladder cancer diagnosis in patients previously treated with bacilli Calmette-Guèrin (Figure 2B). A reduced recurrence rate was reported following HAL fluorescence-guided transurethral resection of the bladder (TURB) as compared to conventional white light TURB (31 vs. 47%) [6].

For the detection of bladder cancer, especially carcinoma in situ, both 5-ALA and HAL present superior sensitivity compared to white light cystoscopy, 96, 97, and 73%, respectively. Nevertheless, the specificity is limited and does not significantly differ from white light cystoscopy, most likely due to the high false-positive rate [11]. However, Frimberger et al. [31] showed that with the addition of autofluorescence imaging to 5-ALA-induced fluorescence endoscopy for the detection of bladder carcinomas, the specificity increased from 67 to 88%, thereby reducing the false-positive rate.

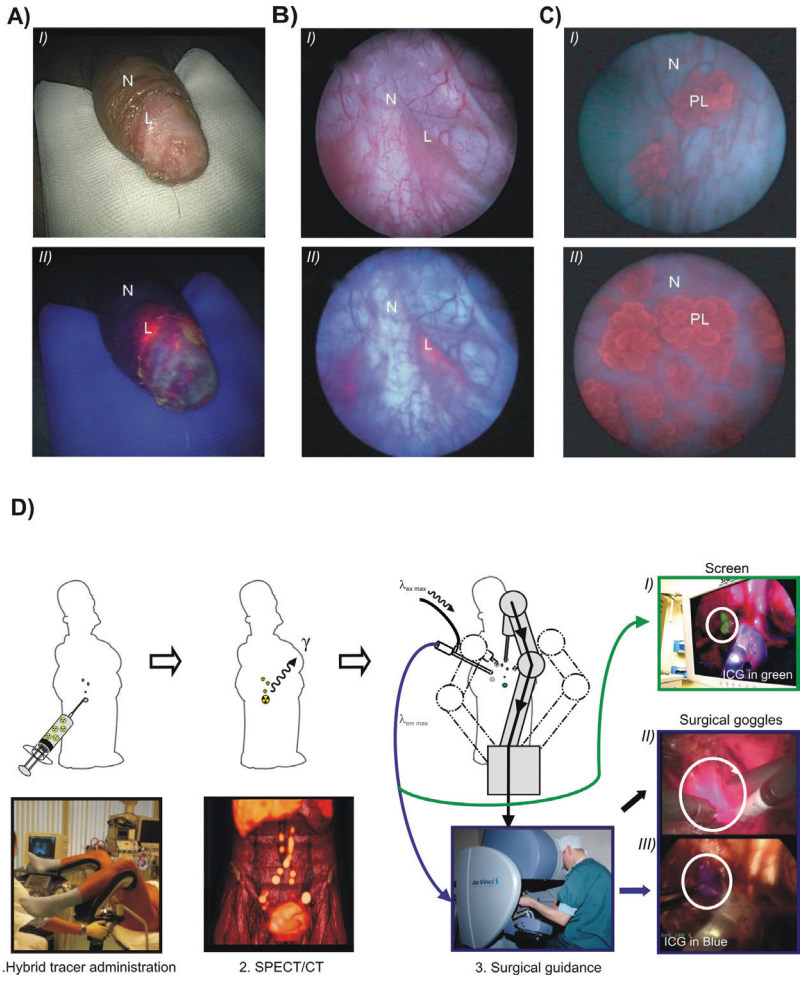

Figure 2. Clinical examples of implementation of fluorescence imaging during surgical procedures. A-C) White light images of the penis (AI) and bladder (BI and CI). Fluorescence imaging of PpIX (A, B) or hypericin (C) discriminated surgical margins of penile carcinoma (AII, L), carcinoma in situ of the bladder (BII, L) and papillary lesions in the bladder (CII, PL) from the normal tissue (N). Images were reprinted from Schlenker et al. [17], Ray et al. [8], and D'Hallewin et al. [24], respectively; D) Implementation of the hybrid tracer ICG-^{99m}Tc-nanocolloid during robot-assisted laparoscopic prostatectomy with SN biopsy procedure. Transrectal ultrasound-guided intra-prostatic injection of the hybrid tracer (1). Preoperative SN identification with SPECT/CT (2). Intraoperative fluorescence-guided SN detection (3; I) Screen). The TilePro function of the da Vinci S surgical goggles allows simultaneous depiction of the three-dimensional surgical field and the intraoperative ICG-image (3; II) and III) Surgical goggles). Dotted lines highlight the fluorescent area. Images were reprinted from van der Poel et al. [1]. ICG = indocyanine green; L = lesion; N = normal tissue; PL = papillary lesion; SN = sentinel node; SPECT/CT = single photon emission computed tomography/computed tomography.

HYPERICIN

Hypericin (Planta Natural Products, Vienna, Austria) is a red fluorescing ($\lambda_{ex\ max}$: 598 nm; $\lambda_{ex\ max}$: 649 nm) hydroxylated phenanthropyrylene-quinone derivative present in plant of the genus Hypericum [32] with a very low quantum yield of less than 0.02 in water [33] (Table 1, Figure 1C). Hypericin as photosensitizer gives low systemic toxicity and accumulates usually in malignant tissue (Figure 2C) [26]. However, administration has been proven difficult due to its water insoluble properties. Recent clinical studies showed comparable sensitivity (82-94%), but increased specificity (91-94%) for the detection of bladder carcinoma as compared to 5-ALA and HAL [23-25] when hypericin was dissolved in ethanol and 1% plasma protein solution. Moreover, Kubin et al. [26] reported water soluble hypericin following polyvinylpyrrolidone (PVP) binding (Hypericin-PVP; Table 1, Figure 1D) for the detection of bladder cancer.

FLUORESCEIN

Fluorescein (FLUORESCITE; Alcon Nederland B.V., Gorinchem, The Netherlands; Figure 1E) is an extremely bright synthetic dye with a quantum yield of 0.76 in water [34] that gives a visual yellow emission (530 nm) following excitation at 488 nm (Table 1). Although this emission is less than 700 nm, the yellow signal provides great contrast in the surgical field. Fluorescein as contrast agent combined with white light cystoscopy during confocal laser endomicroscopy of the bladder was shown to be able to distinguish normal and benign bladder epithelium from bladder carcinoma based on microscopic characteristics [18,19]. With fluorescein, which is considered a good imaging agent for angiography of the eye [35,36], Nguyen et al. [20] showed that the morphology of various intra-abdominal organs could be studied to distinguish diseased from normal tissue during urological interventions. Moreover, individual cells could also be visualized when fluorescein diffused into the interstitial space [20].

INDOCYANINE GREEN

The most widely applied near-infrared tracer is ICG (Pulsion Medical Systems, Munich, Germany; Figure 1F) with an emission in the 820-830 nm range following excitation at 780 nm (quantum yield 0.0028 in water [37]; Table 1). After intravenous injection, ICG binds rapidly to the plasma protein albumin (95%), which results in increased fluorescent properties (quantum yield 0.012 [37]), and a 25 nm red shift of the excitation maximum [37,38]. The emission signal of ICG is not visible with the naked eye and, therefore, a pseudo-color needs to be added. This color may significantly influence the contrast obtained in the surgical field; green provides a better contrast over a bloody background than red and is, therefore, often chosen. Moreover, in order to visualize the emission signal, a fluorescence camera system is required. ICG has a favorable safety profile with anaphylaxis occurring in less than 0.05% of cases.

Outside the field of urology, ICG is used for near-infrared fluorescence angiography [39-41]. Within the field of urology, Tanaka et al. [21] showed clear ureter visualization following retrograde injection of ICG. In addition, renal vasculature and tumors could be visualized during robot-assisted partial nephrectomy [22]. Tobis et al. [22] showed improved tumor detection in 11 patients with small renal masses following intravenous ICG injection. Here the vascular physiology of the tumor provided the diagnostic contrast. Although the short half-life of ICG (2-5 min) required repetitive injections, the recommended maximum dose of 2 mg/kg was not exceeded in any of the cases before resection of the tumor was completed [22]. Furthermore, ICG has found its application in the visualization of lymph vessels and leakage in patients with lymphedema [42].

ICG has most extensively been studied as an alternative for the more common vital dyes methylene blue and patent blue during intraoperative SN biopsy procedures in a variety of tumors such as skin, breast, gastrointestinal, anal, and lung cancer [42,43]. Intratumoral injection of ICG was shown to rapidly migrate to organ-associated lymph nodes that could be visualized via near-infrared fluorescence imaging [42,43]. The increased sensitivity obtained with near-infrared fluorescent tracers may allow for improved identification of lymph nodes at wavelengths not visible by the naked human eye. Binding of ICG to a protein, for example ICG-human serum albumin (ICG-HSA; Figure 1G) [44], increases the hydrodynamic diameter, and might thereby provide better retention and improved detection of the complex in the SNs [43]. Conventional preoperative SN visualization is done by injecting a ^{99m}Tc-labeled sulfur- or nanocolloid (HSA aggregate) to obtain optimal tracer accumulation at the landing sites after (intratumoral) injection. This enables preoperative planar lymphoscintigraphy and SPECT/CT imaging. Moreover, it allows for intraoperative localization of the SN using a gamma probe. The combination of ICG and ^{99m}Tc in the form of the hybrid tracer ICG-^{99m}Tc-nanocolloid (Figure 1H) conveyed the nanocolloid properties to ICG and enabled intraoperative near-infrared imaging of the SNs in animal models for breast and prostate cancer [27,45]. Non-covalent self-assembly of ICG-^{99m}Tc-nanocolloid by premixing ICG with ^{99m}Tc-nanocolloid, but not albumin, resulted in better accumulation in the (sentinel) lymph nodes, thereby increasing specificity [27,45]. The signal to background ratio was found to be superior over 'free' ICG and ICG-HSA. Recently, ICG-^{99m}Tc-nanocolloid-based SN detection was also shown to be useful in prostate cancer patients [1]. This hybrid tracer allowed for preoperative detection of the SNs with SPECT/CT, whereas both the combination of the gamma probe and near-infrared fluorescence detection of ICG enabled intraoperative localization of the SNs (Figure 2D) [1]. Interestingly, following preoperative SPECT/CT imaging, four of 27 SNs were identified outside the extended pelvic lymph node dissection template, all of which were intraoperatively visualized via near-infrared fluorescence imaging [1]. A strong correlation was found between the radioactive and fluorescent contents in the excised lymph nodes indicating that the ICG-^{99m}Tc-nanocolloid complex remained stable in the time period between injection and dissection of the nodes [1,27]. However, 15% of the SNs could not

be intraoperatively detected with fluorescence imaging alone due to the limited tissue penetration of the ICG fluorescent signal [1]. Especially in these instances, guidance to regions of interest by the radioactive component of the hybrid tracer is still desirable.

In summary, fluorescent tracers with visual emissions (PpIX, hypericin, fluorescein) suffer more from poor tissue penetration as compared to tracers with emissions in the near-infrared range. Because of its high quantum yield and therefore bright yellow emission signal, fluorescein can provide sufficient contrast over a bloody background as compared to dyes such as PpIX and hypericin that give a red fluorescence and have a low quantum yield. However, even with a low quantum yield, ICG provides good contrast over a bloody background. Other, the so-called hybrid tracers, may hold two different diagnostic labels for example a radioactive and a fluorescent label (e.g. ICG-^{99m}Tc-nanocolloid). These hybrid tracers are not only suitable for intraoperative fluorescence imaging, but also allow for integration of preoperative imaging using radioactive isotopes. This enables preoperative planning of the fluorescence-guided interventions.

FLUORESCENT IMAGING HARDWARE

The (human) body holds many other molecules that can also be excited by a light source. In order to be able to image the exogenous fluorescent tracer optimally, or to image a more specific endogenous fluorochrome, the excitation light is often tailored to the excitation maximum of the fluorescent tracer of interest by using light emitting diodes (LEDs) or lasers that only emit in a small wavelength region or by using specific band pass filters. Herein it is also important that reflection of the excitation light source does not contaminate the detected fluorescence signal. Using band pass filters in front of the charge coupled device (CCD) camera, collection of the emission signal can be limited to a specific region around the emission maximum of the fluorochrome. Although band pass filters block many of the background signals, it is seldom optimal. For this reason, most open clinical camera systems require darkening of the surgical field to prevent contamination by the surgical lights.

As Table 2 points out, roughly 14 imaging systems have been used in a clinical (urological) setting. Although hardware and software specifications for the individual systems vary significantly, most systems are optimized for near-infrared (ICG) imaging alone (Table 2). Most widely applied are the near-infrared imaging systems for open surgery. Applications using ICG vary from angiography to tumor resection margin imaging, SN detection, and visualization of lymphedema [42,43]. The PhotoDynamic Eye (PDE) system (Hamamatsu Photonics K.K., Hamamatsu, Japan), a commercially available handheld device, provides a black and white image of area of interest following excitation of the fluorochrome with 36 LEDs at 760 nm [46]. Other available near-infrared detection systems for open surgery are the SPY open surgery system (Novadaq Technologies, Concord, ON, Canada) [41], IC-View (Pulsion Medical Systems, Feldkirchen, Germany) [51], HyperEye (Mizuho Medical Co Ltd, Tokyo, Japan) [39], (mini-)FLARE (Beth Israel

Table 2. Clinically available imaging systems

System	*Working distance*	*Excitation settings*	*Detection settings*	*Overlay on visual image*	*FOV*	*REF*
Open surgery systems						
PDE	15-25 cm	36 LEDs; 760 nm	CCD camera; band pass filter >820 nm	NO	NS	[46]
SPY open surgery system	30 cm	Laser; 806 nm	CCD camera; >830 nm	NO	56 cm^2	[41]
HyperEye	30-50 cm	LED; 760 nm	CCD camera; non-Bayer color filters, 380-1200 nm (ICG: cut on filter >840 nm)	YES	76.5 cm^2	[39]
FLARE	45 cm	LED; 656-678 nm and 745-779 nm	CCD camera; band pass filter at 689-725 nm and 800-848 nm	YES	3.7-195 cm^2	[47]
Mini-FLARE	10-32 cm	LED; 656-678 nm and 745-779 nm	CCD camera; band pass filter at 689-725 nm and 800-848 nm	YES	<108 cm^2	[48]
FDPM	<76.2 cm	Laser diode; 785±10 nm	Notch filters at 785 and 830 nm	NO	<900 cm^2	[49]
SurgOptix	21 cm	Laser diode; 750 nm	CCD cameras; band pass filter 750±10 nm and 795±50 nm	YES	1.5-107 cm^2	[50]
IC-View	NS	Laser; 760 nm	CCD camera; >835 nm	NO		[51]
Laparoscopic systems						
D-light	NS	Xe light source; band pass filter 380-440nm	CCD camera; long wavelength filter >520nm	YES	NS	[52]
Olympus NBI	~3mm	Xe light source	CCD camera; 415±15nm, 540±10 nm and 600±10 nm	YES	NS	[53]
NIR D-light	NS	Xe light source; PpIX and ICG settings	NS	YES	NS	[1]
NIR fluorescence for da Vinci Si surgical system	NS	Laser; 806nm	NS	NO	NS	[22]
Microscopy systems						
Confocal laser endomicroscopy	NS	Laser; 488 nm	CCD camera; band pass filter at 530 nm	NS	NS	[20]
Multiphoton microscopy	NS	Ti-Sapphire laser; 780 nm	CCD camera; 380-530 nm	NS	NS	[54]

FOV = field of view; PDE = Photodynamic Eye; LED = light emitting diode; CCD = charge coupled device; NS = not specified; FLARE = fluorescence-assisted resection and exploration; FDPM = frequency-domain photon migration; PpIX = protoporphyrin IX; ICG = indocyanine green; NBI = narrow band imaging; NIR = near-infrared; Xe = xenon; Hg = mercury; Ti = titanium; and REF = reference.

Deaconess Hospital, Boston, MA, USA) [47,48], SurgOptix (Technical University Munich/ Helmholtze Zentrum, Munich, Germany together with SurgOptix Inc., Redwood Shores, CA, USA) [50], and the FDPM system (Texas Medical Center, Houston, TX, USA) [49] (Table 2). SurgOptix and the (mini-)FLARE system also provide white light illumination of the surgical field. Moreover, by using more than one camera, these systems provide an overlay of the fluorescence and visual image. The Hyper Eye provides integration of the white light image with the near-infrared image.

With the rise of minimally invasive urologic interventions, endoscopic and/or laparoscopic systems will be of potential benefit. Currently, four systems are clinically available for laparoscopic fluorescence imaging, although development of new laparoscopic devices is ongoing [55,56]. Storz' D-light (KARL STORZ Endoskope GmbH & Co. KG, Tuttlingen, Germany) provides a system for both white light and collection of fluorescence in the visual emission range [52] and has found wide application for the detection of bladder cancer lesions following fluorescence imaging [2-11, 23-26, 29]. Moreover, Van der Poel et al. [1] used the near-infrared customized D-light system (KARL STORZ Endoskope GmbH & Co. KG) with incorporated near-infrared (ICG) settings for SN detection during robot-assisted laparoscopic prostatectomy procedures. Recently, Intuitive Surgical Inc. (Sunnyvale, CA, USA) introduced an integrated near-infrared imaging system for the da Vinci Si Surgical robot system in collaboration with Novadaq Technologies [22]. Lastly, Olympus Corp. introduced narrow band imaging (NBI) endoscopy in which the visual range emission band pass filters are set very narrow (Table 2). NBI allowed for detailed visualization of the mucosa surface, thereby distinguishing well-vascularized neoplastic lesions from normal bladder mucosa during cystoscopy procedures [53,57,58].

Of the near-infrared imaging systems, five imaging systems enable the detection of fluorochromes at various wavelengths. The customized near-infrared D-light system (KARL STORZ Endoskope GmbH & Co KG) provides both visual and near-infrared emission detection. With the (mini-)FLARE, fluorescence tracers can be excited between 656-678 and 745-779 nm after which emission light is collected via band pass filters from 689-725 and 800-848 nm, respectively [47,38]. SurgOptix provides emission collection using various CCD cameras with band pass filters at 795±50 nm [50]. With the implementation of an extra band pass filter at 750±10 nm, Themelis et al. [50] could perform light-absorption correction. The FDPM system provides Notch filters at 785 and 830 nm for the collection of the emission signal from the near-infrared fluorochrome [49].

Summarizing, the clinical availability of camera systems for fluorescent tracer imaging with emission in the visual range is limited, whereas a lot of research is ongoing in the development of imaging systems optimized for near-infrared dye imaging. Only a limited number of camera systems allows for multispectral imaging, among them the customized near-infrared D-light system (KARL STORZ Endoskope GmbH & Co KG). Although there are many systems available for open fluorescence-guided surgery, only a few laparoscopic devices are available for fluorescence imaging within the urological field.

FUTURE PERSPECTIVES IN FLUORESCENT TRACER DEVELOPMENT AND IMAGING SYSTEMS

The clinical tracers used to date provide merely the initial steps in fluorescence image-guided surgery. Targeting specific tumor markers with fluorescent tracers is expected to improve intraoperative imaging. Various tracers have been developed targeting the $\alpha_v\beta_3$-integrin receptor which plays an important role in the process of (tumor) angiogenesis [59-62]. Moreover, enzyme-activatable tracers [61,63,64] might improve specificity of surgical guidance by making the contrast provided by the imaging agents dependent on local enzymatic activity of, for example, matrix metalloproteinases and cathepsins, which are frequently found to be overexpressed in prostate cancer cells [65]. Although we acknowledge the value of fluorescent tracers, in our opinion, the hybrid tracer approach is superior and therefore has the highest future potential. It enables the conversion of functional imaging (SPECT/CT and/or PET) data to the surgical theatre. Furthermore, it is possible to attach a fluorochrome and radioactive label to most targeting peptides, proteins, and/or antibodies, thereby creating targeted hybrid tracers. Of particular interest would be hybrid tracers for the most common biomarkers in urology. For example, for prostate cancer [65], wherein hybrid tracers have been developed preclinically for biomarkers such as chemokine receptor 4 [66], prostate specific membrane antigen [67], and integrins [66,68,69]. Nevertheless, for all these new compounds currently under development, obtaining clinical approval seems to be the biggest hurdle.

With the introduction of targeted and/or activatable (hybrid) tracers, more sophisticated imaging systems are desired to further improve the detectability of the fluorochromes. To date, most imaging systems are limited to the imaging of only one tracer. However, with the improvements in tracer development, one might think about developing imaging systems providing multispectral imaging. In this way, various fluorochromes can be used during the same procedure, possibly providing more specific imaging of the area of interest. Another interesting development in the field, and possibly applicable during urological interventions, was the introduction of confocal endomicroscopy (Table 2) for cellular structure visualization and vascularization imaging using fluorescein in order to improve surgical guidance [18-20]. Fluorescein, similarly to 'free' ICG, might also be of additional value for the detection of the SN following an intratumoral injection (F.W.B. van Leeuwen, unpublished observations). Moreover, multiphoton microscopy (Table 2) has been used to identify nerve structures based on tissue autofluorescence and might have the potential to improve the precision of nerve-sparing prostatectomy [54]. Lastly, Brouwer et al. described a navigation system for surgical guidance based on preoperative and intraoperatively acquired imaging data with the hybrid tracer ICG-^{99m}Tc-nanocolloid, thereby potentially improving the accuracy of fluorescence-guided surgery even further (Figure 3) [70].

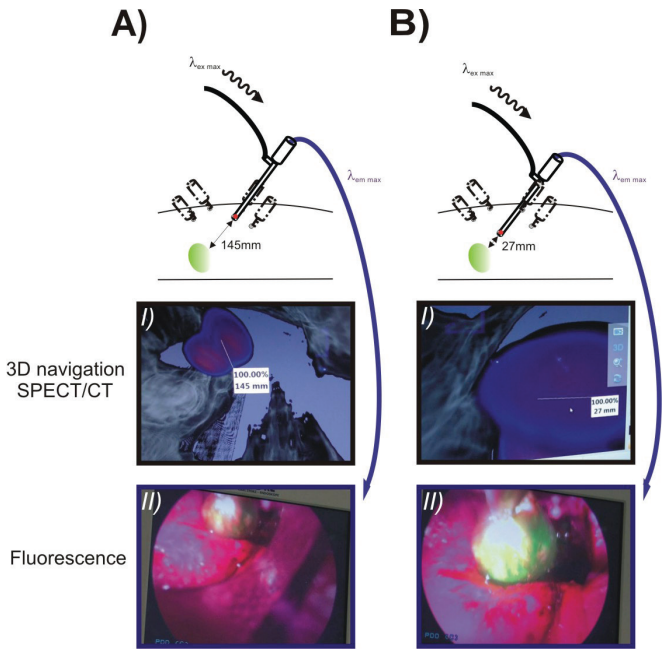

Figure 3. Image navigation towards the target lesion. Based on the preoperatively acquired SPECT/CT data (AI and BI), the laparoscope can be navigated toward the lesion. The navigation system provides the distance toward the lesion (dotted lines highlight the fluorescent area) in millimeters in the schematic SPECT/CT based overview images, whereas the fluorescence laparoscope detects the fluorescent lesions (AII and BII). SPECT/CT = single photon emission computed tomography/ computed tomography.

CONCLUSION

Fluorescence image-guided surgery holds promise for intraoperative identification of anatomical tumor structures within the field of urology. Currently, PpIX precursors 5-ALA and HAL, fluorescein, and ICG have received clinical FDA approval and are used for the identification of tumor locations and surgical tumor margins. Moreover, the hybrid tracer ICG-^{99m}Tc-nanocolloid was used for SN detection during robot-assisted laparoscopic prostatectomy. Challenges lie in the further optimization of targeted and/or activatable (hybrid) imaging agents and the integration between imaging agents and camera systems, thereby enabling more accurate fluorescence image guidance during surgical interventions.

REFERENCES

1. van der Poel HG, Buckle T, Brouwer OR, et al. Intraoperative laparoscopic fluorescence guidance to the sentinel lymph node in prostate cancer patients: clinical proof of concept of an integrated functional imaging approach using a multimodal tracer. Eur Urol. 2011;60:826-833.
2. Babjuk M, Soukup V, Petrik R, et al. 5-aminolaevulinic acid-induced fluorescence cystoscopy during transurethral resection reduces the risk of recurrence in stage Ta/T1 bladder cancer. BJU Int. 2005; 96:798-802.
3. Daniltchenko DI, Riedl CR, Sachs MD, et al. Long-term benefit of 5-aminolevulinic acid fluorescence assisted transurethral resection of superficial bladder cancer: 5-year results of a prospective randomized study. J Urol. 2005; 174:2129-2133.
4. Denzinger S, Burger M, Walter B, et al. Clinically relevant reduction in risk of recurrence of superficial bladder cancer using 5-aminolevulinic acid-induced fluorescence diagnosis: 8-year results of prospective randomized study. Urology. 2007; 69:675-679.
5. Filbeck T, Pichlmeier U, Knuechel R, et al. Clinically relevant improvement of recurrence-free survival with 5-aminolevulinic acid induced fluorescence diagnosis in patients with superficial bladder tumors. J Urol. 2002; 168:67-71.
6. Hermann GG, Mogensen K, Carlsson S, et al. Fluorescence-guided transurethral resection of bladder tumours reduces bladder tumour recurrence due to less residual tumour tissue in Ta/T1 patients: a randomized two-centre study. BJU Int. 2011; 108:E297-303.
7. Lerner SP, Liu H, Wu MF, et al. Fluorescence and white light cystoscopy for detection of carcinoma in situ of the urinary bladder. Urol Oncol. 2011;30:285-9.
8. Ray ER, Chatterton K, Khan MS, et al. Hexylaminolaevulinate fluorescence cystoscopy in patients previously treated with intravesical bacille Calmette-Guerin. BJU Int. 2010; 105:789-794.
9. Ray ER, Chatterton K, Thomas K, et al. Hexylaminolevulinate photodynamic diagnosis for multifocal recurrent nonmuscle invasive bladder cancer. J Endourol. 2009;23:983-988.
10. Stenzl A, Penkoff H, Dajc-Sommerer E, et al. Detection and clinical outcome of urinary bladder cancer with 5-aminolevulinic acid-induced fluorescence cystoscopy: a multicenter randomized, double-blind, placebo-controlled trial. Cancer. 2011;117:938-947.
11. Zaak D, Karl A, Knuchel R, et al. Diagnosis of urothelial carcinoma of the bladder using fluorescence endoscopy. BJU Int. 2005; 96:217-222.
12. Adam C, Salomon G, Walther S, et al. Photodynamic diagnosis using 5-aminolevulinic acid for the detection of positive surgical margins during radical prostatectomy in patients with carcinoma of the prostate: a multicentre, prospective, phase 2 trial of a diagnostic procedure. Eur Urol. 2009;55:1281-1288.

13. Fukuhara H, Inoue K, Satake H, et al. Photodynamic diagnosis of positive margin during radical prostatectomy: preliminary experience with 5-aminole-vulinic acid. Int J Urol. 2011;18:585-591.
14. Ganzer R, Blana A, Denzinger S, et al. Intraoperative photodynamic evaluation of surgical margins during endoscopic extraperitoneal radical prostatectomy with the use of 5-aminolevulinic acid. J Endourol. 2009;23:1387-1394.
15. Zaak D, Sroka R, Khoder W, et al. Photodynamic diagnosis of prostate cancer using 5-aminolevulinic acid: first clinical experiences. Urology. 2008;72:345-348.
16. Frimberger D, Schneede P, Hungerhuber E, et al. Autofluorescence and 5-aminolevulinic acid induced fluorescence diagnosis of penile carcinoma: new techniques to monitor Nd:YAG laser therapy. Urol Res. 2002;30:295-300.
17. Schlenker B, Gratzke C, Seitz M, et al. Fluorescence-guided laser therapy for penile carcinoma and precancerous lesions: long-term follow-up. Urol Oncol. 2011; 29:788-793.
18. Wu K, Liu JJ, Adams W, et al. Dynamic real-time microscopy of the urinary tract using confocal laser endomicroscopy. Urology. 2011;78:225-231.
19. Sonn GA, Jones SN, Tarin TV, et al. Optical biopsy of human bladder neoplasia with in vivo confocal laser endomicroscopy. J Urol .2009; 182:1299-1305.
20. Nguyen NQ, Biankin AV, Leong RW, et al. Real time intraoperative confocal laser microscopy-guided surgery. Ann Surg. 2009;249:735-737.
21. Tanaka E, Ohnishi S, Laurence RG, et al. Real-time intraoperative ureteral guidance using invisible near-infrared fluorescence. J Urol. 2007;178:2197-2202.
22. Tobis S, Knopf J, Silvers C, et al. Near infrared fluorescence imaging with robotic assisted laparoscopic partial nephrectomy: initial clinical experience for renal cortical tumors. J Urol. 2011; 186:47-52.
23. D'Hallewin MA, De Witte PA, Waelkens E, et al. Fluorescence detection of flat bladder carcinoma in situ after intravesical instillation of hypericin. J Urol. 2000;164:349-351.
24. D'Hallewin MA, Kamuhabwa AR, Roskams T, et al. Hypericin-based fluorescence diagnosis of bladder carcinoma. BJU Int. 2002;89:760-763.
25. Sim HG, Lau WK, Olivo M, et al. Is photodynamic diagnosis using hypericin better than white-light cystoscopy for detecting superficial bladder carcinoma? BJU Int. 2005;95:1215-1218.
26. Kubin A, Meissner P, Wierrani F, et al. Fluorescence diagnosis of bladder cancer with new water soluble hypericin bound to polyvinylpyrrolidone: PVP-hypericin. Photochem Photobiol. 2008;84:1560-1563.
27. van Leeuwen AC, Buckle T, Bendle G, et al. Tracer-cocktail injections for combined pre and intraoperative multimodal imaging of lymph nodes in a spontaneous mouse prostate tumor model. J Biomed Opt. 2011;16:016004.
28. Wachowska M, Muchowicz A, Firczuk M, et al. Aminolevulinic acid (ALA) as a product in photodynamic therapy of cancer. Molecules. 2011;16:4140-4164.

29. Celli JP, Spring BQ, Rizvi I, et al. Imaging and photodynamic therapy: mechanisms, monitoring, and optimization. Chem Rev. 2010;110:2795-2838.
30. Lozovaya GI, Masinovsky Z, Sivash AA. Protoporphyrin IX as a possible ancient photosensitizer: spectral and photochemical studies. Orig Life Evol Biosph. 1990;20:321-330.
31. Frimberger D, Zaak D, Stepp H, et al. Autofluorescence imaging to optimize 5-ALA-induced fluorescence endoscopy of bladder carcinoma. Urology. 2001;58:372-375.
32. Kubin A, Wierrani F, Burner U, et al. Hypericin: the facts about a controversial agent. Curr Pharm Des. 2005;11:233-253.
33. Wynn JL, Cotton TM. Spectroscopic properties of hypericin in solution and at surfaces. J Phys Chem. 1995;99:4317-4323.
34. Song A, Zhang J, Zhang M, et al. Spectral properties and structure of fluorescein and its alkyl derivatives in micelles. Colloids and Surfaces A: Physiochem Eng Aspects. 2000;167:253-262.
35. Bienfang DC, McKenna MJ, Papaliodis GN, et al. Case records of the Massachusetts General Hospital. Case 24-2011. A 36-year-old man with headache, memory loss, and confusion. N Engl J Med. 2011;365:549-559.
36. Spaide RF. Peripheral areas of nonperfusion in treated central retinal vein occlusion as imaged by wide-field fluorescein angiography. Retina. 2011;31:829-837.
37. Benson RC, Kues HA. Fluorescence properties of indocyanine green as related to angiography. Phys Med Biol. 1978;23:159-163.
38. Landsman ML, Kwant G, Mook GA, Zijlstra WG. Light-absorbing properties, stability, and spectral stabilization of indocyanine green. J Appl Physiol. 1976;40:575-583.
39. Handa T, Katare RG, Nishimori H, et al. New device for intraoperative graft assessment: HyperEye charge-coupled device camera system. Gen Thorac Cardiovasc Surg. 2010;58:68-77.
40. Sekijima M, Tojimbara T, Sato S, et al. An intraoperative fluorescent imaging system in organ transplantation. Transplant Proc. 2004;36:2188-2190.
41. Taggart DP, Choudhary B, Anastasiadis K, et al. Preliminary experience with a novel intraoperative fluorescence imaging technique to evaluate the patency of bypass grafts in total arterial revascularization. Ann Thorac Surg. 2003;75:870-873.
42. Polom K, Murawa D, Rho YS, et al. Current trends and emerging future of indocyanine green usage in surgery and oncology: a literature review. Cancer. 2011;117:4812-4822.
43. Schaafsma BE, Mieog JS, Hutteman M, et al. The clinical use of indocyanine green as a near-infrared fluorescent contrast agent for image-guided oncologic surgery. J Surg Oncol. 2011;104:323-332.
44. Hutteman M, Mieog JS, van der Vorst JR, et al. Randomized, double-blind comparison of indocyanine green with or without albumin premixing for near-infrared fluorescence imaging of sentinel lymph nodes in breast cancer patients. Breast Cancer Res Treat. 2011;127:163-170.

45. Buckle T, van Leeuwen AC, Chin PT, et al. A self-assembled multimodal complex for combined pre and intraoperative imaging of the sentinel lymph node. Nanotechnology. 2010;21:355101.
46. Unno N, Inuzuka K, Suzuki M, et al. Preliminary experience with a novel fluorescence lymphography using indocyanine green in patients with secondary lymphedema. J Vasc Oncol. 2007;45:1016-1021.
47. Troyan SL, Kianzad V, Gibbs-Strauss SL, et al. The FLARE intraoperative near-infrared fluorescence imaging system: a first-in-human clinical trial in breast cancer sentinel lymph node mapping. Ann Surg Oncol. 2009;16:2943-2952.
48. Mieog JS, Troyan SL, Hutteman M, et al. Toward optimization of imaging system and lymphatic tracer for near-infrared fluorescent sentinel lymph node mapping in breast cancer. Ann Surg Oncol. 2011;18:2483-2491.
49. Sevick-Muraca EM, Sharma R, Rasmussen JC, et al. Imaging of lymph flow in breast cancer patients after microdose administration of a near-infrared fluorophore: feasibility study. Radiology. 2008;246:734-741.
50. Themelis G, Yoo JS, Soh KS, et al. Real-time intraoperative fluorescence imaging system using light-absorption correction. J Biomed Opt. 2009;14:064012.
51. Hirche C, Murawa D, Mohr Z, et al. ICG fluorescence-guided sentinel node biopsy for axillary nodal staging in breast cancer. Breast Cancer Res Treat. 2010;121:373-378.
52. Riedl CR, Plas E, Pfluger H. Fluorescence detection of bladder tumors with 5-amino-levulinic acid. J Endourol. 1999;13:755-759.
53. Kuznetsov K, Lambert R, Rey JF. Narrow-band imaging: potential and limitations. Endoscopy. 2006;38:76-81.
54. Yadav R, Mukherjee S, Hermen M, et al. Multiphoton microscopy of prostate and periprostatic neural tissue: a promising imaging technique for improving nerve-sparing prostatectomy. J Endourol. 2009;23:861-867.
55. Matsui A, Tanaka E, Choi HS, et al. Real-time intra-operative near-infrared fluorescence identification of the extrahepatic bile ducts using clinically available contrast agents. Surgery. 2010;148:87-95.
56. van der Pas MH, van Dongen GA, Cailler F, et al. Sentinel node procedure of the sigmoid using indocyanine green: feasibility study in a goat model. Surg Endosc. 2010;24:2182-2187.
57. Herr HH. Narrow band imaging cystoscopy. Urol Oncol. 2011;29:353-357.
58. Shen YJ, Zhu YP, Ye DW, et al. Narrow-band imaging flexible cystoscopy in the detection of primary nonmuscle invasive bladder cancer: a 'second look' matters? Int Urol Nephrol. 2011;44:451-457.
59. Hutteman M, Mieog JS, van der Vorst JR, et al. Intraoperative near-infrared fluorescence imaging of colorectal metastases targeting integrin alpha(v)beta(3) expression in a syngeneic rat model. Eur J Surg Oncol. 2011;37:252-257.

60. Mery E, Jouve E, Guillermet S, et al. Intraoperative fluorescence imaging of peritoneal dissemination of ovarian carcinomas. A preclinical study. Gyn Oncol. 2011;122:155-162.
61. Penna FJ, Freilich DA, Alvarenga C, Nguyen HT. Improving lymph node yield in retroperitoneal lymph node dissection using fluorescent molecular imaging: a novel method of localizing lymph nodes in Guinea pig model. Urology. 2011;78:232e15-232e18.
62. Themelis G, Harlaar NJ, Kelder W, et al. Enhancing surgical vision by using real-time imaging of avb3-Integrin targeted near-infrared fluorescent agent. Ann Surg Oncol. 2011;18:3506-3513.
63. Liu Y, Bauer AQ, Akers WJ, et al. Hands-free, wireless goggles for near-infrared fluorescence and real-time image-guided surgery. Surgery. 2011;149:689-698.
64. Mieog JS, Hutteman M, van der Vorst JR, et al. Image-guided tumor resection using real-time near-infrared fluorescence in a syngeneic rat model of primary breast cancer. Breast Cancer Res Treat. 2011;128:679-689.
65. Yang SY, Adelstein J, Kassis AI. Putative molecular signatures for the imaging of prostate cancer. Expert Rev Mol Diagn. 2010;10:65-74.
66. Kuil J, Velders AH, van Leeuwen FW. Multimodal tumor-targeting peptides functionalized with both a radio- and a fluorescent label. Bioconjug Chem. 2010; 21:1709-1719.
67. Banerjee SR, Pullambhatla M, Byun Y, et al. Sequential SPECT and optical imaging of experimental models of prostate cancer with a dual modality inhibitor of the prostate-specific membrane antigen. Angew Chem Int Ed Engl. 2011;50:9167-9170.
68. Edwards WB, Akers WJ, Ye Y, et al. Multimodal imaging of integrin receptor-positive tumors by bioluminescence, fluorescence, gamma scintigraphy, and single-photon emission computed tomography using a cyclic RGD peptide labeled with a near-infrared fluorescent dye and a radionuclide. Mol Imaging. 2009;8:101-110.
69. Li C, Wang W, Wu Q, et al. Dual optical and nuclear imaging in human melanoma xenografts using a single targeted imaging probe. Nucl Med Biol. 2006;33:349-358.
70. Brouwer OR, Buckle T, Bunschoten A, et al. Image navigation as a mean to expand the boundaries of fluorescence-guided surgery. Phys Med Biol. 2012:57;3123-36.

SUPPORTING INFORMATION

PRINCIPLE OF FLUORESCENCE

The process of fluorescence can be divided into three steps: 1) Excitation of the molecule by photons; 2) Internal conversion; and 3) Emission of photons. This process is graphically represented in a Jablonski diagram (Figure SI 1A; for more detailed information see Ruggi et al. [1]). Each fluorochrome has its own particular excitation ($\lambda_{ex\ max}$) and emission maximum ($\lambda_{em\ max}$) (Table 1). However, the excitation and emission signals are often very broad (Figure SI1B). In fluorescence imaging this means that you need both a light source matching the excitation maximum of the fluorochrome and a camera system for the detection of the emission light around the emission maximum peak. In general, emissions are classified in visual emissions with a wavelength of 400-650 nm, far-red emissions (650-700 nm), and the by eye invisible near-infrared emissions 700-1000 nm (Figure SI 1C). The efficacy through which this photon emission occurs for a particular molecule is depicted by the fluorescence quantum yield (ranging from 0-1) of the fluorochrome.

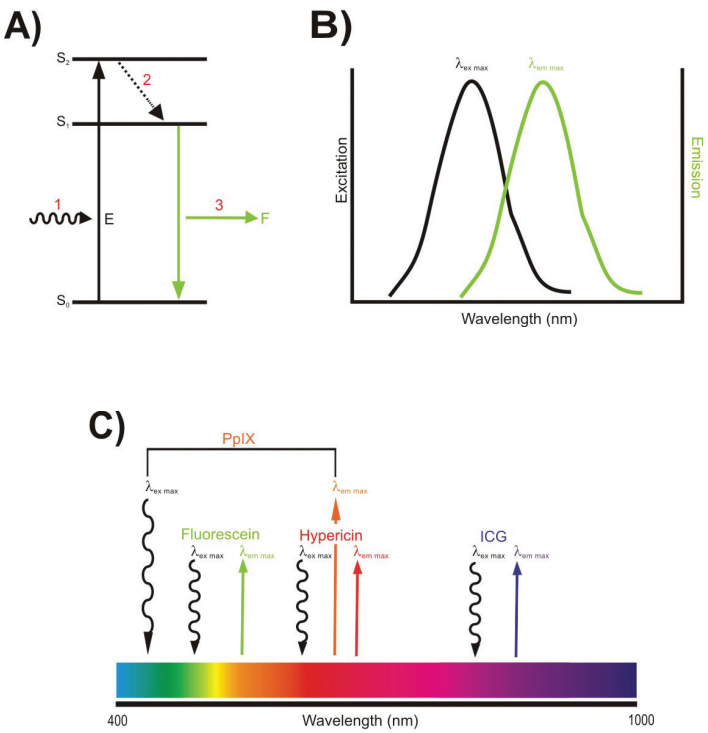

Figure SI1. Basics of fluorescence. A) Jablonski diagram of the process of fluorescence: 1. Excitation of the molecule by photons (E); 2. Internal conversion; and 3. Emission of photons (F). S0, S1 and S2 depict the various energy levels; B) Schematic overview of a general excitation and emission spectrum of a fluorochrome where $\lambda_{ex\ max}$ = excitation maximum and $\lambda_{em\ max}$ = emission maximum; and C) Light spectrum with $\lambda_{ex\ max}$ and $\lambda_{em\ max}$ of various fluorochromes. PpIX = protoporphyrin IX; and ICG = indocyanine green.

Absorption and/or light scatter by tissues limits the penetration of the excitation light and thus the depth at which fluorochromes can be excited. For the fluorescent emissions, the surrounding tissues also cause signal attenuation via absorbance and/or scattering. The major absorbers of visible light are native fluorescent molecules such as oxy- and deoxyhemoglobin in blood, whereas lipids and water are the major absorbers of infrared light at wavelengths >1000 nm [2-4]. Scattering may also occur via these molecules, but tissue architecture and intracellular composition (organelle density) are also of influence [2, 3]. Combined, the depth at which a fluorescent signal can be detected is limited, even in the most optimal near-infrared wavelength window. Signal penetration varies from millimeters (visual emissions 450-650 nm) to centimeters for near-infrared emissions [5, 6]. Moreover, tissue autofluorescence (endogenous fluorescence) may impair the specificity of detection [6]. In the process of autofluorescence, naturally occurring tissue fluorophores generally emit light <700 nm when excited by a light source [3]. Throughout the body, autofluorescence can be caused by various molecules such as nicotinamide (NAD[H]) and flavins. The extracellular matrix can also contribute to autofluorescence due to the intrinsic properties of collagen and elastin [2, 7].

REFERENCES

1. Ruggi A, van Leeuwen FW, Velders AH. Interaction of dioxygen with the electronic excited state of Ir(III) and Ru(II) complexes: Principles and biomedical applications. Coord Chem Rev. 2011;21-22:2542-2554.
2. Bremer C, Ntziachristos V, Weissleder R. Optical-based molecular imaging: contrast agents and potential medical applications. Eur Radiol. 2003:13:231-43.
3. Klohs J, Wunder A, Licha K. Near-infrared fluorescent probes for imaging vascular pathophysiology. Basic Res Cardiol. 2008;103:144-51.
4. Weissleder R, Ntziachristos V. Shedding light onto live molecular targets. Nat Med. 2003;9:123-8.
5. Buckle T, Chin PT, van den Berg NS et al., Tumor bracketing and safety margin estimation using multimodal marker seeds: a proof of concept. J Biomed Opt. 2010;15: 056021.
6. Chin PT, Buckle T, Aguirre de Miguel A et al., Dual-emissive quantum dots for multispectral intraoperative fluorescence imaging. Biomaterials. 2010;31;6823-32.
7. Frimberger D, Zaak D, Stepp H et al. Autofluorescence imaging to optimize 5-ALA-induced fluorescence endoscopy of bladder carcinoma. Urology. 2001;58:372-5.

CHAPTER 3

HYBRID TRACERS FOR SENTINEL NODE BIOPSY

Adapted from: van den Berg NS, Buckle T, KleinJan GH, Klop WMC, Horenblas S, van der Poel HG, Valdés Olmos RA, van Leeuwen FWB. Q J Nucl Med Mol Imaging. 2014;58:193-206.

ABSTRACT

Conventional sentinel node (SN) mapping is performed by injection of a radiocolloid followed by lymphoscintigraphy to identify the number and location of the primary tumor draining lymph node(s), the so-called SN(s). Over the last decade research has focused on the introduction of new imaging agents that can further aid (surgical) SN identification. Different tracers for SN mapping, with varying sizes and isotopes have been reported, most of which have proven their value in a clinical setting. A major challenge lies in transferring this diagnostic information obtained at the nuclear medicine department to the operating theatre thereby providing the surgeon with (image) guidance. Conventionally, an intraoperative injection of vital blue dye or a fluorescence dye is given to allow intraoperative optical SN identification. However, for some indications, the radiotracer-based approach remains crucial. More recently, hybrid tracers, that contain both a radioactive and fluorescent label, were introduced to allow for direct integration of pre- and intraoperative guidance technologies. Their potential is especially high when they are used in combination with new surgical imaging modalities and navigation tools. Next to a description of the known tracers for SN mapping, this review discusses the application of hybrid tracers during SN biopsy and how the introduction of these new techniques can further aid in translation of nuclear medicine information into the operating theatre.

INTRODUCTION

The presence of metastases in the regional lymph node(s) is one of the most important prognostic factors in breast cancer and melanoma, but also in head-and-neck malignancies and cancers of the genitals. For example, in patients with head-and-neck malignancies it was shown that unilateral lymph node metastasis lowered the five-year survival rate with 50% [1].

A regional lymph node dissection can be performed to determine the lymph node status. Unfortunately this procedure is associated with high morbidity such as lymphedema. Assuming the orderly spread of tumor cells through the lymphatic system, identifying the primary tumor draining lymph node(s), the so-called sentinel node(s) (SN(s)) [2], will allow more accurate determination of the lymph node status in patients presenting without clinical evidence of regional lymph node involvement or distant metastasis (clinically N0M0). With roughly 10-30% of these patients presenting with occult lymph node metastases [3-5], SN biopsy can be used to stage these clinically N0 patients and select patients with positive SNs for a regional lymph node dissection as such sparing the pathologically N0 patients an unnecessary regional lymph node dissection. Moreover, with SN biopsy the accuracy of pathological lymph node staging will increase; the pathologist can meticulously examine the SNs only for the presence of isolated tumor cells and/or (micro-)metastases, which is not possible if he/she has to examine a whole regional lymph node dissection specimen (generally >20 lymph nodes).

SN biopsy is most widely validated and implemented in staging patients with breast cancer [6] and melanoma [7]. Over the last decade, SN biopsy has also found its way in staging the regional lymph nodes of the groin in patients with penile [8] or vulvar [9] cancer and for staging the neck in patients with head-and-neck squamous cell carcinoma [10]. The concept has also been validated for prostate cancer in various European countries [11-13], but the procedure has not yet been widely accepted. Initial work is also reported for other urological malignancies like testis [14,15], bladder [16], and kidney [17,18] cancer, as well as SN biopsy for lung [19] and gastric [20] cancer. The potential of lymph node mapping for colorectal cancer has been underlined by ex vivo SN mapping studies [21,22]. Expansion of the SN biopsy technique to these new indications will not only lead to an enlargement of the patient population that will undergo SN biopsy, the widespread implementation of this minimally invasive procedure will also increase the surgical complexity. For example, the surgeon's senses are reduced during laparoscopic applications, driving the need for innovations that aid the surgical identification.

Over the recent years, conventional SN mapping based on lymphoscintigraphy after injection of a radiotracer has been improved by the introduction of single photon emission computed tomography combined with computed tomography (SPECT/CT). Acquisition of SPECT scans enables visualization of the radioactive hot spots (SNs), and fusion of these images with CT images enables anatomical localization of the SN(s) [23,24]. Such an anatomical roadmap can be used to preoperatively plan the most optimal surgical approach towards the SN(s).

Generally, surgical identification of the preoperatively defined SNs can be performed using a gamma-ray detection probe (hereafter referred to as gamma probe) or a portable gamma camera that traces the radioactivity in the nodes, and/or by visual identification after an additional intraoperative injection of a vital blue dye. Unfortunately, in areas where SNs are often located near the injection site, e.g. head-and-neck cancers, radioactivity-based surgical identification can be difficult due to the high background signal coming from the injection site [25,26]. On the other hand, due to its passive diffusion through the lymphatic system, blue dye is unable to accumulate in the SN limiting its effective time window (30-45 minutes) [27]. In contrast, radiotracers are actively incorporated into SNs and can be detected >24 h after administration.

Ideally, the combined use of radiotracing and optical detection allows for optimal use of the nuclear and optical detection technologies. Herein radiotracing is most optimal for (preoperative) total body imaging and the identification of unexpected drainage patterns. Optical imaging, on the other hand, provides detail and real-time feedback during the surgical procedure regarding the location of the SN. Consequently the combination of the vital blue dye approach with radiotracing has been shown to yield a superior SN detection rate compared to either radiotracing or optical vital blue dye detection alone. For melanoma and breast cancer a success rate of identifying nodes with vital blue dye was shown to be 75-80% vs. 97-98% for radiocolloid-based SN detection [28,29]. This increased to 98-99% when using the combined approach of sequential injections. Yet for some indications, e.g. oral cavity carcinoma or prostate cancer, vital blue dye is less sensitive in the identification of the SNs than the radiocolloid approach, principally for the identification of aberrant drainage patterns as was shown in breast cancer where only 55% of SNs outside the axilla had stained blue vs. 84% of the axillary SNs [30]. Moreover, in oral cavity carcinoma and prostate cancer, vital blue dye administration was shown to be of limited value and/or to interfere with the visibility of tumor margins [3, 31, 32].

The limited sensitivity of vital blue dye detection was one of the main reasons to introduce (near-infrared) fluorescence tracers [33], and in particular indocyanine green (ICG) for SN biopsy. Fluorescent dyes show a comparable drainage pattern to vital blue dyes and as such they rapidly flow through the lymphatic system, without accumulation in the SNs [34]. In contrast to vital blue dyes, near-infrared dyes are invisible to the naked eye and can only be visualized using a dedicated near-infrared fluorescence camera system [35]. As such, the use of this type of dye does not interfere with margin visibility or unwanted coloring of the skin.

The difference in migration between the radiocolloid and the dyes can result in a discrepancy between the nuclear techniques used to non-invasively identify the SNs in the pre-surgical setting and the optical techniques used during surgery [28,29]. Direct integration of pre- and intraoperative imaging can be achieved by using hybrid tracers that contain both a radioactive and a fluorescent label [36,37].

This review gives an overview of the available lymphographic agents that are currently

clinically used for SN identification. Next, the application of hybrid tracers in the clinical routine and translation of nuclear medicine information into the operating theatre is discussed.

LYMPHOGRAPHIC AGENTS

RADIOTRACERS

For radiotracing in general colloid-based particles, ranging from albumin to tin, sulfur, antimony-trisulfide, rhenium and phytate are used (Figure 1). Following injection, these technetium-99m (^{99m}Tc) labeled colloids become trapped in the SN via an active physiological process in which the radiotracer is accumulated by macrophages and tissue histiocytes lining the sinuses of the node [38]. Ideally the agent should accumulate in the SN(s) with no, or limited, flow to higher-echelon nodes. However, when the flow is abundant and an excess of particles reaches the SN, saturation can occur, which in turn leads to overflow into higher-echelon nodes.

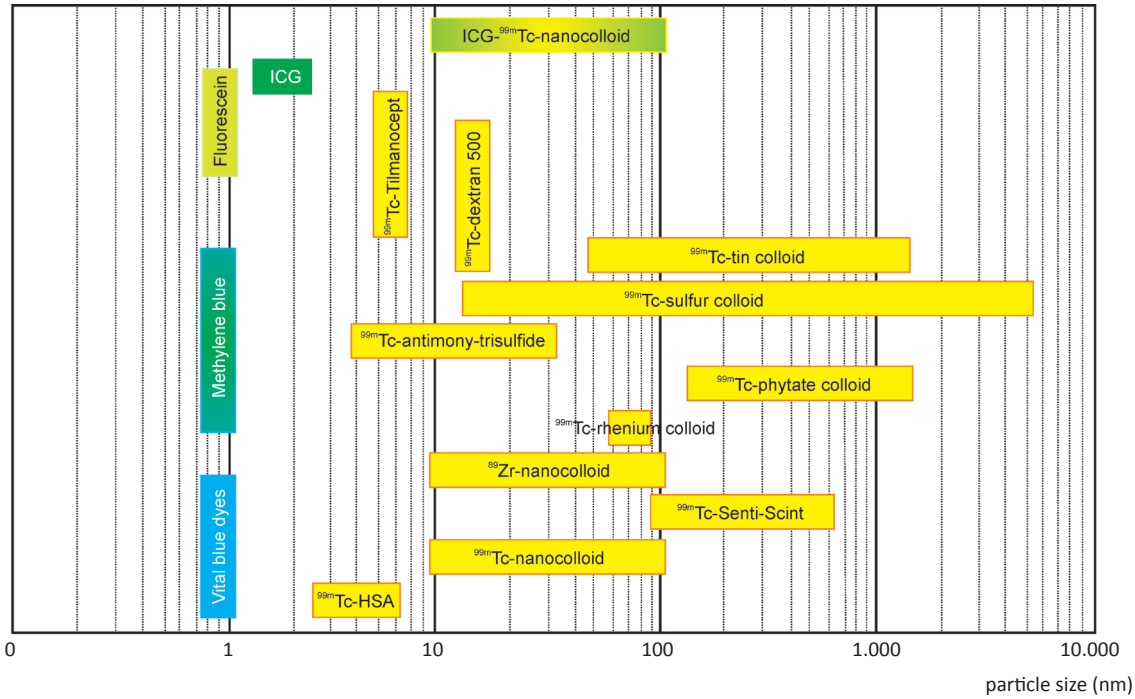

Figure 1. Overview of the particle sizes of the clinically available lymphographic agents. Vital blue dyes = indigo carmine, patent blue (V), isosulfan blue, and lymphazurin blue. ICG = indocyanine green; HSA = human serum albumin; Tc = technetium; Zr = zirkonium.

The composition and size of the current clinically used colloids varies greatly. Particles larger than 500 nm were shown to limit migration from the injection site [39], whereas smaller particles were reported to penetrate the capillary membranes, and as such might be unable to migrate through the lymphatic channel [40]. “Small-particle” radiocolloids (<100 nm) are thought to best enter the lymphatic vessels allowing visualization of the lymphatic tracts during dynamic lymphoscintigraphy [38]. Mariani et al. reported the use of 100-200 nm sized radiocolloids as the best compromise for efficient lymphatic drainage and retention in the SN(s) [29].

For metallic ^{99m}Tc-tin colloid the size depends on the ratio between the ^{99m}Tc-solution and tin solution; sizes ranging 50-1500 nm have been reported [41]. In the United States, the inorganic (filtered) ^{99m}Tc-sulfur colloid is the most frequently used tracer for SN mapping. Sizes ranging 100-400 nm [41] and 15-5000 nm [29] have been reported depending on the type of cut-off filter used. ^{99m}Tc-phytate is formed via a reaction with extracellular calcium and therefore the size of ^{99m}Tc-phytate colloid (diameter ranging 150-1500 nm) strongly depends on the serum calcium concentration [41]. ^{99m}Tc-antimony-trisulfide is mainly used in Australia and Canada and with a size ranging from 3-30 nm it is one of the smallest colloids [29,41] used for SN mapping. In Europe, human serum albumin (HSA)-based nanocolloids (mean diameter 20 nm; range 10-100 nm) are most widely used. Retention of this colloid in the SN is superior compared to that of radiolabeled HSA particles (mean diameter 7 nm) [34]. More recently, the larger HSA-based colloid Senti-Scint was introduced (mean diameter 205 nm; range 100-600 nm) and shown to allow for SN biopsy in amongst others breast [42] and prostate [13] cancer. This increase in size is thought to improve retention in the SNs but with lesser flow to higher-echelon nodes.

Alternatively, dextran-based particles (e.g. ^{99m}Tc-dextran 500 particles; approximately 14.4 nm [43]) have been used for lymphatic mapping in e.g. colon and breast cancer [44,45]. After many preclinical studies, a 7 nm radiocolloid based on mannose was evaluated in phase III studies for SN mapping in breast cancer, melanoma and squamous cell carcinoma of the oral cavity [46-48]. This tracer, better known as ^{99m}Tc-Tilmanocept or Lymphoseek™, is said to accumulate in SNs after binding the mannose-binding protein receptor present on phagocytes [49]. In contrast to the larger radiocolloids, these 7 nm particles also rapidly clear from the injection site due to diffusion into the blood capillaries leading to tracer absorption in the blood stream [49]. Although this diffusion may limit the amount of lymphatic flow, this clearance via the bloodstream reduces the signal intensity at the injection site, which may enable better identification of SN(s) located near the injection site.

As a substitute for the ^{99m}Tc-based radiotracers, zirkonium-89 (^{89}Zr) labeled nanocolloid (^{89}Zr-nanocolloid) has been introduced for positron emission tomography (PET)-based SN mapping in oral cavity carcinoma [50]. Compared to conventional lymphoscintigraphy and SPECT imaging, it is presumed that the increased sensitivity and resolution of PET imaging, in combination with CT, or possibly even magnetic resonance (MR) imaging, might be an

alternative for the ^{99m}Tc-based approach. Similar to the small dextran-based colloid this might also allow for better preoperative detection of SN(s) located near the injection site [50]. However, surgical SN detection using PET tracers has not yet been well-documented. Limiting for the wide implementation of PET/CT or PET/MR, or even PET/CT/MR approaches during SN mapping are the costs associated with production of tracers and the availability of the tracer at the clinical site.

Overall, comparison studies between the different lymphoscintigraphic tracers are limited and mainly focus on the evaluation of different particle sizes (in an in vitro setting) [51,52]. Most SN mapping studies compare the radioguided approach with optical vital blue dye detection. As such it is, at the moment, difficult to state which of the above-mentioned radiocolloids is superior. That said, the current used radiocolloids have proven their value for preoperative SN mapping, suggesting all of them perform to the specific in-house standards required for high-end patient care.

VITAL BLUE DYES

Vital blue dyes can be optically detected by the surgeons' eye during the operation due to absorption of light in the visual wavelength. After intraoperative injection, such a dye allows the surgeon to meticulously track the blue lymphatic duct(s) running from the injection site. Afferent tracts running to the SN(s) can be distinguished from efferent tracts leading to higher-echelon nodes. Literature reports the use of various vital blue dyes such as indigo carmine [53], patent blue (V) [4,5,25,30,37,54-58], isosulfan blue [20,47,48], lymphazurin blue [42,59], and methylene blue [59] (Figure 1). These small dyes (mean diameter <<1 nm) migrate quickly through the lymphatic system, thereby staining the lymphatic tract(s) and the lymph node blue. Unfortunately this occurs without any form of active accumulation in the SNs. In contrast to the other vital blue dyes, methylene blue is thought to be actively taken up by (cancer) cells via targeting the mitochondrial membrane potential [60]. This suggests that cancer cells present in the lymph node(s) might actively take up methylene blue, hereby improving the detection of tumor containing SN(s).

FLUORESCENT TRACERS

Although the principle of their use is the same to that of vital blue dyes, fluorescent dyes can be detected with higher sensitivity. Excitation of a fluorescent dye leads to internal conversion resulting in the emission of photons of a different, longer, wavelength [61]. Every fluorescent dye has its own particular excitation and emission wavelength [35,62]. Fluorescent dyes emitting in the visual range (400-650 nm) can also be detected by eye, but generally detection is more sensitive when a dedicated fluorescence camera is used. Using dedicated band pass filters a light sensitive camera can be used to detect fluorescence signals (photons) in a manner similar to the way gamma-rays are detected. An example of fluorescence imaging in the visual range can be found in fluorescein imaging, which fluoresces in marker-pen-yellow. Clinically fluorescein is used for angiography of the eye

[63] and has been widely used as a fluorescent alternative for the conventional vital blue dyes for lymphatic mapping in e.g. non-small cell lung cancer and colorectal cancer [56,64]. However, the use of fluorescent dyes with an emission in the visible range remains limited to superficial applications, as the tissue penetration of such dyes very limited (mm range).

To improve detection of more deeply situated SNs the use of dyes that emit in the near-infrared range (750-100 nm) have been opted (tissue penetration <1 cm). The best-known example of a clinically applied near-infrared dye can be found in ICG. ICG has been used for vascular perfusion measurements and (lymph-)angiography [65,66]. Currently ICG is widely applied during SN biopsy procedures in, e.g. breast cancer, melanoma, and vulvar cancer [65,66].

Methylene blue can, alternatively to optical blue dye-based detection, also be used as a fluorescent dye. When used at very low concentrations, methylene blue emits in the far-red range (650-750 nm) and has been used for fluorescence-based ureter [67] and parathyroid gland [68] visualization. Logically the same concept can be applied during SN biopsy procedures [69].

Initially it was suggested that the superior signal penetration achieved with a near-infrared fluorescence dye might replace the need for the radiotracer. However, like the blue dyes, fluorescent dyes show a fast migration through the lymphatic system and do not accumulate in the SN. Furthermore, several studies showed that although fluorescence imaging allowed for intraoperative identification of the SN(s), the limited degree of tissue penetration did not allow accurate SN mapping prior to surgery.

HYBRID TRACERS

To take advantage of the excellent properties of radiotracers for preoperative SN mapping and the high detection sensitivity of (near-infrared) fluorescent dyes during the operation, recently hybrid tracers combining radioactivity and fluorescence in one tracer were introduced. A great number of preclinically evaluated tracers potentially suited for hybrid SN mapping have been summarized previously [36]. Although not approved for clinical use, some of these tracers show great potential. For instance, a study in mice showed the combined use of ^{99m}Tc-Tilmanocept labeled with the near-infrared fluorescence dye Cy7 [70]. Alternatively, fluoride-18 fluoxydeglucose (^{18}F-FDG) was shown to allow for SN mapping [71]. Next to β^+-emission, ^{18}F-FDG also emits Cerenkov signals which can be detected similar a fashion as fluorescence [71,72]. Iron-based nanoparticles can also be labeled with fluorescent dyes (and/or and even radiolabels) yielding an alternative class of hybrid SN tracers that are also suitable for MR imaging [73,74].

The hybrid tracer ICG-^{99m}Tc-nanocolloid is formed via non-covalent self-assembly of two well-known lymphatic tracers, namely ICG and ^{99m}Tc-nanocolloid. This self-assembly is driven by the interaction of the dye with e.g. fatty acid binding pockets on albumin. This interaction is not limited to nanocolloid alone, albumin-based colloids in general can be coupled to ICG in a similar manner [34,76]. Other studies have shown that that combining

ICG with the inorganic ^{99m}Tc-sulfur colloid was not feasible and yielded a significant decrease in signal intensity of the fluorescence dye [77]. Clinically, ICG-^{99m}Tc-nanocolloid has, to date, been the most widely used hybrid tracer for SN biopsy. After its introduction for SN biopsy of prostate cancer [75], its application in head-and-neck melanoma [25,37], oral cavity carcinoma [26], breast [57], penile [37], and vulvar [55] cancer was shown. In a recent comparison study it was shown that ICG-^{99m}Tc-nanocolloid shows a similar drainage pattern as its parental compound ^{99m}Tc-nanocolloid [37]. With this tracer it was shown that preoperative SN mapping could be combined with intraoperative radio- and fluorescence guidance to the SN via one single injection of tracer.

Iodization of the dye methylene blue resulted in the formation of iodine-125 (^{125}I)-methylene blue. This compound has been evaluated in a clinical setting during SN biopsy for breast cancer [78,79]. Here, ^{125}I-methylene blue was intraoperatively administrated either subareolarly or intratumorally allowing for radiotracing and optical blue dye detection of the intraoperatively identified SN.

Next to the above-mentioned radioactive and optical tracers for lymphatic mapping, X-ray contrast [80] and magnetic nanoparticles [81] have been opted. In addition to the development of tracers that aid the surgical identification of the SN as such to (histo-) pathologically determine the regional lymph node status, ongoing research focuses on developing a method to non-invasively determine the regional lymph node status. For example, ultrasmall supra-paramagnetic iron oxide particles have been proposed for lymphatic mapping. Here the obtained negative contrast is suspicious of the presence of lymph node metastasis [82]. (Tumor-targeted) PET tracers might also be used for the detection of lymph node metastasis. Contrast-enhanced ultrasound and the injection of microbubbles have also been proposed for SN mapping [83]. From a preclinical point of view, targeted dendrimers, liposomes and even viral particles have been proposed for (tumor-targeted) lymph node mapping [84].

HYBRID TRACERS IN CLINICAL LOGISTICS

Implementation of hybrid tracers into the clinical routine has been shown to be feasible [37]. In case of ICG-^{99m}Tc-nanocolloid tracer preparation is slightly altered compared to the use of radiocolloid only. ICG is added to the radiocolloid solution, which is then almost immediately ready for administration [37]. Consequently use of these tracers does not lead to important alterations in the preparation procedure.

While the clinical advantages of combining preoperative and intraoperative imaging are clear, slight alterations in the workflow have to be made to incorporate both visualization methods simultaneously. Based on the clinical logistics, in the following section, we discuss the challenges and additional possibilities that arise during different steps in the clinical process when using a hybrid tracer (Figure 2).

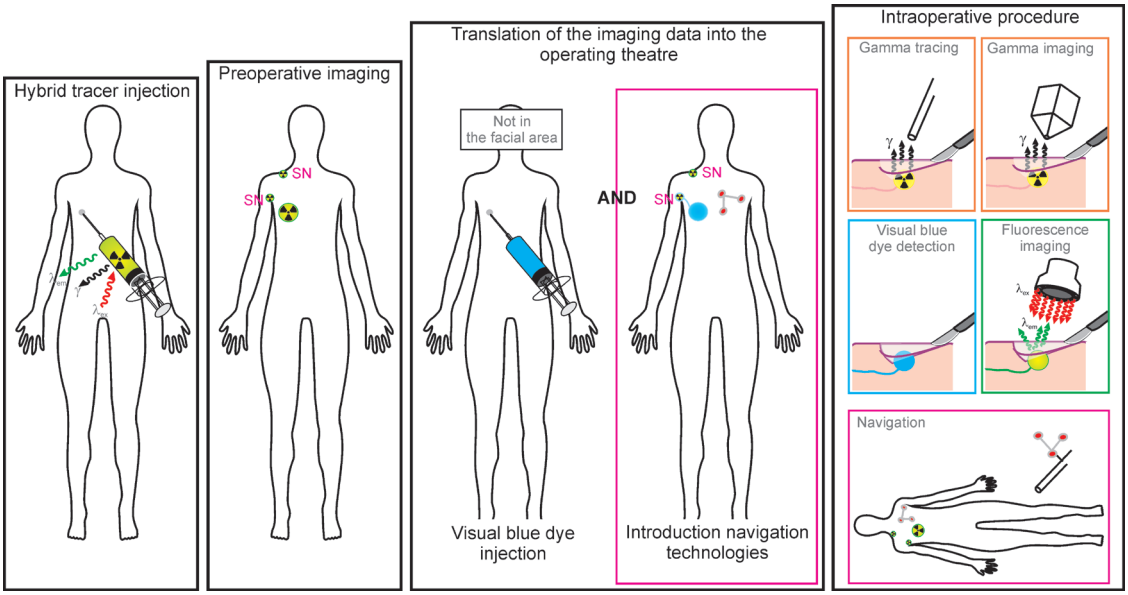

Figure 2. Schematic overview the concept of the use of hybrid tracers in a clinical setting. Following the injection of a hybrid tracer, preoperative lymphoscintigraphy and SPECT/CT imaging is performed to determine the number and anatomical location of the SN(s). An intraoperative injection with blue dye is given to allow for optical SN identification. Additionally, to improve the translation of preoperatively acquired imaging data into the operating theatre, navigation technologies can be introduced. Intraoperatively, a combination of gamma tracing, gamma imaging and fluorescence imaging and blue dye detection is used to identify the SNs. With the introduction of navigation technologies into the operating theatre, navigation of e.g. the gamma probe in the acquired SPECT images can allow for navigation-based identification of the SN(s). λem = emission wavelength of the fluorophore; λex = excitation wavelength of the fluorophore; γ = gamma signal coming from the radioisotope ICG = indocyanine green; SN = sentinel node.

TRACER INJECTION

In line with the SN concept, tracer administration must be related to the site of the tumor. Since the drainage pattern of the various lymphoscintigraphic tracers is dictated by the lymphatic anatomy present at the injection site, the location of tracer deposition is of great influence on the observed drainage pattern and the identification of the SN(s). Multiple injections are administrated around the tumor or excision scar in melanoma or cancer of the genitalia. For breast cancer, there is somewhat of a controversy and injection strategies may differ. Some prefer tumor-related (peritumoral or intratumoral) injections, whereas others prefer injections related to the skin (subdermal or intradermal) or aureolar (subaureolar or periaureolar). The concept here is that a periaureolar or other superficial injections will mainly help visualize only axillary lymphatic drainage [85]. In contrast, an intra- or peritumoral injection not only leads to axillary lymphatic drainage, but often

results in the visualization of drainage outside the axilla to locations such as the intramammary, periscapular or even parasternal regions. Hence, the periaureolar tracer administration approach may not accurately represent the drainage pattern of the tumor. A recent Multisent study, in patients with multifocal and multicentric breast cancer, underlined that each individual breast tumor can have its own specific drainage pattern [54]. Following the identification of the SNs draining from the largest tumor in the breast, additional drainage from the second or third injected tumor was identified in 64% of patients. In 56% of these patients, SNs found after this second/third injection were localized in different basins than those identified after the first injection. In two patients, isolated tumor cells were found in SNs that were only visualized after the second tumor had been injected [54]. For this study, the second/third injection was given 4-26 h after the injection in the largest tumor as such allowing for preoperative discrimination of the SNs from the different tumors. To improve these logistics, here hybrid tracers, in combination with the conventional radiocolloids can possibly be used to assess these multifocal and multicentric tumors via an injection protocol in which the different tumors are injected simultaneously with either the radiocolloid (largest tumor) or with the hybrid tracer (second/third tumor). The presence of fluorescence in the SNs during surgery can then be used to discriminate the different drainage pattern of these tumors.

When performing SN biopsy of e.g. for kidney or prostate cancer, but also for (non-palpable) breast cancer, tracer administration can be more challenging. For breast cancer, (non-palpable) tumors are generally injected under ultrasound or stereotaxic guidance. Tracer injections for abdominal tumors are generally performed under transrectal or endoscopic ultrasound guidance. Commonly an intratumoral injection, or an injection in the area most likely to contain tumor, is aimed for. Limiting in the injection accuracy is the availability of tumor specific needle navigation technologies.

The use of a hybrid tracer does not affect the manner of tracer injection. Like radiotracers, hybrid tracers can be used to assess the accuracy of tracer injection using the radioactive signature. By placing a handheld or portable gamma camera over the site of injection, deposition of the tracer can be checked for [75], and possible leakage into the bloodstream or bladder can be evaluated.

Where the radioactive component of hybrid tracers can be used during pre- and intraoperative imaging, the fluorescent component can also be exploited during ex vivo evaluation of the excised tissue [26, 86]. Not only can the distribution of the tracer in the SN be evaluated, assessment of the relation between the injection site and the corresponding drainage pattern can be used to improve the injection procedure. Assessment of the correlation between the location of the tracer deposits in excised prostate samples and the number and location of the preoperatively visualized SNs suggested that the location at which the tracer is deposited influences the lymphatic drainage pattern [86]. As such we reason that a more tumor directed tracer administration will likely result in improved identification of the true tumor draining lymph node(s) for that specific type of cancer.

PREOPERATIVE SENTINEL NODE MAPPING

Preoperatively, hybrid tracers can be used in an identical manner as the conventional radiotracers are used. Preoperative SN mapping is generally performed by acquisition of dynamic lymphoscintigrams immediately after tracer injection followed by static anterior, lateral and/or posterior lymphoscintigrams. Combined evaluation of these images allows identification of the SN(s) and higher-echelon nodes. With the introduction of SPECT/CT localization of these hot spots within their anatomical context became feasible [24]. This supplementary three-dimensional (3D) information allows the surgeon to plan his/her approach before the start of the operation. SPECT/CT imaging was found to be of particular value for the identification of SNs localized in areas with a complex anatomy and close to the injection site. Moreover, with SPECT/CT being more sensitive that conventional lymphoscintigraphy, non-visualization on planar lymphoscintigraphy can yield a SN when performing SPECT/CT imaging [58]. Additionally, SPECT/CT allows the identification of additional SNs not seen on lymphoscintigrams [58].

The improved resolution and sensitivity of PET/CT may provide a valuable alternative for SPECT/CT, and may allow for more clear identification of SNs located near the injection site [50]. However, a full dynamic procedure that also allows the identification of the lymphatic tract(s) running to the SN is, similar to lymphoscintigraphy, is still lacking for PET tracers.

The use of a handheld or portable gamma cameras can also be used for preoperative SN mapping. With their improved resolution compared that of conventional lymphoscintigraphy, and the ability to position the gamma camera closely to the skin of the patient, this might allow for the identification of near-injection site SNs [87] (an overview of available handheld and portable gamma cameras is given in [88]).

INTRAOPERATIVE IMAGING AND TRANSLATION OF PREOPERATIVE IMAGING INTO THE OPERATING THEATRE

Conform the standard procedure, projection of the data generated at nuclear medicine in the operating theatre, either on-screen [25,26,37,55,75], on an iPad [89] or loading these data into the da Vinci robot during robot-assisted laparoscopic procedures [90,91] can provide the surgeons with feedback regarding the location of the SN during the operation. The most simple way to guide a surgeon to the radioactive hot spots in the patient is probably gamma tracing using a collimator-based gamma probe. The introduction of portable gamma camera technologies into the operating theatre provided surgeons with the ability to generate a pre-incision image of the location of the radioactive hot spots. In a similar fashion this approach was also found to be of value to confirm the removal of the SNs. For example, in six patients with head-and-neck malignancies, with the portable gamma camera nine additional SNs were identified in the wound area after the initial SN had been excised. One of these additionally excised SNs was found to be tumor-positive [92].

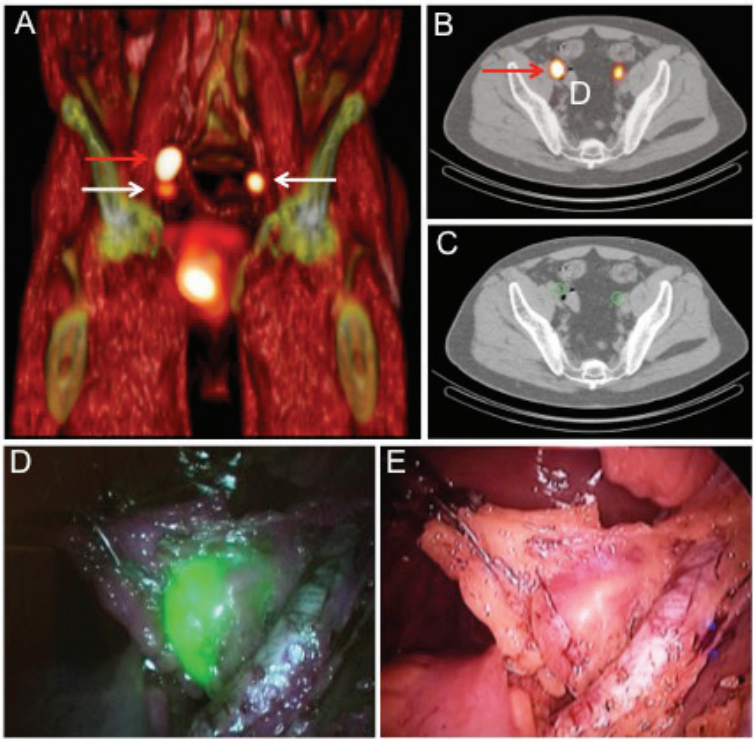

Figure 3. Implementation of the hybrid tracer during robot-assisted laparoscopic sentinel node biopsy of prostate cancer. A) 3D volume rendering of fused SPECT and CT images showing three SNs (arrows); B) axial fused SPECT and CT image showing the location of the most right cranial hot spot in the external iliac area (red arrow). C) Corresponding CT slide; D) Fluorescence imaging of the right most cranial SN using the fluorescence laparoscope from KARL STORZ Endoskope GmbH & Co. KG (Image 1 HUB HD); E) Corresponding white light image of the SN. 3D = three-dimentional; SPECT = single photon emission computed tomography; CT = computed tomography; SN = sentinel node.

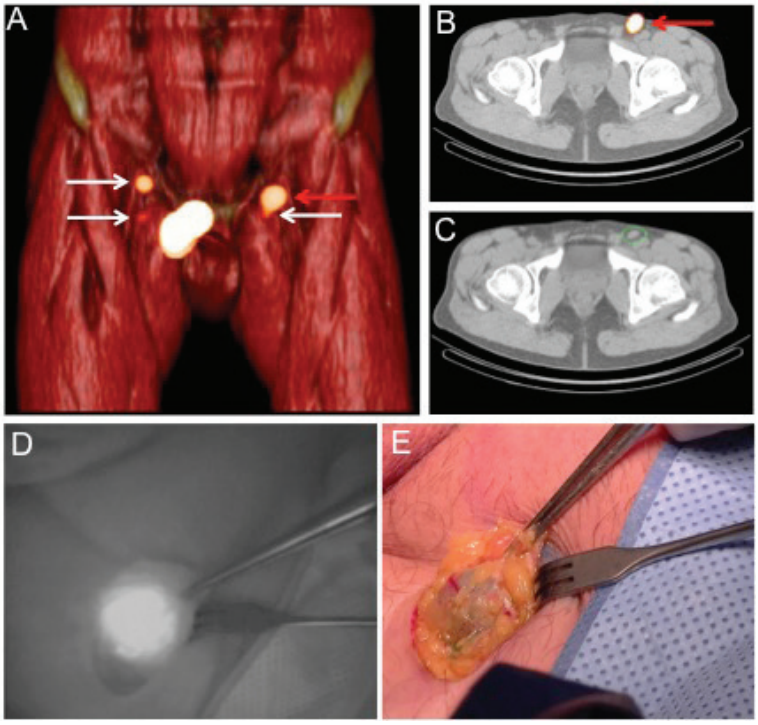

Figure 4. Implementation of the hybrid tracer during SN biopsy for penile cancer. A) 3D volume rendering of fused SPECT and CT images showing 4 of the 5 preoperatively defined SNs (arrows); B) Axial fused SPECT and CT image showing the location of the most left cranial hot spot in the inguinal zone (red arrow); C) Corresponding CT slide; D) Fluorescence imaging of the right most cranial SN using the handheld fluorescence camera from Hamamatsu Photonics K.K. (PhotoDynamic Eye); E) Corresponding white light image of the SN. This SN was found to be slightly blue. 3D = three-dimentional; SPECT = single photon emission computed tomography; CT = computed tomography; SN = sentinel node.

Radioguidance might be hampered with an increased time between injection and the start of surgery, or with SNs being located near the injection site due to signal bleeding. Hybrid tracers such as ICG-^{99m}Tc-nanocolloid enable intraoperative surgical visualization of the preoperatively identified SNs using a dedicated near-infrared fluorescence camera (Figures 3, 4). With the fluorescence signal remaining stable over time, providing its not being exposed to an excess of light, and the limited penetration depth of the fluorescence signal in comparison to that of the radioactive signal, the fluorescence signature of the hybrid tracer can overcome these hurdles. Especially in areas where no vital blue dye is used, in areas with a complex anatomy or in areas with near-injection site SNs, the value of fluorescence imaging was found to be prominent [25,26,75]. In addition, the SN identification rate via the fluorescent signature of the hybrid tracer was found to be superior to that achieved with vital blue dye alone. For example, in vulvar carcinoma intraoperatively 96% of SNs could be visualized with fluorescence imaging whereas only 65% of these nodes were stained blue [55].

Obviously, the implementation of additional visualization methods into the clinical routine affects the surgical workflow. Depending on the type of (handheld) fluorescence camera used in open surgical procedures, the light in the operating theatre needs to be dimmed when fluorescence imaging is initiated to allow for better contrast between the signal in the SN and the background; the light used in the operating theatre contain a fair amount of near-infrared light and the intensity of this light will prohibit the identification of the SN via fluorescence imaging. During laparoscopic procedures, this is not a requirement. This feature is not related to the use of hybrid imaging agents, but to intraoperative fluorescence imaging in general. Improvements of currently available (laparoscopic) camera systems might partially overcome this [35].

In our experience implementation of an additional imaging modality, such as an fluorescence camera, can lead to improved intraoperative detection of the SN. After an initial adjustment period and proper training of surgeons and scrub-nurses, combined radiotracing and intraoperative fluorescence imaging can be fully adopted into the existing surgical routine.

FUTURE APPLICATIONS: INTRODUCTION OF NAVIGATION TECHNOLOGIES INTO THE CLINIC

The introduction of intraoperative navigation can further aid the translation of diagnostic (nuclear medicine-derived) information in the operating theatre. Very simple, for SN biopsy of prostate cancer, the use of a portable gamma camera in combination with real-time on-screen tracking of an ^{125}I-seed placed on a laparoscopic gamma probe was shown to result in two-dimensional navigation to SN(s) [93].

To further improve the intraoperative detection accuracy of the preoperatively defined SN(s), the concept of intraoperative freehandSPECT was introduced by Wendler et al. [94] and implemented firstly in the clinic in 2010 in patients with breast cancer [95]. With this approach, real-time scanning of an area of interest with a gamma probe enables the generation of an intraoperative 3D SPECT scan. Similar to portable gamma cameras, the generation of this intraoperative freehandSPECT scan allows planning of the excision of the SN(s) whereas post-excision scanning of the same area allows confirmation of removal of the SN(s). In addition, the surgeon can navigate the gamma probe, in augmented-reality, in this 3D SPECT scan to the lesion of interest thereby possibly "easing" its identification. Recently this approach was also shown to be feasible for oral cavity carcinoma [96] and melanoma [97].

More recently, navigation based on reference targets in combination with preoperatively acquired nuclear medicine or radiology data was shown [98]. The accuracy of this technology strongly depends on the accuracy with which the preoperative situation can be reproduced; organ movement or deformation due to e.g. patient position changes limit the accuracy [99,100]. These movements are difficult to correct for with internal or external navigation aids, as placement of these aids can also cause additional placement errors [99,100]. The combination of navigation with a real-time imaging technology, e.g. fluorescence imaging, that can determine the navigation accuracy helps the surgeon to correct for errors. In a recent study by Brouwer et al. the feasibility of this approach was shown using ICG-^{99m}Tc-nanocolloid [58]. During preoperative SPECT/CT imaging, a reference target was placed on the patient' body. Repositioning of a sterile reference target on the exact same location on the patient' body in the operating theater allowed a mixed-reality integration of the preoperatively acquired SPECT/CT scan and a visual image of the patient lying on the operating table. Tracking of the fluorescence laparoscope (Image 1 HUB HD; KARL STORZ Endoskope GmbH & Co. KG, Tuttlingen, Germany) allowed reality 3D SPECT/CT-based navigation of this surgical tool. With decreasing distance towards the prostate, the fluorescence signal increased. Hence fluorescence imaging could be used to compensate for errors created due to patient positioning [98].

CONCLUSION

There lies great promise in combining lymphoscintigraphic agents and fluorescent agents for SN mapping. The introduction of hybrid tracers, in which fluorescence dyes and radiotracers are combined, allows for both intraoperative radio- and fluorescence guidance to the SN via one single injection of tracer whereas the protocol of preoperative SN mapping using lymphoscintigraphy and SPECT/CT imaging remains unmodified. The incorporation of fluorescence imaging into the daily used radioguidance technologies opens a whole new line of research.

REFERENCES

1. Ahuja AT, Ying M, Ho SY, Antonio G, Lee YP, King AD et al. Ultrasound of malignant cervical lymph node (s). Cancer Imaging. 2008;8:48-56.
2. Nieweg OE, Tanis PJ, Kroon BB. The definition of a sentinel node. Ann Surg Oncol. 2001;8:538-41.
3. Broglie MA, Stoeckli SJ. Relevance of sentinel node procedures in head and neck squamous cell carcinoma. Q J Nucl Med Mol Imaging. 2011;55:509-20.
4. Horenblas S, Jansen L, Meinhardt W, Hoefnagel CA, de Jong D, Nieweg OE. Detection of occult metastasis in squamous cell carcinoma of the penis using a dynamic sentinel node procedure. J Urol. 2000;163:100-4.
5. Van der Zee AG, Oonk MH, De Hullu JA, Ansink AC, Vergote I, Verheijen RH et al. Sentinel node dissection is safe in the treatment of early-stage vulvar cancer. J Clin Oncol. 2008;26:884-9.
6. Lyman GH, Giuliano AE, Somerfield MR, Benson AB, 3rd, Bodurka DC, Burstein HJ et al. American Society of Clinical Oncology guideline recommendations for sentinel lymph node biopsy in early-stage breast cancer. J Clin Oncol. 2005;23:7703-20.
7. Morton DL, Thompson JF, Cochran AJ, Mozzillo N, Elashoff R, Essner R et al. Sentinel-node biopsy or nodal observation in melanoma. New Engl J Med. 2006;355:1307-17.
8. Sadeghi R, Gholami H, Zakavi SR, Kakhki VR, Tabasi KT, Horenblas S. Accuracy of sentinel lymph node biopsy for inguinal lymph node staging of penile squamous cell carcinoma: systematic review and meta-analysis of the literature. J Urol. 2012;187:25-31.
9. Hassanzade M, Attaran M, Treglia G, Yousefi Z, Sadeghi R. Lymphatic mapping and sentinel node biopsy in squamous cell carcinoma of the vulva: systematic review and meta-analysis of the literature. Gynecol Oncol. 2013;130:237-45.
10. Alkureishi LW, Ross GL, Shoaib T, Soutar DS, Robertson AG, Thompson R et al. Sentinel node biopsy in head and neck squamous cell cancer: 5-year follow-up of a European multicenter trial. Ann Surg Oncol. 2010;17:2459-64.
11. Meinhardt W, van der Poel HG, Valdes Olmos RA, Bex A, Brouwer OR, Horenblas S. Laparoscopic sentinel lymph node biopsy for prostate cancer: the relevance of locations outside the extended dissection area. Prostate Cancer. 2012;2012:751-3.
12. Rousseau C, Rousseau T, Bridji B, Pallardy A, Lacoste J, Campion L et al. Laparoscopic sentinel lymph node (SLN) versus extensive pelvic dissection for clinically localized prostate carcinoma. Eur J Nucl Med Mol Imaging. 2012;39:291-9.
13. Jeschke S, Beri A, Grull M, Ziegerhofer J, Prammer P, Leeb K et al. Laparoscopic radioisotope-guided sentinel lymph node dissection in staging of prostate cancer. Eur Urol. 2008;53:126-32.
14. Brouwer OR, Valdes Olmos RA, Vermeeren L, Hoefnagel CA, Nieweg OE, Horenblas S. SPECT/CT and a portable gamma-camera for image-guided laparoscopic sentinel node biopsy in testicular cancer. J Nucl Med. 2011;52:551-4.
15. Tanis PJ, Horenblas S, Valdes Olmos RA, Hoefnagel CA, Nieweg OE. Feasibility of sentinel

node lymphoscintigraphy in stage I testicular cancer. Eur J Nucl Med Mol Imaging. 2002;29:670-3.
16. Liedberg F, Chebil G, Davidsson T, Gudjonsson S, Mansson W. Intraoperative sentinel node detection improves nodal staging in invasive bladder cancer. J Urol. 2006;175:84-8.
17. Bex A, Vermeeren L, Meinhardt W, Prevoo W, Horenblas S, Valdes Olmos RA. Intraoperative sentinel node identification and sampling in clinically node-negative renal cell carcinoma: initial experience in 20 patients. World J Urol. 2011;29:793-9.
18. Sherif AM, Eriksson E, Thorn M, Vasko J, Riklund K, Ohberg L et al. Sentinel node detection in renal cell carcinoma. A feasibility study for detection of tumour-draining lymph node (s). BJU Int. 2012;109:1134-9.
19. Nomori H, Kohno M, Izumi Y, Ohtsuka T, Asakura K, Nakayama T. Sentinel nodes in lung cancer: review of our 10-year experience. Surg Today. 2011;41:889-95.
20. Kitagawa Y, Takeuchi H, Takagi Y, Natsugoe S, Terashima M, Murakami N et al. Sentinel node mapping for gastric cancer: a prospective multicenter trial in Japan. J Clin Oncol. 2013; 31:3704-10.
21. van der Pas MH, Meijer S, Hoekstra OS, Riphagen II, de Vet HC, Knol DL et al. Sentinel-lymph-node procedure in colon and rectal cancer: a systematic review and meta-analysis. Lanet Oncol. 2011;12:540-50.
22. van der Zaag ES, Bouma WH, Tanis PJ, Ubbink DT, Bemelman WA, Buskens CJ. Systematic review of sentinel lymph node mapping procedure in colorectal cancer. Ann Surg Oncol. 2012;19:3449-59.
23. Mariani G, Bruselli L, Kuwert T, Kim EE, Flotats A, Israel O et al. A review on the clinical uses of SPECT/CT. Eur J Nucl Med Mol Imaging. 2010;37:1959-85.
24. Olmos RA, Vidal-Sicart S, Nieweg OE. SPECT-CT and real-time intraoperative imaging: new tools for sentinel node localization and radioguided surgery? Eur J Nucl Med Mol Imaging. 2009;36:1-5.
25. Brouwer OR, Klop WM, Buckle T, Vermeeren L, van den Brekel MW, Balm AJ et al. Feasibility of sentinel node biopsy in head and neck melanoma using a hybrid radioactive and fluorescent tracer. Ann Surg Oncol. 2012;19:1988-94.
26. van den Berg NS, Brouwer OR, Klop WM, Karakullukcu B, Zuur CL, Tan IB et al. Concomitant radio- and fluorescence-guided sentinel lymph node biopsy in squamous cell carcinoma of the oral cavity using ICG-(^{99m})Tc-nanocolloid. Eur J Nucl Med Mol Imaging. 2012;39:1128-36.
27. Rietbergen DD, van den Berg NS, van Leeuwen FW, Valdes Olmos R. Hybrid techniques for intraoperative sentinel lymph node imaging: early experiences and future prospects. Future Medicine. 2013;5:147-59.
28. Mariani G, Erba P, Manca G, Villa G, Gipponi M, Boni G et al. Radioguided sentinel lymph node biopsy in patients with malignant cutaneous melanoma: the nuclear medicine contribution. J Surg Oncol. 2004;85:141-51.
29. Mariani G, Erba P, Villa G, Gipponi M, Manca G, Boni G et al. Lymphoscintigraphic and

intraoperative detection of the sentinel lymph node in breast cancer patients: the nuclear medicine perspective. J Surg Oncol. 2004;85:112-22.
30. Jansen L, Doting MH, Rutgers EJ, de Vries J, Olmos RA, Nieweg OE. Clinical relevance of sentinel lymph node(s) outside the axilla in patients with breast cancer. Br J Surg. 2000;87:920-5.
31. Kuriakose MA, Trivedi NP. Sentinel node biopsy in head and neck squamous cell carcinoma. Curr Opin Otolaryngol Head Neck Surg. 2009;17:100-10.
32. Egawa M, Fukuda M, Takashima H, Misaki T, Kinuya K, Terahata S. The sentinel node concept in prostate cancer: Present reality and future prospects. Indian J Urol. 2008;24:451-6.
33. Vahrmeijer AL, Frangioni JV. Seeing the invisible during surgery. Br J Surg. 2011;98:749-50.
34. van Leeuwen AC, Buckle T, Bendle G, Vermeeren L, Valdes Olmos R, van de Poel HG et al. Tracer-cocktail injections for combined pre- and intraoperative multimodal imaging of lymph node(s) in a spontaneous mouse prostate tumor model. J Biomed Opt. 2011;16:016004.
35. van den Berg NS, van Leeuwen FW, van der Poel HG. Fluorescence guidance in urologic surgery. Curr Opin Urol. 2012;22:109-20.
36. Buckle T, Chin PT, van Leeuwen FW. (Non-targeted) radioactive/fluorescent nanoparticles and their potential in combined pre- and intraoperative imaging during sentinel lymph node resection. Nanotechnology. 2010;21:482001.
37. Brouwer OR, Buckle T, Vermeeren L, Klop WM, Balm AJ, van der Poel HG et al. Comparing the hybrid fluorescent-radioactive tracer indocyanine green-^{99m}Tc-nanocolloid with ^{99m}Tc-nanocolloid for sentinel node identification: a validation study using lymphoscintigraphy and SPECT/CT. J Nucl Med. 2012;53:1034-40.
38. Uren RF. Lymphatic drainage of the skin. Ann Surg Oncol. 2004;11:179S-85S.
39. Ege GN. Internal mammary lymphoscintigraphy. The rationale, technique, interpretation and clinical application: a review based on 848 cases. Radiology. 1976;118:101-7.
40. Henze E, Schelbert HR, Collins JD, Najafi A, Barrio JR, Bennett LR. Lymphoscintigraphy with Tc-99m-labeled dextran. J Nucl Med. 1982;23:923-9.
41. Higashi H, Natsugoe S, Uenosono Y, Ehi K, Arigami T, Nakabeppu Y et al. Particle size of tin and phytate colloid in sentinel node identification. J Surg Research. 2004;121:1-4.
42. Mirzaei S, Rodrigues M, Hoffmann B, Knoll P, Riegler-Keil M, Kreuzer W et al. Sentinel lymph node detection with large human serum albumin colloid particles in breast cancer. Eur J Nucl Med Mol Imaging. 2003;30:874-8.
43. Li S, Nguyen L, Xion H, Wang M, Hu TC-C, She J-X et al. Nanocarriers for biomedical applications. J S C Aca Sci. 2011;9:30-2.
44. Reasbeck PG, Manktelow A, McArthur AM, Packer SG, Berkeley BB. An evaluation of pelvic lymphoscintigraphy in the staging of colorectal carcinoma. Br J Surg. 1984;71:936-40.
45. Xavier NL, Amaral BB, Cerski CT, Fuchs SC, Spiro BL, Oliveira OL et al. Sentinel lymph

node identification and sampling in women with early breast cancer using 99m-Tc labelled dextran 500 and patent blue V dye. Nucl Med Comm. 2001;22:1109-17.
46. Marcinow AM, Hall N, Byrum E, Teknos TN, Old MO, Agraw-al A. Use of a Novel Receptor-Targeted (CD206) Radiotracer, ^{99m}Tc-Tilmanocept, and SPECT/CT for Sentinel Lymph node Detection in Oral Cavity Squamous Cell Carcinoma: Initial Institutional Report in an Ongoing Phase 3 Study. JAMA Otolaryngol Head Neck Surg. 2013;139:895-902.
47. Sondak VK, King DW, Zager JS, Schneebaum S, Kim J, Leong SP et al. Combined analysis of phase III trials evaluating [(9)(9)mTc]tilmanocept and vital blue dye for identification of sentinel lymph node (s) in clinically node-negative cutaneous melanoma. Ann Surg Oncol. 2013;20:680-8.
48. Wallace AM, Han LK, Povoski SP, Deck K, Schneebaum S, Hall NC et al. Comparative evaluation of [(99m)tc] tilmanocept for sentinel lymph node mapping in breast cancer patients: results of two phase 3 trials. Ann Surg Oncol. 2013;20:2590-9.
49. Vera DR, Wallace AM, Hoh CK, Mattrey RF. A synthetic macromolecule for sentinel node detection: (99m)Tc-DTPA-mannosyl-dextran. J Nucl Med. 2001;42:951-9.
50. Heuveling DA, van Schie A, Vugts DJ, Hendrikse NH, Yaqub M, Hoekstra OS et al. Pilot study on the feasibility of PET/CT lymphoscintigraphy with 89Zr-nanocolloidal albumin for sentinel node identification in oral cancer patients. J Nucl Med. 2013;54:585-9.
51. Jankovic D, Maksin T, Djokic D, Milonjic S, Nikolic N, Mirkovic M et al. Particle size analysis: 90Y and ^{99m}Tc-labelled colloids. J Microsc. 2008;232:601-4.
52. Tsopelas C. Particle size analysis of (^{99m})Tc-labeled and unlabeled antimony trisulfide and rhenium sulfide colloids intended for lymphoscintigraphic application. J Nucl Med. 2001;42:460-6.
53. Uhara H, Yamazaki N, Takata M, Inoue Y, Sakakibara A, Nakamura Y et al. Applicability of radiocolloids, blue dyes and fluorescent indocyanine green to sentinel node biopsy in melanoma. J Dermatol. 2012;39:336-8.
54. Brouwer OR, Vermeeren L, van der Ploeg IM, Valdes Olmos RA, Loo CE, Pereira-Bouda LM et al. Lymphoscintigraphy and SPECT/CT in multicentric and multifocal breast cancer: does each tumour have a separate drainage pattern? Results of a Dutch multicentre study (MULTISENT). Eur J Nucl Med Mol Imaging. 2012;39:1137-43.
55. Matheron HM, van den Berg NS, Brouwer OR, Kleinjan GH, van Driel WJ, Trum JW et al. Multimodal surgical guidance towards the sentinel node in vulvar cancer. Gynecol Oncol. 2013;131:720-5.
56. Meyer A, Cheng C, Antonescu C, Pezzetta E, Bischof-Delaloye A, Ris HB. Successful migration of three tracers without identification of sentinel nodes during intraoperative lymphatic mapping for non-small cell lung cancer. Interact Cardiovasc Thorac Surg. 2007;6:214-8.
57. Schaafsma BE, Verbeek FP, Rietbergen DD, van der Hiel B, van der Vorst JR, Liefers GJ et al. Clinical trial of combined radio- and fluorescence-guided sentinel lymph node biopsy in breast cancer. Br J Surg. 2013;100:1037-44.

58. van der Ploeg IM, Valdes Olmos RA, Kroon BB, Nieweg OE. The Hybrid SPECT/CT as an additional lymphatic mapping tool in patients with breast cancer. World J Surg. 2008;32:1930-4.
59. Liu Y, Truini C, Ariyan S. A randomized study comparing the effectiveness of methylene blue dye with lymphazurin blue dye in sentinel lymph node biopsy for the treatment of cutaneous melanoma. Ann Surg Oncol. 2008;15:2412-7.
60. Eckert GP, Renner K, Eckert SH, Eckmann J, Hagl S, Abdel-Kader RM et al. Mitochondrial dysfunction a pharmacological target in Alzheimer's disease. Mol Neurobiol. 2012;46:136-50.
61. Ruggi A, van Leeuwen FW, Velders AH. Interaction of dioxygen with the electronic excited state of Ir(III) and Ru(II) complexes: Principles and biomedical applications. Coord Chem Rev. 2011;255:2542-54.
62. Yuan L, Lin W, Zheng K, He L, Huang W. Far-red to near infrared analyte-responsive fluorescent probes based on organic fluorophore platforms for fluorescence imaging. Chem Soc Rev. 2013;42:622-61.
63. Spaide RF. Peripheral areas of nonperfusion in treated central retinal vein occlusion as imaged by wide-field fluorescein angiography. Retina. 2011;31:829-37.
64. Dan AG, Saha S, Monson KM, Wiese D, Schochet E, Barber KR et al. 1% lymphazurin vs. 10% fluorescein for sentinel node mapping in colorectal tumors. Arch Surg. 2004;139:1180-4.
65. Polom K, Murawa D, Rho YS, Nowaczyk P, Hunerbein M, M rawa P. Current trends and emerging future of indocyanine green usage in surgery and oncology: a literature review. Cancer. 2011;117:4812-22.
66. Schaafsma BE, Mieog JS, Hutteman M, van der Vorst JR, Kuppen PJ, Lowik CW et al. The clinical use of indocyanine green as a near-infrared fluorescent contrast agent for image-guided oncologic surgery. J Surg Oncol. 2011;104:323-32.
67. Verbeek FP, van der Vorst JR, Schaafsma BE, Swijnenburg RJ, Gaarenstroom KN, Elzevier HW et al. Intraoperative near infrared fluorescence guided identification of the ureters using low dose methylene blue: a first in human experience. J Urol. 2013;190:574-9.
68. van der Vorst JR, Schaafsma BE, Verbeek FP, Swijnenburg RJ, Tummers Q, Hutteman M et al. Intraoperative near-infrared fluorescence imaging of parathyroid adenomas using low-dose methylene blue. Head Neck. 2014;36:853-8.
69. Chu M, Wan Y. Sentinel lymph node mapping using near-infrared fluorescent methylene blue. J Biosci Bioeng. 2009;107:455-9.
70. Emerson DK, Limmer KK, Hall DJ, Han SH, Eckelman WC, Kane CJ et al. A receptor-targeted fluorescent radiopharmaceutical for multireporter sentinel lymph node imaging. Radiology. 2012;265:186-93.
71. Thorek DL, Abou DS, Beattie BJ, Bartlett RM, Huang R, Zanzonico PB et al. Positron lymphography: multimodal, high-resolution, dynamic mapping and resection of lymph node (s) after intradermal injection of 18F-FDG. J Nucl Med. 2012;53:1438-45.
72. Chin PT, Welling MM, Meskers SC, Valdes Olmos RA, Tanke H, van Leeuwen FW. Optical

imaging as an expansion of nuclear medicine: Cerenkov-based luminescence vs fluorescence-based luminescence. Eur J Nucl Med Mol Imaging. 2013;40:1283-91.
73. Zhou Z, Chen H, Lipowska M, Wang L, Yu Q, Yang X et al. A dual-modal magnetic nanoparticle probe for preoperative and intraoperative mapping of sentinel lymph node(s) by magnetic resonance and near infrared fluorescence imaging. J Biomater Appl. 2013;28:100-11.
74. Ma Y, Tong S, Bao G, Gao C, Dai Z. Indocyanine green loaded SPIO nanoparticles with phospholipid-PEG coating for dual-modal imaging and photothermal therapy. Biomaterials. 2013;34:7706-14.
75. van der Poel HG, Buckle T, Brouwer OR, Valdes Olmos RA, van Leeuwen FW. Intraoperative laparoscopic fluorescence guidance to the sentinel lymph node in prostate cancer patients: clinical proof of concept of an integrated functional imaging approach using a multimodal tracer. Eur Urol. 2011;60:826-33.
76. Ohnishi S, Lomnes SJ, Laurence RG, Gogbashian A, Mariani G, Frangioni JV. Organic alternatives to quantum dots for intraoperative near-infrared fluorescent sentinel lymph node mapping. Mol Imaging. 2005;4:172-81.
77. Sevick-Muraca EM, Sharma R, Rasmussen JC, Marshall MV, Wendt JA, Pham HQ et al. Imaging of lymph flow in breast cancer patients after microdose administration of a near-infrared fluorophore: feasibility study. Radiology. 2008;246:734-41.
78. Cundiff JD, Wang YZ, Espenan G, Maloney T, Camp A, Lazarus L et al. A phase I/II trial of 125I methylene blue for one-stage sentinel lymph node biopsy. Ann Surg. 2007;245:290-6.
79. Harkrider WW, Diebold AE, Maloney T, Espenan G, Wang YZ, Stafford SJ et al. An extended phase II trial of iodine-125 methylene blue for sentinel lymph node identification in women with breast cancer. J Am Coll Surg. 2013;216:599-605.
80. Riveros M, Garcia R, Cabanas R. Lymphadenography of the dorsal lymphatics of the penis. Technique and results. Cancer. 1967;20:2026-31.
81. Ahmed M, Douek M. The role of magnetic nanoparticles in the localization and treatment of breast cancer. Biomed Res Int. 2013;2013:281-230.
82. Heesakkers RA, Hovels AM, Jager GJ, van den Bosch HC, Witjes JA, Raat HP et al. MRI with a lymph-node-specific contrast agent as an alternative to CT scan and lymph-node dissection in patients with prostate cancer: a prospective multicohort study. Lancet Oncol. 2008;9:850-6.
83. Sever AR, Mills P, Jones SE, Mali W, Jones PA. Sentinel node identification using microbubbles and contrast-enhanced ultrasonography. Clin Radiology. 2012;67:687-94.
84. Jain R, Dandekar P, Patravale V. Diagnostic nanocarriers for sentinel lymph node imaging. J Control Release.2009;138:90-102.
85. Alazraki NP, Styblo T, Grant SF, Cohen C, Larsen T, Aarsvold JN. Sentinel node staging of early breast cancer using lymphoscintigraphy and the intraoperative gamma-detecting probe. Semin Nucl Med. 2000;30:56-64.
86. Buckle T, Brouwer OR, Valdes Olmos RA, van der Poel HG, van Leeuwen FW. Relationship

between intraprostatic tracer deposits and sentinel lymph node mapping in prostate cancer patients. J Nucl Med. 2012;53:1026-33.
87. Vidal-Sicart S, Brouwer OR, Matheron HM, Bing Tan I, Valdes-Olmos RA. Sentinel node identification with a portable gamma camera in a case without visualization on conventional lymphoscintigraphy and SPECT/CT. Rev Esp Med Nucl Imagen Mol. 2013;32:203-4.
88. Valdes Olmos R, Vidal-Sicart S, Giammarile F, Zaknum JJ, van Leeuwen FW, Mariani G. The GOSST concept and hybrid mixed/virtual/augmented reality environment radioguided surgery. Q J Nucl Med Mol Imaging. 2014;58:207-15.
89. Rassweiler JJ, Muller M, Fangerau M, Klein J, Goezen AS, Pereira P et al. iPad-assisted percutaneous access to the kidney using marker-based navigation: initial clinical experience. Eur Urol. 2012;61:628-31.
90. Volonte F, Buchs NC, Pugin F, Spaltenstein J, Schiltz B, Jung M et al. Augmented reality to the rescue of the minimally invasive surgeon. The usefulness of the interposition of stereoscopic images in the Da Vinci robotic console. Int J Med Robot. 2013;9:e34-8.
91. Volonte F, Pugin F, Buchs NC, Spaltenstein J, Hagen M, Ratib O et al. Console-integrated stereoscopic OsiriX 3D volume-rendered images for da Vinci colorectal robotic surgery. Surg Innov. 2013;20:158-63.
92. Vermeeren L, Klop WM, van den Brekel MW, Balm AJ, Nieweg OE, Valdes Olmos RA. Sentinel node detection in head and neck malignancies: innovations in radioguided surgery. J Oncol. 2009;2009:681746.
93. Vermeeren L, Meinhardt W, Bex A, van der Poel HG, Vogel WV, Hoefnagel CA et al. Paraaortic sentinel lymph node(s): toward optimal detection and intraoperative localization using SPECT/CT and intraoperative real-time imaging. J Nucl Med. 2010;51:376-82.
94. Wendler T, Hartl A, Lasser T, Traub J, Daghighian F, Ziegler SI et al. Towards intra-operative 3D nuclear imaging: reconstruction of 3D radioactive distributions using tracked gamma probes. Med Image Comput Comput Assist Interv. 2007;10:909-17.
95. Wendler T, Herrmann K, Schnelzer A, Lasser T, Traub J, Kutter O et al. First demonstration of 3-D lymphatic mapping in breast cancer using freehand SPECT. Eur J Nucl Med Mol Imaging. 2010;37:1452-61.
96. Heuveling DA, Karagozoglu KH, van Schie A, van Weert S, van Lingen A, de Bree R. Sentinel node biopsy using 3D lymphatic mapping by freehand SPECT in early stage oral cancer: a new technique. Clin Otolaryngol. 2012;37:89-90.
97. Rieger A, Saeckl J, Belloni B, Hein R, Okur A, Scheidhauer K et al. First Experiences with Navigated Radio-Guided Surgery Using Freehand SPECT. Case Rep Oncol. 2011;4:420-5.
98. Brouwer OR, Buckle T, Bunschoten A, Kuil J, Vahrmeijer AL, Wendler T et al. Image navigation as a means to expand the boundaries of fluorescence-guided surgery. Phys Med Biol. 2012;57:3123-36.

99. Baumhauer M, Feuerstein M, Meinzer HP, Rassweiler J. Navigation in endoscopic soft tissue surgery: perspectives and limitations. J Endourol. 2008;22:751-66.
100. Simpfendorfer T, Baumhauer M, Muller M, Gutt CN, Meinzer HP, Rassweiler JJ et al. Augmented reality visualization during laparoscopic radical prostatectomy. J Endourol. 2011;25:1841-5.

PART TWO

CHAPTER 4

CONCOMITANT RADIO- AND FLUORESCENCE-GUIDED SENTINEL NODE BIOPSY IN SQUAMOUS CELL CARCINOMA OF THE ORAL CAVITY USING ICG-^{99M}TC-NANOCOLLOID

Adapted from: van den Berg NS*, Brouwer OR*, Klop WMC, Karkullukçu B, Zuur CL, Tan BI, Balm AJM, van den Brekel MWM, Valdés Olmos RA, van Leeuwen FWB. Eur J Nucl Med Mol Imaging. 2012;39:1128-36. * = Shared first authorship.

ABSTRACT

PURPOSE For oral cavity malignancies, sentinel node (SN) mapping is performed by injecting a radiocolloid around the primary tumor followed by lymphoscintigraphy. Surgically SNs can then be localized using a handheld gamma-ray detection probe. The aim of this study was to evaluate the added value of intraoperative fluorescence imaging to the conventional radioguided procedure. For this we used indocyanine green (ICG)-^{99m}Tc-nanocolloid, a hybrid tracer that is both radioactive and fluorescent.

METHODS Fourteen patients with oral cavity squamous cell carcinoma were peritumourally injected with ICG-^{99m}Tc-nanocolloid. SNs were preoperatively identified with lymphoscintigraphy followed by single photon emission computed tomography combined with computed tomography (SPECT/CT) for anatomical localization. During surgery SNs were detected with a handheld gamma-ray detection probe and a handheld near-infrared fluorescence camera. Pre-incision and post-excision imaging with a portable gamma camera was performed to confirm complete removal of all SNs.

RESULTS SNs were preoperatively identified using the radioactive signature of ICG-^{99m}Tc-nanocolloid. Intraoperatively, 43 SNs could be localized and excised with combined radio- and fluorescence guidance. Additionally, in four patients, an SN located close to the primary injection site (in three patients this SN was located in level I) could only be intraoperatively localized using fluorescence imaging. Pathological analysis of the SNs revealed a metastasis in one patient.

CONCLUSION Combined preoperative SN identification and intraoperative radio- and fluorescence guidance during SN biopsy for oral cavity cancer proved feasible using ICG-^{99m}Tc-nanocolloid. The addition of fluorescence imaging was shown to be of particular value when SNs were located in close proximity to the primary tumor.

INTRODUCTION

The incidence of lymph node metastases in patients with squamous cell carcinoma of the oral cavity is 20-30% [1, 2]. By using sentinel node (SN) biopsy to select patients with occult lymph node metastases, an unnecessary elective neck dissection (END) may be avoided in 70-80% of patients [1, 3]. SN biopsy has several advantages over END: (1) reduced morbidity [4]; (2) improved identification of so-called skip metastases and aberrant lymphatic drainage patterns [5-7]; and (3) improved pathological specimen analysis for the detection of (micro-)metastasis [8, 9]. For SN biopsy, overall sensitivity rates of 91% after five-year follow-up have been reported [10]. However, for floor of mouth (FOM) tumors, the sensitivity and the negative predictive values were much lower compared to other sites, 80 vs. 97% and 88 vs. 98%, respectively [10]. A prospective multi-institutional trial reported false-negative rates of 25 and 10% for FOM and tongue tumors, respectively, whereas this was said to be 0% for other types of oral cavity cancers [11]. In oral cavity malignancies, SNs are often located in close proximity to the primary tumor site, which can render SN biopsy difficult.

Conventional SN mapping is performed by injecting a radiocolloid (^{99m}Tc-nanocolloid or ^{99m}Tc-sulphur colloid) in or around the primary tumor followed by sequential lymphoscintigraphy to identify the lymph nodes on a direct drainage pathway from the primary tumor (the SNs) [12]. To provide an overview of the SNs with regard to their anatomical location, single photon emission computed tomography combined with computed tomography (SPECT/CT) was introduced. Additionally, with SPECT/CT more SNs can be visualized compared to conventional lymphoscintigraphy [13]. Intraoperatively, SN localization is commonly guided by the acoustic signal coming from a handheld gamma-ray detection probe (hereafter referred to as gamma probe). However, since for oral cavity cancers SNs are often located in close proximity to the primary tumor site, the high radioactive background signal coming from the injection site may hamper intraoperative radioguidance towards these SNs [6, 14]. Recently, the intraoperative use of a portable gamma camera was shown to improve the localization of SNs near the injection site [15].

Vital blue dyes are generally applied to enable intraoperative visual detection of the SNs, but have shown to be of limited value in oral cavity tumors as SNs in the head-and-neck area are less frequently stained blue compared to other primary tumor sites [16-18]. Moreover, the use of blue dye may blur the visibility of intraoral tumor margins [1, 19].

To enable visual detection of SNs without affecting the surgical field, the near-infrared fluorescence tracer indocyanine green (ICG) was introduced for SN mapping in various tumor types such as breast, colon and gastric cancers [20, 21]. Recently, Bredell evaluated the use of ICG for SN mapping in oropharyngeal cancer [22]. ICG is not visible by the naked eye and does, therefore, not interfere with the visual identification of tumor margins [23]. However, similar to vital blue dyes, ICG rapidly migrates through the lymphatic system leading to a limited diagnostic window and staining of higher-echelon nodes [24]. To address these migratory limitations of optical dyes, the self-assembled hybrid radiocolloid ICG-^{99m}Tc-nanocolloid was clinically introduced for selective SN biopsy [25, 26].

In this complex, ICG adopts the lymphatic migration properties of the radiocolloid, resulting in a significantly longer retention time in the SNs as compared to ICG alone. With this hybrid tracer being both radioactive and fluorescent, preoperative surgical planning can be combined with intraoperative radioguidance towards the SNs. The fluorescent properties of the hybrid tracer extend the radioguided procedure by providing real-time optical localization using an near-infrared fluorescence camera. For head-and-neck melanoma it was shown that with this approach fluorescence-based SN identification was superior over the use of blue dye [26]. The aim of the current study was to explore the utility of the hybrid tracer during SN biopsy for squamous cell carcinoma of the oral cavity.

MATERIALS AND METHODS

PATIENTS

Between May 2011 and January 2012, 14 patients with squamous cell carcinoma of the oral cavity were included in this study after obtaining written informed consent. Patients were scheduled for surgical removal of the primary tumor followed by SN biopsy. All patients were staged with T1/2 tumors and were clinically node negative as assessed by ultrasound and fine-needle aspiration cytology (USFNAC). Further patient characteristics are listed in Table 1. The study protocol was approved by the Institution's Medical Ethics Committee.

TRACER PREPARATION

^{99m}Tc-nanocolloid was prepared by adding 1400 MBq pertechnetate in 2 mL saline to a vial of nanocolloid (GE Healthcare, Eindhoven, The Netherlands). The mixture was then incubated for 30 min at room temperature after which the excess of reactive elements was removed. Before adding ICG, a quality check was performed in which the color, clarity and pH were determined (colourless, clear and pH 6-7, respectively).

ICG was prepared by adding 5 mL sterile water to a vial containing 25 mg ICG (vial concentration 5 mg/mL; Pulsion Medical Systems, Munich, Germany). Then, 50 µL of ICG solution was added to the ^{99m}Tc-nanocolloid to form ICG-^{99m}Tc-nanocolloid.

All procedures were performed under good manufacturing practice (GMP-z) and under supervision of the institution's pharmacist.

TRACER ADMINISTRATION AND PREOPERATIVE IMAGING

A median of 77 MBq (range 67-94 MBq) ICG-^{99m}Tc-nanocolloid was injected in three or four deposits around the primary tumor (total volume 0.4 mL; Figure 1). To visualize the lymphatic duct(s) with the subsequent SN(s), anterior and lateral dynamic images were obtained during the first 10 min after injection using a dual-head gamma camera (Symbia T, Siemens, Erlangen, Germany). Static planar gamma camera images were acquired 15 min and 2 h post-injection (Figure 2A). The latter was immediately followed by SPECT/CT

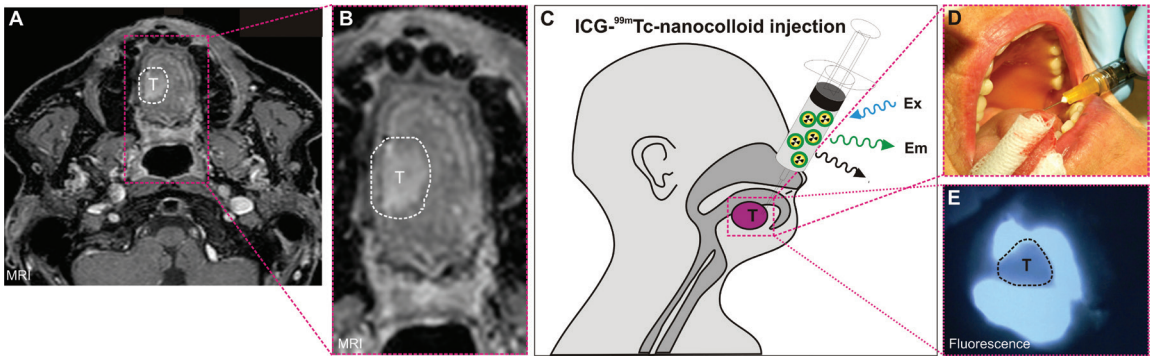

Figure 1. Hybrid ICG-^{99m}Tc-nanocolloid injection. A) Axial diagnostic MRI image showing a tumor on the tongue (T); B) Zoom in on the tongue tumor; C-D) ICG-^{99m}Tc-nanocolloid is peritumourally injected in three to four deposits; E) Intraoperative, near-infrared fluorescence-based visualization of the injection site and tumor (T). MRI = magnetic resonance; ICG = indocyanine green; Ex = exitation light; Em = emission light.

imaging (Symbia T, Siemens, Erlangen, Germany; Figure 2B). SPECT and CT images were obtained on the basis of 2 mm slices. After tissue attenuation correction for the SPECT, fused SPECT/CT images were generated. SPECT, CT and fused SPECT/CT images were simultaneously evaluated using orthogonal multiplanar reconstruction. In addition, three-dimensional (3D) display using volume rendering was performed in order to im-prove anatomical neck level recognition (Figure 2C).

SNs were defined as the lymph nodes on a direct lymphatic drainage pathway from the primary tumor [12]. Early draining lymph nodes in a basin were considered to be the SNs in case of multiple visualized lymph nodes without visible afferent vessels.

SURGICAL PROCEDURE

SN biopsy started 3-19 h after ICG-^{99m}Tc-nanocolloid administration. In the operating room, a portable gamma camera (Sentinella equipped with Sentinella suite software version 7.5; Oncovision, Valencia, Spain) was used to acquire a pre-incision overview image (Figure 3B, pre-incision) and to determine the location for the incision(s) [15]. Initial SN exploration was guided by a gamma probe (Neoprobe, Johnson & Johnson Medical, Hamburg, Germany; Figure 3D). Fluorescence imaging with a dedicated handheld near-infrared fluorescence camera (PhotoDynamic Eye, Hamamatsu Photonics K.K., Hamamatsu, Japan; Figure 3E) was performed to optically detect the SNs. After excision of the SN(s), the portable gamma camera was used to search for remaining radioactive hot spots in the SN excision area (Figure 3B, post-excision) as was previously described by Vermeeren et al. [15]. Higher-echelon nodes (defined by preoperative lymphoscintigraphy and SPECT/ CT) were left in situ.

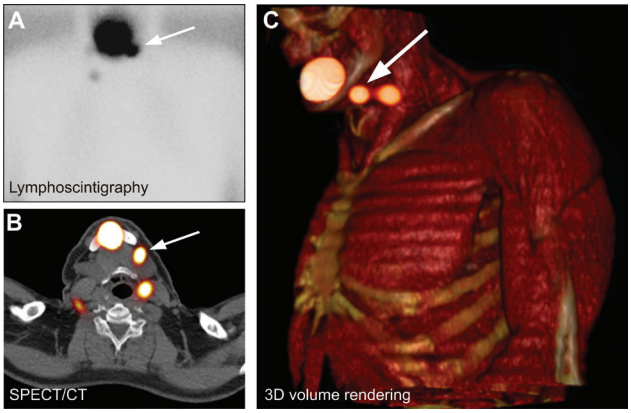

Figure 2. Preoperative sentinel node identification. A) Late planar anterior lymphoscintigram acquired 2 h post-injection showing two SNs on the right side and one SN on the left side (arrow); B) Axial SPECT/CT slice showing two level II SNs (bilateral) and a level I SN close to the injection site (arrow); C) The 3D volume-rendered SPECT/CT showing two SNs on the left side, in level I (arrow) and level II (these SNs were not visible as separate hot spots on the planar lymphoscintgram). 3D = three-dimensional; SPECT/CT = single photon emission computed tomography/computed tomography.

PATHOLOGY

Harvested SNs were fixed in formalin, bisected, embedded in paraffin, cut at a minimum of six levels at 50-150 µM intervals and histologically evaluated for the presence of (micro-) metastases (haematoxylin and eosin (H&E) and anti-cytokeratin (CAM 5.2; Becton Dickinson, San Jose, CA, USA) staining).

RESULTS

PREOPERATIVE FINDINGS

Distribution of the tumor locations of the 14 included patients was as follows: FOM (n=5), tongue (n=7), lower lip (n=1) and buccal mucosa (n=1). Further patient characteristics, and the pre- and intraoperative findings of all 14 patients are outlined in Table 1. A schematic overview of primary tumor and intraoperative SN location is provided in Figures 4A and B, respectively.

Lymphatic drainage was visualized in all patients. Bilateral lymphatic drainage was found in eight patients. In only three of these patients (patients 1, 12 and 14) the tumor had crossed the midline. Using conventional lymphoscintigraphy, a total of 37 SNs were visualized. Four additional SNs were only visible on the SPECT/CT images in three patients (patients 8, 9 and 12) resulting in a total of 41 preoperatively defined SNs (median of 3 SNs per patient; range 1-5) dispersed over 34 basins (median of two basins per patient; range 1-5 basins per patient) (Table 1). In all 14 patients, the fused SPECT/CT images provided an accurate anatomical reference point for surgical planning of the SN biopsy procedure, including the SNs that were found to be located close to the primary injection site (an example is given in Figure 2).

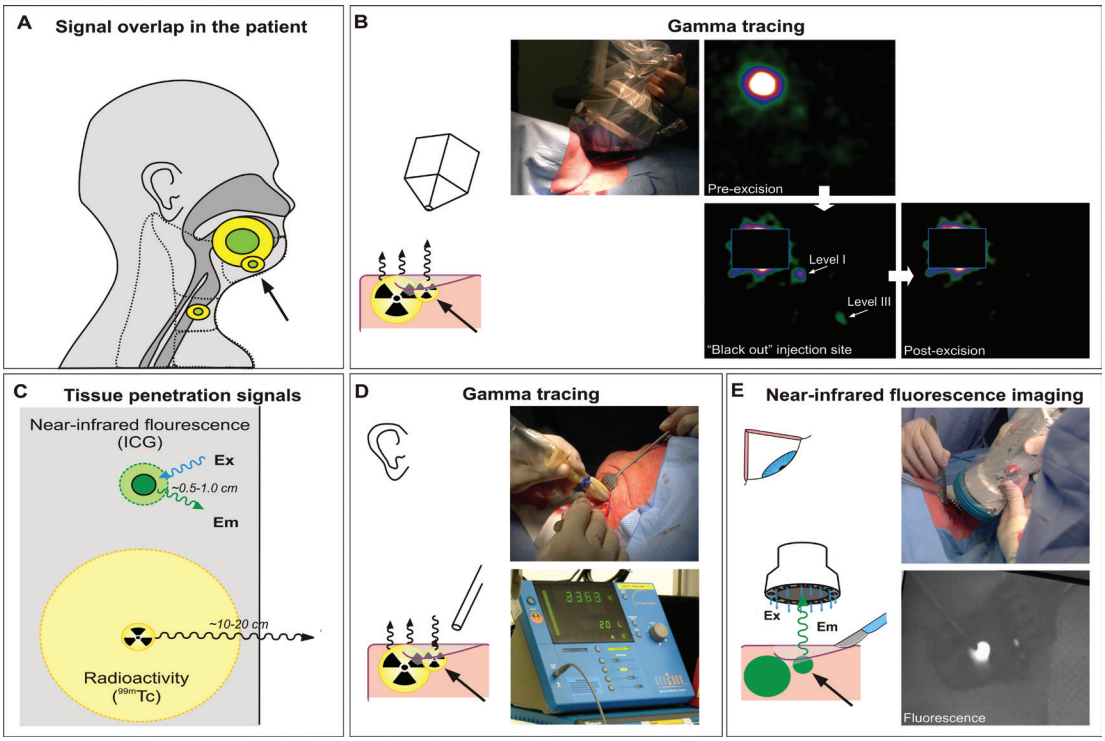

Figure 3. Intraoperative sentinel node identification. A) Schematic overview depicting how detection of an SN residing close to the primary tumor/injection site (arrow) can be difficult with radioguidance alone because of the high background signal coming from the injection site; B) Intraoperative gamma imaging with a portable gamma camera is performed before and after excision of the SN(s) to localize and to confirm complete removal of all predetermined SNs, respectively. The "blackout zone" feature of the portable gamma camera enables masking of the primary injection site, increasing the signal intensities of the weaker radioactive hot spots; C) The fluorescence signal penetration depth of the near-infrared fluorescent dye ICG is limited to approximately 0.5-1.0 cm, whereas the penetration depth of the radioactive signal is much greater depending on the imaging modality used; D) Intraoperatively, SNs are acoustically traced with a gamma probe; E) Near-infrared fluorescence imaging allows for visual identification and excision of the SN(s). Ex = excitation; Em = emission; Tc = technetium; ICG = indocyanine green; SN = sentinel node.

Table 1. Patient characteristics

					Preoperative imaging		Intraoperative findings				Pathology
Pt	*Age (years)*	*Sex*	*Tumor location*	*Time injection - surgery (h)*	*Total # defined SNs*	*SN location*	*Radio guidance*	*Fluore-scence guidance*	*Total # excised SNs*	*Location additional excised SNs*	*Tumor-positive nodes*
1	61	M	FOM midline	4	2	R level III; L level III	3	3	3	R level III	0
2	51	M	Tongue R	5	2	R level I, level III	2	2	2		0
3	58	F	FOM L	19	2	L level I, level III	3	3	3	L level III	0
4	62	F	Tongue R	5	3	R level I, level II; L level III	3	3	3		0
5	59	F	Tongue R	4	2	R level II, level III	1	2	2		1
6	84	F	Buccal mucosa R	19	1	R level II	1	1	1		0
7	82	M	Tongue L	19	3	L level II, 2xlevel III	-§	-§	0		-
8	74	M	Lower lip L	5	5	R level III L 3xlevel I, level III	7	7	7	L 2x level I	0
9	61	F	FOM R	4	4	L 2xlevel III, level I; R level III	3	4	4		0
10	65	M	Tongue R	4	4	R level I, level II; L level II, level III	4*	4*	4*	R level II	0
11	75	M	Tongue L	4	1	L level II	3	3	3	L 2x level II	0
12	60	M	FOM midline	4	4	L level I, level III; R level III, level IV	5	6	6	R 2x level III	0
13	71	M	Tongue R	3	3	R level II; L level III, level V	3	3	3		0
14	54	F	FOM midline	4	5	L level I, level III; R level I, level II, level III	5	6	6	L level I	0
Total					41		43	47	47		1

§ In this patient, the SN procedure was ceased. * In this patient, the L level II SN was not excised. SN = sentinel node; LN = lymph node; M = male; F = female; FOM = floor of mouth; R = right; and L = left.

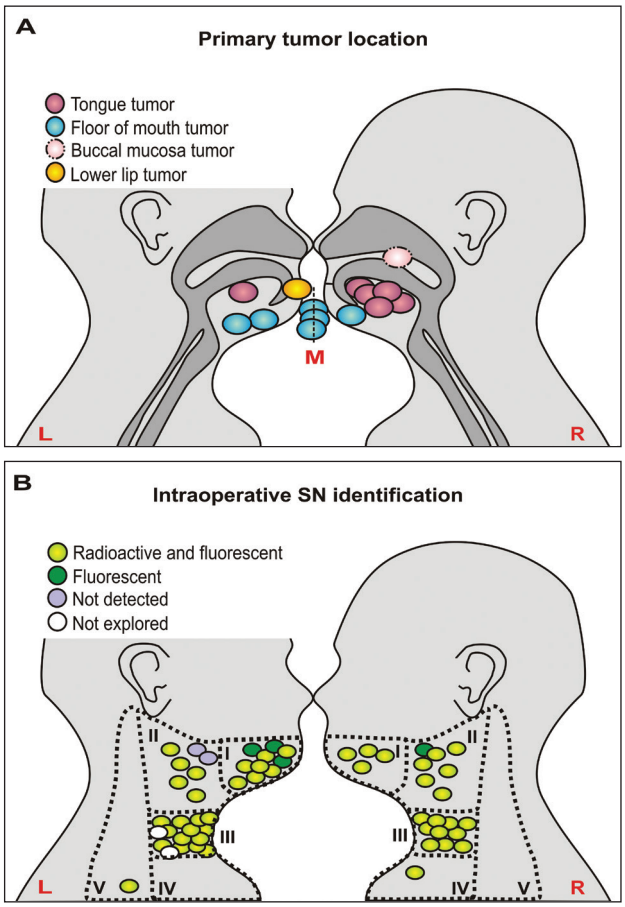

Figure 4. Schematic overview of primary tumor location and the intraoperative sentinel node identification results. A) Primary tumor location; B) Intraoperative SN identification method. The nodes that could be best identified with near-infrared fluorescence imaging during surgery (green dots in the figure) were also radioactive. L = left; R = right; M = midline. SN = sentinel node.

INTRAOPERATIVE FINDINGS

The SN biopsy procedure started 3-19 h post-ICG-^{99m}Tc-nanocolloid-injection and could be completed in all but two patients (patients 7 and 10; Table 1). A total of 47 SNs (median of three SNs per patient; range 0-7) was intraoperatively detected and excised; 43 SNs could be intraoperatively localized with the combined radio- and fluorescence guidance approach (Figure 4B). In four patients (patients 5, 9, 12 and 14), a total of four SNs were found to be located close to the injection site (level I or II; Table 1, Figure 4B). In these patients, SN identification with the gamma probe was hampered due to the high background signal coming from the injection site (Figure 3). Although the portable gamma camera was able to distinguish these SNs from the injection site after masking the injection site using the "blackout zone" function (Figure 3B), fluorescence imaging proved to be the most accurate technology for the identification of these SNs during surgery. To optimize fluorescence-based SN identification, lights were dimmed in the operating room. The SNs could be

pointed out or taken hold of with a surgical forceps (Figure 3E). Subsequently, the light was turned back on and the SN could be excised.

In four patients (patients 3, 8, 10 and 12), a total of 7 additional SNs were identified with the gamma probe. These SNs were not previously identified as separate hot spots on the preoperative images (most probably these SNs were part of a cluster of SNs). These nodes also proved to be fluorescent and were subsequently harvested. Post-excision control with the portable gamma camera revealed residual radioactivity in the excision area in three patients (patients 1, 11 and 14). This resulted in the removal of three additional SNs, again guided by a combination of gamma probe tracing and fluorescence imaging.

In two patients, the SN biopsy procedure was not completed to prevent possible vital structure damage. In patient 7 an SN was located medially of the mandible and very close to the main trunk of the facial nerve (Supporting information Figure SI1). Despite successful detection with the gamma probe and the portable gamma camera, visualization of this SN with the near-infrared fluorescence camera was not possible. In patient 10, an SN was located near branches of the marginal mandibular nerve. This SN could be detected with the portable gamma camera, but its exact location could not be identified with the gamma probe. Initial exploration with the near-infrared fluorescence camera also did not reveal the location of the SN. To reduce the invasiveness of the procedure and to prevent the possible risk of paresis of the lower lip, it was decided not to proceed with the excision. In both cases, the lack of a fluorescent signal suggested that the SN left in situ was located >0.5 cm deeper from the surface imaged; the penetration depth of ICG is limited to 0.5-1.0 cm (Figure 3). Both patients will be closely monitored following the “watch and wait” protocol.

PATHOLOGICAL FINDINGS

Although the SNs were clearly defined in vivo by fluorescence imaging, it was impossible to solely dissect the single SN separately in five patients (patients 1, 5, 8, 10 and 13). Subsequently, in these patients some additional tissue was also excised. This resulted in the identification of 13 additional lymph nodes in these tissue specimens. All of these lymph nodes were evaluated as SNs.

Histopathological examination revealed SNs with largest diameters varying from two to 25 mm with a median of 6 mm. In one patient (patient 5) a level III lymph node metastasis of 3 mm was found. This patient received a subsequent therapeutic neck dissection in which 34 additional tumor-negative lymph nodes from level I-V were removed.

DISCUSSION

The present study shows that a single injection of ICG-^{99m}Tc-nanocolloid enables preoperative SN mapping and intraoperative radio- and fluorescence-guided identification of the SNs draining from primary oral cavity cancers. SPECT/CT and the portable gamma camera allowed for accurate surgical planning, even when SNs were found in close proximity to the injection site. Intraoperatively, surgeons experienced the optical detection of the SNs provided by the fluorescent label of the hybrid tracer as valuable, especially in cases where localization with the gamma probe was impeded by high radioactive background signals. In FOM tumors, SN biopsy is discouraged due to its low sensitivity [10], which we reason may partially be a result of the difficulty to intraoperatively localize such SNs in the vicinity of the injection site. The addition of fluorescence imaging to the conventional radioguided procedure may be of particular benefit in this patient group. In this study, a total of four SNs were found in level I in the five patients with FOM tumors. Three (75%) of these could only be accurately detected with fluorescence imaging.

Contralateral lymph node involvement ranges from 0.9 to 34.7% [27]. Bilateral lymphatic drainage was observed on the lymphoscintigrams in 54% of patients (n=8), even though the primary tumor had crossed the midline in only three of these patients. Hence, by performing an upfront unilateral END, such (potentially tumor-positive) contralateral draining nodes might be missed.

With the rise of minimally invasive surgery, SN biopsy becomes more favorable over END procedures. Lymph nodes are generally small (3-4 mm) and are frequently found in close proximity to each other [18]. These conditions create high demands on the limited spatial resolution of the gamma probe. In the current study, the high spatial resolution (down to the micrometer level) provided by fluorescence imaging enabled the detection and removal of individual SNs as small as 2 mm.

The use of a non-covalent self-assembly approach to generate imaging agents is appealing as it allows for the formation of hybrid agents by combining “simple” and often commercially available, clinically approved building blocks [28]. The hybrid tracer ICG-^{99m}Tc-nanocolloid was built from ^{99m}Tc-nanocolloid particles (used for conventional SN mapping in Europe) and the near-infrared fluorescent dye ICG. Good manufacturing practice (GMP-z)-based preparation of ICG-^{99m}Tc-nanocolloid only adds one additional step to the conventional radiocolloid preparation process, namely the addition of 0.25 mg ICG to a solution of fully prepared ^{99m}Tc-nanocolloid. The pH of the ^{99m}Tc-nanocolloid solution is 6-7, and therefore the preparation protocol does not negatively influence the optical properties of ICG [29]. With this hybrid approach SNs could be accurately visualized using approximately 100 times lower quantities of ICG compared to the study of Bredell [22]. Although one may reason that non-covalent particles may disintegrate in vivo, a large degree of signal overlap was found in the lymphatic system in both preclinical models [24, 30, 31] and in patients [25, 26]. In none of our clinical studies performed thus far did we find nodes that solely contained a fluorescent or a radioactive signal [25, 26].

The use of ICG alone for SN mapping of oropharyngeal cancer was set to be optimal 5 min post-ICG-injection [22], while in the current study SNs were still fluorescent at 19 h after ICG-^{99m}Tc-nanocolloid injection. Clearly the retention of the hybrid tracer in the SNs yields a superior diagnostic window. It therefore does not require additional (intraoperative) injections which helps to optimize the logistics in daily practice. The limited penetration depth of fluorescence imaging compared to modalities based on radioactivity may even be useful, since it can help the surgeon to estimate the depth at which an SN can be localized in order to decide if further exploration is needed (as described for patients 7 and 10). The near-infrared fluorescence signal coming from ICG is invisible to the naked eye and can only be visualized with a dedicated near-infrared fluorescence camera system. As such ICG does not interfere with primary tumor margin visibility [23] like blue dyes do. This study demonstrates how optical guidance provided by the hybrid tracer's fluorescent label offers an excellent alternative over visual blue dyes and facilitates accurate SN localization, even when an SN resides in close proximity to the primary tumor.

Supplementing the conventional radioguided SN biopsy procedure with fluorescence only moderately increases the costs of the procedure as the near-infrared fluorescence imaging system used in this study is in the same price range as a gamma probe. The costs of ICG are also not higher than that of the original tracer ^{99m}Tc-nanocolloid and one vial of ICG can be used for multiple tracer preparations.

CONCLUSION

The hybrid tracer ICG-^{99m}Tc-nanocolloid allows for both preoperative lymphatic mapping and intraoperative SN detection up to 19 h post-injection. The added guidance provided by fluorescence imaging proved especially valuable for the detection of SNs located close to the primary tumor site.

REFERENCES

1. Broglie MA, Stoeckli SJ. Relevance of sentinel node procedures in head and neck squamous cell carcinoma. Q J Nucl Med Mol Imaging. 2011;55:509-20.
2. Coughlin A, Resto VA. Oral cavity squamous cell carcinoma and the clinically n0 neck: the past, present, and future of sentinel lymph node biopsy. Curr Oncol Rep. 2010;12:129-35.
3. Stoeckli SJ, Alkureishi LW, Ross GL. Sentinel node biopsy for early oral and oropharyngeal squamous cell carcinoma. Eur Arch Otorhinolaryngol. 2009;266:787-93.
4. Murer K, Huber GF, Haile SR, Stoeckli SJ. Comparison of morbidity between sentinel node biopsy and elective neck dissection for treatment of the n0 neck in patients with oral squamous cell carcinoma. Head Neck. 2011;33:1260-4.
5. Byers RM, Weber RS, Andrews T, McGill D, Kare R, Wolf P. Frequency and therapeutic implications of "skip metastases" in the neck from squamous carcinoma of the oral

tongue. Head Neck. 1997;19:14-9.
6. Civantos FJ, Moffat FL, Goodwin WJ. Lymphatic mapping and sentinel lymphadenectomy for 106 head and neck lesions: contrasts between oral cavity and cutaneous malignancy. Laryngoscope. 2006;112:1-15.
7. Stoeckli SJ. Sentinel node biopsy for oral and oropharyngeal squamous cell carcinoma of the head and neck. Laryngoscope. 2007;117:1539-51.
8. Civantos Jr F, Zitsch R, Bared A, Amin A. Sentinel node biopsy for squamous cell carcinoma of the head and neck. J Surg Oncol. 2008;97:683-90.
9. Stoeckli SJ, Pfaltz M, Ross GL, Steinert HC, MacDonald DG, Wittekind C, et al. The second international conference on sentinel node biopsy in mucosal head and neck cancer. Ann Surg Oncol. 2005;12:919-24.
10. Alkureishi LW, Ross GL, Shoaib T, Soutar DS, Robertson AG, Thompson R, et al. Sentinel node biopsy in head and neck squamous cell cancer: 5-year follow-up of a European multicenter trial. Ann Surg Oncol. 2010;17:2459-64.
11. Civantos FJ, Zitsch RP, Schuller DE, Agrawal A, Smith RB, Nason R, et al. Sentinel lymph node biopsy accurately stages the regional lymph nodes for T1-T2 oral squamous cell carcinomas: results of a prospective multi-institutional trial. J Clin Oncol. 2010;28:1395-400.
12. Nieweg OE, Tanis PJ, Kroon BB. The definition of a sentinel node. Ann Surg Oncol. 2001;8:538-41.
13. Vermeeren L, Valdés Olmos RA, Klop WM, van der Ploeg IM, Nieweg OE, Balm AJ, et al. SPECT/CT for sentinel lymph node mapping in head and neck melanoma. Head Neck. 2011;33:1-6.
14. de Bree R, Leemans CR. Recent advances in surgery for head and neck cancer. Curr Opin Oncol. 2010;22:186-93.
15. Vermeeren L, Valdés Olmos RA, Klop WM, Balm AJ, van den Brekel MW. A portable gamma-camera for intraoperative detection of sentinel nodes in the head and neck region. J Nucl Med. 2010;51:700-3.
16. Chao C, Wong SL, Edwards MJ, Ross MI, Reintgen DS, Noyes RD, et al. Sentinel lymph node biopsy for head and neck melanomas. Ann Surg Oncol. 2003;10:21-6.
17. Eicher SA, Clayman GL, Myers JN, Gillenwater AM. A prospective study of intraoperative lymphatic mapping for head and neck cutaneous melanoma. Arch Otolaryngol Head Neck Surg. 2002;128:241-6.
18. Tanis PJ, Nieweg OE, van den Brekel MW, Balm AJ. Dilemma of clinically node-negative head and neck melanoma: outcome of “watch and wait” policy, elective lymph node dissection, and sentinel node biopsy-a systematic review. Head Neck. 2008;30:380-9.
19. Kuriakose MA, Trivedi NP. Sentinel node biopsy in head and neck squamous cell carcinoma. Curr Opin Otolaryngol Head Neck Surg. 2009;17:100-10.
20. Polom K, Murawa D, Rho YS, Nowaczyk P, Hünerbein M, Murawa P. Current trends and emerging future of indocyanine green usage in surgery and oncology: a literature review. Cancer. 2011;117:4812-22.

21. Schaafsma BE, Mieog JS, Hutteman M, van der Vorst JR, Kuppen PJ, Löwik CW, et al. The clinical use of indocyanine green as a near-infrared fluorescent contrast agent for image-guided oncologic surgery. J Surg Oncol. 2011;104:323-32.
22. Bredell MG. Sentinel lymph node mapping by indocyanin green fluorescence imaging in oropharyngeal cancer - preliminary experience. Head Neck Oncol. 2010;2:31.
23. Vahrmeijer AL, Frangioni JV. Seeing the invisible during surgery. Br J Surg. 2011;98:749-50.
24. van Leeuwen AC, Buckle T, Bendle G, Vermeeren L, Valdés Olmos R, van de Poel HG, et al. Tracer-cocktail injections for combined pre- and intraoperative multimodal imaging of lymph nodes in a spontaneous mouse prostate tumor model. J Biomed Opt. 2011;16:016004.
25. van der Poel HG, Buckle T, Brouwer OR, Valdés Olmos RA, van Leeuwen FW. Intraoperative laparoscopic fluorescence guidance to the sentinel lymph node in prostate cancer patients: clinical proof of concept of an integrated functional imaging approach using a multimodal tracer. Eur Urol. 2011;60:826-33.
26. Brouwer OR, Klop WM, Buckle T, Vermeeren L, van den Brekel MW, Balm AJ, et al. Feasibility of sentinel node biopsy in head and neck melanoma using a hybrid radioactive and fluorescent tracer. Ann Surg Oncol. 2012;19:1988-94.
27. González-Garcia R, Naval-Gías L, Rodríguez-Campo FJ, Sastre-Pérez J, Muñoz-Guerra MF, Gil-Díez Usandizaga JL. Contralateral lymph neck node metastasis of squamous cell carcinoma of the oral cavity: a retrospective analytic study in 315 patients. J Oral Maxillofac Surg. 2008;66:1390-8.
28. Buckle T, Chin PT, van Leeuwen FW. (Non-targeted) radioactive/fluorescent nanoparticles and their potential in combined pre- and intraoperative imaging during sentinel lymph node resection. Nanotechnology. 2010;21:482001.
29. Björnsson OG, Murphy R, Chadwick VS, Björnsson S. Physiochemical studies on indocyanine green: molar lineic absorbance, pH tolerance, activation energy and rate of decay in various solvents. J Clin Chem Clin Biochem. 1983;21:453-8.
30. Buckle T, van Leeuwen AC, Chin PT, Janssen H, Muller SH, Jonkers J, et al. A self-assembled multimodal complex for combined pre- and intraoperative imaging of the sentinel lymph node. Nanotechnology. 2010;21:355101.
31. Bunschoten A, Buckle T, Kuil J, Luker GD, Luker KE, Nieweg OE, et al. Targeted non-covalent self-assembled nanoparticles based on human serum albumin. Biomaterials. 2012;33:867-75.

SUPPORTING INFORMATION

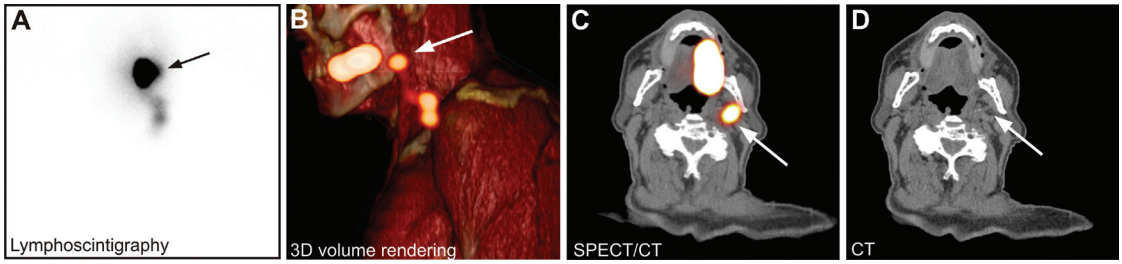

Figure SI1. Preoperative sentinel node mapping (patient 7). A) Anterior planar lymphoscintigram 2 h post-injection vaguely showing three SNs; B) 3D volume-rendered SPECT/CT image confirming the lymphoscintigraphic findings and adding anatomical information; C) Axial fused SPECT/CT image showing the SN located medially of the mandible (arrow) very close to the main trunk of the facial nerve. D) The corresponding SN can be distinguished on the CT image (arrow). SN = sentinel node; 3D = three-dimensional; SPECT/CT = single photon emission computed tomography combined with computed tomography.

CHAPTER 5

A HYBRID RADIOACTIVE AND FLUORESCENT TRACER FOR SENTINEL NODE BIOPSY IN PENILE CARCINOMA AS A POTENTIAL REPLACEMENT FOR BLUE DYE

Adapted from: Brouwer OR*, van den Berg NS*, Mathéron HM, van der Poel HG, van Rhijn BW, Bex A, Valdés Olmos RA, van Leeuwen FWB, Horenblas S. Eur Urol. 2014;65:600-609.
* = Shared first authorship.

ABSTRACT

BACKGROUND Sentinel node (SN) biopsy in penile cancer is typically performed using a combination of radiocolloid and blue dye. Recently, the hybrid radioactive and fluorescent tracer indocyanine green (ICG)-^{99m}Tc-nanocolloid was developed to combine the beneficial properties of both radio-guidance and fluorescence imaging.

OBJECTIVE To explore the added value of SN biopsy using ICG-^{99m}Tc-nanocolloid in patients with penile carcinoma.

DESIGN, SETTING, AND PARTICIPANTS
Sixty-five patients with penile squamous cell carcinoma were prospectively included (January 2011 to December 2012). Preoperative SN mapping was performed using lymphoscintigraphy and single-proton emission computed tomography supplemented with computed tomography (SPECT/CT) after peritumoural injection of ICG-^{99m}Tc-nanocolloid. During surgery, SNs were initially approached using a gamma probe, followed by patent blue dye and/or fluorescence imaging. A portable gamma camera was used to confirm excision of all SNs.

SURGICAL PROCEDURE Patients underwent SN biopsy of the cN0 groin and treatment of the primary tumor.

OUTCOME MEASUREMENTS AND STATISTICAL ANALYSIS The number and location of preoperatively identified SNs were documented. Intraoperative SN identification rates using radio- and/or fluorescence guidance were assessed and compared with blue dye. Statistical evaluation was performed using a two-sample test for equality of proportions with continuity correction.

RESULTS AND LIMITATIONS Preoperative imaging after injection of ICG-^{99m}Tc-nanocolloid enabled SN identification in all patients (a total of 183 SNs dispersed over 119 groins). Intraoperatively, all SNs identified by preoperative SN mapping were localized using combined radio-, fluorescence-, and blue dye guidance. Fluorescence imaging enabled visualization of 96.8% of SNs, while only 55.7% was stained by blue dye ($p<0.0001$). The tissue penetration of the fluorescent signal, and the rapid flow of blue dye limited the detection sensitivity. A tumor-positive SN was found in seven patients.

CONCLUSIONS ICG-^{99m}Tc-nanocolloid allows for both preoperative SN mapping and combined radio- and fluorescence-guided SN biopsy in penile carcinoma patients and significantly improves optical SN detection compared with blue dye.

INTRODUCTION

Penile carcinoma predominantly shows metastatic spread via the lymphatic system. As a consequence, lymph node staging in penile carcinoma has strong prognostic implications [1]. Since only 20-25% of patients have regional metastases, performing a complete lymph node dissection (LND) may be overtreatment, resulting in considerable morbidity [2]. Sentinel node (SN) biopsy is a validated procedure to detect (micro-)metastases in clinically node-negative groins without the morbidity associated with a complete lymph node dissection. Yet the reliability of SN biopsy depends on successful pre-, intra-, and postoperative identification of all (tumor-positive) SNs [3,4].

Generally, SNs are preoperatively identified using lymphoscintigraphy after a peritumoral injection of a radioactive tracer (^{99m}Tc-nanocolloid is the gold standard in Europe). With the introduction of single photon emission computed tomography supplemented with computed tomography (SPECT/CT), it has become possible to detect the SNs in their anatomic context [5]. This three-dimensional (3D) information can be used to accurately plan the surgical approach.

The intraoperative procedure traditionally relies on localization of the radioactive signal using a handheld gamma-ray detection probe (hereafter referred to as gamma probe) that generates an acoustic readout. A portable gamma camera has been introduced with the ability to acquire intraoperative overview images of radioactive hot spots. Unfortunately, the current portable gamma cameras are unable to provide adequate anatomic information, leaving the radioactive signal depicted against a two-dimensional black background [6]. To anatomically visualize the SNs within the surgical field, a second injection with blue dye is usually administered shortly before surgery. However, one of the disadvantages of blue dye is that preoperatively defined (radioactive) SNs may not always be stained blue at the time of excision [7]. Moreover, blue dyes stain the injection site, potentially hindering tumor resection, which is generally performed after SN biopsy.

The use of near-infrared fluorescence imaging has characteristics that can be advantageous for intraoperative SN detection: an improved tissue penetration compared to blue dye, and the fluorescent signal is only visible using a dedicated near-infrared fluorescence camera system, leaving the surgical field unstained [8]. Similar to blue dye, fluorescence imaging normally also requires an additional injection of, for example, the clinically approved indocyanine green (ICG). Like blue dye, ICG migrates quickly through the lymphatic system, resulting in a limited diagnostic window. The larger radioactive ^{99m}Tc-nanocolloid does not have this limitation [9].

To combine the beneficial properties of both radio guidance and fluorescence imaging, ICG-^{99m}Tc-nanocolloid was developed [9,10]. This hybrid tracer expands the gold standard radiotracer ^{99m}Tc-nanocolloid with a near-infrared fluorescent component (ICG) without altering the well-validated tracer kinetics of the gold standard [11]. Pilot studies have demonstrated the feasibility of this hybrid approach in head-and-neck malignancies and prostate cancer [12-14]. Its added value, however, remains to be assessed in a more extensive study population. The purpose of this study was to evaluate the added value of

SN biopsy using ICG-^{99m}Tc-nanocolloid compared with blue dye in a large cohort of patients with penile carcinoma.

METHODS

PATIENTS

A total of 84 consecutive patients presenting with ≥T1G2 tumors were prospectively included. The SN procedure was performed following the European Association of Urology penile cancer guidelines [15]. The study protocol was approved by the institutions' medical ethics committees (N09DRF, NL 26699.031.09).

Seventeen patients were excluded from the study. Nine patients were previously included in a reproducibility study [11]. In five patients, excised SNs were only evaluated ex vivo. In one patient no blue dye was used, one patient presented with a penile melanoma and another patient presented with a carcinoma of the urethra.

Characteristics of the remaining 65 evaluated patients are listed in Table 1. Only patients with at least one cN0 groin were enrolled. In patients with proven unilateral nodal involvement (n=10) or with a previous unilateral lymph node dissection (n=1), only the contralateral cN0 groin was included for SN biopsy, resulting in a total of 119 included groins. Patients were scheduled for SN biopsy or repeat SN biopsy (n=6) in case of a recurrent tumor, followed by treatment of the primary tumor or for SN biopsy only in case of previous penile surgery in another center.

Table 1. Patient characteristics

No of included patients	65
Average age (years)	67 (range 34-93, median 66)
Recurrence (repeat SN biopsy), no.	6
Tumor stage	
- T1	25
- T2	34
- T3	6
Groins	
- cN0 (with or without) FNAC	119
- cN1 (tumor + FNAC)	10
- Previous LND	1
Total included groins for SN biopsy	119

SN = sentinel node; FNAC = fine needle aspiration cytology; LND = lymph node dissection.

TRACER PREPARATION

ICG-^{99m}Tc-nanocolloid was prepared as previously described [11]. Subsequently, approximately 90 MBq±10% was subtracted from the vial containing the ICG-^{99m}Tc-nanocolloid solution. Saline was then added to reach a total volume of 0.4 mL in the syringe. All procedures were performed under good manufacturing practice (GMP-z) and under supervision of the institution's pharmacist.

PREOPERATIVE PROCEDURE

A schematic overview of the study setup is given in Figure 1. ICG-^{99m}Tc-nanocolloid was intradermally injected proximally around the tumor in three or four deposits on the same day or on the day before surgery. No adverse reactions were observed.

Dynamic lymphoscintigraphy was performed during 10 min immediately after injection, using a dual-head gamma camera (Symbia T; Siemens, Erlangen, Germany). Static planar gamma camera images were acquired 15 min post-injection (early) and 2 h post-injection (late), followed by SPECT/CT imaging (Symbia T; Siemens, Erlangen, Germany). Lymph nodes draining from the site of injection through an own lymphatic vessel or a single radioactive lymph node in the groin were identified as SNs [16]. SNs were anatomically localized using multiplanar reconstruction, which enabled comparison of fused SPECT/CT

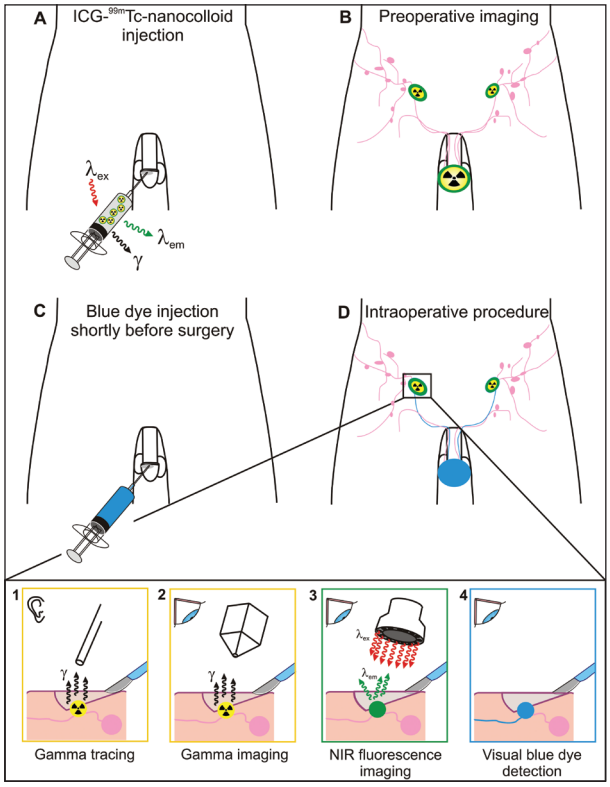

Figure 1. Schematic overview of the study setup. A) After injection of indocyanine green (ICG)-^{99m}Tc-nanocolloid, preoperative imaging of the sentinel nodes (SNs) is performed using lymphoscintigraphy and B) single-proton emission computed tomography supplemented with computed tomography. C) Shortly before surgery, blue dye is also administered. D) Intraoperatively, the radioactive component of the hybrid tracer allows for radioguided SN localization using (1) a gamma-ray detection probe and (2) the portable gamma camera. In addition, the fluorescent component allows for SN visualization using (3) a near-infrared fluorescence camera. (4) Intraoperative SN identification rates using radio- and/or fluorescence guidance were assessed and compared with blue dye. SN = sentinel node. γ = gamma; λ_{ex} = excitation light; λ_{em} = emission light; NIR = near-infrared.

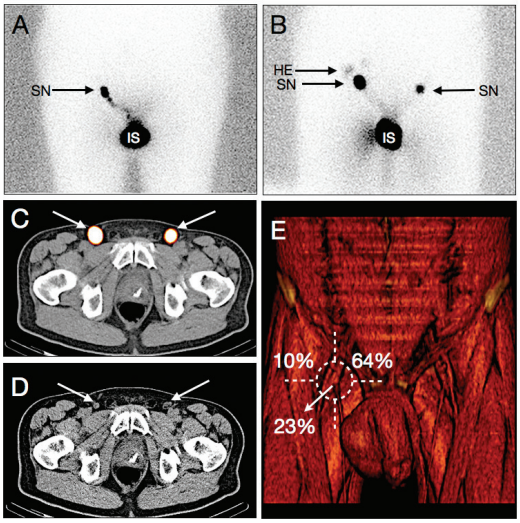

Figure 2. Sentinel node mapping after indocyanine green-^{99m}Tc-nanocolloid injection using lymphoscinti graphy and single proton emission computed tomography supplemented with computed tomography (SPECT/CT). A) Early lymphoscintigram showing drainage to a right inguinal SN (arrow); B) Late lymphoscintigraphy also reveals drainage to the left-side SN, as well as higher (iliac) echelon drainage on the right side (arrows). C) Axial fused SPECT/CT images depicting both radioactive SNs; D) Corresponding CT showing the lymph nodes (arrows). E) Drainage in penile cancer and the five inguinal zones of Daseler: In this study, most of the SNs (64.2%) were located in the medial superior zone, 10.1% in the lateral superior zone, and 23.5% in the central zone, which is concordant with the expected drainage pattern using ^{99m}Tc-nanocolloid alone [5]. SN = sentinel node; HE = higher-echelon node; IS = injection site.

images with the concomitant CT. Additionally, 3D SPECT/CT display of SNs in relation to the anatomic structures was accomplished using volume rendering. Distribution of the SNs on SPECT/CT was determined by dividing the groin into five different zones, according to Daseler (Figure 2E).

INTRAOPERATIVE PROCEDURE

Shortly before surgery, approximately 1.0 mL patent blue dye V (Laboratoire Guerbet, Aulnay-Sous-Bois, France) was intradermally administered in all patients in the same way as the ICG-^{99m}Tc-nanocolloid injection. A portable gamma camera (Sentinella; OncoVision, Valencia, Spain) (Figure 3A) was then used to acquire a pre-incision reference image, as previously described [17]. After incision, SNs were initially pursued with a gamma probe (Neoprobe; Johnson & Johnson Medical, Hamburg, Germany). During surgical exploration, alternating attempts were made to optically visualize the SNs via near-infrared fluorescence imaging using a handheld fluorescence camera (PhotoDynamic Eye; Hamamatsu Photonics K.K., Hamamatsu, Japan) (Figures 3C and 4) and/or visual detection of the blue dye. Fluorescence imaging required the lights in the operating room to be dimmed for a brief period to minimize the background signal. After excision of the SNs, the surgical area was scanned using the gamma probe and palpated to search for clinically suspicious nodes. Subsequently, a second image was acquired with the portable gamma camera to verify complete SN removal.

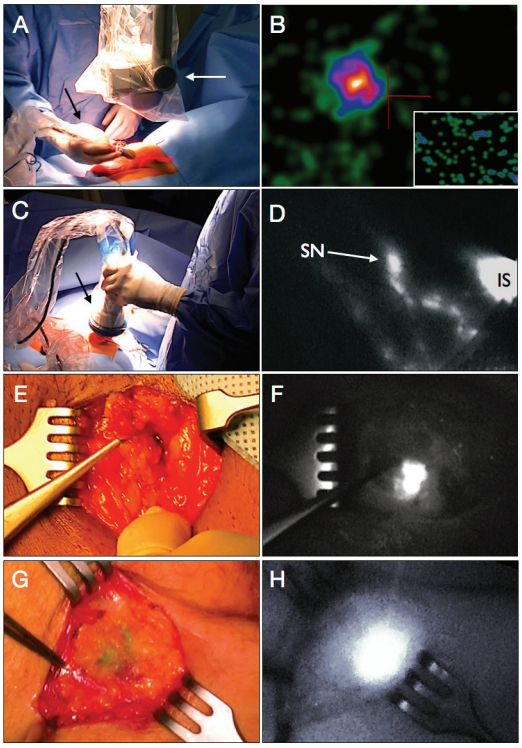

Figure 3. Combined intraoperative radio- and fluorescence-guided sentinel node biopsy. A) The radioactive signature of the hybrid tracer enables initial SN detection using a conventional gamma probe (black arrow) and a portable gamma camera (orange arrow); B) The portable gamma camera provides an overview image of the SNs that can be used to verify complete SN removal after excision (figure inlay); C) As the SN is approached, the fluorescent signature of the hybrid tracer enables SN visualization using a near-infrared fluorescence camera; D) In some patients, the SN (arrow) and its afferent lymphatic duct, as well as the injection site, could be visualized through the intact skin; E-F) A radioactive, non-blue SN clearly seen via fluorescence imaging of the hybrid tracer; G-H) The improved tissue penetration of the fluorescence signal enables clearer visualization of the SN and its borders compared to blue dye. SN = sentinel node.

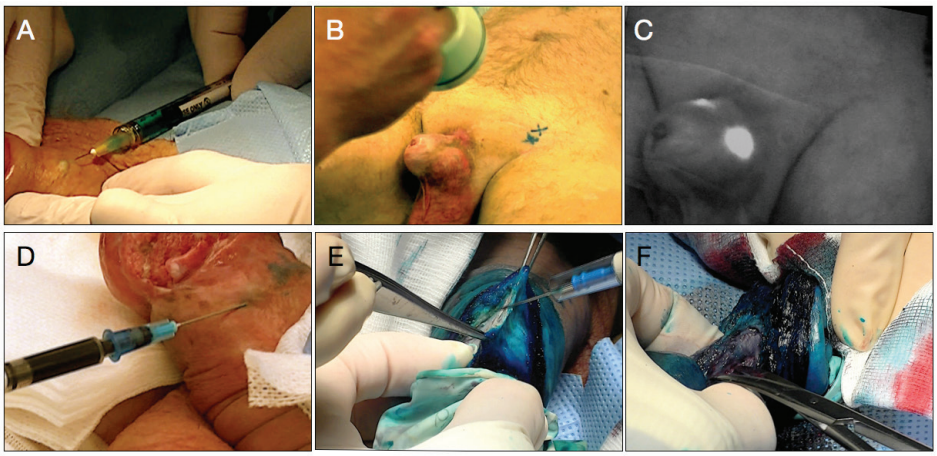

Figure 4. The fluorescent signal is only visible using a dedicated near-infrared fluorescence camera system, leaving the surgical field unstained. A) Hybrid tracer administration; B-C) The injection sites are only visible when using the fluorescence camera; D) Intraoperative blue dye injection; E-F) Blue dye stains the surgical field blue, which may be a hindrance during penile surgery.

If remaining radioactivity was observed at the site of a previously excised SN, it was considered part of a cluster of multiple SNs close together and, thus, as an additional SN, which was also harvested. Intraoperative SN identification rates using radio- and/or fluorescence guidance were assessed and compared with blue dye. Statistical evaluation of the difference between the number of fluorescent- and blue dye stained nodes was performed using a two-sample test for equality of proportions with continuity correction.

PATHOLOGY AND EX VIVO ANALYSES

Harvested SNs were bisected, formalin-fixed, paraffin-embedded, and cut at six or more levels (50-150 µm intervals). Paraffin sections were stained with hematoxylin and eosin and with cytokeratin using an anticytokeratin antibody, clone AE1/AE3 (cat. no. MS-343-P; Thermo Fisher Scientific Inc., Waltham, MA, USA).

To study the distribution of ICG-^{99m}Tc-nanocolloid in tumor-positive SNs, 5-mm sections of four tumor-positive SNs (two patients) were cut and deparaffinized with xylene (twice, 10 min) and rehydrated in 100% ethyl alcohol (EtOH) (twice, 10 min), 70% EtOH (twice, 5 min), and water (twice, 5 min). Slides were subsequently air dried for 2 h and scanned on an Odyssey scanner (LI-COR Biosciences, Lincoln, NE, USA) for the presence of ICG (setting: 800 nm; focus offset: 0 mm; intensity: 10).

RESULTS

PREOPERATIVE RESULTS

An average dose of 79 MBq ICG-^{99m}Tc-nanocolloid was preoperatively injected on the same day (n=38) or on the day before surgery (n=27). Lymphoscintigraphy and SPECT/CT visualized at least one SN in all patients (100% visualization rate). Only 89 SNs (48.5%) were visible on the early planar lymphoscintigrams, whereas 160 SNs (87.4%) were identified on the late planar lymphoscintigrams. One patient declined to undergo SPECT/CT due to claustrophobia (four SNs at lymphoscintigraphy). In the remaining 64 patients, SPECT/CT revealed 26 SNs in 18 patients that were not seen on the lymphoscintigrams. Furthermore, SPECT/CT helped to define three nodes (in three patients) as iliac higher-echelon nodes (these were considered as inguinal SNs based on lymphoscintigraphy). In sum, a total of 183 SNs were preoperatively identified dispersed over 119 groins (median: three SNs per patient; range 1-6) (Table 2).

Table 2. Results

Preoperative SN results	
- Lymphoscintigraphy, early	89
- Lymphoscintigraphy, late	160
- SPECT/CT*	179
Total number of identified SNs	183 (average 2.9; median 3, range 1-6)
Location of SNs, no.	
- Medial superior zone	115 (64.2%)
- Lateral superior zone	18 (10.1%)
- Central zone	42 (23.5%)
- Medial inferior zone	3 (1.7%)
- Lateral inferior zone	1 (0.6%)
Total	179*
Intraoperative SN results	
- Traceable with probe (in vivo)	215 (97.3%)
- Radioactive (ex vivo)	220 (99,6%)
- Fluorescent (in vivo)	214 (96.8%)**
- Fluorescent (ex vivo)-	220 (99.6%)
- Blue (+ radioactive/fluorescent)	123 (55.7%)**
- Blue (non-radioactive/non-fluorescent)	1 (0.45%)
Total number of excised SNs	221 (average 3.4; median 3, range 1-9)
Pathology	
Total number of SNs	221 (average 3.4; median 3, range 1-9)
Total number of lymph nodes	239
Number of tumor-positive SNs	10 (7 patients, 7 groins)

*One patient refused to undergo SPECT/CT. **Statistical significant difference between surgically visualized fluorescent and blue SNs ($p<0.0001$). SN = sentinel node; SPECT/CT = single photon emission computed tomography combined with computed tomography.

Bilateral drainage was observed in 52 of the 54 patients (96.3%) with clinically N0 groins. The remaining two patients received tracer re-injection; lymphoscintigraphy 1 h later showed bilateral drainage in both cases. In seven of the ten patients with a clinically N1 groin based on ultrasound and fine-needle aspiration cytology, bilateral drainage was observed. The remaining three patients only showed drainage to the unaffected groin. One patient who presented with a recurrent tumor already had received a previous unilateral lymph node dissection and only showed drainage to the contralateral side.

Most of the SNs (64.2%) were located in the medial superior zone of the groin, 10.1% was located in the lateral superior zone and 23.5% in the central zone (Figure 2E). Drainage to an inferior quadrant was seen in four patients (2.2%) with a recurrent tumor who had already received a previous SN biopsy, which may have caused an altered lymphatic drainage pattern.

INTRAOPERATIVE RESULTS

SN biopsy was started 3-27 h (mean: 13 h; median: 7 h) after injection of ICG-^{99m}Tc-nanocolloid. All 183 preoperatively defined SNs could be localized using a combination of radio- and fluorescence guidance. Only one blue node was found during surgery that was neither radioactive nor fluorescent. This node was also considered a SN and harvested.

Post-excision imaging with the portable gamma camera revealed remaining activity at the location of the previously excised SN in 22 of 65 patients (33.8%). In these patients, the area was explored once again, yielding 37 additional SNs. In six of these cases, a remaining SN was identified using the portable gamma camera after no residual activity was detected during initial scanning with the gamma probe (Figure 5).

Of the total of 221 excised SNs (Table 2, Figure 6), 97.3% could be roughly localized using the gamma probe. The remaining 2.7% (in four patients) could not be detected using the gamma probe because the radioactive signal was too weak due to radioactive decay (surgery was performed >24 h after tracer injection and relatively low tracer uptake in these SNs was observed on preoperative images). These nodes were localized using fluorescence imaging, which does not suffer from decay.

In total, 96.8% of the excised SNs were intraoperatively visualized with the fluorescence camera during surgery; 55.7% had stained blue at the time of excision. This means that 41.1% more SNs could be optically identified via fluorescence imaging ($p<0.0001$). In only 22 patients, all of the preoperatively defined radioactive SNs were also stained blue. In eight patients, no blue SN was found at all, whereas a fluorescent SN could be visualized in every patient. Fluorescence imaging offered an improved tissue penetration compared with blue dye, allowing earlier visualization of the SNs. This was exemplified by cases in which superficially located SNs were visible through the skin (Figure 3).

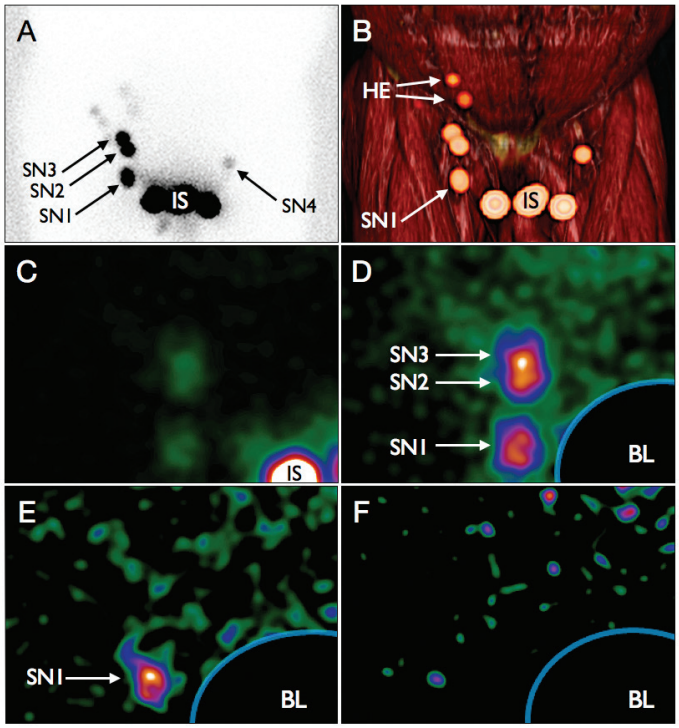

Figure 5. Post-excision confirmation of complete sentinel node removal using a portable gamma camera. A) Lymphoscintigram showing the injection site (IS) and three SNs on the right side and on SN on the left side; B) 3D volume-rendered SPECT/CT image revealing that the most caudal SN on the right side is located in an inferior Daseler zone; C) Initial image acquired with the portable gamma during surgery mainly depicting the high radioactive signal coming from the injection site (IS); D) Blocking the injection site using the Sentinella suite software visualizes the three SNs on the right side; E) Post-excision image after removal of three radioactive and fluorescent nodes shows that the most caudal SN is still in situ; F) After excision of the remaining SN, which proved to be tumor-positive at histopathology, complete SN removal is verified. SN = sentinel node; HE = higher-echelon node; BL = blocked injection site using Sentinella suite software. 3D = three-dimension, IS = injection site.

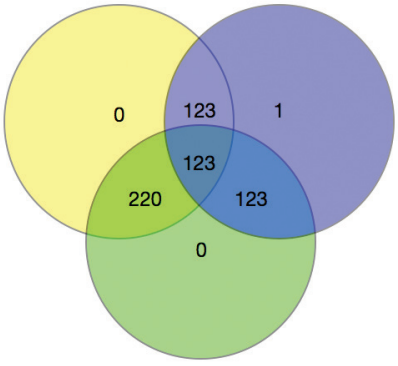

Figure 6. Ex vivo sentinel node evaluation. Excised nodes were radioactive (yellow circle), fluorescent (green circle) and/or blue (blue circle). Of the excised SNs, 220 were both radioactive and fluorescent. Of these SNs 123 were also blue. Only one SN was non-radioactive, non-fluorescent, but blue. SN = sentinel node.

HISTOPATHOLOGY FINDINGS AND EX VIVO ANALYSES

Pathologic analyses of the excised SNs revealed metastases in 10 SNs (seven of 65 patients (19.8%), seven of 119 groins (6%)). Three patients with a tumor-positive SN also had a tumor-positive node at ultrasound guided fine needle aspiration cytology in the contralateral groin, for which they received an LND in the same session. All seven patients with a tumor-positive SN were scheduled for an LND of the affected groin.

The median size of the SN metastases was 8 mm (mean: 7.94 mm; range: 1.5-14 mm). In one patient, one of the tumor-positive SNs was an additional SN, which was excised after being identified using the portable gamma camera (Figure 5). While all 10 tumor-positive SNs were both radioactive and fluorescent only seven stained blue. The single non-radioactive and non-fluorescent SN that was blue was tumor-negative.

Additional ex vivo examination of four tumor-positive SNs revealed that the fluorescent signal was mainly present in the unaffected lymphatic tissue of the SN (Figure 7).

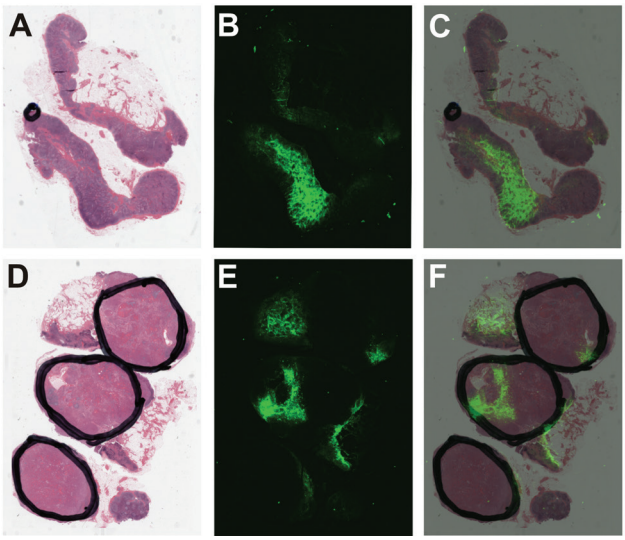

Figure 7. Ex vivo examination of the fluorescent signal in tumor-positive sentinel nodes. A) A SN containing a micrometastases (black circle); B-C) Ex vivo fluorescence imaging reveals that the fluorescent signal is mainly present in the remaining unaffected lymphatic tissue of the node; D) A SN containing a macrometastases (black circle); E-F) Ex vivo fluorescence imaging.

DISCUSSION

SN biopsy for penile carcinoma, using a radiocolloid (^{99m}Tc-nanocolloid) in combination with blue dye, is a well-established procedure to accurately stage clinically node-negative groins [7,15,18]. Here, we demonstrate that the hybrid tracer ICG-^{99m}Tc-nanocolloid improves optical SN detection in comparison with blue dye. In our series of 65 patients, all of whom were injected with both the hybrid tracer ICG-^{99m}Tc-nanocolloid and blue dye, 96.8% of the SNs could be intraoperatively visualized using fluorescence imaging, whereas merely 55.7% of the SNs were stained blue at time of excision ($p<0.0001$). This statistically significant difference suggests that optical SN detection using ICG-^{99m}Tc-nanocolloid can potentially replace blue dye. The low percentage of blue-stained nodes identified in this study is in line with a recent meta-analysis of 19 studies by Sadeghi et al. that reported a pooled SN detection rate of 60% for blue dye alone [7].

There are several potential explanations as to why >40% of the SNs that were identified using ICG-^{99m}Tc-nanocolloid were not stained blue. Consistent with previous reports in areas with rapid lymphatic drainage (e.g., the head-and-neck region), the blue dye may already have passed the SN at the time of excision [13,19]. However, lymphatic drainage in penile carcinoma can also be more delayed, as demonstrated by the limited number of visualized SNs on early lymphoscintigraphy in this series. Hence, the blue dye may not yet have reached the SN at the time of excision in some cases. Together these factors limit the diagnostic window and potentially require timed (re-)injections prior to, or during, the operation. It is also important to note that only 70% of the tumor-positive SNs identified with ICG-^{99m}Tc-nanocolloid stained blue, whereas the single SN (0.45%) that was blue, but did not contain ICG-^{99m}Tc-nanocolloid, was tumor-negative.

SN distribution in this study was similar to a previous anatomic SN mapping study using SPECT/CT, showing that drainage was mainly directed to the superior and central inguinal zones [5]. The current study further substantiates results from a previous reproducibility study showing that ICG-^{99m}Tc-nanocolloid preserves the gold standard in preoperative SN mapping (lymphoscintigraphy and SPECT/CT) [11]. The addition of the fluorescent moiety extends the window for optical SN detection using fluorescence imaging up to (or possibly even beyond) 27 h after tracer injection. This enables the use of ICG-^{99m}Tc-nanocolloid in both one- and two-day protocols, without the need for additional injections during surgery.

Ex vivo fluorescence imaging confirmed the presence of fluorescence in all radioactive SNs. Therefore, the 3.2% of SNs that could not be visualized intraoperatively using the near-infrared fluorescence camera were probably covered with overlying (fatty) tissue so the fluorescent signal was blocked. This illustrates that while the tissue penetration of near-infrared fluorescence imaging is superior to blue dye, it is still limited compared with the radioactive signal. This is further demonstrated by the finding that SNs were only visible through the skin when located superficially in patients with a low body mass index (Figure 3), which is in line with a previous report on the use of ICG in patients with vulvar

cancer [20]. Improvement of near-infrared fluorescence camera systems may help further expand the applicability of intraoperative fluorescence guidance [21]. For the time being, the radioactive signature of the hybrid tracer still remains crucial to enable reliable SN mapping. For example, the ability to acquire an overview image with the portable gamma camera during surgery allowed the identification of residual SNs that could have been missed with the gamma probe or near-infrared fluorescence camera (Figure 5), thereby providing confirmation of complete SN removal in the operating room.

The fluorescent signature of ICG-^{99m}Tc-nanocolloid provides the unique possibility to study tracer distribution in ex vivo tissue specimens, long after the radioactive signal has decayed [22]. In this study, ex vivo imaging using a sensitive fluorescence camera confirmed the presence of a fluorescent signal in all tumor-positive SNs with metastases ≤14 mm (Figure 7). Apparently, when unaffected lymphatic tissue is still present, the presence of tumor tissue in a node does not necessarily cause rerouting of the lymph flow [23].

CONCLUSION

ICG-^{99m}Tc-nanocolloid allows for combined radio- and fluorescence-guided SN biopsy in penile carcinoma patients while retaining the properties of the radiocolloid that are optimal for preoperative SN identification using lymphoscintigraphy and SPECT/CT. The fluorescent component significantly improved intraoperative optical SN identification compared with blue dye, indicating that by using this hybrid approach, blue dye may be omitted.

SURGERY IN MOTION

The Surgery in Motion video accompanying this article can be found in the online version at http://dx.doi.org/10.1016/j.eururo.2013.11.014 and via www.europeanurology.com.

REFERENCES

1. Cabanas RM. Anatomy and biopsy of sentinel lymph nodes. Urol Clin North Am. 1992;19:267-76.
2. Horenblas S, Jansen L, Meinhardt W, et al. Detection of occult metastasis in squamous cell carcinoma of the penis using a dynamic sentinel node procedure. J Urol. 2000;163:100-4.
3. Leijte JAP, Hughes B, Graafland NM, et al. Two-center evaluation of dynamic sentinel node biopsy for squamous cell carcinoma of the penis. J Clin Oncol. 2009;27:3325-9.
4. Kroon BK, Horenblas S, Estourgie SH, et al. How to avoid false-negative dynamic sentinel node procedures in penile carcinoma. J Urol. 2004;171:2191-4.

5. Leijte JAP, Valdés Olmos RA, Nieweg OE, et al. Anatomical mapping of lymphatic drainage in penile carcinoma with SPECT-CT: implications for the extent of inguinal lymph node dissection. Eur Urol. 2008;54:885-90.
6. Vermeeren L, Valdés Olmos RA, Meinhardt W, et al. Intraoperative radioguidance with a portable gamma camera: a novel technique for laparoscopic sentinel node localisation in urological malignancies. Eur J Nucl Med Mol Imaging. 2009;36:1029-36.
7. Sadeghi R, Gholami H, Zakavi SR, et al. Accuracy of sentinel lymph node biopsy for inguinal lymph node staging of penile squamous cell carcinoma: systematic review and meta-analysis of the literature. J Urol. 2012;187:25-31.
8. Vahrmeijer AL, Frangioni JV. Seeing the invisible during surgery. Br J Surg. 2011;98:749-50.
9. van Leeuwen AC, Buckle T, Bendle G, et al. Tracer-cocktail injections for combined pre- and intraoperative multimodal imaging of lymph nodes in a spontaneous mouse prostate tumor model. J Biomed Opt. 2011;16:016004.
10. Buckle T, van Leeuwen AC, Chin PTK, et al. A self-assembled multimodal complex for combined pre- and intraoperative imaging of the sentinel lymph node. Nanotechnology. 2010;21:355101.
11. Brouwer OR, Buckle T, Vermeeren L, et al. Comparing the hybrid fluorescent-radioactive tracer indocyanine green-^{99m}Tc-nanocolloid with ^{99m}Tc-nanocolloid for sentinel node identification: a validation study using lymphoscintigraphy and SPECT/CT. J Nucl Med. 2012;53:1034-40.
12. van der Poel HG, Buckle T, Brouwer OR, et al. Intraoperative laparoscopic fluorescence guidance to the sentinel lymph node in prostate cancer patients: clinical proof of concept of an integrated functional imaging approach using a multimodal tracer. Eur Urol. 2011;60:826-33.
13. Brouwer OR, Klop WMC, Buckle T, et al. Feasibility of sentinel node biopsy in head and neck melanoma using a hybrid radioactive and fluorescent tracer. Ann Surg Oncol. 2012;19:1988-94.
14. van den Berg NS, Brouwer OR, Klop WMC, et al. Concomitant radio- and fluorescence-guided sentinel lymph node biopsy in squamous cell carcinoma of the oral cavity using ICG-(^{99m})Tc-nanocolloid. Eur J Nucl Med Mol Imaging. 2012;39:1128-36.
15. Pizzocaro G, Algaba F, Horenblas S, et al. EAU penile cancer guidelines 2009. Eur Urol. 2010;57:1002-12.
16. Valdés Olmos RA, Vidal Sicart S. SPECT/CT image generation and criteria for sentinel node mapping. In: Mariani G, Manca G,Orisini F, Vidal Sicart S, Valdés Olmos RA (eds). Atlas of lymphoscintigraphy and sentinel node mapping. Milan: Springer-Verlag, 2012:111-9.
17. Vermeeren L, Valdés-Olmos RA, Klop WMC, et al. A portable gamma-camera for intraoperative detection of sentinel nodes in the head and neck region. J Nucl Med. 2010;51:700-3.

18. Djajadiningrat RS, Graafland NM, van Werkhoven E, et al., Contemporary management of regional nodes in penile cancer-improvement of survival? J Urol. 2014;191:68-73.
19. Chao C, Wong SL, Edwards MJ, et al. Sentinel lymph node biopsy for head and neck melanomas. Ann Surg Oncol. 2003;10:21-6.
20. Crane LMA, Themelis G, Arts HJG, et al. Intraoperative near-infrared fluorescence imaging for sentinel lymph node detection in vulvar cancer: first clinical results. Gynecol Oncol. 2011;120:291-5.
21. van den Berg NS, van Leeuwen FWB, van der Poel HG. Fluorescence guidance in urologic surgery. Curr Opin Urol. 2012;22:109-20.
22. Buckle T, Brouwer OR, Valdés Olmos RA, et al. Relationship Between Intraprostatic Tracer Deposits and Sentinel Lymph Node Mapping in Prostate Cancer Patients. J Nucl Med. 2012;53:1026-33.
23. Leijte JAP, van der Ploeg IMC, Valdés Olmos RA, et al. Visualization of tumor blockage and rerouting of lymphatic drainage in penile cancer patients by use of SPECT/CT. J Nucl Med. 2009;50:364-7.

CHAPTER 6

MULTIMODAL SURGICAL GUIDANCE DURING SENTINEL NODE BIOPSY FOR MELANOMA: COMBINED GAMMA TRACING AND FLUORESCENCE IMAGING OF THE SENTINEL NODE THROUGH USE OF THE HYBRID TRACER ICG-^{99M}TC-NANOCOLLOID

Adapted from: van den Berg NS, Brouwer OR, Schaafsma BE, Mathéron HM, Klop WMC, Balm AJM, van den Brekel MWM, van Tinteren H, Nieweg OE, van Leeuwen FWB, Valdés Olmos RA. Radiology. 2015:275;530-537.

ABSTRACT

PURPOSE To evaluate the hybrid approach in a large population of patients with melanoma in the head-and-neck, on the trunk, or on an extremity who were scheduled for sentinel node (SN) biopsy.

MATERIALS AND METHODS This prospective study was approved by the institutional review board. Between March 2010 and March 2013, 104 patients with a melanoma, including 48 women (average age: 54.3 years; range 18.5-87.4) and 56 men (average age: 55.2 years; range 22.4-77.4) (p=0.76) were enrolled after obtaining written informed consent.

Following intradermal hybrid tracer administration, lymphoscintigraphy and single photon emission computed tomography combined with computed tomography were performed. Blue dye was intradermally injected prior to the start of the surgical procedure (not in patients with a facial melanoma). Intraoperatively, SNs were initially pursued via gamma tracing followed by fluorescence imaging and, when applicable, blue dye detection. A portable gamma camera was used to confirm SN removal. Collected data included the number and location of the pre- and intraoperatively identified SNs, and the intraoperative number of SNs that were radioactive, fluorescent, and/or blue. A two-sample test for equality of proportions was performed to evaluate differences in intraoperative SN visualization through fluorescence imaging and blue dye detection.

RESULTS Preoperative imaging revealed 2.4 SNs (range 1-6) per patient. Intraoperatively, 93.8% (286 of 305) of the SNs were radioactive, 96.7% (295 of 305) of the SNs were fluorescent, while only 61.7% (116 of 188) of the SNs stained blue ($p<0.0001$). Fluorescence imaging was of value for the identification of near-injection site SNs (two patients), SNs located in complex anatomic areas (head-and-neck (28 patients)), and SNs that failed to accumulate blue dye (19 patients).

CONCLUSION The hybrid tracer enables both preoperative SN mapping and intraoperative SN identification in melanoma patients. In the setup of this study, optical identification of the SNs through the fluorescent signature of the hybrid tracer was superior compared with blue dye-based SN visualization.

INTRODUCTION

Sentinel node (SN) biopsy has evolved into a routine procedure to determine the presence of lymph node metastasis, allowing melanoma patients with nodal metastasis to be treated in a relatively early phase of their disease. Generally, for SN biopsy a combination of technetium-99m (^{99m}Tc)-labeled colloid and blue dye is used. Where radiolabeled colloids enable preoperative SN mapping and intraoperative detection of these particular SNs by using a handheld gamma ray detection probe (hereafter referred to as gamma probe) [1], intraoperative administration of a blue dye can allow the surgeon to optically identify SNs by visualizing their afferent lymphatic vessels. Although successful, this approach has limitations [2]. A deeply located blue lymph vessel may be difficult to find, and its dissection requires substantial expertise. Occasionally, blue dye causes an allergic reaction and it can stain the injection site for months [3,4]. Also, SNs do not always take up blue dye, particularly in the neck. Consequently, the false-negative rate of SN biopsy in melanoma patients is high, 9-21% [5,6].

For radiologically guided SN identification in the preoperative setting, single photon emission computed tomography combined with computed tomography (SPECT/CT) was shown to help place SNs in their anatomic context, enabling better planning of the operation [7-9]. In the surgical suite, the introduction of a portable gamma camera complemented the traditional acoustic guidance provided by the gamma probe [10].

The introduction of near-infrared fluorescence imaging of indocyanine green (ICG) was shown to provide an alternative mode of optical SN identification during the operation [11-16]. Because the near-infrared window lies beyond the visible spectrum, ICG can only be visualized by using a dedicated near-infrared fluorescence camera. Consequently, the use of ICG does not alter the surgical field, nor does it cause tattooing effects of the skin, as does blue dye. However, similar to blue dye, ICG migrates quickly through the lymphatic system, resulting in a limited diagnostic detection window [17]. Although the sensitivity of the signal detection is improved considerably when ICG is used instead of blue dye, the penetration depth of a near-infrared fluorescence dye (<1.0 cm) still prevents preoperative SN mapping.

The hybrid tracer ICG-^{99m}Tc-nanocolloid was developed to combine the attractive migrational properties of a radiolabeled colloid with the favorable optical imaging features of ICG [17,18]. Because of its long-lasting retention in the SNs, a single injection with this hybrid tracer allows preoperative SN mapping and intraoperative radioguided SN identification in a similar fashion as its parental compound ^{99m}Tc-nanocolloid [19]. In addition, it allows fluorescence imaging-based SN visualization of the preoperatively identified SNs. Previously we demonstrated the feasibility of this hybrid approach in various pilot studies [19-25]. In our current study, we evaluated the hybrid approach in a large population of patients with melanoma in the head-and-neck, on the trunk, or on an extremity that were scheduled for SN biopsy.

MATERIALS AND METHODS

PATIENTS

The study protocol was approved by the institutional review board of the Dutch Cancer Institute-Antoni van Leeuwenhoek Hospital (Amsterdam, the Netherlands).

Between March 2010 and March 2013, patients were prospectively included after obtaining written informed consent. Patient inclusion criteria were as follows: (a) age 18 years or older; (b) histologically proven melanoma in the head-and-neck, on the trunk, or on an extremity (Breslow thickness of at least 1.0 mm); (c) no tumor-positive lymph nodes in the regional lymph node basin, as defined by palpation and ultrasonography-guided fine needle aspiration cytology examination; and (d) scheduled for SN biopsy and repeat excision of the melanoma site. Exclusion criteria were as follows: (a) pregnant or breast-feeding woman (in our study no patients were excluded on this basis); (b) patients with a known allergy to iodine (in our study no patients were excluded on this basis); and (c) fluorescence imaging was not performed intraoperatively; because of scheduling logistics, there was no fluorescence camera available in the operating room (in our study 17 patients were excluded on this basis).

Our population consisted of 104 patients, including 48 women (average age: 54.3 years, range 18.5-87.4) and 56 men (average age: 55.2 years; range 22.4-77.4) (p=0.76), with an average Breslow thickness of 2.7 mm (range 1.0-10.0 mm). The first 13 patients were also included in previous feasibility trials [19,21].

TRACER PREPARATION

ICG-^{99m}Tc-nanocolloid (size 10-100 nm) was prepared via non-covalent self-assembly of ^{99m}Tc-labeled nanocolloid (GE Healthcare, Eindhoven, the Netherlands) and ICG (Pulsion Medical Systems, Munich, Germany), as previously described [20].

^{99m}Tc-nanocolloid is approved for lymphatic mapping by the European Medicines Agency, and ICG is used off-label for this application but is U.S. Food and Drug Administration approved for intravenous use (up to 2.0 mg/kg body weight). In the ICG-^{99m}Tc-nanocolloid complex, the ratio of ICG to human serum albumin is 18:1 [26]. While the amount of ^{99m}Tc-nanocolloid is identical to that used for radioguided SN biopsy [19], the dose of ICG used (<0.05 mg) is substantially lower than the amount of ICG allowed for intravenous use.

PREOPERATIVE PROCEDURE

Operating room logistics aided in determining whether the patient was injected with the hybrid tracer on the day before, or on the morning of, the operation. An average of 78.5 MBq (range 57.4-112.9 MBq) of ICG-^{99m}Tc-nanocolloid was intradermally injected around the melanoma site (four deposits; total volume, 0.4 mL). This variability is tracer-decay-dependent and was influenced by the time the volume for injection was extracted from the vial.

To visualize the draining lymphatic vessels and the first draining lymph nodes, during the first 10 min after injection, anterior and lateral dynamic lymphoscintigraphy was performed by using a dual-head gamma camera (Symbia T; Siemens, Erlangen, Germany). This step was followed by acquisition of static planar lymphoscintigrams at 15 min after injection. At 2 h after injection, again static planar lymphoscintigrams were obtained, followed by SPECT and low-dose CT (40 mAs, 130 kV) (Symbia T; Siemens) acquisitions. After correction for scatter and tissue attenuation, SPECT and CT images were fused. Multiplanar reconstruction enabled comparison of fused SPECT/CT images with concomitant CT images (Osirix medical imaging software; Pixmeo, Geneva, Switzerland). One author (R.A.V.O., with 21 years of experience with SN biopsy for melanoma) and three other nuclear medicine physicians who are not authors of our study (with 7, 10, and 14 years of experience with SN biopsy) evaluated the acquired imaging data for the number of SNs visualized, and the basin in which the SN was located. Lymph nodes on a direct drainage pathway from the site of injection were classified as SNs (hereafter referred to as preoperative SNs) [27,28].

SURGICAL PROCEDURE

Before the start of the operation, 1.0 mL of blue dye V (Laboratoire Guerbet, Aulnay-Sous-Bois, France) was injected intradermally around the melanoma site (circular injection) in the patients with melanoma located outside the facial area (n=69). Operations were performed by three authors (W.M.C.K., A.J.M.B., O.E.N., with 7, 7, and 21 years of experience with SN biopsy for melanoma, respectively) and others who are not authors of our study.

Generally, SN biopsy was performed before excision of the melanoma site. However, in 44 patients with a head-and-neck melanoma, the surgeon removed the melanoma site prior to performing SN biopsy; here, the surgeon reasoned that leaving the melanoma site in situ would affect radioactivity-based SN identification because of the high background signal coming from the injected melanoma site.

Preceding the start of SN biopsy, an overview image of the radioactive hot spots was acquired by using a portable gamma camera (Sentinella; Oncovision, Valencia, Spain) [10]. Preoperative SNs were initially pursued with the gamma probe (Neoprobe; Johnson & Johnson Medical, Hamburg, Germany), and when possible, attempts were made to visualize the tumor draining lymphatic vessels via blue dye. Alternating attempts were then made to optically visualize the preoperative SN through fluorescence imaging by using a handheld near-infrared fluorescence camera (PhotoDynamic Eye; Hamamatsu Photonics K.K., Hamamatsu, Japan) and, when applicable, visual detection of blue dye. Fluorescence imaging required the lights in the operating room to be dimmed to minimize the background signal.

To verify complete preoperative SN removal, after excision of the preoperative SNs, another portable gamma camera image was acquired. If residual radioactivity was

observed at the site of a previously excised SN, the node was considered part of a cluster of multiple adjacent SNs. Since it is not possible to discriminate between nodes in a cluster, these nodes were considered to be additional intraoperative SNs and also were harvested using the above described combination. In case of clustered nodes, after the operation, the acquired SPECT and CT images were retrospectively evaluated for visibility of these clusters on the images by three authors (R.A.V.O., O.R.B., N.S.v.d.B., with 21, 5, and 3 years of experience, respectively).

Prior to closing, the wound area was evaluated for non-radioactive non-fluorescent but blue nodes and palpated for enlarged lymph nodes suspicious for metastasis that were not radioactive, fluorescent, or blue.

Intraoperatively, SNs were classified for being radioactive (yes or no), fluorescent (yes/no), or blue (yes/no) by the surgeon (W.M.C.K., A.J.M.B., O.E.N., and others who are not authors of our study. The data were collected by a clinical researcher (N.S.v.d.B., O.R.B., B.E.S., H.M.M., with 3 years, 5 years, 3 years, and 1 year of experience with image-guided SN biopsy, respectively).

HISTOPATHOLOGY AND EX VIVO ANALYSES

Excised SNs were formalin fixed, bisected, and paraffin embedded, and they were cut at a minimum of six levels at 50-150 µm intervals. Histopathological evaluation was performed by a pathologist (3-20 years of experience) and included staining (hematoxylin and eosin (S-100, catalog no. Z0311; Dako, Heverlee, Belgium) and MART-1 (catalog no. M7196; Dako)).

STATISTICAL ANALYSIS

A two-sample test for equality of proportions with continuity correction (R version 3.0.2; www.r-project.org) was performed to evaluate the difference in average age between male and female patients and to evaluate differences in the number of fluorescent and blue nodes in the overall population and for each subgroup. A p-value <0.05 was considered to indicate a significant difference.

RESULTS

PREOPERATIVE RESULTS

A total of 246 SNs were preoperatively identified in 104 patients (average 2.4 preoperative SNs per patient; range 1-6; Table 1). A SPECT/CT scan was acquired in all patients, and in all but one patient, this scan provided useful anatomic landmarks that facilitated virtual planning of the surgical procedure. In the remaining patient, the portable gamma camera was used to locate a pre-auricular SN close to the injection site that was not seen on the acquired lymphoscintigrams or on the SPECT/ CT images.

Table 1. Preoperative sentinel node mapping results

	Overall			
Primary melanoma location		***Head-and-Neck***	***Trunk***	***Extremity***
# Patients	104	53	33	18
Total # SNs visualized (av; range)	246 (2.4; 1-6)	137 (2.6; 1-6)	76 (2.3; 1-4)	33 (1.8; 1-3)
- Lymphoscintigraphy (% total)	232/246 (94.3%)	127/137 (92.7%)	73/76 (96.1%)	32/33 (97.0%)
- SPECT/CT (% total)	245/246 (99.6%)	136/137 (99.3%)	76/76 (100.0%)	33/33 (100.0%)
- Portable gamma camera (% total)	1/246 (0.4%)	1/137 (0.7%)	-	-
Total # basins in which SNs were visualized (av; range)	183 (1.8; 1-6)	111 (2.1; 1-5)	53 (1.6; 1-4)	19 (1.1; 1-2)
Distribution of SNs visualized according to basins				
- Suboccipital	8/183 (4.4%)	8/111 (7.2%)	-	-
- Temporal	1/183 (0.5%)	1/111 (0.9%)	-	-
- Parotid gland	8/183 (4.4%)	8/111 (7.2%	-	-
- Retro- or pre-auricular	18/183 (9.8%)	18/111 (16.2%)	-	-
- Neck	75/183 (41.0%)	74/111 (66.7%)	1/53 (1.9%)	-
- Supraclavicular	4/183 (2.2%)	2/111 (1.8%)	2/53 (3.8%)	-
- Scapular	2/183 (1.1%)	-	2/53 (3.8%)	-
- Pectoral	1/183 (1.1%)	-	1/53 (1.9%)	-
- Epitrochlear	1/183 (1.1%)	-	-	1/19 (5.3%)
- Axilla	44/183 (24.0%)	-	40/53 (75.5%)	4/19 (21.1%)
- Intermediate trunk	1/183 (0.5%)	-	1/53 (1.9%)	-
- Groin	20/183 (10.9%)	-	6/53 (11.3%)	14/19 (73.7%)

= number; SPECT/CT = single photon emission computed tomography combined with computed tomography; SN = sentinel node; av = average.

INTRAOPERATIVE RESULTS

In the one-day protocol, the surgical procedure started, on average, 5 h after injection (range 3-10 h after injection; 58 patients). In the two-day protocol, the procedure started approximately 21 h after injection (range 18-27 hours after injection; 46 patients).

All but four preoperatively identified SNs could be intraoperatively localized through the combined use of gamma tracing, fluorescence imaging, or blue dye guidance. In 33 patients, 59 additional SNs (intraoperatively identified SNs) were excised on the basis of the combination of gamma detection and fluorescence imaging. Re-analysis of the respective CT images revealed the presence of clustered nodes located at the location of a single hot spot on the corresponding SPECT images (Figures SI1-3). Intraoperatively, in total, 301 SNs were harvested (average 2.9 SNs per patient; range, 1-9(; (Table 2).

Table 2. Intraoperative sentinel node detection

	Overall (104 patients	***No blue dye used (35 patients)***	***Blue dye used (69 patients)***						
			Injection site first (13 patients)	***Sentinel node biopsy first (56 patients)***					
									Total
Basin		***Head-and-Neck[±]***	***Other[@]***	***Head-and-Neck[±]***	***Head-and-Neck[±]***	***Axilla***	***Groin***	***Aberrant[%]***	***Other[@]***	
# Excised SNs	301	112	2	49	18	72	38	6	4	138
# Not-excised SNs	4	3	-	-	-	1	-	-	-	1
Total	305	115	2	49	18	73	38	6	4	139
Intraoperative SN detection										
- With gamma tracing	286/305 (93.8%)	102/115 (88.6%)	2/2 (100.0%)	46/49 (93.9%)	17/18 (94.4%)	71/73 (97.3%)	38/38 (100.0%)	6/6 (100.0%)	4/4 (100.0%)	136/139 (97.8%)
- With fluorescence guidance	295/305 (96.7%)	111/115 (96.5%)	2/2 (100.0%)	49/49 (100.0%)	16/18 (88.9%)	69/73 (94.5%)	38/38 (100.0%)	6/6 (100.0%)	4/4 (100.0%)	133/139 (95.7%)
- With blue dye visualization	116/188 (61.7%)	-	-	19/49 (38.8%)	4/18 (22.2%)	54/73 (74.0%)	35/38 (92.1%)	2/6 (33.3%)	2/2 (50.0%)	97/139 (69.8%)
p-value[$]	p<0.0001	-	-	p<0.0001	p=0.0002	p=0.0008	p=0.24	p=0.14	p=0.41	p<0.0001

[±] head-and-neck includes subocciptial, temporal, retro- and pre-auricular basins, the parotid gland, and the neck basins. [@] Other includes supraclavicular and epitrochlear basins. [%] Abberant includes intermediate trunk, pectoral, and scapular basins. [$] Two-sample test for equality of proportions with continuity correction between detection by fluorescence imaging and visual blue dye detection. # = number; pts = patients; SN = sentinel node.

In the overall population, 93.8% (286 of 305) of the excised SNs could be intraoperatively localized with gamma tracing by using the gamma probe. Optical identification of the SNs with fluorescence imaging identified 96.7% (295 of 305) of the nodes, while only 61.7% (116 of 188) of the SNs had stained blue at the time of excision ($p<0.0001$; Table 2). Intraoperatively, no SNs were found that were solely blue.

To allow continuous drainage after the intraoperative injection of blue dye, SN biopsy is ideally performed before repeat excision of the melanoma site. Looking more closely at this specific subset of patients (Table 2, "Blue dye used" columns, "SNB first" column, "Total" column), merely 69.8% (97 of 139) of the SNs were blue at the time of excision, whereas fluorescence imaging allowed visualization of 95.7% (133 of 139) of the SNs ($p<0.0001$).

In 23 patients with drainage to the head-and-neck and two patients with drainage to the groin, fluorescence imaging allowed the surgeon to determine the exact location of the preoperative SNs. Fluorescence imaging was used by the surgeon to pinpoint the preoperative SNs with a forceps in eight of these 25 patients. In five of these patients, preoperative SNs were already visualized transcutaneously (Figure 1), allowing the surgeon to determine the site of incision.

In five patients, fluorescence imaging aided in the localization of the preoperative SN as radioactivity-based detection of the preoperative SNs was not possible because of the high background signal coming from the nearby injection site. In four of these five patients, the preoperative SN was located in the parotid gland (melanoma site, temporal bone (n=3) or preauricular area (n=1)) and in the other patient, the preoperative SN was located in level III (melanoma site, cheek).

Fluorescence imaging confirmed gamma probe-based localization of the preoperative SNs when no blue dye was used (n=3 patients) but also allowed for optical identification of preoperative SNs that failed to take up blue dye (n=19 patients; Figures 2, 3). In three patients, through fluorescence imaging the lymphatic duct running to the preoperative SN could be visualized (Figures 3, 4).

Pathologic analysis of the excised nodes revealed 36 SN metastases in 25 patients. Nodal involvement was found in 15.1% (eight of 53), 33.3% (11 of 33), and 33.3% (six of 18) of patients with head-and-neck melanoma, melanoma of the trunk, or on an extremity, respectively. In five patients with a melanoma on the trunk, aberrant drainage was seen. In two of these five patients, the aberrantly located SN was the only tumor-positive node.

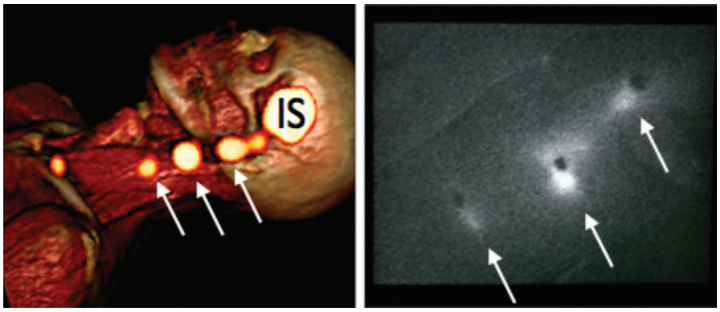

Figure 1. Transcutaneous sentinel node identification through fluorescence imaging in a 70-year-old female with melanoma on the head (temporal left; Breslow thickness 2.0 mm). The patient was scheduled for re-excision of the melanoma scar and subsequent SN biopsy. Due to the location of the melanoma, no blue dye was injected intraoperatively. Left) 3D SPECT/CT-based volume rendering after cropping of the skin. The image shows three SNs (white arrows); Right) Intraoperative fluorescence imaging visualized the temporal, pre-auricular and level II SN already transcutaneously. SN = sentinel node; SPECT/CT = single photon emission computed tomography combined with computed tomography.

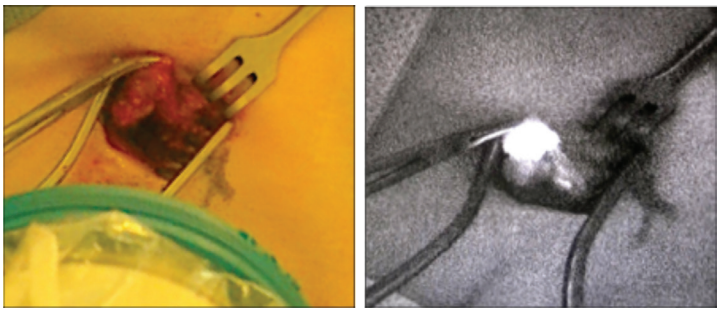

Figure 2. Optical sentinel node identification via fluorescence imaging in a 25-year-old female with a melanoma of the trunk (on the back, paramedian; Breslow thickness 1.1 mm). The patient was scheduled for re-excision of the melanoma scar and subsequent SN biopsy. Preoperatively two SNs were visualized (left and right axilla). Directly before the start of the operation 1.0 mL blue dye was injected. Left) Axillary tissue harbouring the SN; Right) Fluorescence imaging-based identification of the SN which did not stain blue. SN = sentinel node.

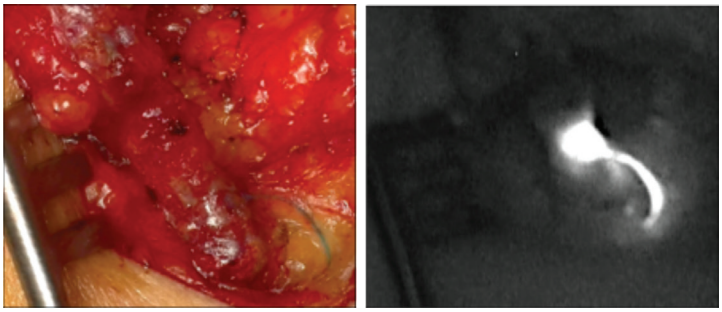

Figure 3. Optical sentinel node identification vial fluorescence imaging in a 20-year-old female with a melanoma of the trunk (abodomen, paramedian right; Breslow thickness 1.1 mm). The patient was scheduled for re-excision of the melanoma scar and subsequent SN biopsy. Preoperatively three SNs were visualizd (right and left groin and in the right axilla). Directly before the start of the operation 1.0 mL blue dye was injection. Left) Identification of a blue afferent lymphatic duct running to a SN in the left groin; Right) Fluorescence imaging-based identification of the SN and its afferent lymphatic duct. SN = sentinel node.

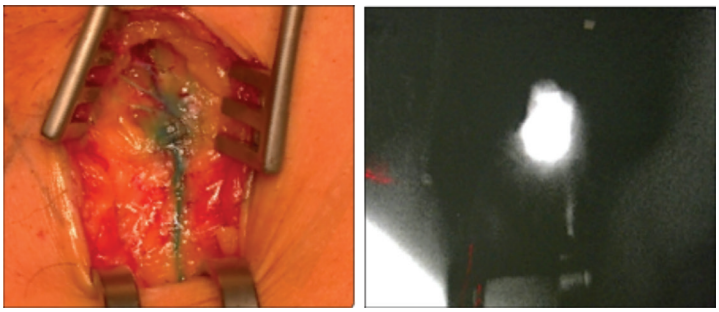

Figure 4. Optical sentinel node identification in a 51-year-old female patient with a melanoma of an extremity (left upper leg; Breslow thickness 2.0 mm). The patient was scheduled for re-excision of the melanoma scar and subsequent SN biopsy. Preoperatively a SN was visualized in the left groin. Directly before the start of the operation 1.0 mL blue dye was injected. Left) Clear blue dye-based visualization of the afferent lymphatic duct running to the blue stained SN; Right) Fluorescence imaging-based visualization of the same SN and its afferent lymphatic duct. SN = sentinel node.

DISCUSSION

Our study in 104 patients with melanoma confirms what previous feasibility studies suggested, namely that the hybrid approach, making use of ICG-^{99m}Tc-nanocolloid, provides improved intraoperative guidance toward preoperative SNs; with additional fluorescence imaging during surgery, 35.1% more SNs could be optically visualized than with blue dye (in the group of patients in which blue dye was used, fluorescence imaging allowed visualization of 182 of 188 SNs (96.8%), whereas with blue dye, 116 of 188 SNs (61.7%) were visualized).

Overall, the percentage of SNs that could be identified during the operation by using gamma tracing and fluorescence imaging was comparable (93.8% (286 of 305) and 96.7% (295 of 305), respectively). The finding that SNs were more often fluorescent than blue (96.7% (295 of 305) vs. 61.7% (116 of 188), respectively; $p<0.0001$) may imply a superior optical identification rate for the hybrid tracer in comparison with conventional blue dye. This advantage was most pronounced in patients with drainage to the head-and-neck.

In our study, we did not solely rely on intraoperative fluorescence imaging to identify the preoperative SNs; rather, the hybrid approach was taken in which preoperative images provided a roadmap for initial surgical exploration. Results of recent studies with the use of 'free' ICG further underline the value of preoperative imaging by stating that in-depth SN identification provided by radiolabeled colloids is superior to that provided by ICG [13,14]. Namikawa et al. [14] showed that, especially in patients with axillary SNs or patients with a high body mass index, fluorescence imaging alone was found insufficient. In addition, preoperative SN mapping also allows the identification of aberrant drainage profiles, which might be missed when only fluorescence imaging is performed.

The intraoperative detection of additional intraoperative SNs is not uncommon, but it is striking that, in our overall study population, 19.3% (59 of 305) additional SNs were intraoperatively identified through the combined use of gamma detection (using a portable gamma camera and gamma probe) and fluorescence imaging. Previous studies from our institute showed that, with the conventional approach (gamma probe and blue dye), next to the preoperatively identified SNs, 8-11.6% additional SNs were harvested [8,29,30]. Because leaving an SN behind constitutes one of the possible causes for false-negative results, this finding indicates that thorough confirmation of SN removal (e.g. by using a portable gamma camera) remains of importance. Retrospective analysis suggests that more careful evaluation of the preoperatively acquired CT and corresponding SPECT images may have helped to better predict the number of preoperative SNs in that area.

While the particle charge was shown not to affect the migratory behavior of tracers in the lymphatic system [31], migration is reversely related to the particle size [32]. Logically, the use of tracers such as ICG (size of ICG <1 nm and 6-7 nm when bound to human serum albumin) or blue dye (<1 nm) may result in the visualization of more nodes compared with the use of large colloidal tracers. For example, through the use of ICG, Fujisawa et al. [11] showed the identification of 24% additional nodes compared with preoperatively identified SNs by using ^{99m}Tc-tin colloid. In addition to their more extensive drainage pattern

compared with large colloidal tracers, the fast drainage of small tracers limits the effective time window in which nodes can be detected through fluorescence imaging. It has been suggested that the optimal time window between injection and visualization of the nodes is 5-30 min [33,34]. For colloidal tracers such as ^{99m}Tc-nanocolloid, retention in the SNs is at least 24 h, thereby allowing both preoperative lymphatic mapping and intraoperative gamma tracing. In our study, in which ICG-^{99m}Tc-nanocolloid was formed via non-covalent self-assembly of ICG and ^{99m}Tc-nanocolloid, we were able to detect the SNs with both gamma tracing and fluorescence imaging up to 27 h after injection. During ex vivo analysis, we did not observe any SNs that were only fluorescent and not radioactive, suggesting the stability of our hybrid tracer over time.

In addition to the difference in nodal retention, there is a clear difference in the optical detection mechanisms for blue dye and near-infrared fluorescence tracers. Blue dye is visible to the eye when it reflects light [35], which is a very superficial effect. On the other hand, the generation of a near-infrared fluorescent signal is an active process in which the fluorescent molecule (in this case ICG) is excited by light of a near-infrared wavelength (±780 nm). Its subsequent relaxation to the ground state results in the emission of light of an even higher wavelength (±820 nm). With the excitation and emission both taking place in the near-infrared window, the near-infrared fluorescence signal can penetrate a tissue layer up to 1.0 cm [36]. However, it must be noted that the signal becomes very diffuse at this depth. The use of ICG facilitates superior in-depth optical identification compared with the use of blue dye; in five patients, near-infrared fluorescence imaging allowed transcutaneous visualization of the SN. In three patients, we could clearly visualize a fluorescent lymphatic duct running to the SN. For future studies, it would be interesting to investigate the hybrid tracer's potential to follow the afferent lymph vessel in comparison with blue dye [32].

Literature has shown that only 0.34-0.92% of the injected tracer is retained per SN; most of the rest of the tracer resides at the injection site [37]. Thus, when an SN is located near the injected melanoma site, radioactivity-based SN identification may be facilitated by removing the site of injection (and thus this unwanted background signal) prior to performing the SN biopsy procedure. Using a hybrid tracer, which combines the fluorescent and radioactive signature in one compound, may improve logistics in daily clinical practice, as no additional injections during the operation are required to allow for optical SN identification (usable in both one- and two-day protocols). This renders the effectiveness of the hybrid approach independent from the order in which the repeat excision of the melanoma site and SN biopsy are performed.

In our study population, most patients (n=69) received both the injection with the hybrid tracer and the injection with the blue dye. This might have led to a bias toward blue dye but not favorable to fluorescence imaging-based SN visualization. Because blue dye is visible to the naked eye, a surgeon cannot be blinded to this factor. However, for visualization of the fluorescent signature of the hybrid tracer, a dedicated fluorescence camera is required, meaning that the surgeon is initially blinded to it. Moreover, during the

operation, surgeons approached the preoperative SNs first with the gamma probe and then blue dye detection. Fluorescence imaging was used last so that its findings could be compared with the findings of the other techniques. In that order It would have been unethical to blind them for these routine technologies. To determine the true value of ICG-^{99m}Tc-nanocolloid (particularly the added value of the hybrid approach) in comparison with the use of a radioactive tracer and blue dye, prospective multicenter randomized studies have to be initiated in which both methods are compared. The potential advantages also need to be weighed against the complexity of the implementation of this hybrid approach into the clinical routine and the associated costs [24]. Fluorescence imaging is rather intuitive and can be used successfully with minimal training. However, the highest additional costs lie in obtaining a near-infrared fluorescence camera system, which, depending on the system chosen (e.g. goggles, handheld, or stand alone), varies from several thousands to hundreds of thousands of U.S. dollars [38]; the list price of the system used in our study is approximately $40,000 in U.S. dollars.

CONCLUSION

ICG-^{99m}Tc-nanocolloid enables both preoperative SN mapping and intraoperative SN identification in patients with melanoma. In our setup, optical identification of the SNs through the fluorescent signature of the hybrid tracer was superior compared with SN identification with blue dye. The fluorescent signature of the hybrid tracer was found to be of additional value for the detection of SNs close to the injection site (two patients), SNs located in an area of complex anatomy (head and neck, 28 patients), and SNs that failed to accumulate blue dye (19 patients).

REFERENCES

1. Valsecchi ME, Silbermins D, de Rosa N, Wong SL, Lyman GH. Lymphatic mapping and sentinel lymph node biopsy in patients with melanoma: a meta-analysis. J Clin Oncol. 2011;29:1479-87.
2. Nieweg OE, Jansen L, Kroon BB. Technique of lymphatic mapping and sentinel node biopsy for melanoma. Eur J Surg Oncol. 1998;24:520-4.
3. Chao C, Wong SL, Edwards MJ, Ross MI, Reintgen DS, Noyes RD, et al. Sentinel lymph node biopsy for head and neck melanomas. Ann Surg Oncol. 2003;10:21-6.
4. Govaert GA, Oostenbroek RJ, Plaisier PW. Prolonged skin staining after intradermal use of patent blue in sentinel lymph node biopsy for breast cancer. Eur J Surg Oncol. 2005;31:373-5.
5. Nieweg OE, Veenstra HJ. False-negative sentinel node biopsy in melanoma. J Surg Oncol. 2011;104:709-10.

6. van Akkooi AC, Voit CA, Verhoef C, Eggermont AM. New developments in sentinel node staging in melanoma: controversies and alternatives. Curr Opin Oncol. 2010;22:169-77.
7. Uren RF. SPECT/CT Lymphoscintigraphy to locate the sentinel lymph node in patients with melanoma. Ann Surg Oncol. 2009;16:1459-60.
8. Veenstra HJ, Vermeeren L, Olmos RA, Nieweg OE. The additional value of lymphatic mapping with routine SPECT/CT in unselected patients with clinically localized melanoma. Ann Surg Oncol. 2012;19:1018-23.
9. Vermeeren L, Valdes Olmos RA, Klop WM, van der Ploeg IM, Nieweg OE, Balm AJ, et al. SPECT/CT for sentinel lymph node mapping in head and neck melanoma. Head Neck. 2011;33:1-6.
10. Vermeeren L, Valdes Olmos RA, Klop WM, Balm AJ, van den Brekel MW. A portable gamma-camera for intraoperative detection of sentinel nodes in the head and neck region. J Nucl Med. 2010;51:700-3.
11. Fujisawa Y, Nakamura Y, Kawachi Y, Otsuka F. Indocyanine green fluorescence-navigated sentinel node biopsy showed higher sensitivity than the radioisotope or blue dye method, which may help to reduce false-negative cases in skin cancer. J Surg Oncol. 2012;106:41-5.
12. Gilmore DM, Khullar OV, Gioux S, Stockdale A, Frangioni JV, Colson YL, et al. Effective low-dose escalation of indocyanine green for near-infrared fluorescent sentinel lymph node mapping in melanoma. Ann Surg Oncol. 2013;20:2357-63.
13. Nakamura Y, Fujisawa Y, Nakamura Y, Maruyama H, Furuta J, Kawachi Y, et al. Improvement of the sentinel lymph node detection rate of cervical sentinel lymph node biopsy using real-time fluorescence navigation with indocyanine green in head and neck skin cancer. J Dermatol. 2013 Jun;40:453-7.
14. Namikawa K, Tsutsumida A, Tanaka R, Kato J, Yamazaki N. Limitation of indocyanine green fluorescence in identifying sentinel lymph node prior to skin incision in cutaneous melanoma. Int J Clin Oncol. 2014;19:190-203.
15. Stoffels I, von der Stuck H, Boy C, Poppel T, Korber N, Weindorf M, et al. Indocyanine green fluorescence-guided sentinel lymph node biopsy in dermato-oncology. J Dtsch Dermatol Ges. 2012 Jan;10:51-7.
16. van der Vorst JR, Schaafsma BE, Verbeek FP, Swijnenburg RJ, Hutteman M, Liefers GJ, et al. Dose optimization for near-infrared fluorescence sentinel lymph node mapping in patients with melanoma. Br J Dermatol. 2013;168:93-8.
17. van Leeuwen AC, Buckle T, Bendle G, Vermeeren L, Valdes Olmos R, van de Poel HG, et al. Tracer-cocktail injections for combined pre- and intraoperative multimodal imaging of lymph nodes in a spontaneous mouse prostate tumor model. J Biomed Opt. 2011;16:016004.
18. Buckle T, van Leeuwen AC, Chin PT, Janssen H, Muller SH, Jonkers J, et al. A self-assembled multimodal complex for combined pre- and intraoperative imaging of the sentinel lymph node. Nanotechnology. 2010;21:355101.

19. Brouwer OR, Buckle T, Vermeeren L, Klop WM, Balm AJ, van der Poel HG, et al. Comparing the hybrid fluorescent-radioactive tracer indocyanine green-^{99m}Tc-nanocolloid with ^{99m}Tc-nanocolloid for sentinel node identification: a validation study using lymphoscintigraphy and SPECT/CT. J Nucl Med. 2012;53:1034-40.
20. Brouwer OR, van den Berg NS, Matheron HM, van der Poel HG, van Rhijn BW, Bex A, et al. A hybrid radioactive and fluorescent tracer for sentinel node biopsy in penile carcinoma as a potential replacement for blue dye. Eur Urol. 2014;65:600-9.
21. Brouwer OR, Klop WM, Buckle T, Vermeeren L, van den Brekel MW, Balm AJ, et al. Feasibility of sentinel node biopsy in head and neck melanoma using a hybrid radioactive and fluorescent tracer. Ann Surg Oncol. 2012;19:1988-94.
22. Mathéron HM, van den Berg NS, Brouwer OR, Kleinjan GH, van Driel WJ, Trum JW, et al. Multimodal surgical guidance towards the sentinel node in vulvar cancer. Gynecol Oncol. 2013;131:720-5
23. Schaafsma BE, Verbeek FP, Rietbergen DD, van der Hiel B, van der Vorst JR, Liefers GJ, et al. Clinical trial of combined radio- and fluorescence-guided sentinel lymph node biopsy in breast cancer. Br J Surgery. 2013;100:1037-44.
24. van den Berg NS, Brouwer OR, Klop WM, Karakullukcu B, Zuur CL, Tan IB, et al. Concomitant radio- and fluorescence-guided sentinel lymph node biopsy in squamous cell carcinoma of the oral cavity using ICG-(^{99m})Tc-nanocolloid. Eur J Nucl Med Mol Imaging. 2012;39:1128-36.
25. van der Poel HG, Buckle T, Brouwer OR, Valdes Olmos RA, van Leeuwen FW. Intraoperative laparoscopic fluorescence guidance to the sentinel lymph node in prostate cancer patients: clinical proof of concept of an integrated functional imaging approach using a multimodal tracer. Eur Urol. 2011;60:826-33.
26. Bunschoten A, Buckle T, Kuil J, Luker GD, Luker KE, Nieweg OE, et al. Targeted non-covalent self-assembled nanoparticles based on human serum albumin. Biomaterials. 2012;33:867-75.
27. Nieweg OE, Tanis PJ, Kroon BB. The definition of a sentinel node. Ann Surg Oncol. 2001;8:538-41.
28. Valdés Olmos RA, Vidal-Sicart S. SPECT/CT image generation and criteria for sentinel node mapping. In: Mariani G., Manca G, Orsini P., Vidal-Sicart S., Valdés Olmos R., eds. Atlas of Lymphoscintigraphy and Sentinel Node Mapping. Milan, Italy: Springer; 2012. p. 269-83.
29. Klop WM, Veenstra HJ, Vermeeren L, Nieweg OE, Balm AJ, Lohuis PJ. Assessment of lymphatic drainage patterns and implications for the extent of neck dissection in head and neck melanoma patients. J Surg Oncol. 2011;103:756-60.
30. Veenstra HJ, Klop WM, Speijers MJ, Lohuis PJ, Nieweg OE, Hoekstra HJ, et al. Lymphatic drainage patterns from melanomas on the shoulder or upper trunk to cervical lymph nodes and implications for the extent of neck dissection. Ann Surg Oncol. 2012;19:3906-12.

31. Ballou B, Lagerholm BC, Ernst LA, Bruchez MP, Waggoner AS. Noninvasive imaging of quantum dots in mice. Bioconjug Chem. 2004;15:79-86.
32. Uren RF. Lymphatic drainage of the skin. Ann Surg Oncol. 2004;11:179S-85S.
33. Bredell MG. Sentinel lymph node mapping by indocyanin green fluorescence imaging in oropharyngeal cancer - preliminary experience. Head Neck Oncol. 2010;2:31.
34. Jeschke S, Lusuardi L, Myatt A, Hruby S, Pirich C, Janetschek G. Visualisation of the lymph node pathway in real time by laparoscopic radioisotope- and fluorescence-guided sentinel lymph node dissection in prostate cancer staging. Urology. 2012;80:1080-6.
35. van den Berg NS, van Leeuwen FW, van der Poel HG. Fluorescence guidance in urologic surgery. Curr Opin Urol. 2012;22:109-20.
36. Vahrmeijer AL, Frangioni JV. Seeing the invisible during surgery. Br J Surg. 2011;98:749-50.
37. Mariani G, Erba P, Manca G, Villa G, Gipponi M, Boni G, et al. Radioguided sentinel lymph node biopsy in patients with malignant cutaneous melanoma: the nuclear medicine contribution. J Surg Oncol. 2004;85:141-51.
38. Liu Y, Bauer AQ, Akers WJ, Sudlow G, Liang K, Shen D, et al. Hands-free, wireless goggles for near-infrared fluorescence and real-time image-guided surgery. Surgery. 2011;149:689-98.

SUPPORTING INFORMATION

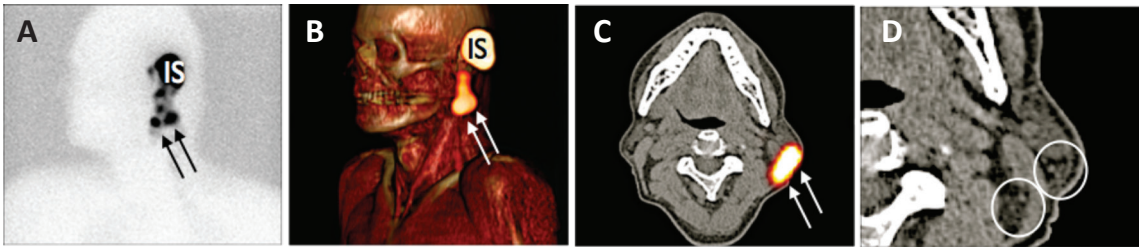

Figure SI1. Preoperative sentinel node mapping in a 59-year-old male patient with head-and-neck melanoma (left ear; Breslow thickness 1.0 mm). The patient was scheduled for re-excision of the melanoma scar and subsequent SN biopsy. Due to the location of the melanoma, no patent blue dye was injected intraoperatively. Conventional lymphoscintigrams (A) and SPECT/CT images (B) showing SNs in the parotid gland and level II (marked with arrows). Intraoperatively, additional SNs were from both locations. Retrospective analysis revealed the SNs in the parotid gland and level II being part of clusters (four and two nodes harvested, respectively; C and D) SN = sentinel node; IS = injection site; SPECT/CT = single photon emission computed tomography combined with computed tomography.

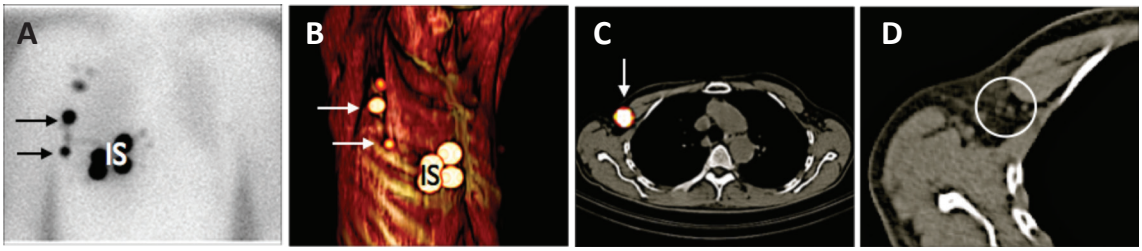

Figure SI2. Preoperative sentinel node mapping in 69-year-old male patient with a melanoma of the trunk (thorax right; Breslow thickness 4.0 mm). The patient was scheduled for re-excision of the melanoma scar and subsequent SN biopsy. Directly before the start of the operation 1.0 mL patent blue dye was injected. Conventional lymphoscintigrams (A) and SPECT/CT. images (B) showing two SNs (pectoral and axilla; marked with arrows) with regard to the injection site (IS). Intraoperatively, four SNs were removed from the axilla. Retrospective analysis revealed these SNs being part of a cluster (C and D). SN = sentinel node; IS = injection site; SPECT/CT = single photon emission computed tomography combined with computed tomography.

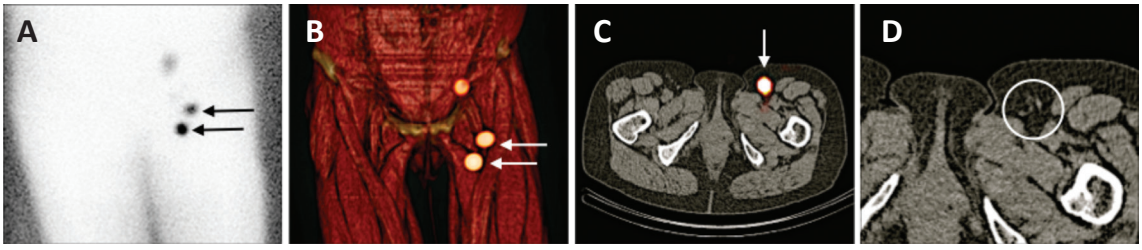

Figure SI3. Preoperative sentinel node mapping in a 65-year-old female patient with melanoma of an extreemity (left medial knee; Breslow thickness 2.1 mm). The patient was scheduled for re-excision of the melanoma scar and subsequent SN biopsy. Directly before the start of the operation 1.0 mL patent blue dye was injected. Conventional lymphoscintigrams (A) and SPECT/CT images (B) showing two SNs in the groin (marked with arrows) with regard to the injection site (IS). Intraoperatively, three SNs were removed from the groin. Retrospective analysis revealed these SNs being part of a cluster (C and D). SN = sentinel node; IS = injection site; SPECT/CT = single photon emission computed tomography combined with computed tomography.

PART THREE

CHAPTER 7

(NEAR-INFRARED) FLUORESCENCE GUIDED SURGERY UNDER AMBIENT LIGHT CONDITIONS, A NEXT STEP TO EMBEDMENT OF THE TECHNOLOGY IN CLINICAL ROUTINE

Adapted from: van den Berg NS, KleinJan GH, Miwa M, Sato T, Maeda Y, van Akkooi ACJ, Horenblas S, Karakullukçu B, van Leeuwen FBW. Ann Surg Oncol. 2016;23:2586-95.

ABSTRACT

BACKGROUND AND PURPOSE In open surgery procedures, after temporarily dimming the lights in the operation theatre, the PhotoDynamic Eye (PDE) fluorescence camera has, amongst others, been used for fluorescence-guided sentinel node (SN) biopsy procedures. To improve the clinical utility and logistics of fluorescence-guided surgery, we developed and evaluated a prototype modified PDE (m-PDE) fluorescence camera system.

METHODS The m-PDE works under ambient light conditions and includes a white light mode and a pseudo-green-colored fluorescence mode (including a gray-scaled anatomical background). Twenty-seven patients scheduled for SN biopsy for (head and neck) melanoma (n=16), oral cavity (n=6), or penile (n=5) cancer were included. The number and location of SNs were determined following an indocyanine green-^{99m}Tc-nanocolloid injection and preoperative imaging. Intraoperatively, fluorescence guidance was used to visualize the SNs. The m-PDE and conventional PDE were compared head-to-head in a phantom study, and in seven patients. In the remaining 20 patients, only the m-PDE was evaluated.

RESULTS Phantom study: The m-PDE was superior over the conventional PDE, with a detection sensitivity of 1.20×10^{-11} M (vs. 3.08×10^{-9} M) ICG in human serum albumin. In the head-to-head clinical comparison (n=7), the m-PDE was also superior: (i) SN visualization: 100 versus 81.4%; (ii) transcutaneous SN visualization: 40.7 versus 22.2%; and (iii) lymphatic duct visualization: 7.4 versus 0%. Findings were further underlined in the 20 additionally included patients.

DISCUSSION The m-PDE enhanced fluorescence imaging properties compared with its predecessor, and provides a next step towards routine integration of real-time fluorescence guidance in open surgery.

INTRODUCTION

Different groups have reported that for effective intraoperative (near-infrared) fluorescence imaging the lights in the operating room have to be dimmed, or switched off, in order to visualize the fluorescence signal [1,2]. This results in temporary stalling of the surgical procedure, even when the fluorescence camera itself is equipped with a white light source [2]. Therefore, in general, the fluorescence guidance technology is primarily used to provide static confirmatory information regarding the location of lesions [3]. Ideally, during a surgical procedure the technique would be used to allow the surgeon to excise the lesion of interest under real-time fluorescence guidance.

Previously, in laparoscopic studies using the hybrid tracer indocyanine green (ICG)-^{99m}Tc-nanocolloid, we showed that the value of real-time fluorescence guidance significantly increased when the fluorescent signal was displayed within the anatomical context of the patient [4]. For open surgery procedures, using the PhotoDynamic Eye fluorescence camera (PDE; Hamamatsu Photonics K.K., Hamamatsu, Japan), we saw that in some cases the background signal helped provide anatomical context [5-7]. We reasoned that exploiting this feature further could aid the routine embedment of the technology. Allowing fluorescence guidance under ambient light conditions would, at the same time, help simplify clinical logistics. To achieve our goals, we set out to develop a prototype modified-PDE (m-PDE) fluorescence camera, and evaluated it in both a phantom and patient study.

MATERIALS AND METHODS

FLUORESCENCE CAMERA SYSTEMS

We evaluated the newly developed prototype m-PDE fluorescence camera and compared it to the commercially available conventional-PDE (c-PDE) fluorescence camera (Hamamatsu Photonics K.K.).

The main differences between the c-PDE and the m-PDE are shown in Table 1. Briefly, the light-emitting diode (LED)-based near-infrared excitation light of the c-PDE works in a continuous wave mode, while the illumination source of the m-PDE is pulsed in synchronization with the frame rate of the charge coupled device (CCD). Here, pulsation means the CCD detector obtains both a fluorescence image containing ambient light background signal and an image of the ambient light background only. Real-time subtraction of the two images then allows the m-PDE to obtain a 'pure' fluorescence image (in gray-scale or pseudo-green-color) under ambient light conditions. Second, the m-PDE also allows real-time mixing of the 'pure' pseudo-green-colored fluorescence image with the gray-scale anatomical context image. As a third improvement, the m-PDE can also show a white light image in a non-fluorescence imaging setting.

table 1

Table 1. Characteristics of the conventional-PDE fluorescence camera and the modified-PDE fluorescence camera

	Conventional-PDE	***Modified-PDE***
Excitation light source	LED (continuous)	LED (pulsed)
Imaging device	CCD	CCD
Excitation / Emission wavelength	760 / >820nm	760 / >820nm
Handheld	Yes	Yes
Pulsed fluorescence imaging	No	Yes
White light imaging	No	Yes
Focus adjustment	No	Yes
Effective under ambient light conditions	No	Yes
Pseudo-coloring	No	Yes (green)
Fluorescence image presented in	Black-and-white	1. Black-and-white 2. Pseudo-colored green on a grey-scaled anatomical background

LED = light emitting diode; CCD = charge coupled device.

PHANTOM STUDY

A 5.0 mg/mL (6.45 x 10^{-3} M) ICG (ICG-Pulsion, 25 mg vial; Pulsion Medical Systems, Munich, Germany)-human serum albumin (HSA; Albuman 200 g/L; Sanquin, Amsterdam, The Netherlands) solution was prepared and diluted 1:1 with HSA in 30 steps down to 9.31 ng/mL (1.20 x 10^{-11} M). From each dilution 100 µL was pipetted in a black 96-well plate (Cellstar; Greiner Bio-One GmbH, Frickenhausen, Germany). The complete dilution range was then evaluated to determine the detection sensitivity of the m-PDE and c-PDE fluorescence camera systems. Hereby, the head of the fluorescence cameras was fixed, perpendicular, at a 14 cm distance from the well-plate surface. This allowed capture of the whole dilution range in the field of view.

Imaging of the plate was performed under different settings (white light (m-PDE only) and fluorescence (both systems)), and under various light conditions: (i) all lights in the operating room turned on (halogen satellite lamps directly lighting the sterile field (angle of approximately 45° with regard to the plate surface), the plenum and surrounding lights (both tubular lights)); (ii) satellite lamps directly lighting the sterile field turned off, but the plenum and surrounding lights on (referred to as 'ambient light' conditions); and (iii) all lights in the operating room dimmed. For the m-PDE fluorescence camera system evaluation, in all experiments the pseudo-colored green setting was used.

As a reference for the fluorescence intensity measured with the c-PDE and m-PDE fluorescence camera systems, the ICG-HSA-based dilution range was also measured on preclinical, cooled, black box, camera systems (IVIS Spectrum, (Xenogen Corporation, San Francisco, CA, USA) and the Pearl Impulse (LI-COR Biotechnology GmbH, Hombur, Germany)). The fluorescence image obtained with the IVIS Spectrum was presented in a pseudo-colored glow scale, whereas for the Pearl Impulse, the fluorescence signal was presented in a pseudo-colored green scale. For both systems, the fluorescence images were overlaid onto a black-and-white background image.

For quantification of the fluorescence signal measured with the IVIS Spectrum, in the acquired fluorescence image, regions of interest were drawn surrounding the wells after which Living Image 3D analysis software (version 1.0; Xenogen Corporation) was used to quantify the signal intensity per well.

LIGHT SPECTRA MEASUREMENTS

Light spectra of the different lamps present in the operating room were determined using a Jobin Yvon VS140 linear array fiber spectrometer (Horiba, Kyoto, Japan) in the 300-1200 nm range, with an integration time of 0.1 ms. The fiber was held at a 2-meter distance from the lamp from which the light spectra were measured.

ABSORPTION AND EMISSION SPECTRA MEASUREMENTS OF ICG-HSA

The absorption and emission spectrum of ICG-HSA (concentration: 1.5 x 10^{-9} M) was measured using an Ultrospec 3000 UV/Vis spectrophotometer (Pharmacia Biotech/GE Healthcare Europe GmbH, Eindhoven, The Netherlands) and an LS55 fluorescence spectrometer (PerkinElmer, Groningen, The Netherlands). Solutions were prepared in a 3 mL quartz cuvet (Hellma GmbH & Co. KG, Müllheim, Germany).

PATIENT STUDY

PATIENTS

Patients with squamous cell carcinoma of the oral cavity (n=6) or penis (n=5), head-and-neck melanoma (n=11), or melanoma on the trunk or on an extremity (n= 5) scheduled for sentinel node (SN) biopsy with subsequent treatment of the primary tumor/re-excision of the melanoma scar were prospectively enrolled after obtaining written informed consent. All included patients were clinically node-negative as defined by palpation and ultrasound-guided fine needle aspiration cytology. Patient characteristics are shown in Table 2. The study protocol was conducted in accordance with the Helsinki Declaration and approved by the Medical Ethical Committee of the Netherlands Cancer Institute-Antoni van Leeuwenhoek Hospital.

Table 2. Pre- and intraoperative sentinel node identification findings, and pathology results

	Direct camera comparison		***Evaluation modified-PDE system***
	Conventional-PDE	***Modified-PDE***	
Patient characteristics			
Patients	7		20
Age, average (range) (years)	64.6 (58-74)		54.4 (34-81)
Male / Female ratio	5 / 2		14 / 6
Tumor type + tumor stage			
- SCC, oral cavity	4		2
- T1	4		2
- Melanoma (head and neck, trunk, or extremity)	3 (1, 1, 1)		13 (10, 1, 2)
- Breslow thickness, average (range) (mm)	1.6 (1.2-2.1)		2.1 (0.6-4.0)
- Ulceration, yes/no	0 / 3		3 / 10
- SCC, penis	-		5
- T1	-		2
- T2	-		3
Preoperative sentinel node mapping			
Injected dose, average (range) (MBq)	69.6 (62.1-77.1)		80.6 (67.3-156)
Preoperative # SNs identified using SPECT/CT (average, range)	21 (3, 2-5)		51 (2.6, 1-6)
# Basins (% total), # SNs (% total)	16 (100%), 21 (100%)		40 (100%), 51 (100%)
- Head	1 (6.3%), 1 (4.8%)		5 (12.5%), 6 (11.8%)
- Auricular	-		-
- Parotid gland	-		2 (5.0%), 3 (5.9%)
- Neck (level I-V)	11 (68.8%), 15 (71.4%)		19 (47.5%), 23 (45.1%)
- Axilla	2 (12.5%), 2 (9.5%)		2 (5.0%), 2 (3.9%)
- Supraclavicular	-		1 (2.5%), 1 (2.0%)
- Scapular	1 (6.3%), 1 (4.8%)		-
- Groin	1 (6.3%), 2 (9.5%		11 (27.5%), 16 (31.4%)
Time injection - operation, average (range) (hrs)	5.5 (4.3-6.5)		6.4 (3.5-19.5)

PDE = PhotoDynamic Eye; T = tumor; SCC = squamous cell carcinoma; MBq = Mega Becquerel; SN = sentinel node; SPECT/CT = single photon emission computed tomography combined with computed tomography. [#] In two patients blue dye was used. Here 2 SNs were excised of which 1 was blue at the time of excision. [$] In two patients blue dye was used. Here 2 SNs were excised of which were both blue at the time of excision.

	Direct camera comparison		***Evaluation modified-PDE system***
	Conventional-PDE	***Modified-PDE***	
Intraoperative sentinel indentification			
Intraoperatively # excised SNs (average, range)	27 (3.9, 2-7)		73 (3.7, 1-7)
- Radioactive	27		73
- Fluorescent	27		73
- Blue	1[#]		12[$]
Intraoperatively # fluorescent SNs (% total) (# pts)			
- Visibility through skin	6 (22.2%) (2 pts)	11 (40.7%) (4 pts)	26 (35.6%) (11 pts)
# SNs per basin			
- Head	1	1	1
- Auricular	-	-	1
- Parotid gland	-	-	2
- Neck (level I-V)	5	5	17
- Axilla	-	2	2
- Supraclavicular	-	-	-
- Scapular	-	1	-
- Groin	-	2	3
- Visibility in vivo (prior to excision)	22 (81.4%) (6 pts)	27 (100%) (7 pts)	75 (100%) (20 pts)
# SNs per basin			
- Head	1	1	5
- Auricular	-	-	1
- Parotid gland	-	-	8
- Neck (level I-V)	19	21	35
- Axilla	1	2	2
- Supraclavicular	-	-	4
- Scapular	1	1	-
- Groin	0	2	18
- Visibility lymphatic duct	-	2 (7.4%) (2 pts)	33 (45.2%) (13 pts)
# SNs per basin			
- Head	-	-	2
- Auricular	-	-	1
- Parotid gland	-	-	4
- Neck (level I-V)	-	2	15
- Axilla	-	-	2
- Supraclavicular	-	-	4
- Scapular	-	-	-
- Groin	-	-	5
	Note: determined under dark conditions	Note: determined under ambient light conditions	Note: determined under ambient light conditions
Pathology			
# Tumor-positive SNs (% total)	0 / 34		4 / 91 (4.4%)
# Tumor-positive patients (% total)	0 / 7		4 / 20 (20.0%)

HYBRID TRACER PREPARATION, ADMINISTRATION, PREOPERATIVE SENTINEL NODE MAPPING AND (HISTO-)PATHOLOGY

Preparation and administration of the hybrid tracer ICG-^{99m}Tc-nanocolloid, preoperative imaging, and (histo-)pathological specimen analysis for oral cavity cancer [6], penile cancer [8], and (head-and-neck) melanoma [7] have been previously described.

SURGICAL PROCEDURE

In patients with head-and-neck malignancies, primary tumor removal or re-excision of the melanoma scar was completed prior to performing SN biopsy. In penile cancer patients and patients with a melanoma on the trunk or on an extremity, SN biopsy was performed prior to treatment of the primary tumor site or the melanoma scar. A schematic overview of the intraoperative SN excision procedure is given in Figure 1.

RESULTS

PHANTOM STUDY

REFERENCE FLUORESCENCE DATA

Figure 2A illustrates the relation between the ICG-HSA concentration and the fluorescence intensity measured with the IVIS Spectrum. Under black-box conditions, the lowest concentration evaluated (1.20 x 10^{-11} M ICG-HSA) could be easily detected using this system (Figure 2B). The Pearl Impulse showed a similar detection range (data not shown).

Figure 1. Workflow for sentinel node localization and excision. Following preoperative image analysis by the surgeon to virtually determine the location of the SNs (1), blue dye can be injected (2). Prior to incision a portable gamma camera (Sentinella; Oncovision, Valencia, Spain), a gamma probe (Neoprobe; Johnson & Johnson Medical, Hamburg, Germany), and the fluorescence camera (c-PDE or m-PDE; Hamamatsu Photonics K.K., Hamamatsu, Japan) are use to determine the location of the SNs (3). After incision (4) the SN is pursued via gamma tracing, after which alternating attempts were made to visualize the SN via fluorescence imaging and, when applicable, blue-dye visualization (5). After identification of the SN, the node was excised, after which the wound bed was checked for the presence of residual radioactivity/remaining fluorescence activity at the site of a previously excised SN. Additionally excised nodes were considered part of a cluster of multiple adjacent SNs (6). Following completion of SN biopsy via the combined radio- and fluorescence-guided (and, when applicable, blue dye) approach, the wound-bed was palpated for the presence of suspicious non-radioactive, non-fluorescent and, when applicable, non-blue-dye-stained lymph nodes (8). Thereafter the wound bed was closed (9). SN = sentinel node; PDE = PhotoDynamic Eye.

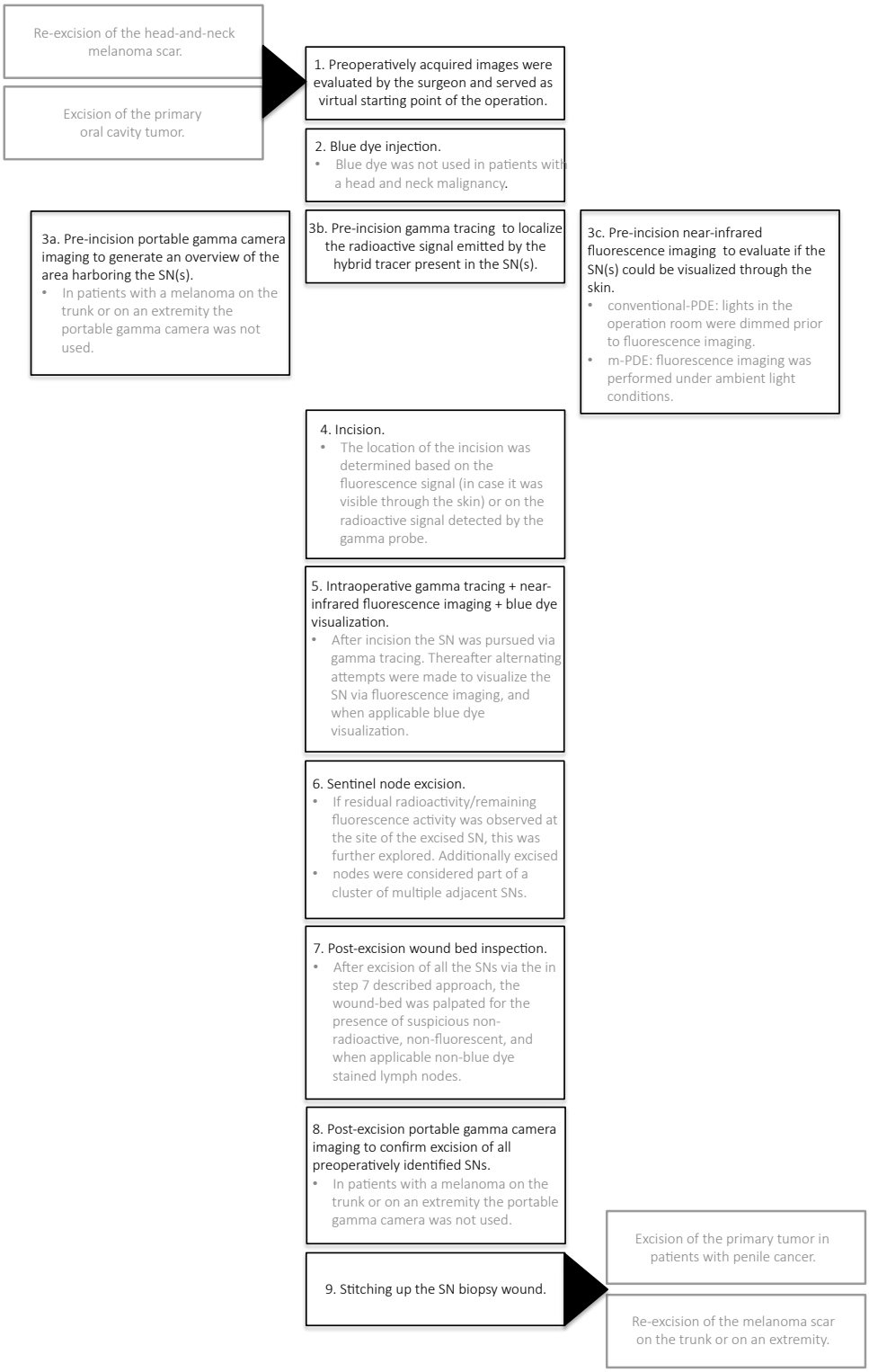
Re-excision of the head-and-neck melanoma scar.
Excision of the primary oral cavity tumor.
1. Preoperatively acquired images were evaluated by the surgeon and served as virtual starting point of the operation.
2. Blue dye injection.
• Blue dye was not used in patients with a head and neck malignancy.
3a. Pre-incision portable gamma camera imaging to generate an overview of the area harboring the SN(s).
• In patients with a melanoma on the trunk or on an extremity the portable gamma camera was not used.
3b. Pre-incision gamma tracing to localize the radioactive signal emitted by the hybrid tracer present in the SN(s).
3c. Pre-incision near-infrared fluorescence imaging to evaluate if the SN(s) could be visualized through the skin.
• conventional-PDE: lights in the operation room were dimmed prior to fluorescence imaging.
• m-PDE: fluorescence imaging was performed under ambient light conditions.
4. Incision.
• The location of the incision was determined based on the fluorescence signal (in case it was visible through the skin) or on the radioactive signal detected by the gamma probe.
5. Intraoperative gamma tracing + near-infrared fluorescence imaging + blue dye visualization.
• After incision the SN was pursued via gamma tracing. Thereafter alternating attempts were made to visualize the SN via fluorescence imaging, and when applicable blue dye visualization.
6. Sentinel node excision.
• If residual radioactivity/remaining fluorescence activity was observed at the site of the excised SN, this was further explored. Additionally excised
• nodes were considered part of a cluster of multiple adjacent SNs.
7. Post-excision wound bed inspection.
• After excision of all the SNs via the in step 7 described approach, the wound-bed was palpated for the presence of suspicious non-radioactive, non-fluorescent, and when applicable non-blue dye stained lymph nodes.
8. Post-excision portable gamma camera imaging to confirm excision of all preoperatively identified SNs.
• In patients with a melanoma on the trunk or on an extremity the portable gamma camera was not used.
9. Stitching up the SN biopsy wound.
Excision of the primary tumor in patients with penile cancer.
Re-excision of the melanoma scar on the trunk or on an extremity.

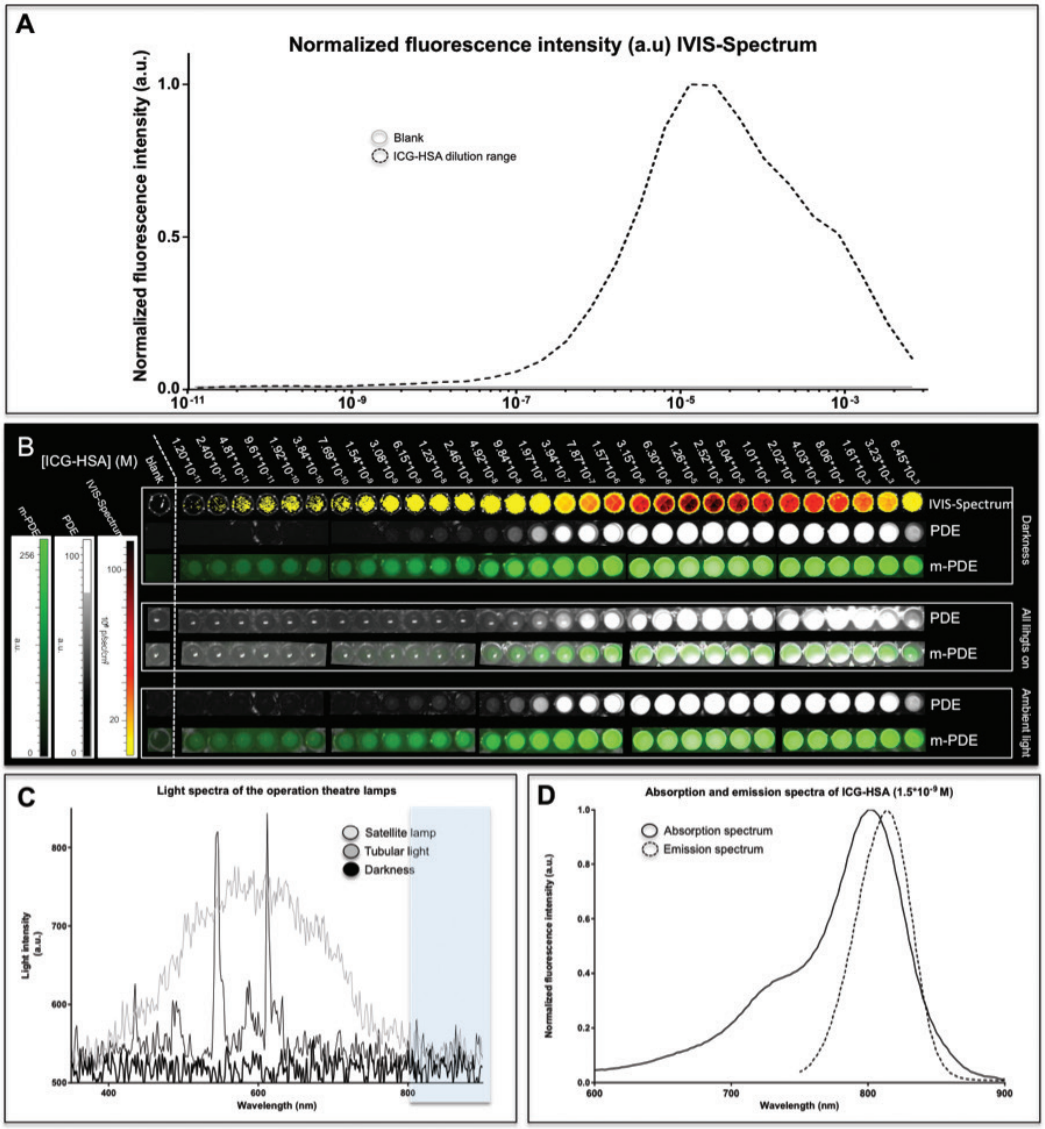

Figure 2. Determination of the sensitivity of the m-PDE and c-PDE fluorescence camera systems for ICG-HSA. A) Fluorescence intensity curve of the various steps of the dilution range measured with the IVIS Spectrum; B) Visual fluorescence images obtained with the IVIS Spectrum, c-PDE, and m-PDE when measured in full darkness, with all lights in the operating room turned on (satellite lamps, plenum, and surrounding lights), and with the satellite lamps directly lighting the sterile field turned off, but the plenum and surrounding lights on; C) Light spectrum of the lamps present in the operating room. The light blue area shows the area in which ICG emits its light; D) Absorption and emission spectrum of 1.50×10^{-9} M ICG-HSA. ICG = indocyanine green; HSA = human serum albumin; PDE = PhotoDynamic Eye.

Spectral analysis of the light emissions encountered for the different light settings evaluated in the operating room (Figure 2C) revealed that the light spectrum of the (halogen) satellite lamps gives a broad emission spectrum that shows significant overlap with the spectral area where the ICG emission is collected. The severity with which the satellite lamps influenced ICG detection depended on the angle under which the satellite lamp was placed relative to the phantom. Hereby, the sensitivity for ICG was highest when the satellite lamp was angled so that the reflected satellite lamplight did not align with the position of the fluorescence camera. The normal surrounding lamps (tubular lights) displayed an assembly of light peaks, with the most pronounced emission maxima at 545 and 612 nm, which showed a limited degree of spectral overlap with the emission peak of ICG (Figure 2C, D).

DETECTION SENSITIVITY PDE FLUORESCENCE CAMERA SYSTEMS

Visual inspection of the fluorescence images generated by the m-PDE yielded similar detection sensitivities as reported for the IVIS Spectrum above (1.20×10^{-11} M ICG-HSA) (Figure 2B) when fluorescence imaging was performed in the dark or under ambient light conditions (surrounding lights and plenum turned on; Figure 2B). With all the lights turned on, including the satellite lamps, the fluorescence detection sensitivity for the m-PDE system slightly dropped to 2.40×10^{-11} M ICG-HSA.

With the c-PDE system, a detection sensitivity of 3.08×10^{-9} M ICG-HSA was found under dark conditions (Figure 2B). This dropped to 4.92×10^{-8} M ICG-HSA when all the lights in the operating room were turned on (Figure 2B). This two-to-three orders of magnitude difference indicates the m-PDE fluorescence camera system can better cope with the background light present in an intraoperative setting.

PATIENT STUDIES

CONVENTIONAL-PDE VS. MODIFIED-PDE FLUORESCENCE CAMERA

In the comparison study in seven patients (oral cavity cancer (n=4) and melanoma (n=3)), a total of 27 SNs were harvested (average 3.9, range 2-7; Table 2). Initial evaluations performed with the satellite lamps turned on were of limited success and proved to be highly dependent on the positioning of the lamps. For that reason, in this comparison study evaluations were performed with either the satellite lamps dimmed or with these lights turned on, but faced away from the surgical wound bed.

With the m-PDE, under ambient light conditions all SNs evaluated could be easily visualized (100%). For the c-PDE, with all lights in the operating room dimmed an overall detection rate of 81.4% was found. The m-PDE system visualized 40.7% of the SNs transcutaneously (11 SNs, four patients; ambient light conditions), while the c-PDE system visualized only 22.2% (6 SNs, two patients; dimmed light conditions). In two patients, a lymphatic duct leading to an SN was visualized with the m-PDE (ambient light conditions), whereas no lymphatic ducts could be visualized with the c-PDE (dimmed light conditions).

Further detailed results can be found in Table 2.

Supporting information Figure SI1 presents the surgical workflow for the c-PDE (Figure SI1A) and m-PDE (Figure SI1B) fluorescence camera system. When using the c-PDE (Figure SI1A), lights in the operating room had to be dimmed in order to visualize the SNs. This temporarily stalled the surgical procedure. Forceps were often placed at the location of the SN, after which the lights in the operating room were turned back on to visually confirm the localization of the SN. This was followed by SN excision and fluorescence imaging to confirm removal of the SN. This process was repeated for each individual SN.

When working with the m-PDE (Figure SI1B), the presence of ambient light, presentation of the pseudo-colored green fluorescence images on a gray-scaled anatomical background, and the ability to switch the m-PDE to white light mode, combined, allowed the surgeon to directly verify the anatomical location of the SNs and proceed with their excision in a sequential manner. Here, the white light mode allowed us to optimally focus the camera. Please see Figure 3 for a stepwise illustration on the real-time fluorescence-guided excision of three SNs in a cluster under ambient light conditions. It is interesting to note that even with the increased detection sensitivity of the m-PDE fluorescence camera system, excision of the SNs was not hindered by background signals as a consequence of leakage of tracer from damaged lymphatic ducts (Figure 3).

EXTENDED CLINICAL EVALUATION OF THE MODIFIED-PDE FLUORESCENCE CAMERA SYSTEM

The m-PDE fluorescence camera was further evaluated in an additional 20 patients: oral cavity (n=2) and penile cancer (n=5), and (head-and-neck) melanoma (n=13). From these patients, 73 SNs were harvested (average 3.7, range 1-7), of which 35.6% (26 SNs; 11 patients) could be visualized transcutaneously (Table 2). Lymphatic ducts draining from the primary tumor were identified in 13 patients and 33 SNs (45.2%; Table 2). Transcutaneous SN visualization, as well as visualization of the lymphatic ducts, was most pronounced in patients with drainage to SNs in the neck (Table 2). Examples of our findings are shown in Figure 3 and supporting information Figures SI2 and SI3.

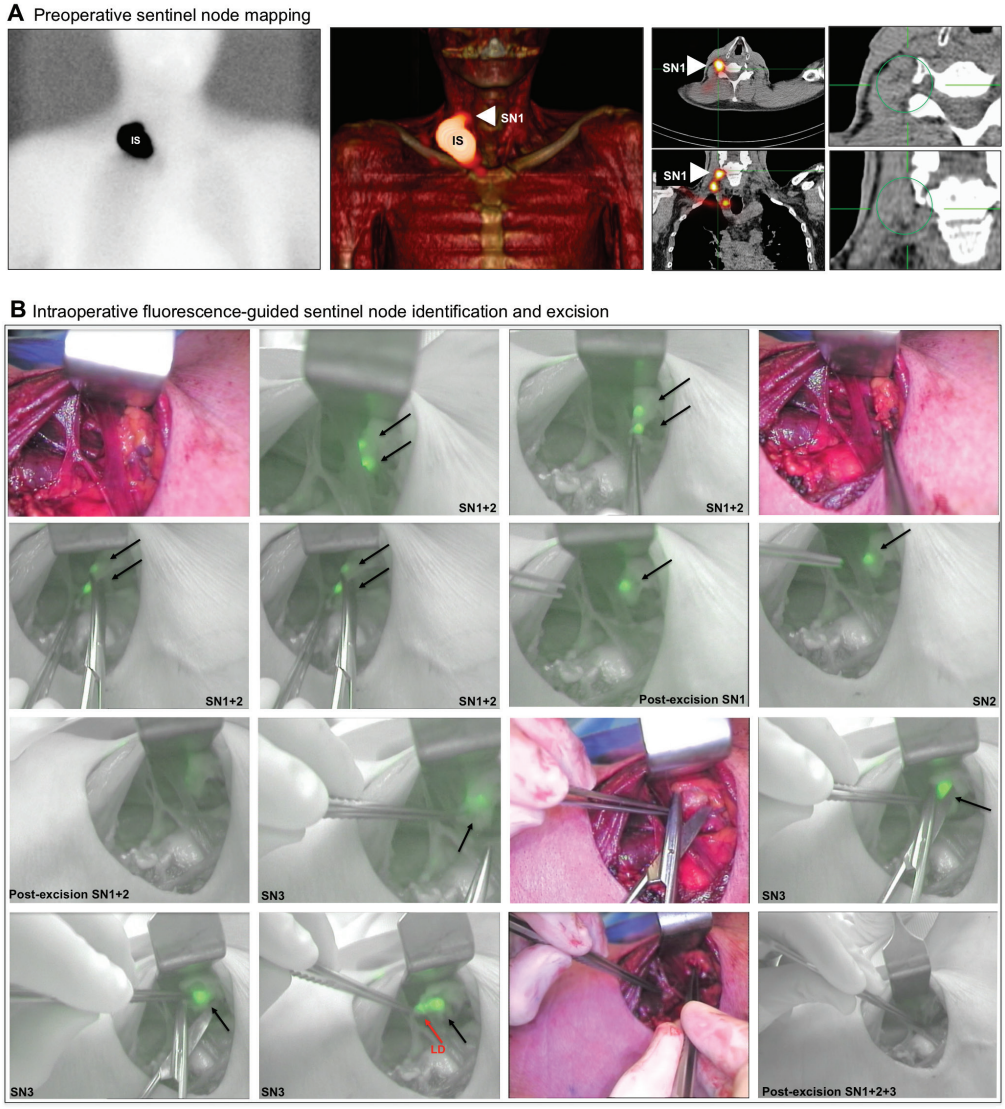

Figure 3. Fluorescence-guided sentinel node excision in a patient with a melanoma of the neck. A) Preoperative imaging. Left: Static lymphoscintigram acquired 2 h after hybrid tracer injection showing only the IS. Middle: Following fusion of the acquired SPECT and CT images, a three dimensional volume rendering was generated showing the injection site, as well as an SN in level IV (white arrow) and a supraclavicular SN. Right: Axial fused SPECT/CT (left) and CT (right) slice showing the SN in level IV being part of a cluster (indicated because no clear node could be identified on the CT, only a strand of tissue); B) After re-excision of the melanoma scar, the SN cluster in level IV was pursued via fluorescence imaging using the m-PDE fluorescence camera. The timeline shows fluorescence-guided excision of this cluster of SNs. Switching between the fluorescence and white light image allowed the surgeon to work under continuous fluorescence guidance. A total of three fluorescent (and radioactive) SNs were removed from the area where the hotspot was seen on SPECT/CT imaging. IS = injection site; SN = sentinel node; SPECT/CT = single photon emission computed tomography combined with computed tomography.

DISCUSSION

In the current study, we evaluated the effect that technical improvements have on the performance of the fluorescence camera. For this, the 'new' prototype m-PDE fluorescence camera was evaluated in relation to the 'old' c-PDE. After evaluation in a phantom set-up, its value was defined in patients who were to undergo an SN biopsy procedure for (head-and-neck) melanoma, oral cavity or urological malignancies using the hybrid tracer ICG-^{99m}Tc-nanocollloid. We have previously reported that this hybrid tracer, in combination with the m-PDE's predecessor (the c-PDE), allowed superior optical SN visualization compared to blue dye in, for example, patients with vulvar or penile cancer [8,9] or melanoma [7] (on average, 60.7 vs. 96.5%, respectively).

The increased sensitivity of the m-PDE compared with the c-PDE, as concluded from the phantom studies, translated nicely in an improved clinical utility of the m-PDE. In a comparative series of seven patients, the reported two-to-three orders of magnitude increase in detection sensitivity resulted in a 14.8% increase in SN visualization. The value of the m-PDE fluorescence camera system was further underlined in 20 additional patients. With the m-PDE, 35.6% of the SNs could be visualized transcutaneously and, for 45.2% of the SNs, lymphatic ducts were visualized. Its utility was further enhanced by (1) the fact that the fluorescence image of the m-PDE is corrected real-time for the influence of ambient light, meaning that the lights in the operating theatre did not have to be dimmed when performing fluorescence imaging; (2) the ability of the m-PDE to show the pseudo-colored green fluorescence image on a gray-scale anatomical background image; and (3) its ability to directly switch between the fluorescence light and white light mode. Given the clear clinical potential of this approach for ICG, which is not a particularly bright dye with a relatively short luminescence lifetime, this concept may, in the future, be successfully expanded to other luminescent tracers that have found their way into the clinic [10].

The technological evolutions realized in the m-PDE help minimize the disturbance of the clinical workflow and help to transform fluorescence imaging from a confirmatory modality to one that provides real-time 'on-screen' guidance during SN excision (as illustrated in Figures 3, SI1 and SI2). This optimized 'on-screen' guidance set-up is comparable to the type of guidance obtained during (fluorescence-guided) laparoscopic surgery [4,11]. However, during open surgery procedures, the small overlap of the ICG light spectrum and the light emitted by the satellite lamp (Figure 2), in combination with the high intensity of this light source (Figure 2), still meant that the satellite lamps had to be faced away from the surgical wound bed (or turned off) for optimal guidance. With the upcoming modernized operating rooms, in which halogen satellite lamps are exchanged for LED lamps, this effect will likely become less prominent.

In the current study, we evaluated the m-PDE in combination with ICG-^{99m}Tc-nanocollloid, a hybrid tracer that was specifically designed as an SN tracer [12,13]. The specificity of this tracer was further confirmed by the minimal leakage from the lymphatic ducts that we observed with the m-PDE (Figure 3). When compared with other studies

using 'free' ICG where such leakage is more common [11], this outcome underlines the advantage of using an SN-specific tracer for SN biopsy procedures. From a technical perspective, the advantages the m-PDE has can, in the future, also provide value in applications for which 'free' ICG is used, e.g. during angiography applications such as free-flap reconstruction [14] or partial nephrectomy [15], for lymphedema imaging [16], lymphatic mapping [11] or the identification of postoperative lymphatic leaks [17], or the for the identification of metastases in the liver [18].

CONCLUSION

The m-PDE fluorescence camera system enhances the fluorescence imaging properties and simplifies the workflow compared with its predecessor. We thus think it provides a critical next step in the routine use of fluorescence-guided surgery.

REFERENCES

1. Crane LM, Themelis G, Arts HJ, Buddingh KT, Brouwers AH, Ntziachristos V, et al. Intraoperative near-infrared fluorescence imaging for sentinel lymph node detection in vulvar cancer: first clinical results. Gynecol Oncol. 2011;120:291-5.
2. Mieog JS, Troyan SL, Hutteman M, Donohoe KJ, van der Vorst JR, Stockdale A, et al. Toward optimization of imaging system and lymphatic tracer for near-infrared fluorescent sentinel lymph node mapping in breast cancer. Ann Surg Oncol. 2011;18:2483-91.
3. Kusano M, Kokudo N, Toi M, Kaibori M (eds). ICG fluorescence imaging and navigation surgery. New York: Springer; 2016.
4. KleinJan GH, van den Berg NS, Brouwer OR, de Jong J, Acar C, Wit EM, et al. Optimisation of fluorescence guidance during robot-assisted laparoscopic sentinel node biopsy for prostate cancer. Eur Urol. 2014;66:991-8.
5. Brouwer OR, Klop WM, Buckle T, Vermeeren L, van den Brekel MW, Balm AJ, et al. Feasibility of sentinel node biopsy in head and neck melanoma using a hybrid radioactive and fluorescent tracer. Ann Surg Oncol. 2012;19:1988-94.
6. van den Berg NS, Brouwer OR, Klop WM, Karakullukcu B, Zuur CL, Tan IB, et al. Concomitant radio- and fluorescence-guided sentinel lymph node biopsy in squamous cell carcinoma of the oral cavity using ICG-(99m)Tc-nanocolloid. Eur J Nucl Med Mol Imaging. 2012;39:1128-36.
7. van den Berg NS, Brouwer OR, Schaafsma BE, Matheron HM, Klop WM, Balm AJ, et al. Multimodal surgical guidance during sentinel node biopsy for melanoma: combined gamma tracing and fluorescence imaging of the sentinel node through use of the hybrid tracer indocyanine green-(99m)Tc-nanocolloid. Radiology. 2015;275:521-9.
8. Brouwer OR, van den Berg NS, Matheron HM, van der Poel HG, van Rhijn BW, Bex A, et

al. A hybrid radioactive and fluorescent tracer for sentinel node biopsy in penile carcinoma as a potential replacement for blue dye. Eur Urol. 2014;65:600-9.
9. Mathéron HM, van den Berg NS, Brouwer OR, Kleinjan GH, van Driel WJ, Trum JW, et al. Multimodal surgical guidance towards the sentinel node in vulvar cancer. Gynecol Oncol. 2013;131:720-5.
10. van Leeuwen FW, Hardwick JC, van Erkel AR. Luminescence-based imaging approaches in the field of interventional molecular imaging. Radiology. 2015;276:12-29.
11. Manny TB, Patel M, Hemal AK. Fluorescence-enhanced robotic radical prostatectomy using real-time lymphangiography and tissue marking with percutaneous injection of unconjugated indocyanine green: the initial clinical experience in 50 patients. Eur Urol. 2014;65:1162-8.
12. van Den Berg NS, Buckle T, Kleinjan GH, Klop WM, Horenblas S, van Der Poel HG, et al. Hybrid tracers for sentinel node biopsy. Q J Nucl Med Mol Imaging. 2014;58:193-206.
13. Brouwer OR, Buckle T, Vermeeren L, Klop WM, Balm AJ, van der Poel HG, et al. Comparing the hybrid fluorescent-radioactive tracer indocyanine green-^{99m}Tc-nanocolloid with ^{99m}Tc-nanocolloid for sentinel node identification: a validation study using lymphoscintigraphy and SPECT/CT. J Nucl Med. 2012;53:1034-40.
14. Holm C, Dornseifer U, Sturtz G, Basso G, Schuster T, Ninkovic M. The intrinsic transit time of free microvascular flaps: clinical and prognostic implications. Microsurgery. 2010;30:91-6.
15. Bjurlin MA, Gan M, McClintock TR, Volpe A, Borofsky MS, Mottrie A, et al. Near-infrared fluorescence imaging: emerging applications in robotic upper urinary tract surgery. Eur Urol. 2014;65:793-801.
16. Unno N, Nishiyama M, Suzuki M, Tanaka H, Yamamoto N, Sagara D, et al. A novel method of measuring human lymphatic pumping using indocyanine green fluorescence lymphography. J Vasc Surg. 2010;52:946-52.
17. Tan IC, Balaguru D, Rasmussen JC, Guilliod R, Bricker JT, Douglas WI, et al. Investigational lymphatic imaging at the bedside in a pediatric postoperative chylothorax patient. Pediatr Cardiol. 2014;35:1295-300.
18. Ishizawa T, Fukushima N, Shibahara J, Masuda K, Tamura S, Aoki T, et al. Real-time identification of liver cancers by using indocyanine green fluorescent imaging. Cancer. 2009;115:2491-504.

SUPPORTING INFORMATION

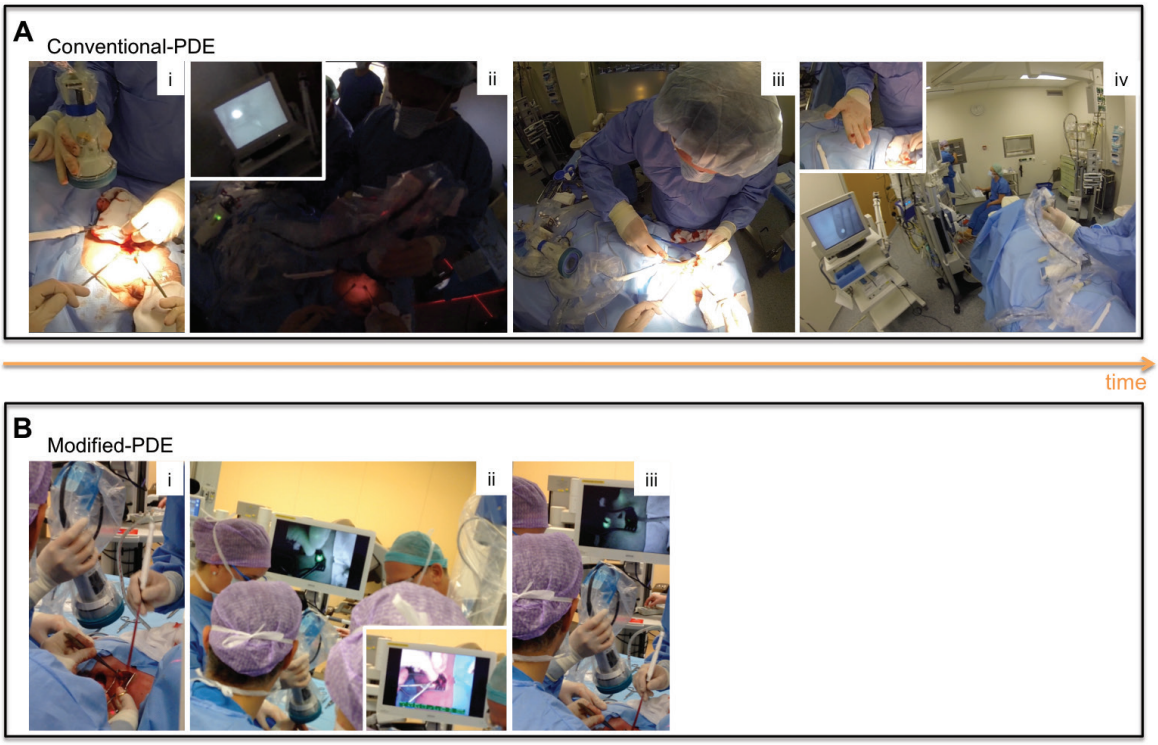

Figure SI1. Operation room logistics for the conventional-PDE and modified-PDE fluorescence camera. A) Workflow when using the conventional-PDE fluorescence camera: Upon presumed localization of the SN, the camera is brought into position by the operating surgeon (i). Thereafter lights in the operation room are switched off and the surgeon, on-screen, inspects the wound area for the presence of a fluorescence hotspot indicating the SN (ii). A black-and-white fluorescence image is generated by the system (ii, insert). After pinpointing the SN with a forceps, lights in the operation room are turned back on and the SN is excised (iii). Post-excision fluorescence imaging to confirm SN removal (iv; the insert shows the SN lying on the hand of the surgeon); B) Workflow when using the modified-PDE fluorescence camera: Upon presumed localization of the SN, the camera is brought into position by the operating surgeon after which the assisting scrub-nurse or fellow will hold the camera to allow for fluorescence-guided SN excision (i). Fluorescence imaging is performed under ambient light conditions. Here the fluorescence signal is displayed on-screen in green on a grey-scaled background. Under real-time fluorescence imaging conditions, the surgeon explores the area harboring the SN (ii; the insert shows the corresponding white light image) and excises it accordingly (iii). SN = sentinel node; PDE = PhotoDynamic Eye.

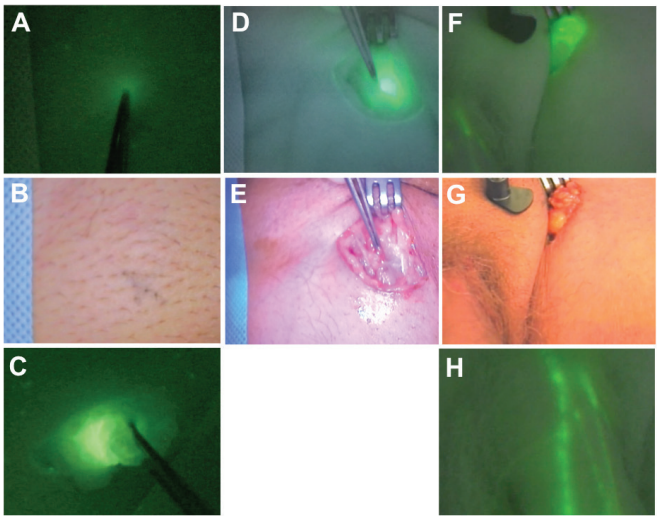

Figure SI2. Examples of the images acquired with the modified-PDE system in patients with penile cancer. A) Transcutaneous visualization of a SN located in the groin; B) Corresponding white light image; C) Fluorescence-based SN visualization after the skin was opened; D) Intraoperative identification of a non-blue, but radioactive and fluorescent SN in the groin; E) Corresponding white light image; F) Visualization of the SN in the groin. The left side of the image also shows the lymphatic duct(s) draining to this specific SN; G) Fluorescence-based visualization of lymphatic ducts over the penis running to SNs in the groin; H) Visualization of lymphatic ducts running over the penis to the SN(s) in the groin. SN = sentinel node; PDE = PhotoDynamic Eye; SPECT/CT = single photon emission computed tomography combined with computed tomography.

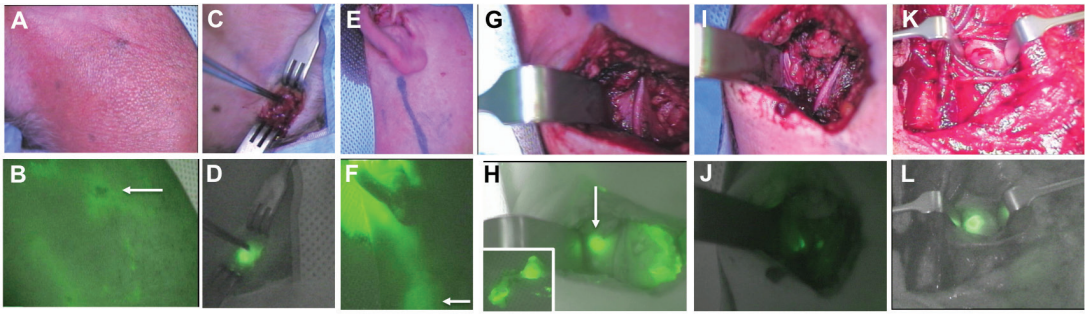

Figure SI3. Examples of the images acquired with the modified-PDE system in patients with head-and-neck malignancies. A) Transcutaneous visualization of a suboccipital SN together with the ducts running from the melanoma on the crown of the head to the neck; B) Corresponding white light image; C) Fluorescence-based visualization of a suboccipital SN; D) Corresponding white light image; E) Transcutaneous visualization of the lymphatic duct running from the injected melanoma site on the ear to a cluster of SNs in level II of the neck; F) Corresponding white light image; G) After opening of the skin, a clear fluorescence hotspot could be visualized. During excision here two SNs were visualized (insert); H) Corresponding white light image; I) Post-excision visualization of the remaining lymphatic ducts; J) Corresponding white light image; K) Fluorescence-based visualization of a deep lying SN in level V in a patient with a melanoma just below the mandibular in the neck; L) Corresponding white light image. SN = sentinel node; PDE = PhotoDynamic Eye.

CHAPTER 7

CHAPTER 8

OPTIMISATION OF FLUORESCENCE GUIDANCE DURING ROBOT-ASSISTED LAPAROSCOPIC SENTINEL NODE BIOPSY FOR PROSTATE CANCER

Adapted from: Kleinjan GH*, van den Berg NS*, Brouwer OR, de Jong J, Acar C, Wit EM, Vegt E, van der Noort V, Valdés Olmos RA, van Leeuwen FWB, van der Poel HG. Eur Urol. 2014:66(6);991-8. * = Shared first authorship.

ABSTRACT

BACKGROUND The hybrid tracer was introduced to complement intraoperative radiotracing towards the sentinel nodes (SNs) with fluorescence guidance.

OBJECTIVE Improve in vivo fluorescence-based SN identification for prostate cancer by optimizing hybrid tracer preparation, injection technique, and fluorescence imaging hardware.

DESIGN, SETTING, AND PARTICIPANTS Forty patients with a Briganti nomogram-based risk >5% of lymph node metastases were included. After intraprostatic tracer injection, SN mapping was performed (lymphoscintigraphy and single photon emission computed tomography with computed tomography (SPECT/CT)).

In groups 1 and 2, SNs were pursued intraoperatively using a laparoscopic gamma probe followed by fluorescence imaging. In group 3, SNs were initially located via fluorescence imaging. Compared with group 1, in groups 2 and 3, a new tracer formulation was introduced that had a reduced total injected volume (2.0 mL vs. 3.2 mL but increased particle concentration. For groups 1 and 2, the Tricam SLII with D-Light C laparoscopic fluorescence imaging system was used. In group 3, the laparoscopic fluorescence imaging system was upgraded to an Image 1 HUB HD with D-Light P system.

INTERVENTION Hybrid tracer-based SN biopsy, extended pelvic lymph node dissection, and robot-assisted radical prostatectomy.

OUTCOME MEASUREMENTS AND STATISTICAL ANALYSIS Number and location of the preoperatively identified SNs, in vivo fluorescence-based SN identification rate, tumor status of SNs and lymph nodes, postoperative complications, and biochemical recurrence (BCR).

RESULTS AND LIMITATIONS Mean fluorescence-based SN identification improved from 63.7% (group 1) to 85.2% and 93.5% for groups 2 and 3, respectively (p=0.012). No differences in postoperative complications were found. BCR occurred in three pN0 patients.

CONCLUSIONS Stepwise optimization of the hybrid tracer formulation and the laparoscopic fluorescence imaging system led to a significant improvement in fluorescence-assisted SN identification. Preoperative SPECT/CT remained essential for guiding intraoperative SN localization.

INTRODUCTION

Sentinel node (SN) biopsy using a radioactive tracer was introduced for prostate cancer to minimize the extent of the pelvic lymph node dissection (PLND) while retaining diagnostic accuracy [1]. The concept behind SN biopsy is to identify the lymph nodes that are most likely to contain metastatic cells in case migration from the primary prostate tumor has occurred, the so-called SNs. Visualization of this direct drainage pathway transcends the anatomic location of the SN. Therefore, this technique also enables the identification of potential tumor-bearing lymph nodes outside the extended PLND (ePLND) template [2,3] that would otherwise have been missed. When performing SN biopsy in combination with an ePLND, improved lymphatic staging can be achieved; pathologists can evaluate the SNs more extensively, decreasing the possibility of sampling errors, which can result in improved diagnostic accuracy [4,5].

Since its introduction, the procedure has been subject to various refinements. In the past 15 years, the surgical technique has shifted from a mainly open procedure to a laparoscopic and later a robot-assisted procedure. For preoperative SN mapping, following the injection of a radioactive tracer, lymphoscintigrams are taken. The introduction of single photon emission computed tomography with computed tomography (SPECT/CT) resulted in improved anatomic SN localization, allowing better planning of the operation and reducing operative time [6].

To date, intraoperative SN identification is based primarily on the use of a (laparoscopic) gamma probe (radioguided approach). The recent introduction of fluorescence imaging during surgery was shown to aid the surgeon in optical, fluorescence-based, visualization of the SNs [7,8]. Yet, the limited penetration depth of the near-infrared fluorescent dye indocyanine green (ICG; <1.0 cm) prohibits preoperative SN mapping, meaning that during surgery meticulous scanning of, and beyond, the entire ePLND template is required [2,6]. This exploration is extensive and time-consuming and may potentially miss SNs. Hence, the use of ICG is often combined with radiocolloid-based preoperative SN mapping methods [8]. To facilitate the integrated use of preoperative imaging with fluorescence guidance, we introduced the hybrid tracer ICG-^{99m}Tc-nanocolloid [6]. Being both radioactive and fluorescent, a single ICG-^{99m}Tc-nanocolloid administration allows for preoperative SN mapping as well as intraoperative fluorescence guidance to these exact hot spots. In our previous studies, the hybrid nature of this tracer was shown to complement the radio-guided approach and outperformed blue dye [9,10].

Following our initial feasibility study in prostate cancer [11], 40 additional prostate cancer patients were included. In these patients, we systematically evaluated whether optimization of the tracer formulation and fluorescence imaging hardware improvements could help increase in vivo fluorescence-based SN identification during robot-assisted laparoscopic procedures.

METHODS

PATIENTS

Between December 2010 and July 2013, 40 patients with localized prostate cancer and a Briganti nomogram-estimated risk >5% of lymph node metastases were included after informed consent was obtained. Patients were scheduled for robot-assisted radical prostatectomy (RARP) and SN biopsy followed by an ePLND. The first nine patients were included under registration of the feasibility study (N09IGF), and the patient population was completed through off-label use of the hybrid tracer. Three groups were formed for statistical analysis. In group 1 (n=11; December 2010-April 2011), the previously described hybrid tracer preparation [11] and the Tricam SLII with D-Light C laparoscopic fluorescence imaging system (KARL STORZ Endoskope GmbH & Co. KG, Tuttlingen, Germany) was used. In group 2 (n=13; April 2011-November 2012), the particle concentration was increased, and the injected volume decreased. In group 3 (n=16; December 2012-July 2013), the tracer formulation was identical to that used in group 2, but an upgraded laparoscopic fluorescence imaging system (Image 1 HUB HD with D-Light P system (KARL STORZ Endoskope GmbH & Co. KG)) was introduced.

TRACER PREPARATION

Two different tracer formulations were used. In group 1 we prepared the hybrid tracer as previously described (0.4 mL in the syringe; referred to as the previously described tracer formulation) [11]. In groups 2 and 3 we used the new tracer formulation.

The new tracer formulation was prepared as follows: ^{99m}Tc-nanocolloid was made by adding 2.0 mL pertechnetate (approximately 300 MBq) to a vial of nanocolloid (GE Healthcare, Eindhoven, The Netherlands). ICG-^{99m}Tc-nanocolloid was then formed by adding 0.05 mL (0.25 mg) of ICG solution (5.0 mg/mL; Pulsion Medical, Feldkirchen, Germany) to the vial. After in situ formation of ICG-^{99m}Tc-nanocolloid, the tracer was subtracted from the vial and diluted with saline to a total volume of 2.0 mL in the syringe. Procedures were performed in accordance with the Dutch guidelines for good manufacturing practice and with approval of the local pharmacist.

TRACER INJECTION

The hybrid tracer was injected transrectally into the peripheral zone of each quadrant of the prostate under ultrasound guidance [11]. In group 1, four deposits of 0.1 mL ICG-^{99m}Tc-nanocolloid were given. After each injection, the needle was flushed with 0.7 mL saline (total injected volume: 3.2 mL). In groups 2 and 3, patients received four deposits of 0.5 mL ICG-^{99m}Tc-nanocolloid (total injected volume: 2.0 mL).

PREOPERATIVE SENTINEL NODE MAPPING

Static planar lymphoscintigraphy was performed 15 min and 2 h after injection, followed by a SPECT and low-dose CT scan (Symbia T; Siemens Healthcare, Erlangen, Germany).

SPECT and low-dose CT images were fused, and a three-dimensional (3D) SPECT/CT-based volume-rendering reconstruction was created using OsiriX medical imaging software (Pixmeo, Geneva, Switzerland). Images were analyzed by an experienced nuclear medicine physician according to previously described criteria [12].

SURGICAL PROCEDURE

Operations were performed by HGvdP using the da Vinci S Surgical system (Intuitive Surgical Inc., Sunnyvale, CA, USA). Patients first underwent SN biopsy, followed by ePLND and RARP.

In the case of a one-sided SN non-visualization following preoperative imaging, an ePLND was performed on that side. The ePLND comprised all lymph nodes in the internal, obturator, and external regions proximal of the ureter vessel crossing and distally from the pubic bone. SNs outside the ePLND template were defined as described by Meinhardt et al. [13]. Preoperatively acquired SPECT/CT images and the 3D volume-rendered image were used as a virtual roadmap for the localization of the individual SNs. Intraoperatively, in groups 1 and 2, SNs were initially pursued using an laparoscopic gamma probe (Europrobe 2; Eurorad S.A., Eckbolsheim, France) followed by confirmatory fluorescence imaging. In group 3, SNs were initially localized via fluorescence imaging followed by ex vivo confirmation via gamma tracing. Real-time fluorescence images were introduced into the da Vinci S system via the TilePro function [11].

In this study, fluorescence imaging was performed using two generations of laparoscopic fluorescence imaging systems: the Tricam SLII with D-Light C system (groups 1 and 2) and the Image 1 HUB HD with D-Light P system (group 3) (both KARL STORZ Endoskope GmbH & Co. KG).

PATHOLOGIC EXAMINATION

Lymph nodes and SNs were formalin fixed, cut at 2 mm, and paraffin embedded. Lymph nodes sections were stained with haematoxylin and eosin. SNs were cut at three levels (150 µm intervals), and sections were haematoxylin and eosin stained. In addition, on the second level, an immunohistochemical stain was performed using a CAM5.2 antibody (catalogue number 345779; Becton Dickinson Biosciences, San Jose, CA, USA). Prostatectomy specimens were formalin fixed, paraffin embedded, and classified according to the 2009 TNM classification.

FOLLOW-UP

Postoperative complications (within 90 days after surgery) were scored using the Clavien-Dindo score [14]. Patients were evaluated for biochemical recurrence (BCR; prostate-specific antigen >0.1 ng/mL) during follow-up.

STATISTICAL ANALYSIS

For continuous variables, the mean or median and interquartile range (IQR; 25-75%) is

given. For discrete variables, frequencies and percentages are reported. Study endpoints were as follows: 1) intraoperative fluorescence-based SN identification rate; defined for each patient as ((number of SNs intraoperatively visualized via fluorescence imaging)/(total number of SNs seen on preoperative imaging)) x 100%; 2) postoperative complications, and 3) BCR.

A one-way analysis of variance was performed for evaluation of the number of postoperative complications in the three groups. We used the nonparametric Kruskal-Wallis test for evaluation of between-group differences in intraoperative fluorescence-based SN identification rate and the number of harvested SNs and lymph nodes. For BCR-free survival, we performed a log-rank test comparing groups 1 and 2 with group 3. A chi-square test was performed to evaluate whether there was a difference in pN1 patients among the three groups. Statistical analysis was performed using SPSS version 20 (IBM Corp., Armonk, NY, USA).

In general, viewing our 40 patients as a random sample of the entire population, our null hypothesis is that the unknown distributions of these rates in the population are the same across the three groups. A p-value <0.05 was considered significant.

RESULTS

PREOPERATIVE IMAGING

Patient characteristics are shown in Table 1. At least one SN was preoperatively identified in 38 of the 40 patients. Bilateral non-visualization occurred in two patients (5.0%) and unilateral non-visualization in five patients (12.5%). Lymphoscintigraphy and SPECT/CT imaging identified a total of 119 SNs (median: 3, IQR 0-2). Results per subgroup are specified in supplementary information Table SI1.

Changing the hybrid tracer formulation did not yield a significant difference in the number of preoperatively visualized SNs (Table 2). However, with the new tracer formulation flushing was no longer necessary between placement of the difference tracer deposits, thereby reducing injection time and increasing the ease of the procedure.

INTRAOPERATIVE SENTINEL NODE IDENTIFICATION

Six of the preoperatively identified SNs could not be resected because of the risk of injury or mechanical limitations of the robot (location: pararectal region inside the mesorectal fascia (n=3), presacral region (n=2), and right iliac region (n=1) Table 3).

In seven patients, 14 additional SNs were removed during surgery based on their fluorescent and radioactive appearance in the same region as the SNs detected with preoperative imaging. In retrospect, in six of these seven patients, lumph node clusters could be visualised on CT (Figure 1). Overall, 127 SNs (median: 3 per patient; IQR: 2-4; Table 2) were identified during surgery. In 16 patients (40.0%), an SN was located outside the ePLND template (Figures 2 and 3; Table 3).

Table 1. Patient characteristics

	Total	***Group 1***	***Group 2***	***Group 3***
No. patients	40	11	13	16
Age, median (IQR)	64 (60-68)	62 (59-69)	64 (61-67)	65 (60-70)
Preoperative PSA-level (ng/mL), median (IQR)	8.5 (6.4-13.9)	12.0 (8.1-17.2)	9.0 (6.9-15.5)	6.8 (5.2-9.0)
Clinical T-stage				
- 1c (%)	7	2	3	2
- 2a (%)	3	1	1	1
- 2b (%)	10	4	3	4
- 2c (%)	9	1	3	4
- 3a (%)	9	3	2	4
- 3b (%)	2	0	1	1
Biopsy Gleason sum score				
- 6 (%)	4	4	0	0
- 7 (%)	30	6	8	16
- 8 (%)	5	1	4	0
- 9 (%)	1	0	1	0
- 10 (%)	0	0	0	0
Pathologic T-stage				
- 2a (%)	0	0	0	0
- 2b (%)	6	2	1	3
- 2c (%)	16	3	5	8
- 3a (%)	16	5	6	5
- 3b (%)	2	1	1	0
Pathologic Gleason sum score				
- 6 (%)	4	0	2	2
- 7 (%)	28	9	6	14
- 8 (%)	3	1	2	0
- 9 (%)	4	0	3	0
- 10 (%)	1	1	0	0

IQR = interquartile range; no. = number; PSA = prostate specific antigen.

Table 2. Intraoperative sentinel node identification and ex vivo measurements

	Total (n=38[@])	***Group 1***	***Group 2***	***Group 3***	***p-value***
Number of intraoperatively detected SNs, per patient, median (IQR)	3 (2-4)	2 (2-3)	4 (2.5-4)	4 (2-4)	0.2[a]
In vivo SN identification					
- Fluorescence-based SN identification rate# in vivo, per patient,mean % (mean % corrected for malfunctioning equipment)	72.9% (84.0%*)	50.9% (63.7%*)	63.8% (85.2%*)	93.5% (93.5%*)	0.005a (0.012a)
- Radioactivity-based SN detection in vivo, per patient, mean %	100%	100%	100%	NA	-
Ex vivo SN measurements					
- Fluorescence-based SN detection ex-vivo, %	96.9%	92.6%	97.7%	100.0%	-
- Radioactivity-based SN detection ex vivo, %	100.0%	100.0%	100.0%	100.0%	-
Time per combined SN, ePLND and prostatectomy procedure (h), median (IQR)	2:07 (2:00-2:12)	2:01 (1:50-2:01)	2:04 (2:00-2:14)	2:06 (2:02-2:14)	0.2[b]

[@] Two patients were excluded due to non-visualization on preoperative images (one patient in group 1, and one patient in group 2).

\# Intraoperative fluorescence-based SN identification rate is defined as: defined for each patient as: ((number of SNs intraoperatively visualized via fluorescence imaging) / (total number of SNs seen on preoperative imaging)) x 100%.

* Intraoperative fluorescence-based SN identification rate after correction for non-visualization due to malfunctioning equipment.

[a] = Kruskal-Wallis test; [b] = ANOVA-test; n = number; NA = not applicable; IQR = interquartile range; SN = sentinel node; n = number of patients.

Table 3. Number and location of the intraoperatively identified sentinel nodes

	Total	*Group 1*	*Group 2*	*Group 3*
SNs removed from ePLND template, no. (% total)				
- Left obturator region	19 (15.0%)	4 (3.1%)	4 (3.1%)	11 (8.7%)
- Right obturator region	28 (22.0%)	7 (5.5%)	10 (7.9%)	11 (8.7%)
- Left external region	18 (14.2%)	6 (4.7%)	8 (6.3%)	4 (3.1%)
- Right external region	16 (12.6%)	5 (3.9%)	5 (3.9%)	6 (4.7%)
- Left internal region	9 (7.1%)	0	5 (3.9%)	4 (3.1%)
- Right internal region	7 (5.5%)	0	2 (1.6%)	5 (3.9%)
- Left common Iliac trunk	10 (7.9%)	3 (2.4%)	4 (3.1%)	3 (2.4%)
- Right common Iliac trunk	2 (1.6%)	0	0	2 (1.6%)
Subtotal	109 (85.8%)	25 (19.7%)	38 (29.9%)	46 (36.2%)
SN removed outside ePLND template, no. (% total)				
- Pararectal (mesorectal fascia) region	5 (3.9%)	1 (0.8%)	0	4 (3.1%)
- Presacral region	5 (3.9%)	1 (0.8%)	2 (1.6%)	2 (1.6%)
- Paravesical region	4 (3.1%)	0	0	4 (3.1%)
- Right umbilical ligament	1 (0.8%)	0	1 (0.8%)	0
- Left umbilical ligament	1 (0.8%)	0	1 (0.8%)	0
- Para-aortal region	2 (1.6%)	0	2 (1.6%)	0
Subtotal	18 (14.2%)	2 (1.6%)	6 (4.7%)	10 (7.9%)
Total	127 (100.0%)	27 (21.3%)	44 (34.6%)	56 (44.1%)
Not removed SN, no.				
- Pararectal region	3	1	1	1
- Presacral region	2	0	1	1
- Right iliac region	1	1	0	0
Total	6	2	2	2

SN = sentinel node; ePLND = extended pelvic lymph node dissection; no. = number.

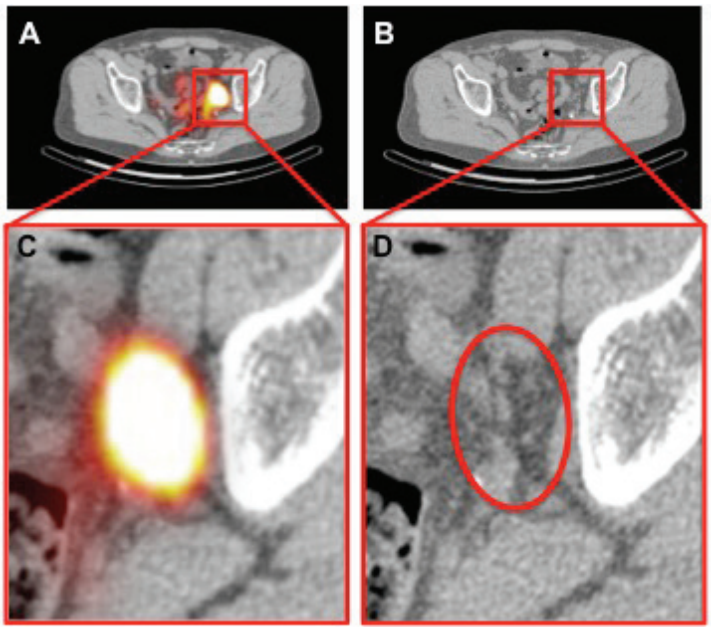

Figure 1. Clustered lymph nodes as seen on SPECT/CT imaging. A) Fused SPECT/CT image showing the location of a single radioactive hotspot in the left obturator region; B) Corresponding CT image; C) Zoom showing the radioactive hotspot; D) Multiple lymph nodes were visualized on the CT image in the area of the radioactive hotspot. SPECT/CT = single photon emission computed tomography combined with computed tomography; CT = computed tomography.

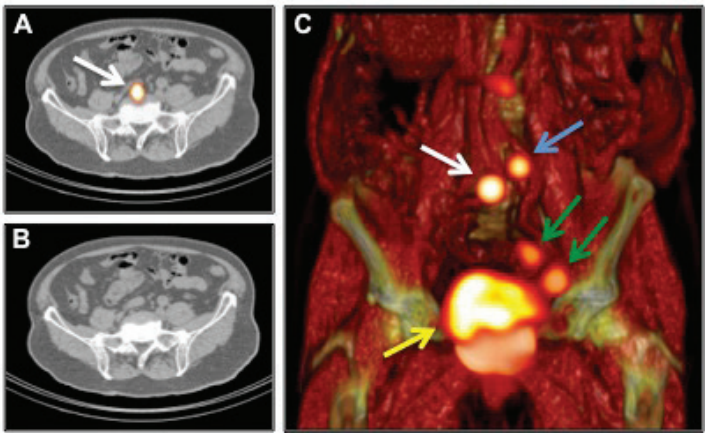

Figure 2. Illustration of the localization of sentinel nodes outside the extended pelvic lymph node dissection template. A) Fused SPECT/CT image showing the location of a single radioactive hotspot at the aorto-caval level (white arrow); B) Corresponding CT image; C) three dimensional volume rendering showing the injection site (yellow arrow), the aorto-caval sentinel node (white arrow) as well as two sentinel nodes at the external iliac and obturator region (green arrows). A higher-echelon para-aortic lymph node (blue arrow) was also visualized. SPECT/CT = single photon emission computed tomography combined with computed tomography; CT = computed tomography.

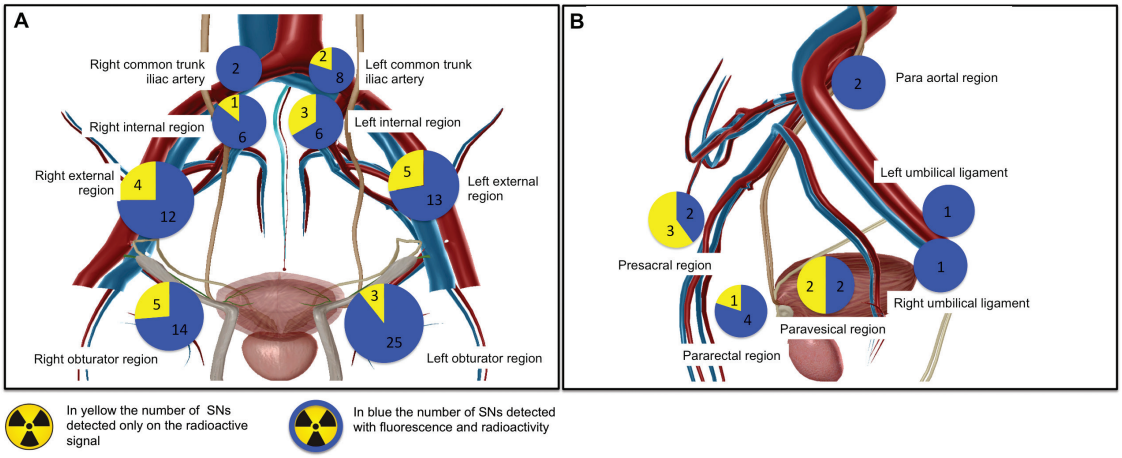

Figure 3. Intraoperative sentinel node location. A) Sentinel nodes inside extended pelvic lymph node dissection template; B) Sentinel nodes outside the extended pelvic lymph node dissection template. Intraoperatively, nodes were detected using radioguidance (yellow) or radio- and fluorescence guidance (blue). The schematic images used to illustrate the location of the detected sentinel nodes were generated with Visible Body software (Argosy Publishing Inc, Newton Upper Falls, MA, USA).

The two patients who had non-visualization on preoperative imaging were excluded from the intraoperative SN detection outcome analysis. With every stepwise modification, the intraoperative fluorescence-based SN visualization rate increased (Table 2). The mean optical SN visualization percentage modestly increased from 50.9% (group 1) to 63.8% (group 2) after the tracer formulation was altered. In these two groups, in five patients (group 1: two patients; group 2: three patients), none of the SNs could be intraoperatively visualized via fluorescence imaging for reasons of malfunctioning equipment (damaged light cable). After excluding these patients, the in vivo fluorescence-based SN visualization percentage of groups 1 and 2 was found to be 63.7% and 85.2%, respectively. Following the introduction of the upgraded laparoscopic fluorescence imaging system (group 3), the mean intraoperative visualization percentage went up to 93.5% (p=0.012). Ex vivo measurements in the operating room revealed a fluorescent signal in 123 of the 127 excised SNs (96.9%), while all excised SNs were radioactive (100.0%; Table 2).

PATHOLOGIC EXAMINATION

Overall, histopathological analysis of the excised tissues yielded 467 lymph nodes: 160 nodes in the SN specimens and 307 additional nodes resected from the subsequent ePLND template. In eight patients, a total of 32 tumor-positive nodes were found: 16 SNs and 16 lymph nodes (Table 4; supplementary information Table SI2). In three patients, the SN was

the only tumor-positive node. In three other patients, next to a tumor-positive SN, a tumor-positive lymph nodes was also found. Strikingly, in one of these three patients, next to two tumor-positive SNs, we found 12 tumor-positive lymph nodes (supporting information Table SI2). In the last two positive patients, SNs were tumor free, but a tumor-positive lymph nodes was found. In one of these two patients, the positive lymph nodes was found in the ePLND tissue (false-negative SN biopsy procedure). In the other patient, a small positive lymph nodes (3 mm) was found in the prostatectomy specimen. This particular lymph nodes was not seen on preoperative images.

On a per-patient basis, the sensitivity of the SN biopsy procedure was 75.0% (six out of eight pN1 patients correctly staged with SN biopsy), with a negative predictive value of 94.1%. On a per-tumor-positive node basis, this sensitivity is 50.0% (16 tumor-positive SNs on a total of 32 positive nodes; Table 4).

Table 4. Pathological node evaluation

	Total	***Group 1***	***Group 2***	***Group 3***	***p-value***
No. patients pN1	8	2	3	3	0.9[b]
SN evaluation					
- No. harvested SNs / patient, median (IQR)	4 (2.3-5.0)	3 (2.0-3.0)	4 (2.5-5.5)	4 (3.0-5.8)	0.028[a]
- Total no. SNs	160	29	57	74	
- Total no. tumor-positive SNs	16	1	5	9	
LN evaluation					
- No. harvested LNs from ePLND/ patient, median (range)	8 (4.5-11.0)	4 (4.0-10.0)	6 (4.5-12.0)	9 (7.3-11.0)	0.2[a]
- Total no. LNs	307	65	95	147	
- Total no. tumor-positive LN	16	1	13	2	
SN + LN evaluation					
- Total no. removed nodes per patient (SN + ePLND), median (IQR)	12 (9.0-14.8)	9 (6.0-11.0)	11 (8.0-15.5)	12 (11.0-16.0)	0.026[a]
- Total no. harvested SNs + LNs	467	94	152	221	

[a] = Kruskal-Wallis test; [b] = Chi-square test.
no. = number of patients; IQR = interquartile range; No. = number; SN = sentinel node; LN = lymph node; ePLND = extended pelvic lymph node dissection; pN1 = positive for regional lymph node metastases.

FOLLOW-UP

No significant differences in postoperative complications were found among the three groups (p=0.9; Table 5). Although follow-up was relatively short, in patients without nodal metastases (pN0), the Kaplan-Meier curve showed an improvement in BCR-free survival in group 3 (n=0; total follow-up 25 months) versus men in groups 1 and 2 (n=3; total follow-up 38 months; p=0.2; Figure 4).

Table 5. Patient follow-up

	Total	***Group 1***	***Group 2***	***Group 3***
Follow-up months, median (range)	10.5 (3.0-35.0)	22 (5.0-35.0)	12 (8.0-22.0)	8 (3.0-12.0)
Complications				
- Clavien-Dindo				
- Lymphocele (Clavien-Dindo IIIa)	2	0	2	0
- Urinary tract infection (Clavien-Dindo II)	2	0	1	1
- Postoperative bowel obstruction (Clavien-Dindo II)	1	1	0	0
- Micturition obstruction (Sachse Ureterotomy) (Clavien -Dindo IIIb)	1	1	0	0
- Postoperative wound infection (Clavien-Dindo II)	1	0	0	1
- Hematoma of the ventral abdominal wall (Clavien-Dindo I)	1	0	1	0
- Epididymitis (Clavien-Dindo II)	1	0	0	1
- Hydronephrosis (Clavien-Dindo IIIa)	1	1	0	0
Total	10	3	4	3
- Erectile dysfunction	24	5	6	13
- Micturition problems	11	2	4	5

Follow-up in postoperative complications reported within 90 days after the prostatectomy combined with extended pelvic lymph node dissection and sentinel node procedure.

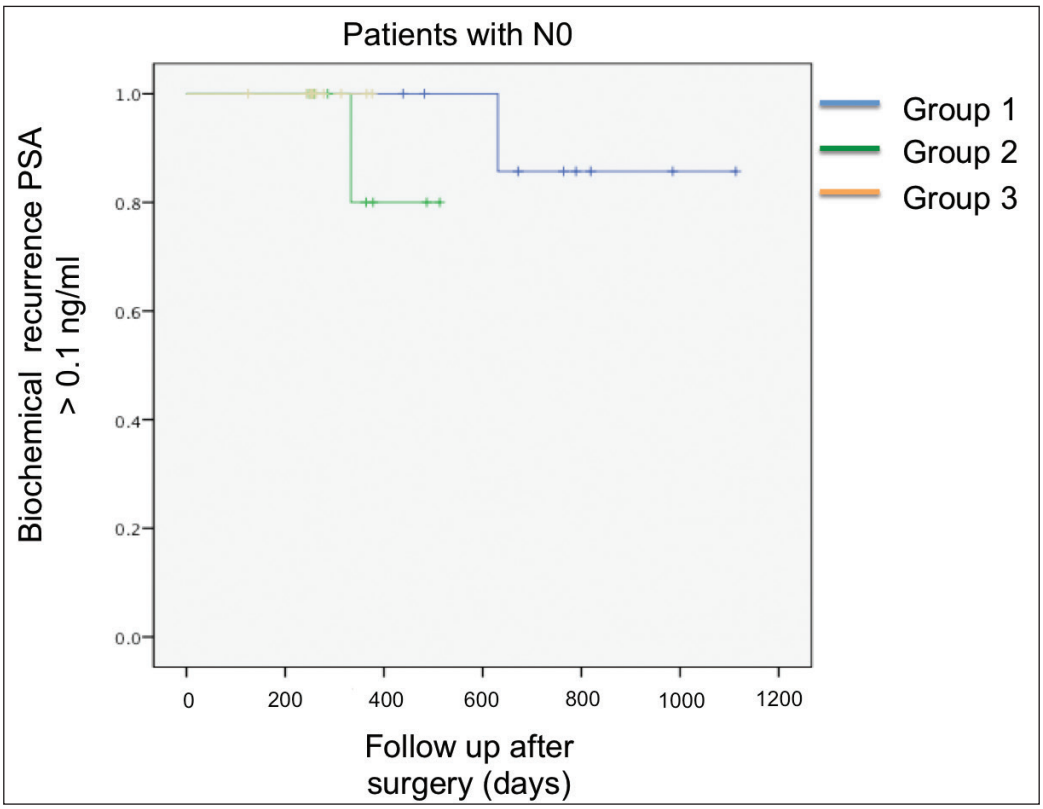

Figure 4. Kaplan Meier curve illustrating the biochemical recurrence. The blue line represents group 1 and 2 in which three biochemical recurrences were found. The green line represents group 3.

DISCUSSION

This study demonstrates that optimization of the hybrid tracer formulation and injection technique, as well as upgrading the laparoscopic fluorescence imaging system, improved in vivo fluorescence-based SN identification during RARP. Without altering the efficacy of preoperative SN mapping, the new tracer formulation increased the injected amount of ICG-^{99m}Tc-nanocolloid particles 2.5-fold and reduced the injected volume 1.6-fold. In combination with initial laparoscopic gamma probe exploration, the in vivo fluorescence visualization efficiency increased by 21.5% (group 1 vs. group 2). This increase contradicts our previous findings in breast cancer patients, where a 2-fold increase in the amount of injected particles did not lead to a change in fluorescence visualization efficiency [15]. Feedback from previous studies has taught us that the SN has to be exposed within mms of the surface to allow for in vivo fluorescence-based detection [9,10,16]. Hence, an explanation for this finding may lie in the time taken for the now more routine surgical

exploration; findings in group 1 turned out lower than the reported 85% in our feasibility study, which was based on the same approach.

After upgrading the laparoscopic fluorescence imaging system (group 3), the mean intraoperative fluorescence-based SN visualization percentage increased to 93.5%, transforming the procedure in a potential driver to improve intraoperative localization of tumor-positive SNs, even within the standard ePLND template. This improvement may provide better nodal staging (the "Will Rogers" phenomenon) and help improve the BCR-free survival rate, as was seen in group 3 [17]. The tailored filter settings allowed visualization of the near-infrared fluorescence signal (displayed in blue) as an integral part of the patient anatomy (displayed in "normal" colored view; Figure 5). Despite a slight loss in sensitivity this continuous exploration of the surgical field via fluorescence imaging proved extremely valuable for the localization of the SN(s). In combination wit the 3D information that SPECT/CT provided, this improvement may render initial exploration with the laparoscopic gamma probe in vivo redundant, provided that the fluorescence-based SN identification rate equals that of its radioactive counterpart. This is attractive because fluorescence does not suffer from the shine-through phenomenon from the tracer deposits in the prostate, as is the case for the radioguided approach [18].

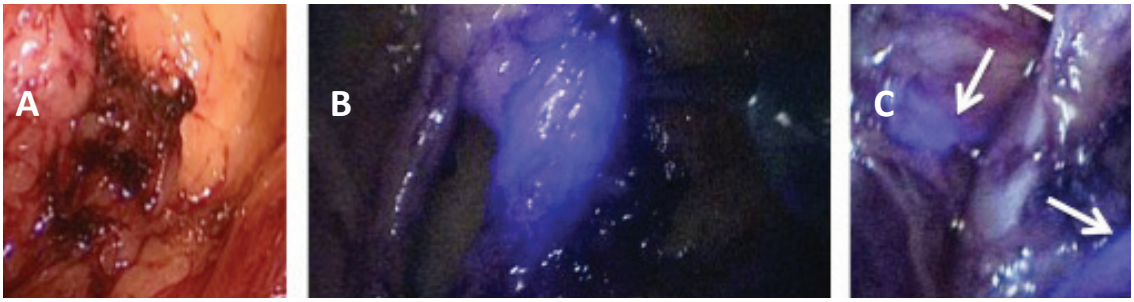

Figure 5. Intraoperative sentinel node (and lymphatic duct) identification via fluorescence guidance. A) White light image illustrating the area that harbors the sentinel node; B) Fluorescence guidance clearly shows the contours of the sentinel nodes. The adjusted filter settings of the Image 1 HUB HD + D-light P system (KARL STORZ Endoskope GmbH & Co. KG) allows clear visualization of anatomical detail in the background; C) Lymphatic ducts visualized via fluorescence imaging (white arrows).

Of the 16 tumor-positive SNs that were resected during the operation, one was located outside the ePLND template (6.3%). This finding underlines previous reports stating that metastatic spread may occur beyond the ePLND template [13,19]. In five of the eight patients with positive nodes, we found positive lymph nodes beyond the resected lumph nodes; in total 16 additional tumor-positive lymph nodes were recovered from the ePLND specimens. It must be noted that one patient accounts for 75% of these positive lymph nodes (supporting information Table SI2). Based on our findings, we believe that SN identification via the hybrid approach (including SPECT/CT) combined with ePLND provides the best approach for nodal staging in combination with RARP.

The main limitations of the study are the small patient population, the possibility that SN identification rates may increase over time because of a learning curve, and the relatively low number of overall nodes removed. The cost-effectiveness and the independent use of intraoperative fluorescence guidance remain to be investigated; currently, an international multicenter study is being initiated to address this question. Still an important question remains to be answered: What is the best hybrid tracer injection technique? In our current, ongoing, study (N12IGP) we will evaluate whether the location of hybrid tracer injection (intraprostatic vs. intratumoral) is relevant for the detection and localization of tumor-positive SNs.

CONCLUSION

Altering the hybrid tracer formulation and injection technique and upgrading the laparoscopic fluorescence imaging system significantly improved in vivo fluorescence-based SN identification. Further improvement of in vivo fluorescence-based SN detection, reaching rates similar to that of the conventional radio-guided approach, may make intraoperative laparoscopic gamma tracing redundant. Still, SPECT/CT remains an essential tool for preoperative SN localization.

REFERENCES

1. Wawroschek F, Vogt H, Weckermann D, Wagner T, Harzmann R. The sentinel lymph node concept in prostate cancer - first results of gamma probe-guided sentinel lymph node identification. Eur Urol. 1999;36:595-600.
2. van Leeuwen FWB, Hruby S. Fluorescence guidance during radical prostatectomy. Eur Urol. 2014;65:1169-1170.
3. Rousseau C1, Rousseau T, Campion L, Lacoste J, Aillet G, Potiron E, Lacombe M, Le Coguic G, Mathieu C, Kraeber-Bodéré F. Laparoscopic sentinel lymph node versus hyperextensive pelvic dissection for staging clinically localized prostate carcinoma: a prospective study of 200 patients. J Nucl Med. 2014;55:753-8.

4. Staník M, Capák I, Macík D, Vašina J, Lžičařová E, Jarkovský J, et al. Sentinel lymph node dissection combined with meticulous histology increases the detection rate of nodal metastases in prostate cancer. Int Urol Nephrol. 2014;46:1543-1549.
5. Wawroschek F, Wagner T, Hamm M, Weckermann D, Vogt H, Ma B. The influence of serial sections, immunohistochemistry, and extension of pelvic lymph node dissection on the lymph node status in clinically localized prostate cancer. Eur Urol. 2003;43:132-7.
6. Warncke SH, Mattei A, Fuechsel FG, Brun SZ, Krause T, Studer UE. Detection rate and operating time required for probe-guided sentinel lymph node resection after injection of technetium-99m nanocolloid into the prostate with and without preoperative imaging. Eur Urol. 2007;52:126-33.
7. Manny TB, Patel M, Hemal AK. Fluorescence-enhanced robotic radical prostatectomy using real-time lymphangiography and tissue marking with percutaneous injection of unconjugated indocyanine green: The initial clinical experience in 50 patients. Eur Urol. 2014:65;1162-8.
8. Jeschke S, Lusuardi L, Myatt A, Hruby S, Pirich C, Janetschek G. Visualisation of the lymph node pathway in real time by laparoscopic radioisotope- and fluorescence-guided sentinel lymph node dissection in prostate cancer staging. Urology. 2012;80:1080-7.
9. Brouwer OR, van den Berg NS, Mathéron HM, van der Poel HG, van Rhijn BW, Bex A, et al. A hybrid radioactive and fluorescent tracer for sentinel node biopsy in penile carcinoma as a potential replacement for blue dye. Eur Urol. 2014;65:600-9.
10. Mathéron HM, van den Berg NS, Brouwer OR, Kleinjan GH, van Driel WJ, Trum JW, et al. Multimodal surgical guidance towards the sentinel node in vulvar cancer. Gynecol Oncol. 2013;131:720-5.
11. van der Poel HG, Buckle T, Brouwer OR, Valdés Olmos RA, van Leeuwen FWB. Intraoperative laparoscopic fluorescence guidance to the sentinel lymph node in prostate cancer patients: clinical proof of concept of an integrated functional imaging approach using a multimodal tracer. Eur Urol. 2011;60:826-33.
12. Nieweg OE, Tanis PJ, Kroon BB. The definition of a sentinel node. Ann Surg Oncol. 2001;8:538-41.
13. Meinhardt W, van der Poel HG, Valdés Olmos RA, Bex A, Brouwer OR, Horenblas S. Laparoscopic sentinel lymph node biopsy for prostate cancer: the relevance of locations outside the extended dissection area. Prostate Cancer. 2012;2012:751753.
14. Dindo D, Demartines N, Clavien P-A. Classification of surgical complications: a new proposal with evaluation in a cohort of 6336 patients and results of a survey. Ann Surg. 2004;240:205-13.
15. Schaafsma BE, Verbeek FPR, Rietbergen DDD, van der Hiel B, van der Vorst JR, Liefers GJ, et al. Clinical trial of combined radio- and fluorescence-guided sentinel lymph node biopsy in breast cancer. Br J Surg. 2013;100:1037-44.
16. Brouwer OR, Klop WMC, Buckle T, Vermeeren L, van den Brekel MWM, Balm AJM, et

al. Feasibility of sentinel node biopsy in head and neck melanoma using a hybrid radioactive and fluorescent tracer. Ann Surg Oncol. 2012;19:1988-94.
17. Fukuda M, Egawa M, Imao T, Takashima H, Yokoyama K, Namiki M. Detection of sentinel node micrometastasis by step section and immunohistochemistry in patients with prostate cancer. J Urol. 2007;177:1313-7.
18. Joniau S, Van den Bergh L, Lerut E, Deroose CM, Haustermans K, Oyen R, et al. Mapping of pelvic lymph node metastases in prostate cancer. Eur Urol 2013;63:450-8.
19. Gofrit ON, Zorn KC, Steinberg GD, Zagaja GP, Shalhav AL. The Will Rogers phenomenon in urological oncology. J Urol. 2008;179:28-33.

SUPPORTING INFORMATION

Table SI1. Preoperative imaging results

	Total	*Group 1*	*Group 2*	*Group 3*
No. patients	40	11	13	16
Injected dose (MBq), median (IQR)	217.8 (205.3-228.7)	218.2 (205.7-236.7)	223.8 (207.8-236.7)	209.6 (203.8-222.8)
Preoperative imaging results, no. per patient				
- SNs on early lymphoscintigrams, median (IQR)	1 (0-2)	1 (0-2)	1 (0-2)	1 (0-2)
- SNs on late lymphoscintigrams, median (IQR)	2 (1-3)	2 (2-3)	2 (1-3)	2 (2-3)
- SNs on SPECT/CT, median (IQR)	3 (0-6)	2 (2-3)	4 (2-4)	3 (2-4)
- Higher-echelon LNs, median (IQR)	0 (0-1)	1 (0-2)	0 (0-1)	0 (0-.75)
Time from injection to surgery (h), median (IQR)	5:44 (4.15-5.07)	4:34 (4:15-5:05)	5:05 (4:14-5:35)	4:42 (4:13-5:04)

MBq = Mega Bequerel; IQR = interquartile range; SN = sentinel node; LN = lymph node; n = number of patients; no. = number; SPECT/CT = single photon emission computed tomography combined with computed tomography

Table SI2. pN1 pathological findings

Patient	*No. tumor-positive SNs*	*Location tumor-positive SNs*	*No. tumor-positive LNs from ePLND*	*Total no. tumor-positive SNs + LNs from ePLND*
1	0/1	-	1/3	1/4
2	1/7	Right external region	0/4	1/13
3	1/12	Right external region	1/7	2/19
4	2/2	Left internal region, Right obturator region	12/13	14/15
5	3/3	Left external region (2x), Left paravesical region	0/8	3/11
6	0/3	-	1/12	1/15
7	5/9	Left internal region (4x), Right obturator region	0/12	5/21
8	4/6	Left external region, Left obturator region, Right internal region, Right obturator region	1/13	5/19
Total	16/43		16/72	32/115

SN = sentinel node; LN = lymph node; ePLND = extended pelvic lymph node dissection.

CHAPTER 9

MULTISPECTRAL FLUORESCENCE IMAGING DURING ROBOT-ASSISTED LAPAROSCOPIC SENTINEL NODE BIOPSY: A FIRST STEP TOWARDS A FLUORESCENCE-BASED ANATOMIC ROADMAP

Adapted from: van den Berg NS, Buckle T, KleinJan GH, van der Poel HG, van Leeuwen FWB. Eur Urol 2016. DOI: 10.1016/j.eururo.2016.06.012.

ABSTRACT

BACKGROUND During (robot-assisted) sentinel node (SN) biopsy procedures, intraoperative fluorescence imaging can be used to enhance radioguided SN excision. For this combined pre- and intraoperative SN identification was realized using the hybrid SN tracer, indocyanine green-^{99m}Tc-nanocolloid. Combining this dedicated SN tracer with a lymphangiographic tracer such as fluorescein may further enhance the accuracy of SN biopsy.

OBJECTIVE Clinical evaluation of a multispectral fluorescence guided surgery approach using the dedicated SN tracer ICG-^{99m}Tc-nanocolloid, the lymphangiographic tracer fluorescein, and a commercially available fluorescence laparoscope.

DESIGN, SETTING, AND PARTICIPANTS Pilot study in ten patients with prostate cancer. Following ICG-^{99m}Tc-nanocolloid administration and preoperative lymphoscintigraphy and single photon emission combined with computed tomography imaging, the number and location of SNs were determined. Fluorescein was injected intraprostatically immediately after the patient was anesthetized. A multispectral fluorescence laparoscope was used intraoperatively to identify both fluorescent signatures.

SURGICAL PROCEDURE Multispectral fluorescence imaging during robot-assisted radical prostatectomy with extended pelvic lymph node dissection and SN biopsy.

MEASUREMENTS (1) Number and location of preoperatively identified SNs. (2) Number and location of SNs intraoperatively identified via ICG-^{99m}Tc-nanocolloid imaging. (3) Rate of intraoperative lymphatic duct identification via fluorescein imaging. (4) Tumor status of excised (sentinel) lymph node(s). (5) Postoperative complications and follow-up.

RESULTS AND LIMITATIONS Near-infrared fluorescence imaging of ICG-^{99m}Tc-nanocolloid visualized 85.3% of the SNs. In 8/10 patients, fluorescein imaging allowed bright and accurate identification of lymphatic ducts, although higher background staining and tracer washout were observed. The main limitation is the small patient population.

CONCLUSION Our findings indicate that a lymphangiographic tracer can provide additional information during SN biopsy based on ICG-^{99m}Tc-nanocolloid. The study suggests that multispectral fluorescence image-guided surgery is clinically feasible.

INTRODUCTION

Fluorescence imaging is rapidly finding its way into the operating theatre. A wide spectrum of fluorescent tracers has already been explored in clinical (first-in-human) studies as either free dye or a dye-functionalized targeting agent [1]. In the field for urology, fluorescence guidance has amongst others been used for sentinel node (SN) biopsy of prostate cancer [2, 3]. For this procedure, the near-infrared fluorescent dye indocyanine green (ICG), especially in the form of the hybrid tracer ICG-^{99m}Tc-nanocolloid was shown to enhance the more traditional radioguided ^{99m}Tc-nanocolloid-based SN biopsy procedure [4-6].

During the widely applied radioguided SN biopsy procedure of for example melanoma and breast cancer, intraoperatively blue dye is injected to allow the surgeons to optically define the lymphatic flow (lymphangiography) of a tumor; lymphangiographic tracers such as blue dye help to visualize the lymphatic ducts that run from the injection site to the SN [7, 8]. As alternatives to blue dye, the visible fluorescent dye fluorescein and the near-infrared fluorescent dye ICG in its 'free' form have been used [4,9-11]. While the fluorescent alternatives provide enhanced detection sensitivity compared to blue dye, their detection can be complex in combination with ICG-^{99m}Tc-nanocolloid. In this context, the concept of multi-color, or multispectral, fluorescence imaging can provide a solution.

Multispectral imaging involves concurrent use of multiple fluorescent dyes to highlight various molecular, physiological, and/or anatomical features [12, 13]. Factors critical in achieving successful multispectral imaging guidance are: 1) the clinical availability of fluorescence tracers that do not spectrally overlap (e.g. fluorescein ($\lambda_{em\ max}$ = 515 nm) and ICG ($\lambda_{em\ max}$ = 820 nm)); and 2) a (laparoscopic) fluorescence camera capable of detecting different fluorescence emissions. It should be noted that some of the currently available near-infrared fluorescence laparoscopes, designed for combined use with ICG, have evolved from laparoscopes developed for photodynamic diagnostics, which detects fluorescence emitted in the visual region [14].

In this study we investigated if intraoperative lymphangiography with fluorescein can provide additional guidance during ICG-^{99m}Tc-nanocolloid-based SN biopsy for prostate cancer. To this end we required intraoperative multispectral imaging. Hence, the secondary aim of the study was to prove the clinical feasibility of intraoperative multispectral fluorescence imaging.

METHODS

PRECLINICAL EVALUATION OF FLUORESCEIN AS LYMPH-ANGIOGRAPHIC AGENT

Initial preclinical experiments using fluorescein are described and discussed in the supporting information.

CLINICAL EVALUATION OF THE MULTISPECTRAL FLUORESCENCE IMAGING APPROACH

PATIENTS

Between October 2013 and August 2015, ten patients with intermediate or high-risk prostate cancer with a >5% risk of lymph node metastases as estimated using the Briganti nomogram [15] were included in a clinical study approved by the local medical ethical committee (Dutch trial register: NTR4451) after they provided written informed consent.

Patients were scheduled for robot-assisted radical prostatectomy (RARP) and SN biopsy followed by an extended pelvic lymph node dissection (ePLND). The patient characteristics are shown in Table 1.

PREOPERATIVE PROCEDURE

A detailed description of ICG-^{99m}Tc-nanocolloid preparation, the injection procedure and preoperative imaging approach is provided in the supporting information. In brief, ICG-^{99m}Tc-nanocolloid (204.49 MBq, range 191.56-218.20) was injected into the prostate 4.75 h before surgery (range 3.5-5.5) under transrectal ultrasound guidance. Then preoperative SN mapping using a combination of lymphoscintigraphy and single photon emission computed tomography combined with computed tomography (SPECT/CT) was performed to determine the number and location of the SN(s).

SURGICAL PROCEDURE

HARDWARE

Surgical procedures were performed by one surgeon (HvdP) using the da Vinci S(i) surgical system (Intuitive Surgical Inc., Sunnyvale, CA, US).

Multispectral fluorescence imaging requires multiple dyes that do not overlap spectrally for sequential excitation and detection. We used the Image 1 HUB HD + D-light P system (KARL STORZ Endoskope GmbH & Co. KG, Tuttlingen, Germany) with customized filter settings [5] for sequential visualization of ICG and fluorescein. ICG is excited (780 nm) and detected (820 nm) in the near-infrared mode (Supplementary Figure 1A, B), whereas fluorescein is excited (488 nm) and detected (515 nm) in the autofluorescence (AF) mode (Supplementary Figure 1A, C) [1].

Table 1 Patient characteristics, pathology and follow-up

		Preoperatieve data				*Pathology data*								
Patient	***Age***	***Pre-operative PSA (ng/mL)***	***cProstate size (cc)***	***cTNM***	***Biopsy-based Gleason sum score***	***pTNM, pR***	***Post-operative Gleason sum score***	***# SNs***	***# LNs***	***# Tumor-positive SNs / LNs***	***Post-operative complications (Clavien-Dindo)***	***Biochemical recurrence (PSA (ng/mL))***	***Adjuvant therapy***	***Follow-up (m)***
1	57	7.4	11	cT3bN0M0	3+4=7	pT3aN0Mx, pR0	3+4=7	4	10	0 / 0	-	0.12 (at 4.5 m F/U)	Adjuvant radio-therapy and hormonal therapy	26
2	73	3.4	19	cT3aN0M0	3+4=7	pT2cN0Mx, pR0	3+4=7	5	13	0 / 0	-	-	-	24
3	68	12.7	25	cT2cN0M0	3+5=8	pT4aN1M1a, pR0	3+5=8	3	22	3 / 18	-	4.95 (at 2 m F/U)	Adjuvant hormonal therapy	27
4	69	10.8	37	cT2aN0M0	3+4=7	pT2cN0Mx, pR0	3+4=7	1	6	0 / 0	-	-	-	25
5	68	5.2	92	cT3aN0M0	4+5=9	pT2cN0Mx, pR0	3+3=6	9	11	0 / 0	-	-	-	20
6	68	15.0	37	cT2bN0M0	4+3=7	pT3aN0Mx, pR0	3+5=8	4	11	0 / 0	-	-	-	18
7	70	9.4	52	cT2aN0M0	4+3=7	pT2cN0Mx, pR0	4+3=7	6	12	0 / 0	-	-	-	16
8	66	6.3	44	cT1cNxMx	3+4=7	pT2cN1Mx, pR0	3+4=7	1	19	0 / 1	I	-	-	14
9	66	9.4	40	cT3aN0M0	3+4=7	pT2aN1M0, pR1	3+4=7	7	17	2 / 17	II	-	-	14
10	65	6.6	70	cT2cN0M0	3+4=7	pT3aN0Mx, pR0	3+4=7	12	11	0 / 0	-	un-known*	un-known*	un-known*
Average	67	8.6	55.6					5.2	13.2					
Total								52	132	5 / 36				

PSA = prostate specific antigen; c = clinical; p = pathological; T = tumor; N = node; M = metastasis;
# = number; SNs = sentinel nodes; LNs = lymph nodes. *Patient follow-up elsewhere.

The fluorescence laparoscope was inserted via the assistant-port. The TilePro function of the da Vinci S(i) robot was utilized to present the fluorescence imaging data to the urologist.

Intraoperative procedure

Clinical grade fluorescein (fluorescite, 100 mg/mL) was obtained from Alcon Nederland B.V. (Gorinchem, the Netherlands). For injection of fluorescein, a total volume of 2.0 mL (200 mg fluorescein) was extracted from the vial and injected into the prostate similar to as described for ICG-^{99m}Tc-nanocolloid. The aim was to place the fluorescein deposits at the same location as for the hybrid tracer. Then the surgical field was sterilized.

Before incision, preoperatively acquired SPECT/CT images and the corresponding three-dimensional volume-rendered image were used as a virtual roadmap. Better knowledge of the location of the SN(s) with regard to the patient's anatomic context was achieved by scrolling through the images. These images served as the initial starting point for intraoperative SN localization. After entering the area of interest, the SNs (and the lymphatic ducts) were visualized via fluorescence imaging of ICG-^{99m}Tc-nanocolloid (near-infrared mode). The afferent lymphatic ducts (and SNs) were visualized via fluorescence imaging of fluorescein in the AF mode. As described previously, after excision of the SN(s), ex vivo gamma tracing was performed to confirm SN removal [5].

Following completion of SN biopsy, ePLND was performed, followed by RARP as described by KleinJan et al. [5]. In patients in whom preoperative SN mapping did not reveal a SN on one side, only an ePLND on that side was performed.

Scoring of the sentinel node and lymphangiographic findings

Intraoperatively, for each SN it was scored if 1) it could be visualized via ICG-^{99m}Tc-nanocolloid (yes/no) or fluorescein (yes/no) imaging; and 2) if the afferent lymphatic duct(s) could via fluorescein (yes/no) or ICG-^{99m}Tc-nanocolloid (yes/no) imaging. The general distribution of the two tracers in the surgical field was also evaluated.

(histo-)pathological examination of the tumor status

The prostate and the excised nodes were processed and evaluated for the presence and localization of tumor tissue as previously described [5].

Ex vivo multispectral fluorescence imaging of the injection site (prostate) and nodal samples

To confirm the presence of both fluorescent dyes, samples were evaluated ex vivo using the multispectral fluorescence laparoscope.

Table 2. Intraoperative imaging findings

Patient	*Injection hybrid tracer - start operation (hours)*	*Side that was operated on first*	*# SNs NIR fluorescent in vivo (ex vivo) L + R*	*# SNs with a fluorescein positive lymphatic duct L + R*	*Location excised SNs*	*Location SNs to which a lymphatic duct was seen*	*Location SNs not excised*
1	4.5	L	1 (1) + 2 (2)	1 + 0	L: ext iliac[$] R: int iliac, ext iliac	L: ext iliac R: -	L: presacral R: -
2	5.5	R	2 (2) + 3 (3)	0 + 1	L: obt fossa (2) R: int iliac, ext iliac, pararectal	L: - R: int iliac	-
3	3.5	L	1 (1) + 1 (1)	0 + 0	L: int iliac R: int iliac	-	-
4	5.5	L	1 (1) + nonvis	1 + nonvis	L: int iliac R: -	L: int iliac	L: presacral
5	4.5	R	1 (2) + 2 (3)	0 + 3	L: obt fossa, ext iliac R: obt fossa, int iliac, common iliac trunk	L: - R: obt fossa, int iliac, common iliac trunk	-
6	5	L	1 (1) + 3 (3)	1 + 2	L: int iliac R: int iliac (2), ext iliac	L: int iliac R: int iliac, ext iliac	L: presacral (2) R: -
7	4.5	L	1 (3) + 0 (1)	1 + 0	L: obt fossa (2), ext iliac R: int iliac	L: ext iliac R: -	L: - R: common iliac trunk
8	4.5	L	1 (1) + nonvis	0 + nonvis	L: obt fossa R: -	-	-
9	4.5	R	1 (1) + 4 (4)	0 + 2	L: common iliac trunk R: obt fossa (2), ext iliac, near umbiliacal ligamentum	L: - R: obt fossa (2)	-
10	5.5	L	3 (3) + 1 (1)	3 + 0	L: obt fossa (3) R: obt fossa	L: obt fossa (3)* R: -	
Average	4.75		2.9 (3.4)	1.5	3,4		0,5
Total		2 R / 8 L	29 (34)	15	34		5

In patients 2 and 10, 1 and 3 SNs were not evaluated for fluorescein-based visualization of the lymphatic ducts. [$] Next to being stained with ICG-^{99m}Tc-nanocolloid, this SN was also fluorescein positive; * Next to being stained with fluorescein, these lymphatic ducts were also ICG-^{99m}Tc-nanocolloid positive. L = left; R = right; # = number; SN = sentinel node; NIR = near-infraread; nonvis = non-visualization on preoperative imaging; ext = external; int = internal; obt = obturator.

POSTOPERATIVE COMPLICATIONS AND FOLLOW-UP

Postoperative complications (within 90 d after surgery) were scored using the Clavien-Dindo classification [16, 17]. Patients were also evaluated for biochemical recurrence (prostate specific antigen > 0.1 ng/mL) at follow-up.

RESULTS

Following intraprostatic ICG-^{99m}Tc-nanocolloid administration, preoperative imaging revealed 36 SNs in ten patients (mean 3.6; range 1-5; Figure 1 and Table SI1), of which 85.3% were visualized intraoperatively via real-time (video-rate) near-infrared fluorescence imaging (in 10/10 patients; Table 2, Figure 2). For superficially located SNs, fluorescein visualized lymphatic ducts to 44.1% of the SNs (in 8/10 patients; Table 2, Figure 2). This visualization was also in real-time and was achieved with good contrast and high resolution. In one patient bilateral lymphatic ducts were visualized via fluorescein imaging. In two patients, no lymphatic ducts could be visualized via fluorescein imaging, which may be a result of prostate site mismatch for fluorescein and ICG-^{99m}Tc-nanocolloid administration (Figure 3).

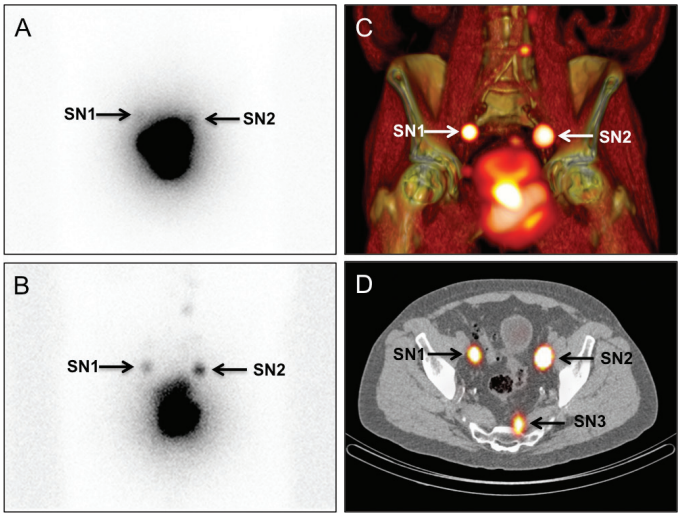

Figure 1. Preoperative sentinel node mapping. Following ICG-^{99m}Tc-nanocolloid administration, lympho-scintigrams were acquired at A) 15 min and B) 2 h after injection, followed by single photon emission computed tomography (SPECT) and computed tomography (CT) image acquisition. C) Following reconstruction, SPECT and CT images were fused and a three-dimensional volume rendering was generated. D) Axial SPECT/CT slices show the sentinel nodes being located in the external iliac (left and right) and the internal iliac (right). SN = sentinel node.

In one patient the lymphatic ducts could be identified via imaging of both fluorescein and ICG-^{99m}Tc-nanocolloid (Table 2, Figure 2A, B). In another patient fluorescein was also detected in an SN containing ICG-^{99m}Tc-nanocolloid (Table 2, Figure 2D), which was confirmed ex vivo in the excised SN specimen (Figure 3).

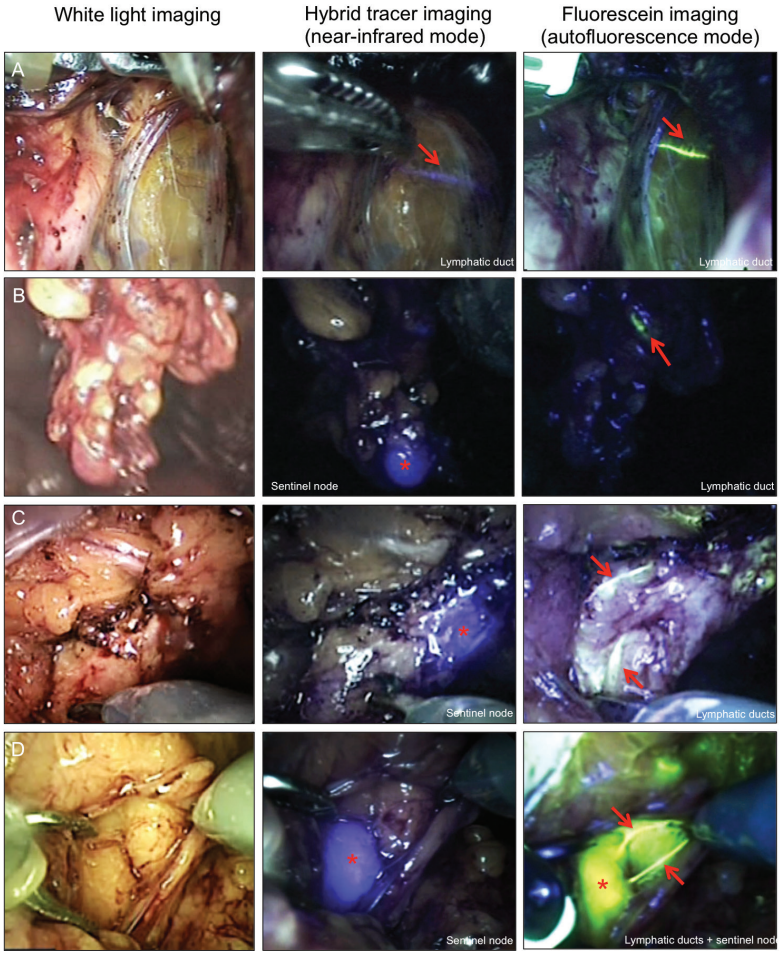

Figure 2. Intraoperative multispectral fluorescence imaging. Laparoscopic fluorescence imaging was performed of the areas of interest (left column). A) Visualization of a lymphatic duct via both near-infrared fluorescence imaging of the hybrid tracer (middle column; arrow) and visible fluorescence imaging of fluorescein (right column; arrow); B) The lymphatic duct seen under A ended in a sentinel node visualized via fluorescence imaging of the hybrid tracer (middle column; asterisk). No fluorescein was found in the sentinel node here (right column); C) Example of a sentinel node that could be visualized via fluorescence imaging of the hybrid tracer (right column; asterisk) whereas via fluorescein imaging clear lymphatic ducts were visualized running to this sentinel node (right column; arrows); D) Clear sentinel node visualization via both near-infrared fluorescence imaging of the hybrid tracer (middle column; asterisk) and fluorescence imaging of fluorescein (right column; asterisk). With fluorescein also two clear lymphatic ducts running to the sentinel node were visualized (right column; arrows).

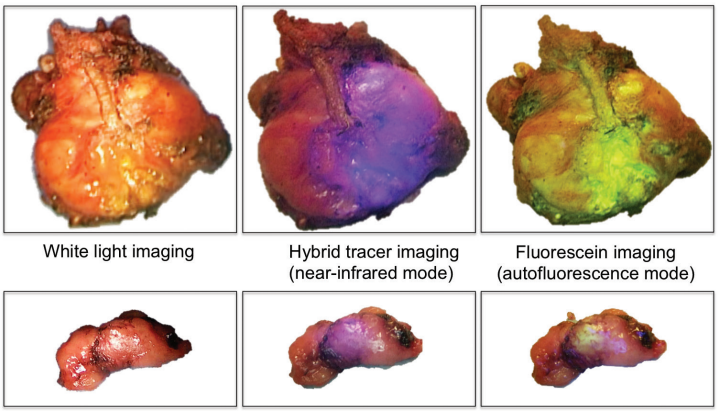

Figure 3. Ex vivo multispectral fluorescence imaging of the prostate and a sentinel node. Top row: White light image showing the prostate (left). Multispectral fluorescence imaging of the near-infrared ICG-^{99m}Tc-nanocolloid (shown in blue) to determine the injected site of the hybrid tracer (middle). Visible fluorescence imaging in the auto-fluorescence mode to visualize location where fluorescein was injected (shown in yellow). Bottom row: White light imaging of a sentinel node (left). This sentinel node contained both the hybrid tracer (middle; shown in blue) and fluorescein (right; shown in yellow).

For this particular surgical procedure, manipulation of the prostate (injection site) resulted in release of fluorescein into the surgical field. Moreover, when disconnecting the prostate from the bladder, fluorescein-containing urine started to leak into the surgical field. In addition, a strong overall background signal was encountered with fluorescein, possibly as a result of shunting; in most patients, the injection of a tracer into the prostate results in some loss into the vascular system. It should be mentioned that this background signal was not a consequence of autofluorescence, since these signals were not visible in the AF mode when fluorescein was not present.

Nodal metastases were found in three patients, with a false-negative SN in one man (a metastatic lymph node was found in the ePLND but no metastases in the concomitant SN) (Table 1).

Postoperative complications within 90 days after surgery were seen in two patients, epididymitis and hematoma with a Clavien-Dindo score of II, and I, respectively (Table 1). Biochemical recurrence occurred in two patients (Table 1).

DISCUSSION

We present a first-in-human multispectral fluorescence imaging approach in which ICG-^{99m}Tc-nanocolloid-based SN identification was supported by additional lymphangiographic guidance provided by fluorescein. We demonstrated that both fluorescent dyes could be detected efficiently using a commercially available (fluorescence) laparoscope.

Unfortunately, the proof-of-concept nature of this study, with a relatively small number of patients included, makes it hard to make statements regarding the clinical impact of this technology.

The small molecule fluorescein was injected directly before the start of the operation and rapidly drained through the lymphatic system without specific accumulation in the (sentinel) lymph node(s), but brightly staining the lymphatic duct(s) running to the SN(s). The number of lymphatic ducts visualized using this technique was higher than the ductal visualization achieved using ICG-^{99m}Tc-nanocolloid (Table 2, Figure 2). Similar to blue dye, another small molecule used for lymphangiography, the time-window in which fluorescein can be detected is limited. Because of this limitation, fluorescein-positive lymphatic ducts could only be observed at the site where the urologist started his exploration (seven patients; Table 2). Presumably the signal on contralateral pelvic side had already disappeared by the time the surgical exploration started. It should also be noted that 'free' ICG can be considered a lymphangiographic agent with a relatively short effective time-window [4]. Another shortcoming is that these lymphangiographic tracers potentially suffer from spillage as a result of tissue manipulation during the resection process, and can thus contaminate the surgical field [18]. By contrast, the dedicated SN tracer ICG-^{99m}Tc-nanocolloid provides specific uptake and remains present in the SN for more than 29 h after administration [19], providing more logistical freedom. Concomitant use of ICG-^{99m}Tc-nanocolloid provides a solid basis for fluorescein to add additional value, without suffering much from its shortcomings, similar to the routine clinical use of blue dye in combination with ^{99m}Tc-nanocolloid in other malignancies [7, 8].

The hybrid nature of ICG-^{99m}Tc-nanocolloid facilitated preoperative checking of correct injection of the hybrid tracer into the prostate, which is not possible with fluorescein. Preoperative imaging also demonstrated that ICG-^{99m}Tc-nanocolloid is hepatically cleared, as previously reported for ICG [20]. By contrast, fluorescein is cleared renally, so it has been used as an imaging agent for ureter visualization [21]. This renal clearance of fluorescein was not considered a limitation during the SN biopsy procedure, but did lead to contamination of the surgical field during prostatectomy. This could affect the use of future tumor-receptor targeted tracers, as it indicates that fluorescence guidance towards cancer in the prostate (or bladder) may suffer from false-positive signals when a renally cleared tracer is used [18]. Depending on the excitation light and the detection filters used in the laparoscope, such a signal may also limit the identification of surgical resection margins.

Intraoperative fluorescein detection was straightforward, suggesting that use of a near-infrared fluorescence tracer is not a perquisite. Of course, searching for an additional fluorescence signal took additional effort and time, but because the same clinical grade laparoscope could be used, this process was rather intuitive. In comparison to the conventional radioguided SN approach, the additional costs of ICG-^{99m}Tc-nanocolloid is negligible [22], and use of fluorescein involves only minor additional costs [11]. As the laparoscope used for fluorescence imaging also provides high-definition white light

imaging, its conversion to multispectral fluorescence imaging can be covered when upgrading the clinical modalities routinely used for laparoscopic surgery. However, one limitation is that a multispectral laparoscope is not yet available as part of the robotic platform.

Although some will be of the opinion that combining a lymphangiographic tracer with a dedicated SN tracer can lead to further refinement of the SN biopsy procedure, others may believe that this will make the procedure more complex. However, bearing in mind the large number of (tumor-receptor) targeted fluorescent tracers with varying fluorescent signatures that have been applied in clinical studies [1], and the rapid development of new imaging tracers, the ability to perform multispectral imaging lays a basis for future surgical guidance applications. Ideally image guidance will facilitate identification not only of diseased areas but also of distinct anatomic landmarks such as ligaments, vessels, nerves, and/or ureters. A potential future application of multispectral fluorescence guidance could be nerve-sparing prostatectomy using tracers targeting prostate-specific membrane antigen [23] and nerves [24]. A read-out of two (or more) features would allow the generation of an intraoperative multispectral fluorescence imaging-based roadmap highlighting different (diseased) anatomic structures in real time. This could help to improve surgical accuracy and reduce procedure-associated morbidity.

CONCLUSION

Simultaneous use of a dedicated SN tracer and a lymphangiographic tracer during robot-assisted laparoscopic SN biopsy for prostate cancer is feasible. Ultimately this multispectral surgical guidance concept will allow the generation of an intraoperative multispectral fluorescence imaging-based roadmap that can highlight different (diseased) anatomical structures in real-time.

SURGERY IN MOTION

The Surgery in Motion video accompanying this article can be found in the online version at http://dx.doi.org/10.1016/j.eururo. 2016.06.012 and via www.europeanurology.com.

REFERENCES

1. van Leeuwen FW, Hardwick JC, van Erkel AR. Luminescence-based Imaging Approaches in the Field of Interventional Molecular Imaging. Radiology. 2015;276:12-29.
2. Greco F, Cadeddu JA, Gill IS, Kaouk JH, Remzi M, Thompson RH, et al. Current perspectives in the use of molecular imaging to target surgical treatments for genitourinary cancers. Eur Urol. 2014;65:947-64.
3. van den Berg NS, van Leeuwen FW, van der Poel HG. Fluorescence guidance in urologic

surgery. Curr Opin Urol. 2012;22:109-20.
4. Jeschke S, Lusuardi L, Myatt A, Hruby S, Pirich C, Janetschek G. Visualisation of the lymph node pathway in real time by laparoscopic radioisotope- and fluorescence-guided sentinel lymph node dissection in prostate cancer staging. Urology. 2012;80:1080-6.
5. KleinJan GH, van den Berg NS, Brouwer OR, de Jong J, Acar C, Wit EM, et al. Optimisation of fluorescence guidance during robot-assisted laparoscopic sentinel node biopsy for prostate cancer. Eur Urol. 2014;66:991-8.
6. Weckermann D, Dorn R, Trefz M, Wagner T, Wawroschek F, Harzmann R. Sentinel lymph node dissection for prostate cancer: experience with more than 1,000 patients. J Urol. 2007;177:916-20.
7. Kapteijn BA, Nieweg OE, Liem I, Mooi WJ, Balm AJ, Muller SH, et al. Localizing the sentinel node in cutaneous melanoma: gamma probe detection versus blue dye. Ann Surg Oncol. 1997;4:156-60.
8. Kapteijn BA, Nieweg OE, Petersen JL, Rutgers EJ, Hart AA, van Dongen JA, et al. Identification and biopsy of the sentinel lymph node in breast cancer. Eur J Surg Oncol. 1998;24:427-30.
9. Dan AG, Saha S, Monson KM, Wiese D, Schochet E, Barber KR, et al. 1% lymphazurin vs 10% fluorescein for sentinel node mapping in colorectal tumors. Arch Surg. 2004;139:1180-4.
10. Doss LL, Alyea JL, Waggoner CM, Schroeder TT. Fluorescein-aided isolation of lymphatic vessels for lymphangiography. AJR Am J Roentgenol. 1980;134:603-4.
11. Lee CM, Park S, Park SH, Jung SW, Choe JW, Sul JY, et al. Sentinel Node Mapping Using a Fluorescent Dye and Visible Light During Laparoscopic Gastrectomy for Early Gastric Cancer: Result of a Prospective Study From a Single Institute. Ann Surg. 2016. DOI: 10.1097/SLA.0000000000001739.
12. Kobayashi H, Koyama Y, Barrett T, Hama Y, Regino CA, Shin IS, et al. Multimodal nanoprobes for radionuclide and five-color near-infrared optical lymphatic imaging. ACS Nano. 2007;1:258-64.
13. Chin PT, Buckle T, Aguirre de Miguel A, Meskers SC, Janssen RA, van Leeuwen FW. Dual-emissive quantum dots for multispectral intraoperative fluorescence imaging. Biomaterials. 2010;31:6823-32.
14. van der Poel HG, Buckle T, Brouwer OR, Valdes Olmos RA, van Leeuwen FW. Intraoperative laparoscopic fluorescence guidance to the sentinel lymph node in prostate cancer patients: clinical proof of concept of an integrated functional imaging approach using a multimodal tracer. Eur Urol. 2011;60:826-33.
15. Briganti A, Larcher A, Abdollah F, Capitanio U, Gallina A, Suardi N, et al. Updated nomogram predicting lymph node invasion in patients with prostate cancer undergoing extended pelvic lymph node dissection: the essential importance of percentage of positive cores. Eur Urol. 2012;61:480-7.

16. Clavien PA, Barkun J, de Oliveira ML, Vauthey JN, Dindo D, Schulick RD, et al. The Clavien-Dindo classification of surgical complications: five-year experience. Ann Surg. 2009;250:187-96.
17. Dindo D, Demartines N, Clavien PA. Classification of surgical complications: a new proposal with evaluation in a cohort of 6336 patients and results of a survey. Ann Surg. 2004;240:205-13.
18. van Leeuwen FWB, van der Poel HG. Surgical guidance in prostate cancer: from molecule to man translations. Clin Cancer Res. 2016:5;22:1304-6 .
19. Brouwer OR, van den Berg NS, Matheron HM, van der Poel HG, van Rhijn BW, Bex A, et al. A hybrid radioactive and fluorescent tracer for sentinel node biopsy in penile carcinoma as a potential replacement for blue dye. Eur Urol. 2014;65:600-9.
20. Ishizawa T, Fukushima N, Shibahara J, Masuda K, Tamura S, Aoki T, et al. Real-time identification of liver cancers by using indocyanine green fluorescent imaging. Cancer. 2009;115:2491-504.
21. Udshmadshuridze NS, Asikuri TO. Intra-operative imaging of the ureter with sodium fluorescein. Z Urol Nephrol. 1988;81:635-9.
22. van den Berg NS, Brouwer OR, Klop WM, Karakullukcu B, Zuur CL, Tan IB, et al. Concomitant radio- and fluorescence-guided sentinel lymph node biopsy in squamous cell carcinoma of the oral cavity using ICG-(99m)Tc-nanocolloid. Eur J Nucl Med Mol Imaging. 2012;39:1128-36.
23. Vargas HA, Grimm J, O FD, Sala E, Hricak H. Molecular imaging of prostate cancer: translating molecular biology approaches into the clinical realm. Eur Radiol. 2015;25:1294-302.
24. Cotero VE, Siclovan T, Zhang R, Carter RL, Bajaj A, LaPlante NE, et al. Intraoperative fluorescence imaging of peripheral and central nerves through a myelin-selective contrast agent. Mol Imaging Biol. 2012;14:708-17.

SUPPORTING INFORMATION

METHODS

HYBRID TRACER PREPARATION, INJECTION AND PREOPERATIVE SENTINEL NODE MAPPING

^{99m}Tc-nanocolloid was prepared by adding 2.0 mL pertechnetate (≈300 MBq) to a vial of nanocolloid (GE Healthcare, Eindhoven, the Netherlands). The hybrid tracer was then formed by adding 0.05 mL (0.25 mg) of ICG solution (5.0m g/mL; Pulsion Medical, Feldkirchen, Germany) to this vial. After formation of ICG-^{99m}Tc-nanocolloid, the total volume was subtracted from the vial and diluted with saline to a total volume of 2.0 mL in the syringe. Procedures were performed in accordance with the Dutch guidelines for good manufacturing practice and with approval of the local pharmacist.

On average 4.75 h before surgery (range 3.5-5.5) ICG-^{99m}Tc-nanocolloid (average of 204.49 MBq (range 191.56-218.20)) was injected under transrectal ultrasound guidance into the prostate. Randomization was performed between an intratumoral injection (2 deposits of 1.0 mL on site where the dominant lesion was located) and an intraprostatic injection (4 deposits of 0.5 mL; 2 on the left site of the gland and 2 on the right site).

The injection was followed by preoperative SN mapping in the form of lymphoscintigraphy (15 min and 2 h post-hybrid-tracer-injection; 5 min acquisition time per image) and single photon emission computed tomography combined with computed tomography (SPECT/CT; approximately 2.5 h post-hybrid-tracer-injection, 25 min acquisition time)) as described previously [1]. After fusion of the SPECT and CT images, a 3D SPECT/CT-based volume rendering reconstruction was created using Osirix medical imaging software (Pixmeo, Geneva, Switzerland). Images were analyzed by an experienced nuclear medicine physician and for each patient the number and location of visualized SNs was determined (Table SI1).

ABSORPTION AND EMISSION SPECTRA MEASUREMENTS

Absorption and emission spectra of ICG-human serum albumin (concentration: 13.38 µM) and fluorescein-human serum albumin (concentration: 1.12 µM) were measured using an Ultrospec 3000 UV/Vis spectrophotometer (Pharmacia Biotech/GE Healthcare Europe GmbH, Eindhoven, The Netherlands) and an LS55 fluorescence spectrometer (PerkinElmer, Groningen, The Netherlands). Solutions were prepared in a 3 mL quartz cuvet (Hellma GmbH & Co. KG, Müllheim, Germany).

PRECLINICAL STUDY

Non-tumor bearing male TRAMP mice (n=3) were injected with 10-20 µL of fluorescein solution (1 mg/mL; Sigma-Aldrich, Zwijndrecht, The Netherlands) into the left lobe of the prostate of the mouse as previously described [2]. After dye administration, the injection site was massaged for up to 1 min.

For intraoperative detection of fluorescein dynamic fluorescence imaging was performed using a self-made fluorescence camera exciting fluorescein (excitation 488 nm; emission >520 nm). A total of six inguinal lymph node(s) were evaluated.

RESULTS

ABSORPTION AND EMISSION SPECTRA MEASUREMENTS

The absorption and emission spectra of ICG and fluorescein are given in Figure SI1.

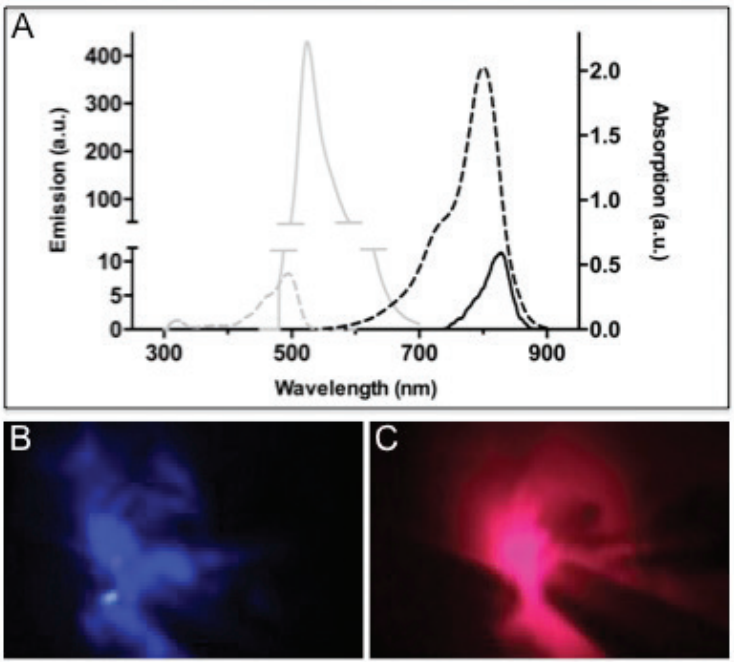

Figure SI1. Excitation and emission spectra fluorescein and ICG-human serum albumin. A) Absorption (dashed lines) and emission spectrum of ICG (black) and fluorescein (grey); B) Blue light is used to excite fluorescein; C) Near-infrared light is used to excite ICG.

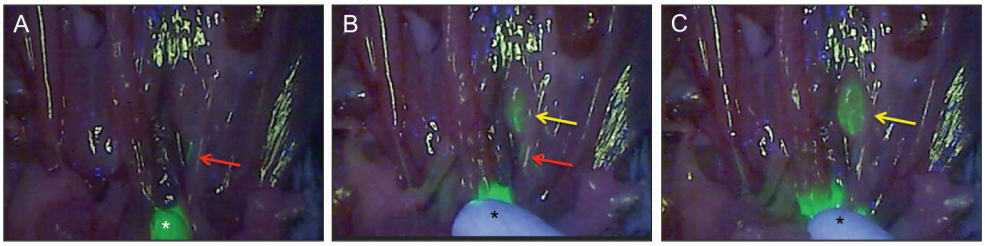

Figure SI2. Lymphangiography using the visible fluorescence dye fluorescein. Upon fluorescein injection into the mouse prostate (*) real-time lymphatic mapping was found feasible. Within 10 s (A) drainage occurs into the lymphatic vessels (red arrow). Already at 30 s (B) fluorescein reached the lymph node (yellow arrow), which is fully filled roughly 1 min post-injection of fluorescein (C).

PRECLINICAL STUDY

Fluorescence imaging enabled real-time (at video-rate) intraoperative visualization of the lymphatic ducts and the inguinal lymph nodes (Figure SI2). In all mice, drainage from the injection site into the lymphatic ducts could be visualized within 10 s after injection of fluorescein. Staining of the lymph node(s) occurred immediately thereafter. Washout of fluorescein from the nodes was seen >2 min post-injection and suggested a quick migration of the dye trough the lymphatic system comparable to what we previously showed for ICG [2].

Table SI1. Preoperative imaging findings

Patient	*Injected dose (MBq)*	*# SNs early LSG L + R*	*# SNs late LSG L + R*	*# SNs SPECT/CT L + R*	*Location SNs*
1	224.31	1 + 0	2 + 1	2 + 2	L: ext iliac, presacral R: ext iliac, int iliac
2	202.08	1 + 2	1 + 2	1 + 3	L: obt fossa R: obt fossa, int iliac, ext iliac
3	208.91	0 + 0	0 + 0	1 + 1	L: obt fossa R: obt fossa
4	192.29	1 + 0	1 + 0	2 + 0	L: int iliac, presacral R: -
5	218.20	1 + 3	1 + 3	1 + 3	L: obt fossa R: obt fossa (2), paracaval
6	197.07	0 + 0	1 + 2	3 + 2	L: int iliac, presacral (2) R: obt fossa (2)
7	193.98	2 + 1	2 + 1	3 + 2	L: obt fossa, int iliac, ext iliac R: obt fossa, bifurcation common iliac trunk
8	200.19	0 + 0	0 + 0	1 + 0	L: obt fossa R: -
9	216.35	1 + 3	1 + 3	1 + 3	L: common iliac trunk R: obt fossa, ext iliac, bifurcation common iliac trunk
10	191.56	2 + 0	2 + 2	2 + 3	L: int iliac, paravesical R: obt fossa, bifurcation common iliac trunk (2)
Average	204.49	1.8	2.3	3.6	
Total		18	23	36	

MBq = Mega Bequerel; LSG = lymphoscintigraphy; SPECT/CT = single photon emission computed tomography combined with computed tomography; L = left; R = right; SN = sentinel node; obt = obturator; int = internal; ext = external.

REFERENCES

1. van Leeuwen AC, Buckle T, Bendle G, Vermeeren L, Valdes Olmos R, van de Poel HG, et al. Tracer-cocktail injections for combined pre- and intraoperative multimodal imaging of lymph nodes in a spontaneous mouse prostate tumor model. J Biomed Opt. 2011;16:016004.
2. KleinJan GH, van den Berg NS, Brouwer OR, de Jong J, Acar C, Wit EM, et al. Optimisation of fluorescence guidance during robot-assisted laparoscopic sentinel node biopsy for prostate cancer. Eur Urol. 2014;66:991-8.

CHAPTER 10

A PILOT STUDY OF SPECT/CT-BASED MIXED-REALITY NAVIGATION TOWARDS THE SENTINEL NODE IN PATIENTS WITH MELANOMA OR MERKEL CELL CARCINOMA

Adapted from: van den Berg NS, Brouwer OR, Mathéron HM, Nieweg OE, Valdés Olmos RA, van Leeuwen FWB. Nucl Med Comm. 2016;37:812-7.

ABSTRACT

OBJECTIVE To explore the feasibility of an intraoperative navigation technology based on preoperatively acquired single photon emission computed tomography combined with computed tomography (SPECT/CT) images during sentinel node (SN) biopsy in patients with melanoma or Merkel cell carcinoma.

MATERIALS AND METHODS Patients with a melanoma (n=4) or Merkel cell carcinoma (n=1) of a lower extremity scheduled for wide re-excision of the primary lesion site and SN biopsy were studied. Following a ^{99m}Tc-nanocolloid injection and lymphoscintigraphy, SPECT/CT images were acquired with a reference target (ReTp) fixed on the leg or the iliac spine. Intraoperatively, a sterile ReTp was placed at the same site to enable SPECT/CT-based mixed-reality navigation of a gamma ray detection probe also containing a reference target (ReTgp). The accuracy of the navigation procedure was determined in the coronal plane (x, y-axis) by measuring the discrepancy between standard gamma probe-based SN localization and mixed-reality-based navigation to the SN. To determine the depth accuracy (z-axis), the depth estimation provided by the navigation system was compared to the skin surface-to-node distance measured in the CT component of the SPECT/CT images.

RESULTS In four of five patients, it was possible to navigate towards the preoperatively defined SN. The average navigational error was 8.0 mm in the sagittal direction and 8.5 mm in the coronal direction. Intraoperative sterile ReTp positioning and tissue movement during surgery exerted a distinct influence on the accuracy of navigation.

CONCLUSION Intraoperative navigation during melanoma or Merkel cell carcinoma surgery is feasible and can provide the surgeon with an interactive three dimensional roadmap towards the SN or SNs in the groin. However, further technical optimization of the modality is required before this technology can become routine practice.

INTRODUCTION

In patients with intermediate-thickness melanoma, sentinel node (SN) biopsy has become a routine procedure that provides staging and prognostic information, reduces the risk of nodal recurrence and results in improved melanoma-specific survival when combined with completion node dissection in patients who are node positive [1]. The procedure typically entails the injection of a radiocolloid around the melanoma site, followed by two-dimensional lymphoscintigraphy to outline the lymphatic drainage pattern [2]. Nowadays, single photon emission computed tomography (SPECT) is combined with computed tomography (CT) imaging providing three-dimensional (3D) images. As a result, SNs are depicted within their anatomical context, facilitating the planning of the surgical procedure [3].

Intraoperatively, most surgeons use a gamma-ray detection probe (hereafter referred to as a gamma probe) to find the hot node that is depicted on the preoperative images. Yet a gamma probe only provides an acoustic signal and no visual information or read-out for the distance to the SN. Moreover, the commonly used blue dye can only be seen when the SN is already exposed. It would thus be beneficial if the spatial anatomical information provided by preoperative SPECT/CT imaging can also be used in the operation theatre. Recently, navigation in a mixed-reality environment using preoperatively acquired SPECT/CT images has shown potential during SN biopsy procedures for urological malignancies [4,5]. The current pilot study explores the feasibility of this technology in four patients with melanoma and one patient with a Merkel cell carcinoma.

MATERIALS AND METHODS

PATIENTS

Five patients (mean age 47.4 years, range 29-65) were enrolled in the current study. Four of these five patients presented with a melanoma (average Breslow thickness 3 mm, range 1.7-5.3) of a lower extremity (Table 1). The other patient presented with a Merkel cell carcinoma of a lower extremity (Table 1), which, in our institution, is also indicated for SN biopsy [6]. All patients were scheduled for wide re-excision of the primary lesion site and SN biopsy.

All procedures performed in our study were in accordance with the ethical standards of our institution and the 1964 Helsinki declaration and its later amendments or comparable ethical standards. Informed consent was obtained from all patients who participated in the current study.

Table 1. Patient characteristics, pre- and intraoperative findings, and pathology outcome

Patient	*Age*	*Primary*	*Injected dose (MBq)*	*# SNs identified on SPECT/CT*	*Patient target location*	*Error in coronal plane (X,Y-position; mm)*	*Error in sagittal plane (Z-position; mm)*	*# Excised SNs*	*# Blue SNs*	*# Tumor-positive nodes*
1	50	Melanoma, thigh L	73.5	1	ASIS, R	10	-4	1	1	0
2	54	Melanoma, thigh R	67.8	1	ASIS, L	10	-10	2	2	0
3	29	Melanoma, thigh R	139.4	1	Thigh, R	not determined	>45 mm	1	0	0
4	65	Melanoma, lower leg R	79.7	3	Thigh, R	9	-2	3	2	0
5	39	Merkel cell carcinoma, lower leg R	70.4	2	ASIS, L	5	-16	3	3	0
Average	47.4		86.2			8.5±2.1	-8.0±5.5			
Total				8				10		

L = left; R = right; ASIS = anterior superior iliac spine.

PREOPERATIVE PROCEDURE

^{99m}Tc-nanocolloid was administered intradermally in four deposits surrounding the primary lesion site (0.4 mL; average 86.2 MBq, range 68-139). Dynamic lymphoscintigraphy was performed immediately after tracer injection and was followed by static imaging at 15 min and 2 h after injection using a dual-head gamma camera (Symbia-T; Siemens, Erlangen, Germany) (Figure 1A). Following late imaging, a reference target (ReTp) was placed on the contralateral anterior superior iliac spine in three patients and on the ipsilateral thigh in two patients. The location of the ReTp was marked on the skin with indelible ink. Thereafter, SPECT images were acquired with a 128 x 128 matrix and 60 frames at 25 s per view. This was combined with a low-dose CT (40 mAs, 5 mm slices). Attenuation-corrected SPECT and CT images were fused using Osirix medical imaging software (Pixmeo, Geneva, Switzerland). Orthogonal multiplanar reconstructions and three dimensional volume-rendered images (Figure 1B) were generated from the fused images. Afterwards, the nuclear medicine physician determined the number and location of SNs and marked these on the skin with

indelible ink. An SN was defined as a lymph node on a direct lymphatic drainage pathway from the primary lesion [7].

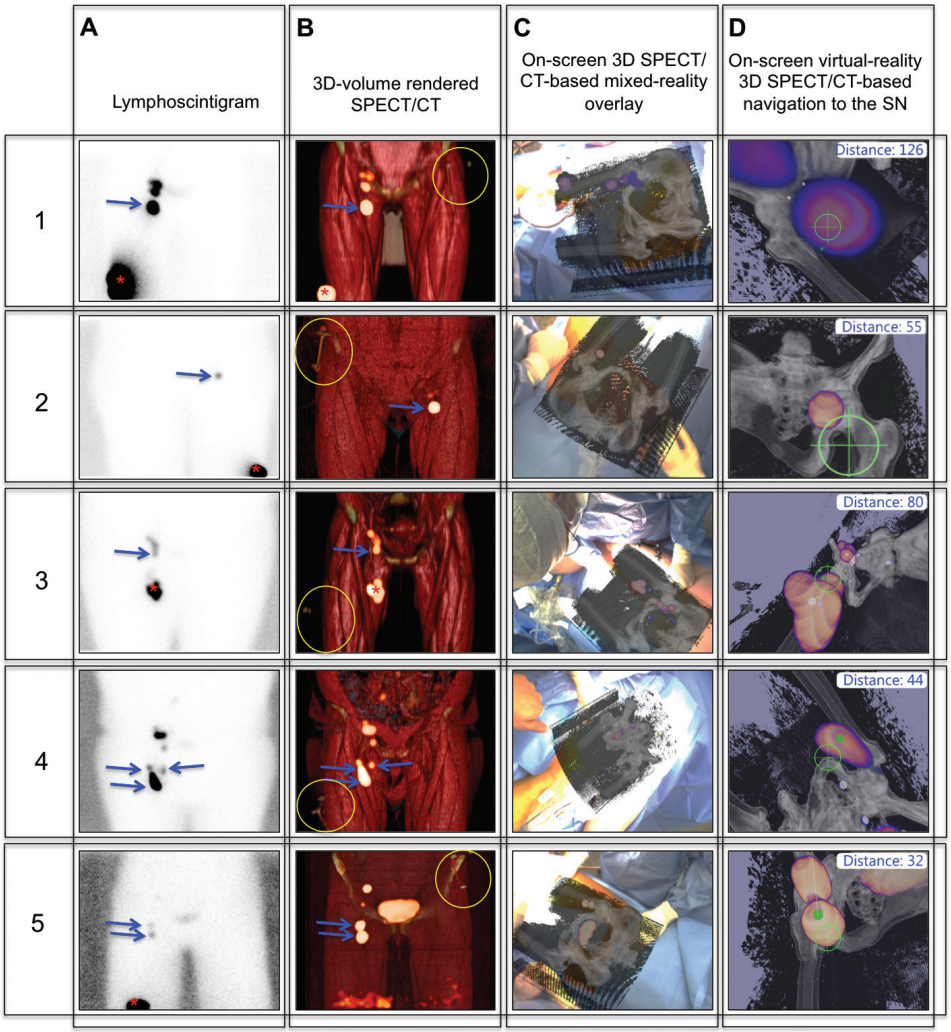

Figure 1. Imaging datasets of the five included patients. A) Anterior lymphoscintigram taken 2 h after a radiocolloid injection showing the sentinel node in the groin (arrow) and the injected site (asterisk); B) 3D volume-rendered SPECT/CT image showing the sentinel node in the groin (arrow) and the patient reference tracer (circle); C) The mixed-reality overlay of the preoperatively acquired SPECT/CT and the video feed of the patient is presented onscreen; D) On-screen 3D virtual-reality based navigation to the sentinel node in the groin. 3D = three-dimensional; SPECT/CT = single photon emission computed tomography/computed tomography.

NAVIGATION SYSTEM: IMAGE REGISTRATION IN THE OPERATION THEATRE

The tracked attenuation-corrected SPECT images and the low-dose CT images were loaded into the navigation system (declipseSPECT; SurgicEye, Munich, Germany) and the location of the reference target on the patient (ReTp) was automatically segmented from the low-dose CT.

After sterile prepping and draping, a sterile ReTp was again placed on the patient at the preoperatively marked position and fixed with Steri-Strips (3M Health Care, St. Paul, Minnesota, USA). A video camera at the top of the navigation system provided an on-screen image-feed of the surgical field. This real-time video signal was then combined with the SPECT/CT information and matched to the location and orientation of the patient ReTp, which resulted in a (on-screen) mixed-reality representation (Figure 1C). Subsequently, a second sterile reference target (ReTgp) was placed on the gamma probe (Crystal Photonics, Des Plaines, Illinois, USA). After calibration, this allowed for navigation of the tip of the gamma probe in the on-screen in 3D, SPECT/CT-based, virtual-reality view (Figure 1D).

NAVIGATION PROTOCOL IN THE OPERATION THEATRE

To determine the accuracy of the intraoperative navigation in the coronal plane, the gamma probe was navigated in the on-screen 3D SPECT/CT-based virtual-reality view to the location of the SN over the intact skin without the acoustic signal. This location was then marked on the skin with indelible ink. Subsequently, the SN was localized through the intact skin in the conventional manner using the acoustic signal of the gamma probe (Neoprobe; Johnson & Johnson Medical, Amersfoort, the Netherlands). The point with the highest gamma ray count rate was also marked on the skin. The accuracy error of the SPECT/CT-based virtual-reality view in the coronal plane (x and y position) was then determined by measuring the distance between the two marks using a caliper.

During the navigation process, the system provided an estimate of the distance between the center of the SN and the tip of the gamma probe, which enabled determination of the depth of the node (z position; sagittal plane) for surgical exploration. This estimate was compared with the depth measured on the corresponding low-dose CT image that served as the gold standard.

SENTINEL NODE EXCISION AND (HISTO-)PATHOLOGICAL EVALUATION

After completing the experimental preincision navigation procedure, the SN biopsy procedure was performed as described previously [8]. Serial sectioning, haematoxylin-eosin and immunohistochemistry staining of the SNs were performed as described previously [9].

RESULTS

Preoperative lymphoscintigraphy and SPECT/CT imaging revealed a total of eight inguinal SNs (Figure 1A, B). The intraoperative feasibility of the navigation approach was assessed for one SN in each of the five patients (Table 1).

Intraoperative placement of the sterile ReTp was easy and did not affect the surgical workflow. Superimposition of the SPECT/CT images onto the patient image provided a visual confirmation of the ReTp repositioning accuracy. The anterior superior iliac spine was found to be the most suitable location for ReTp placement as it provided a rigid orientation point in comparison with the soft tissue of the thigh. Although the latter location ensured constant visibility of the tracker, in one patient, it yielded a 45 mm error, which could be attributed to intraoperative abduction and rotation of the leg compared with the patient position during SPECT/CT acquisition (Figure 1, patient 3). Such an obvious movement artifact led us to exclude this patient from further analysis, a point that is addressed further in the discussion section.

In the remaining four patients, the navigation approach could be executed successfully. The locating error of 3D virtual-reality SPECT/CT-based navigation, compared with conventional gamma probe localization, in the coronal plane was found to be 8.5 mm on average (SD 2.1 mm, range 5.0-10.0; Table 1). The average sagittal (in-depth; z-position) error was found to be 8.0 mm (SD 5.4 mm, range 2.0-16.0; Table 1). Compared with the low-dose CT measurement, navigation underestimated the depth in all four patients.

After completion of the navigation protocol, a total of ten SNs were excised. Histopathological evaluation indicated one SN to be tumor-positive.

DISCUSSION

The current pilot study shows the feasibility of on-screen navigation in a mixed-reality environment using preoperatively acquired SPECT/CT images. Preoperative SPECT/CT imaging has been shown to make intraoperative SN biopsy procedure in melanoma patients easier [10,11], with significantly more SNs detected [12] as well as patient benefit [13]. In this context, intraoperative technologies that exploit the 3D SPECT/CT information may increase its value even further. The additional information provided by 3D SPECT/CT-based navigation helped not only to reproduce the anatomical environment as preoperatively displayed by SPECT/CT, but also has the potential to facilitate intraoperative SN localization. This can be especially useful in localizing SNs that contain little radioactivity, SNs deeper inside the body, near the primary lesion or in areas with an intricate anatomy.

It is generally assumed that in soft tissues, registration and motion artefacts limit the value of navigation technologies [14]. The current proof-of-concept study shows that on-screen 3D virtual-reality SPECT/CT-based navigation is feasible with reasonable accuracy. On average, navigation errors were found to be around 8 mm in both the x,y-direction (coronal) and the z-direction (sagittal). This study also shows the importance of

correct placement of the patient ReTp as the error was larger when the ReTp was placed on the thigh (non-rigid anatomy) compared with the anterior superior iliac spine (rigid anatomy). This indicates that the ReTp should be placed on a rigid reference point rather than in a non-rigid area that is prone to change during the operation compared with preoperative image acquisition. This was underlined in one patient, where the ReTp was placed on the thigh (error >45 mm; Table 1). The deviation in the z-direction may be explained by the pressure that surgeons intuitively place on the gamma probe to increase the count rate. Although the navigation errors that we encountered did not limit the identification of the relatively large lymph nodes in the groin, this could prove a limitation in the head-and-neck area. The SNs in the latter area are considerably smaller, often in close proximity to non-SNs, and are surrounded by important structures that the surgeon should preserve [15].

Our current study clearly indicates that SPECT/CT-based navigation is feasible in this patient group, but at the same time suggests that this type of navigation is susceptible to movement-induced errors. Intraoperatively obtained freehandSPECT datasets could help omit errors as result of patient positioning differences in the preoperative or intraoperative setting. This alternative approach has shown clinical potential in a number of SN related studies [16-18]. Nevertheless, compared with the use of preoperative SPECT/CT data sets, the generation of freehandSPECT data sets is more time consuming, lacks the anatomical detail provided by the (low-dose) CT image and may have a lower image quality. One could, however, envision that in the future, intraoperative freehandSPECT could be used to correct for motion-induced artefacts in the SPECT/CT-based navigation set-up.

Intraoperative guidance modalities that help correct for the navigation-induced error can be especially beneficial. Here, the conventionally used gamma probe already provides a means to validate the navigation accuracy because of its real-time acoustic feedback, but the spatial resolution and in-depth view of the technology is limited. Other disadvantages of the gamma probe are that it does not provide images and the tracing process can be time consuming. Alternative to gamma ray-based guidance, blue dye or even fluorescence guidance may be used to confirm the accuracy of the navigation procedure as they provide the surgeon with real-time visual feedback in terms of the location of the lymphatic ducts and/or SNs [4,19]. Incorporation of fluorescence imaging into the navigation approach can be a particularly interesting technique for further refinement of the navigation procedure.

CONCLUSION

Surgical navigation in preoperatively acquired SPECT/CT images in patients with melanoma or Merkel cell carcinoma of a lower extremity is feasible. For wider implementation, the accuracy of the procedure needs to be optimized.

REFERENCES

1. Morton DL, Thompson JF, Cochran AJ, Mozzillo N, Nieweg OE, Roses DF, et al. Final trial report of sentinel-node biopsy versus nodal observation in melanoma. N Engl J Med. 2014; 370:599-609.
2. van den Berg NS, Buckle T, Kleinjan GI, Klop WM, Horenblas S, van der Poel HG, et al. Hybrid tracers for sentinel node biopsy. Q J Nucl Med Mol Imaging. 2014; 58:193-206.
3. van der Ploeg IM, Valdés Olmos RA, Nieweg OE, Rutgers EJ, Kroon BB, Hoefnagel CA. The additional value of SPECT/CT in lymphatic mapping in breast cancer and melanoma. J Nucl Med. 2007; 48:1756-1760.
4. Brouwer OR, Buckle T, Bunschoten A, Kuil J, Vahrmeijer AL, Wendler T, et al. Image navigation as a means to expand the boundaries of fluorescence guided surgery. Phys Med Biol. 2012; 57:3123-3136.
5. Brouwer OR, van den Berg NS, Mathéron HM, Wendler T, van der Poel HG, Horenblas S, et al. Feasibility of intraoperative navigation to the sentinel node in the groin using preoperatively acquired single photon emission computerized tomography data: transferring functional imaging to the operating room. J Urol. 2014; 192:1810-1816.
6. Ortin-Perez J, van Rijk MC, Valdes-Olmos RA, Vidal-Sicart S, Nieweg OE, Vilalta A, et al. Lymphatic mapping and sentinel node biopsy in Merkel's cell carcinoma. Eur J Surg Oncol. 2007; 33:119-122.
7. Nieweg OE, Tanis PJ, Kroon BB. The definition of a sentinel node. Ann Surg Oncol. 2001; 8:538-541.
8. Nieweg OE, Jansen L, Kroon BB. Technique of lymphatic mapping and sentinel node biopsy for melanoma. Eur J Surg Oncol. 1998; 24:520-524.
9. van den Berg NS, Brouwer OR, Schaafsma BE, Mathéron HM, Klop WM, Balm AJ, et al. Multimodal surgical guidance during sentinel node biopsy for melanoma: combined gamma tracing and fluorescence imaging of the sentinel node through use of the hybrid tracer indocyanine green-(99m)Tc-nanocolloid. Radiology. 2015; 275:521-529.
10. van der Ploeg IM, Valdés Olmos RA, Kroon BB, Wouters MW, van den Brekel MW, Vogel WV, et al. The yield of SPECT/CT for anatomical lymphatic mapping in patients with melanoma. Ann Surg Oncol. 2009;16:1537-1542.
11. Veenstra HJ, Vermeeren L, Olmos RA, Nieweg OE. The additional value of lymphatic mapping with routine SPECT/CT in unselected patients with clinically localized melanoma. Ann Surg Oncol. 2012;19:1018-1023.
12. Jimenez-Heffernan A, Ellmann A, Sado H, Huić D, Bal C, Parameswaran R, et al. Results of a prospective multicenter international atomic energy agency sentinel node trial on the value of SPECT/CT over planar imaging in various malignancies. J Nucl Med. 2015; 56:1338-1344.
13. Stoffels I, Boy C, Pöppel T, Kuhn J, Klötgen K, Dissemond J, et al. Association between sentinel lymph node excision with or without preoperative SPECT/CT and metastatic node detection and disease-free survival in melanoma. JAMA. 2012; 308:1007-1014.

14. Baumhauer M, Feuerstein M, Meinzer HP, Rassweiler J. Navigation in endoscopic soft tissue surgery: perspectives and limitations. J Endourol. 2008; 22:751-766.
15. Grégoire V, Ang K, Budach W, Grau C, Hamoir M, Langendijk JA, et al. Delineation of the neck node levels for head and neck tumors: a 2013 update. DAHANCA, EORTC, HKNPCSG, NCIC CTG, NCRI, RTOG, TROG consensus guidelines. Radiother Oncol. 2014;110:172-181.
16. Bluemel C, Herrmann K, Kübler A, Buck AK, Geissinger E, Wild V, et al. Intraoperative 3-D imaging improves sentinel lymph node biopsy in oral cancer. Eur J Nucl Med Mol Imaging. 2014; 41:2257-2264.
17. Engelen T, Winkel BM, Rietbergen DD, KleinJan GH, Vidal-Sicart S, Olmos RA, et al. The next evolution in radioguided surgery: breast cancer related sentinel node localization using a freehandSPECT-mobile gamma camera combination. Am J Nucl Med Mol Imaging. 2015; 5:233-245.
18. Heuveling DA, Karagozoglu KH, van Schie A, van Weert S, van Lingen A, de Bree R. Sentinel node biopsy using 3D lymphatic mapping by freehand SPECT in early stage oral cancer: a new technique. Clin Otolaryngol. 2012;37:89-90.
19. Kapteijn BA, Nieweg OE, Liem I, Mooi WJ, Balm AJ, Muller SH, et al. Localizing the sentinel node in cutaneous melanoma: gamma probe detection versus blue dye. Ann Surg Oncol. 1997;4:156-160.

CHAPTER 11

FIRST-IN-HUMAN EVALUATION OF A HYBRID MODALITY THAT ALLOWS COMBINED RADIO- AND (NEAR-INFRARED) FLUORESCENCE TRACING DURING SURGERY

Adapted from: van den Berg NS, Simon H, KleinJan GH, Engelen T, Bunschoten A, Welling MN, Tijink BM, Horenblas S, Chambron J, van Leeuwen FWB. Eur J Nucl Med Mol Imaging. 2015;2:1639-47.

ABSTRACT

PURPOSE

The clinical introduction of the hybrid tracer indocyanine green (ICG)-^{99m}Tc-nanocolloid, composed of a radioactive and a near-infrared fluorescence component, has created the need for surgical (imaging) modalities that allow for simultaneous detection of both signals. This study describes the first-in-human use of a prototype opto-nuclear probe during sentinel node (SN) biopsy using ICG-^{99m}Tc-nanocolloid.

METHODS

To allow for fluorescence tracing, a derivative of the conventional gamma probe technology was generated in which two optical fibers were integrated to allow for excitation (785 nm) and emission signal collection (>810 nm). The ability of this opto-nuclear probe to detect the fluorescence signal of the hybrid tracer ICG-^{99m}Tc-nanocolloid was firstly determined ex vivo in (non)SNs samples obtained from 41 patients who underwent hybrid tracer-based SN biopsy in the head-and-neck or urogenital area. In an in vivo proof-of-concept study in nine of these 41 patients, SNs were localized using combined gamma and fluorescence tracing with the opto-nuclear probe. Fluorescence tracing was performed in a similar manner as gamma tracing and under ambient light conditions.

RESULTS

Ex vivo, the gamma tracing option of the opto-nuclear probe correctly identified the SN in all 150 evaluated (non)SN samples. Ex vivo fluorescence tracing in the low-sensitivity mode correctly identified 71.7% of the samples. This increased to 98.9% when fluorescence tracing was performed in the high-sensitivity mode. In vivo fluorescence tracing (high-sensitivity mode) accurately identified the SNs in all nine patients (20 SNs evaluated; 100%).

CONCLUSION

This study demonstrates the first-in-human evaluation of a hybrid modality capable of detecting both gamma and fluorescence signals during a surgical procedure. Fluorescence tracing could be performed in ambient light.

INTRODUCTION

In Europe, sentinel node (SN) biopsy is routinely performed via a radioguided surgery approach that involves a technetium-99m-labeled colloid (standard in Europe: ^{99m}Tc-nanocolloid) [1]. For some indications, radioguidance is accompanied by the intraoperative use of a blue dye that aids visual identification of the SNs and their draining lymphatic vessels. Although this procedure can be considered relatively straightforward, e.g. for the identification of SNs in the axilla, for the identification of SNs in the head-and-neck or in the pelvic area several issues remain to be resolved: i) the complexity of the anatomy and the abundance of delicate anatomical structures that surround the SN may complicate intraoperative SN detection; ii) blue dye is of limited value in these areas and may obscure resection margins [2]; and iii) detection of an SN located in close proximity to the injection site may be hampered due to the high radioactive background signal coming from the injection site [3]. The integrated use of the near-infrared dye indocyanine green (ICG) and ^{99m}Tc-nanocolloid in the form of the hybrid tracer ICG-^{99m}Tc-nanocolloid [4] was shown to extend the conventional radioguided technology. For example, it showed promise in optical identification of SNs in the parotid gland [5] and near the injection site [5, 6]. Moreover, fluorescence imaging of the hybrid tracer demonstrated improved detection sensitivity compared to blue dye [7, 8].

It was recently reported that a conventional gamma probe could be modified to allow for fiber-based illumination and detection of light. This initial modification allowed optical tracing of patent blue V via light absorption measurements [9]. For the current study, we modified the optical properties of this set-up in order to excite and detect ICG (laser; λ_{ex}: 785 nm and λ_{em}: >810 nm). We evaluated this prototype opto-nuclear probe for gamma tracing and near-infrared fluorescence tracing during ICG-^{99m}Tc-nanocolloid-based SN biopsy in patients with head-and-neck, penile, and prostate cancer.

MATERIALS AND METHODS

OPTO-NUCLEAR PROBE

From an engineering perspective, the prototype opto-nuclear probe (Eurorad S.A., Eckbolsheim, France) itself is highly similar to the conventional gamma probe. However, for excitation of ICG, a narrow-band 785 nm laser excitation source was integrated into the device. In addition, for detection of the fluorescent emission signal of ICG, and to exclude reflected laser light, a broadband cut-off filter (>810 nm) was placed in front of the detector. An adjustable photomultiplier tube (PMT; range: 0.7 V (1.0×10^5; low-sensitivity mode) to 0.9 V (1.0×10^6; high-sensitivity mode)) was integrated into the opto-nuclear probe to fine-tune the sensitivity for fluorescence tracing. The resulting prototype opto nuclear probe is shown in Figure 1.

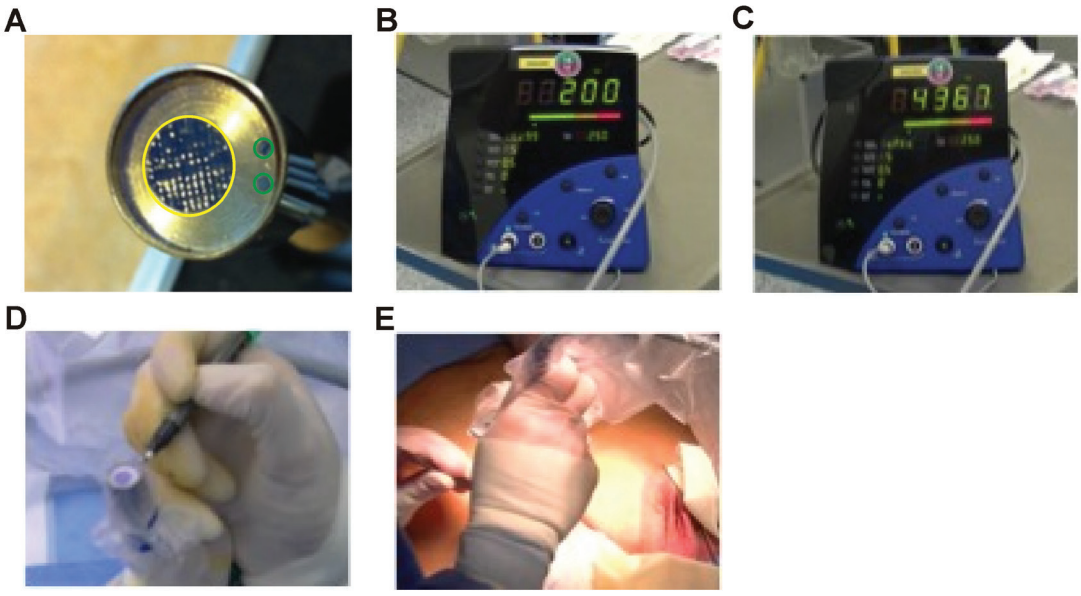

Figure 1. Prototype opto-nuclear probe. A) In the head of the prototype opto-nuclear probe, next to the crystal for gamma detection (yellow circle), two optical fibers are embedded (green circles); B-C) Traced gamma (B) and near-infrared fluorescence (C) signals are presented to the surgeon via an acoustic output; D) Intraoperatively, to effectively perform near-infrared fluorescence tracing using the opto-nuclear probe, the location of the optical fibers is marked on the probe; E) Intraoperative fluorescence tracing is performed in a similar way as conventional gamma tracing.

FLUORESCENCE SENSITIVITY MEASUREMENTS IN A PHANTOM SET-UP

^{99m}Tc-nanocolloid was prepared by adding 400 MBq pertechnetate in saline to a vial of nanocolloid (GE Healthcare, Leiderdorp, The Netherlands). To form the hybrid tracer, 50 µL of a 5 mg/mL ICG-sterile water for injection solution (ICG-Pulsion, 25 mg vial; Pulsion Medical Systems, Munich, Germany) was added to the ^{99m}Tc-nanocolloid vial.

To obtain an indication for the optimal concentration range wherein fluorescence tracing can be performed, and to determine the correlation between gamma- and fluorescence tracing using the opto-nuclear probe, 121.91 MBq of the hybrid tracer ICG-^{99m}Tc-nanocolloid (containing 0.125 mg/mL ICG) was diluted with saline in 11 steps down to 0.22 MBq (containing 0.061 ng/mL ICG). The dilution range was prepared in Eppendorf tubes containing a total volume of 0.4 mL. After each dilution step, the amount of radioactivity present in the Eppendorf tube was counted in a dose calibrator (CII radioisotope calibrator CRC®-5, Capintec Inc., Montvale, NJ, USA). Subsequently, gamma

tracing was performed by placing the head of the opto-nuclear probe directly in front of the Eppendorf tube. The 5-s and 2-s count rates were then measured in triplicate.

Thereafter, 10 µL of each step of the dilution range was pipetted onto a paper towel and air-dried (in the dark). Fluorescence tracing was performed by placing the tip of the optonuclear probe on the surface of the paper towel. Both the 5-s and 2-s count rates were measured with the PMT set at 0.7 and at 0.9 V (low- and high-sensitivity mode, respectively). Measurements were performed in triplicate. The correlation (r^2-value; linear regression analysis) between the results obtained with the gamma tracing and fluorescence tracing mode of the opto-nuclear probe was calculated in the linear range of the measured hybrid tracer dilution range.

To provide a quantitative reference for the fluorescence emission signal, 100 µL of each step of the hybrid tracer dilution range was transferred into a black 96-well plate (Cellstar, Greiner Bio-One GmbH, Frickenhausen, Germany), and a fluorescence emission curve was measured with a PerkinElmer LS 55 fluorescence spectrophotometer (λ_{ex}: 760 nm and λ_{em}: 800 nm; PerkinElmer Health Sciences B.V., Groningen, The Netherlands). The correlation (r^2-value; linear regression analysis) between the results obtained with fluorescence tracing using the opto-nuclear probe and the spectrophotometry results was calculated in the linear range of the measured hybrid tracer dilution range.

To determine the responsiveness of the opto-nuclear probe to blue dye, a dilution range of patent blue V dye (Laboratoire Guerbet, Aulnay-Sous-Bois, France) was generated by diluting 25 mg/mL patent blue V dye with sterile water for injection in 13 steps down to a final concentration of 3.1 ng/mL. The dilution range was prepared in a black 96-well plate (Cellstar), and the fluorescence emission signal was measured with the LS 55 fluorescence spectrophotometer (λ_{ex}: 610 nm and λ_{em}: 670 nm; PerkinElmer). Subsequently, 10 µL of each step of the dilution range was pipetted onto a paper towel and air-dried (in the dark). Thereafter, fluorescence tracing was performed as described above.

PATIENTS

Between January 2013 and April 2014, 150 nodal samples from 41 patients who underwent hybrid tracer-based SN biopsy (head-and-neck (n=13), penile (n=23), and prostate cancer (n=5)) were collected for ex vivo analysis using the opto-nuclear probe. Of these 41 patients, the opto-nuclear probe was evaluated in vivo in nine patients (head-and-neck (n=2) or penile cancer (n=7)).

The study protocol was approved by the local medical ethical committee, and written informed consent was obtained from all patients in whom the opto-nuclear probe was evaluated intraoperatively. All procedures performed were in accordance with the ethical standards of our institution and with the 1964 Declaration of Helsinki and its later amendments or comparable ethical standards.

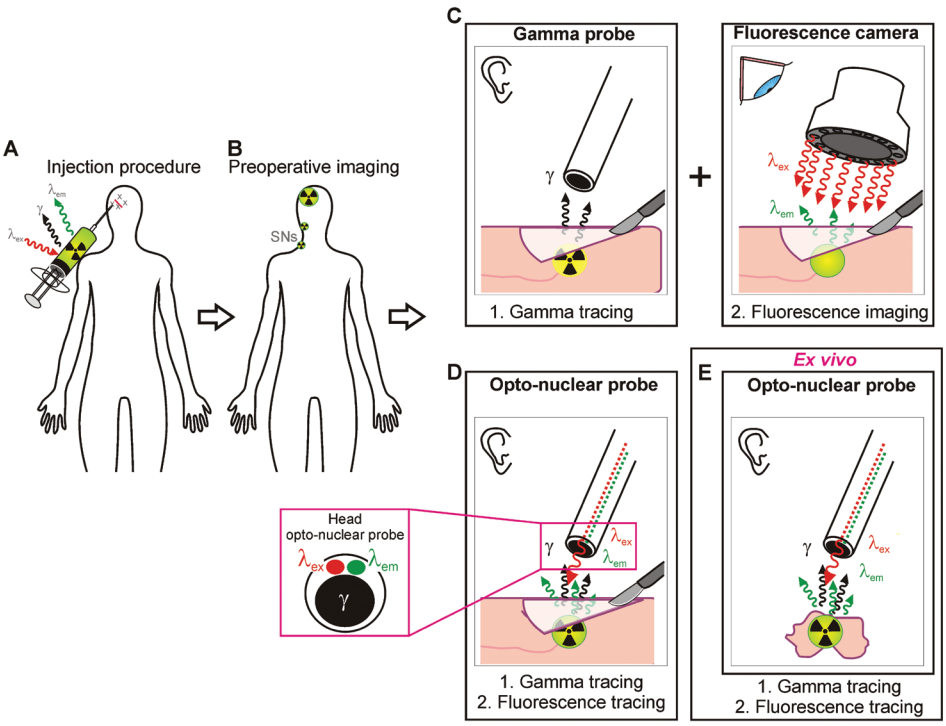

Figure 2. A hybrid approach for intraoperative lesion identification. Schematic overview of the sentinel node biopsy procedure using a hybrid tracer composed of a radioactive and a near-infrared fluorescence moiety. Following hybrid tracer injection (A), preoperative imaging (lymphoscintigraphy and SPECT/CT imaging) (B) is performed to identify the lesion of interest. Intraoperatively, the conventional approach (C) consists of the use of a gamma probe (gamma tracing of the lesion) and a near-infrared fluorescence camera (visualization of the fluorescence signal in the lesion). With the newly proposed approach, one modality is used that allows both gamma tracing and near-infrared fluorescence tracing (D). The opto-nuclear probe can be used both in vivo and ex vivo and (E) to evaluate the gamma and near-infrared fluorescence signal. SPECT/CT = single photon emission computed tomography combined with computed tomography. SN = sentinel node. λem = emission wavelength of the fluorophore; λex = excitation wavelength of the fluorophore; γ = gamma signal coming from the radioisotope

CLINICAL TRACER PREPARATION AND SENTINEL NODE BIOPSY PROCEDURE

For illustration, a schematic overview of the pre- and intraoperative SN biopsy procedure is provided in Figure 2. ICG-^{99m}Tc-nanocolloid preparation, administration, preoperative SN mapping, routine surgical guidance (gamma tracing and fluorescence imaging) and (histo-) pathological evaluation for head-and-neck [5, 6], penile [7], and prostate [10] cancer were performed as previously described.

In patients with penile cancer, an injection with patent blue V dye was given intraoperatively [7]. In patients with head-and-neck or prostate cancer, no patent blue V dye was used [5, 6, 10].

EX VIVO SENTINEL NODE MEASUREMENTS

Similar to our previous studies, during the operation, nodal samples were evaluated by the surgeon as being radioactive (yes/no), fluorescent (yes/no) and, in patients in whom blue dye was used, blue (yes or no) [5-7, 10].

To determine the sensitivity of the opto-nuclear probe on human tissue, after excision, nodal samples were evaluated using the opto-nuclear probe. Firstly, gamma tracing was performed with 5-s count rates measured. After switching the settings to the fluorescence mode, fluorescence tracing was performed with the PMT set at 0.7 V (low-sensitivity mode). In the case that a node positive with gamma tracing could not be fluorescence-traced, the PMT was increased to 0.9 V (high-sensitivity mode) and measurements were repeated. All measurements were performed in triplicate. The results were compared to those obtained with our conventional approach (gamma tracing (Neoprobe; Johnson & Johnson Medical B.V., Amersfoort, The Netherlands, or Europrobe; Eurorad S.A.) and fluorescence imaging (PDE; Hamamatsu Photonics K.K., Hamamatsu, Japan)) and scored for correct or incorrect prediction by the opto-nuclear probe.

In all experiments, fluorescence tracing with the opto-nuclear probe was performed in ambient light.

INTRAOPERATIVE SENTINEL NODE IDENTIFICATION USING THE OPTO-NUCLEAR PROBE

The opto-nuclear probe was evaluated intraoperatively in nine patients scheduled for SN biopsy (Table 1). Operations were performed by six different surgeons.

Table 1. Characteristics of the patients included for intraoperative opto-nuclear probe evaluation

						Opto-nuclear probe					
Patient	***Age***	***Sex***	***Primary tumor***	***Time injection – surgery (hours)***	***# SNs evaluated with ONP / total # preoperatively defined SNs***	***Location of the ONP-evaluated SNs***	***Gamma tracing with OMP***	***Fluorescence tracing with ONP***		***Blue dye***	***Pathology: SN + or -***
								0.9 Volt	0.7 Volt		
1	73	M	SCC penis	7.25	3/3	L: 2x groin R: groin	3	3	1	2	Negative
2	65	M	SCC penis	5.25	2/3	L: 2x groin	2	2	0	2	Negative
3	71	M	SCC penis	6.25	1/2	L: groin	1	1	0	1	Negative
4	53	M	SCC penis	4	2/2	L: groin R: groin	2	2	1	2	Negative
5	59	M	SCC penis	22.75	4/4	L: 2x groin R: 2x groin	4	4	2	-	Negative
6	63	M	SCC penis	18	2/2	L: groin R: 2x groin	2	2	2	-	Negative
7	66	M	SCC tongue L	4	2/4	L: level IA, IB	2	2	1	-	Positive (2x)
8	54	F	Merkel cell cheek L	4.5	1/1	L: level II	1	1	0	-	Negative
9	64	M	SCC penis	20.5	3/3	L: 2x groin R: groin	3	3	0	3	Negative
Average	64			9.75							
Total					20/24		20/20 (100%)	20/20 (100%)	7/20 (35.0%)	10/11 (90.9%)	

SN = sentinel node; ONP = opto-nuclear probe; SN + = tumor-positive sentinel node; SN - = tumor-negative sentinel node; SCC = squamous cell carcinoma; L = left; R = right.

During the operation, the SN was first pursued with the gamma tracing option of the opto-nuclear probe. After localization of the node, the opto-nuclear probe was switched to the fluorescence tracing mode. Here, the PMT was initially set at 0.9 V (high-sensitivity mode). When a signal was obtained, the PMT voltage was reduced to 0.7 V (low-sensitivity mode). Fluorescence tracing with the opto-nuclear probe was performed in ambient light.

Validation of the in vivo fluorescence signalwas performed using a handheld fluorescence camera (PDE; Hamamatsu Photonics K.K.). For the detection of the fluorescence signal using the fluorescence camera, the lights in the operation theatre had to be dimmed. Obtained results were scored for correct or incorrect prediction by the opto-nuclear probe.

After excision of the SN(s), ex vivo SN measurements were performed as described in the 'Ex vivo sentinel node measurements' section above.

RESULTS

Since gamma tracing of radiolabeled colloids (e.g. the hybrid tracer ICG-^{99m}Tc-nanocolloid) is already a well-known and thoroughly proven surgical guidance method, the current study focused on the evaluation and validation of the novel fluorescence tracing mode of the opto-nuclear probe. Initially, the system was evaluated in a phantom set-up. These findings provided the basis for the evaluation of the opto-nuclear probe technology on resected nodal samples. As a last step, we evaluated the technology in an image-guided surgery set-up during SN biopsy.

SENSITIVITY MEASUREMENTS IN A PHANTOM SET-UP

In the phantom experiments, where a dilution range of ICG-^{99m}Tc-nanocolloid was measured using the opto-nuclear probe, a strong correlation was found between gamma- and fluorescence tracing intensities (Figure 3A and B, respectively). With the PMT set at 0.7 V (low-sensitivity mode), r^2-values of 0.73 and 0.91 were found for the measured 5-s and 2-s count rates, respectively (Figure 3C). At 0.9 V (high- sensitivity mode), however, continuous oversaturation of the opto-nuclear probe prevented us from obtaining an r^2-value.

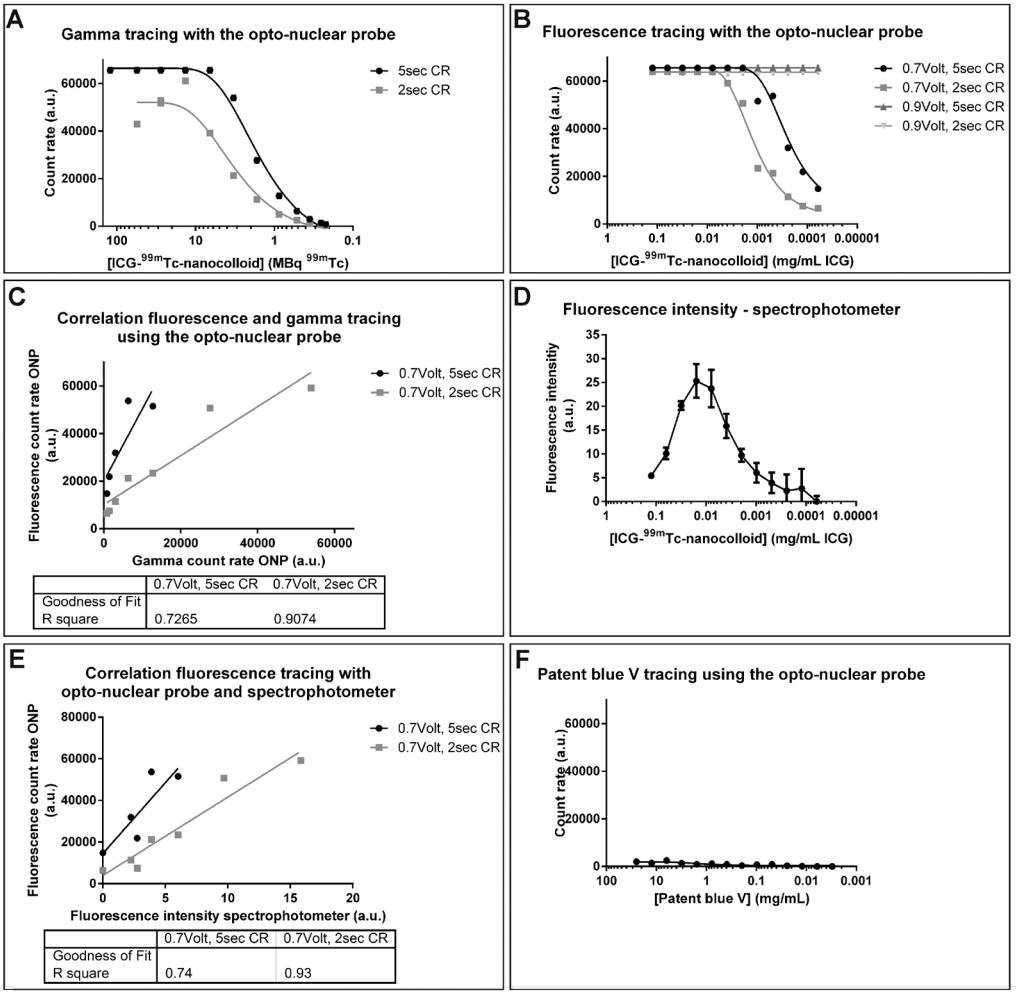

	0.7Volt, 5sec CR	0.7Volt, 2sec CR
Goodness of Fit R square	0.7265	0.9074

	0.7Volt, 5sec CR	0.7Volt, 2sec CR
Goodness of Fit R square	0.74	0.93

Figure 3. Phantom experiments evaluating the opto-nuclear probe. A) A dilution range of the hybrid tracer ICG-^{99m}Tc-nanocolloid was prepared (x-axis), after which gamma tracing using the opto-nuclear probe was performed. The 2-s and 5-s count rates were measured during performance of opto-nuclear probe-based gamma tracing (y-axis) of the hybrid tracer; B) A dilution range of the hybrid tracer ICG-^{99m}Tc-nanocolloid was prepared (x-axis), after which near-infrared fluorescence tracing using the opto-nuclear probe was performed. For near-infrared fluorescence tracing, 2-s and 5-s count rates were measured with the PMT set at 0.7 V (low-sensitivity) and 0.9 V (high-sensitivity) (y-axis); C) The correlation between the counts measured via gamma tracing (x-axis) and near-infrared fluorescence tracing (y-axis) was calculated; D) The hybrid tracer dilution range (x-axis; concentration hybrid tracer) was also measured on a fluorescence spectrophotometer (y-axis, fluorescence intensity in a.u.); E) Correlation between opto-nuclear probe-based near-infrared fluorescence tracing (x-axis) and measurements of the fluorescence spectrophotometer (y-axis) when evaluating the hybrid tracer dilution range; F) Opto-nuclear probe-based near-infrared fluorescence tracing of a dilution range of patent blue V dye (x-axis) with the PMT set at 0.9 V (high-sensitivity mode). 5-s count rates were measured (y-axis). In the low-sensitivity mode (PMT set at 0.7 V), no fluorescence signal was detected with the opto-nuclear probe. ICG = indocyanine green; ONP = opto-nuclear probe; a.u. = arbitrary units; sec = seconds; CR = count rate; PMT = photomultiplier tube.

A comparison between the fluorescence count rates obtained with the opto-nuclear probe (Figure 3A) and the signal intensities measured with a fluorescence spectrophotometer (the standard method for fluorescence intensity quantification) (Figure 3D) gave an r^2-value of 0.74 at a 5-s count rate, which increased to 0.93 at the 2-s count rate (Figure 3E). Again the r^2-value could not be calculated at 0.9 V (high-sensitivity mode) due to signal oversaturation. The fluorescence spectrophotometer measurements showed that the fluorescence peak intensity was highest at the concentration range 7.0-30.0 µg/mL ICG-^{99m}Tc-nanocolloid (Figure 3E).

With the PMT set at 0.7 V (low-sensitivity mode) the presence of patent blue V dye in the samples did not interfere with fluorescence tracing. However, when the PMT was set to 0.9 V (high-sensitivity mode), a continuous number of background counts was measured at various concentrations of blue dye (ranging 25 mg/mL- 3.1 ng/mL; Figure 3F). Surprisingly the fluorescence spectrophotometer did not record any additional fluorescence signal for patent blue V dye.

EX VIVO SAMPLE EVALUATION

A total of 150 nodal samples from 41 patients were analyzed ex vivo. All SNs (n=131) were radioactive and fluorescent. The 19 additionally excised samples (referred to as nonSNs) were not radioactive and not fluorescent and functioned as negative control. During ex vivo evaluation (Figure 4A, B), all radioactivity-containing nodes were able to be gamma traced with the opto-nuclear probe. The fluorescence tracing efficacy, however, was dependent on the PMT settings. With the PMT set at 0.7 V (low-sensitivity mode), merely 70.7% of the evaluated nodes could be correctly staged for their fluorescent content (Figure 4C).

A strong increase in detection sensitivity to 98.9% was achieved by adjusting the PMT voltage to 0.9 V (high-sensitivity mode; Figure 4C). Most of the nodal samples contained some additional dissected tissue (see Figure 4B for an example), which influenced the fluorescence tracing efficacy. For example, in contrast to the above-described phantom measurements, the influence of the tissue in the nodal samples resulted in a poor correlation between the signal intensities measured using gamma and fluorescence tracing (Figure 4D). The presence of patent blue V dye in the nodal samples did not influence the fluorescence tracing.

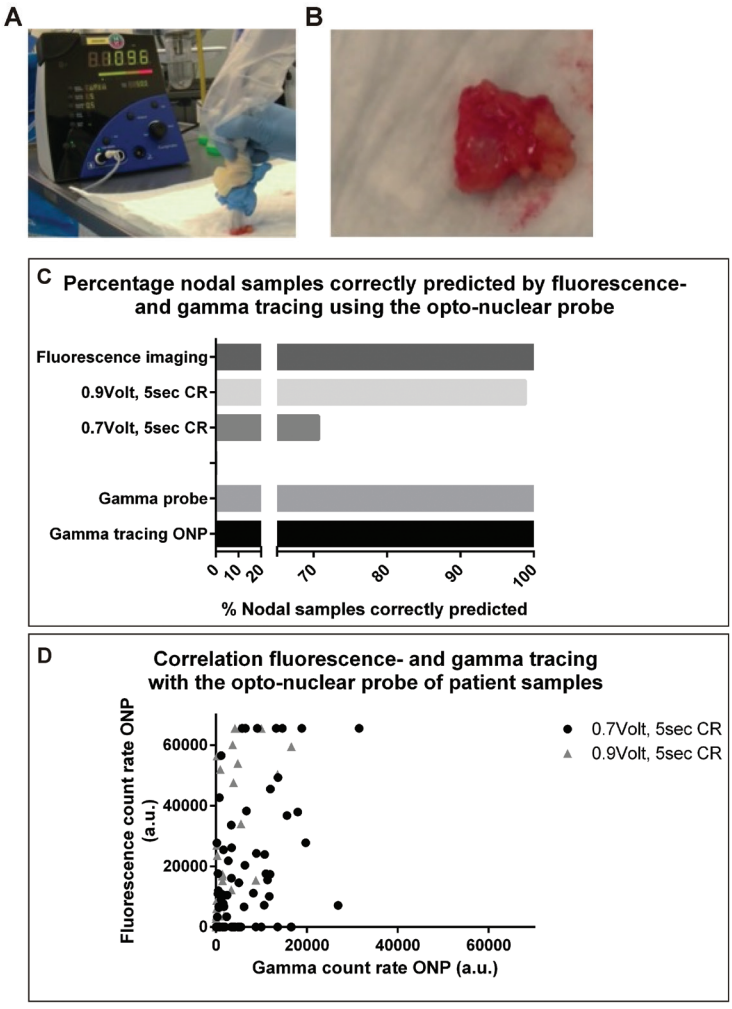

Figure 4. Patient sample evaluation with the opto-nuclear probe. A) Illustration showing ex vivo fluorescence tracing of a sentinel node; B) Sentinel node illustrating that not only the sentinel node is excised but also some surrounding (fatty) tissue; C) Percentage of sentinel nodes correctly predicted with the opto-nuclear probe. Of the 150 evaluated nodal samples, gamma tracing and near-infrared fluorescence tracing results obtained with the opto-nuclear probe were compared to the results obtained with the conventional gamma probe and near-infrared fluorescence camera, respectively; D) 150 nodal samples were evaluated with the opto-nuclear probe. The graph shows the correlation between count-rates measured for gamma tracing and near-infrared tracing using the opto-nuclear probe. ONP = opto-nuclear probe; a.u. = arbitrary units; CR = count rate; sec = seconds.

INTRAOPERATIVE SENTINEL NODE IDENTIFICATION USING THE OPTO-NUCLEAR PROBE

We then set out to evaluate the potential of the modality to provide in vivo guidance in the form of gamma and fluorescence tracing in nine patients scheduled for SN biopsy. Findings are specified in Table 1.

Intraoperatively, 20 SNs were evaluated with the opto-nuclear probe (Figure 1). Similar to the results of the ex vivo situation, the gamma tracing option of the opto-nuclear probe allowed localization of 100% of the SNs, and fluorescence tracing of all of these SNs (100%) was possible when the PMT was set to 0.9 V (high-sensitivity mode). At low-sensitivity mode (0.7 V), however, accurate fluorescence tracing with the opto-nuclear probe was achieved for only seven of the 20 evaluated nodes (35.0%). This detection percentage is markedly lower than that obtained at these settings in the above-described ex vivo measurements. In contrast to the findings in the phantom set-up, in vivo, the presence of patent blue V dye did not lead to false-positive results at 0.9 V (high-sensitivity mode).

The surgeons found the use of the fluorescence tracing option of the opto-nuclear probe to be intuitive. Handling, the method of fluorescence tracing, and acoustic read-out (Figure 1) were similar to that of the conventional gamma probe that is routinely used for SN identification. To improve the ease of probe placement during the operation, the location of the optical fibers was marked on the opto-nuclear probe with a marker pen (Figure 1D). Making circularly rotating movements while performing fluorescence tracing allowed scanning of a larger area and easier detection of the fluorescence signal. This effect was strengthened in the high-sensitivity mode (PMT set at 0.9 V). Importantly, the fact that the technology was effective in ambient light conditions had a minimal influence on surgical logistics. The ability to get a quantitative feel of the fluorescence signal intensity (counts) in relation to the gamma tracing findings was considered advantageous. Nevertheless, the inability to visualize the SNs was considered a disadvantage by some surgeons.

DISCUSSION

To the best of our knowledge, this is the first clinical study reporting on a hybrid modality that allows for combined gamma and near-infrared fluorescence tracing during a surgical procedure. Following the positive results of the initial phantom and ex vivo evaluation experiments, our first-in-human study in nine patients nicely illustrated the clinical feasibility of this technology. The integration of the fluorescence tracing option into an existing modality saves both additional investment and valuable space in the operation theatre. Though it should be apparent that larger clinical evaluation studies are needed to determine the true clinical potential of this technology.

Interestingly, the different experiments performed illustrated a small discrepancy in findings among the phantom, ex vivo, and in vivo setting. For example, at 0.9 V (high-sensitivity mode), the phantom experiments indicated that detection of the fluorescent signal was oversaturated, making 0.7 V (low-sensitivity mode) the preferred setting for the fluorescence tracing measurements. Moreover, at 0.9 V the presence of patent blue V dye induced a background signal during fluorescence tracing. Ex vivo, though, we found that the fluorescence tracing ability was improved when switching from low-sensitivity (PMT set at 0.7 V) to high-sensitivity (0.9 V) mode (from 70.7% to 98.9%, respectively), and no influence of patent blue V dye was observed at either setting. During the in vivo evaluation, this effect was even more profound, resulting in an improvement of detection, from 35 to 100% (0.7 and 0.9 V, respectively). Evidently, the attenuation of the fluorescence signal in the nodal sample tissue influences the detection of the fluorescence signal with the optonuclear probe. Moreover, the limited penetration depth of the fluorescence signal as a result of tissue attenuation also influenced the correlation between the signal intensities obtained in the ex vivo set-up. In the phantom experiments, a strong correlation was found between gamma and fluorescence tracing, underscoring the utility of the technology, while measurements in clinical samples yielded a poor correlation. Distribution of the tracer through the node, and thus the degree of tissue attenuation at different points of measurement, may also vary; earlier histopathological evaluation of fluorescent SNs also indicated that the tracer is not homogeneously distributed through the node [7]. This result supports previous findings indicating that tissue attenuation of the fluorescent emission signal [11] severely limits the ability to acquire a quantitative read-out in tissue specimens.

Existing, routinely used clinical procedures such as the SN biopsy procedure provide advantages for the valorization of new techniques. Initially, we demonstrated the value of this concept by the evolution of the radiotracer ^{99m}Tc-nanocolloid into the hybrid tracer ICG-^{99m}Tc-nanocolloid that allows for both radio- and fluorescence-based SN detection [4]. In the current study, we showed that the extension of a gamma probe with fluorescence tracing capabilities resulted in a unique hybrid surgical guidance modality, which could also be rapidly evaluated in a clinical trial. Because the opto-nuclear probe is directly derived from the existing gamma probe technology, its use was considered intuitive for surgeons with experience in SN biopsy. Implementation of this hybrid tracing technology in clinical routine may therefore have a short learning curve. Since the read-out is acoustic rather than visual, the technology can easily be used in combination with fluorescence imaging. For the detection of gamma photons, a combination of acoustic (gamma tracing) and visible (gamma imaging using portable camera systems) feedback has already proven its value [12, 13].

Importantly, with the opto-nuclear technology, fluorescence tracing can be performed in ambient light, which is a significant improvement to the application of the current generation of surgical (near-infrared) fluorescence cameras that require the lights in the operating theatre to be dimmed or switched off completely [14-16]. This means that with

the opto-nuclear probe technology, the impact that fluorescence detection has on operation theatre logistics is minimized.

Although we specifically focused on the combined use of a hybrid tracer and opto-nuclear tracing technology, use of the latter is not confined to ICG-^{99m}Tc-nanocolloid. The probe settings can easily be switched between gamma and fluorescence tracing, thus allowing for the use of tracers other than the hybrid tracer, e.g. other ^{99m}Tc-labeled colloids [1], or separately administered ICG. This makes it a versatile technology that is easy implemented. For future purposes, one may also want to apply the fluorescence tracing technology during ICG perfusion measurements (e.g. kidney ischemia [17]), ICG-based tumor tracing (e.g. exploring the liver for the presence of colorectal metastasis [18]), or even in combination with tumor receptor targeting tracers functionalized with a fluorescence dye like ICG [19] or alternative near-infrared dyes such as Cy7 (λ_{ex}: 750 nm; λ_{em}: 773 nm; Luminoprobe GmbH, Hannover, Germany), CW800 (λ_{ex}: 778 nm; λ_{em}: 794 nm; LI-COR Biosciences, Lincoln, NE, USA), or ZW800 (λ_{ex}: 772 nm; λ_{em}: 78[8] nm [20]). Here it should be noted that using optical tracing alone will severely limit the surgical guidance provided to superficial structures with a known location, due to the limited penetration depth of the fluorescent dye [11].

CONCLUSION

This proof-of-concept study demonstrated the first clinical evaluation of a hybrid surgical modality capable of detecting both gamma and near-infrared fluorescence signals. Because near-infrared fluorescence tracing is performed in a similar manner as conventional gamma tracing, the technology could be easily adopted by surgeons.

REFERENCES

1. van den Berg NS, Buckle T, Kleinjan GH, KlopWM, Horenblas S, van der Poel HG, et al. Hybrid tracers for sentinel node biopsy. Q J Nucl Med Mol Imaging. 2014;58:193-206.
2. Broglie MA, Stoeckli SJ. Relevance of sentinel node procedures in head and neck squamous cell carcinoma. Q J Nucl Med Mol Imaging. 2011;55:509-20.
3. Heuveling DA, van Schie A, Vugts DJ, Hendrikse NH, Yaqub M, Hoekstra OS, et al. Pilot study on the feasibility of PET/CT lymphoscintigraphywith 89Zr-nanocolloidal albumin for sentinel node identification in oral cancer patients. J Nucl Med. 2013;54:585-9.
4. Brouwer OR, Buckle T, Vermeeren L, KlopWM, Balm AJ, van der Poel HG, et al. Comparing the hybrid fluorescent-radioactive tracer indocyanine green-^{99m}Tc-nanocolloid with ^{99m}Tc-nanocolloid for sentinel node identification: a validation study using lymphoscintigraphy and SPECT/CT. J Nucl Med. 2012;53:1034-40.
5. van den Berg NS, Brouwer OR, Schaafsma BE, Matheron HM, Klop WM, Balm AJ, et al. Multimodal surgical guidance during sentinel node biopsy for melanoma: combined gamma tracing and fluorescence imaging of the sentinel node through use of the

hybrid tracer indocyanine green-Tc-nanocolloid. Radiology. 2015;275:530-7.
6. van den Berg NS, Brouwer OR, Klop WM, Karakullukcu B, Zuur CL, Tan IB, et al. Concomitant radio- and fluorescence-guided sentinel lymph node biopsy in squamous cell carcinoma of the oral cavity using ICG-(99m)Tc-nanocolloid. Eur J Nucl Med Mol Imaging. 2012;39:1128-36.
7. Brouwer OR, van den Berg NS, Matheron HM, van der Poel HG, van Rhijn BW, Bex A, et al. A hybrid radioactive and fluorescent tracer for sentinel node biopsy in penile carcinoma as a potential replacement for blue dye. Eur Urol. 2014;65:600-9.
8. Matheron HM, van den Berg NS, Brouwer OR, Kleinjan GH, van Driel WJ, Trum JW, et al. Multimodal surgical guidance towards the sentinel node in vulvar cancer. Gynecol Oncol. 2013;131:720-5.
9. Tellier F, Ravelo R, Simon H, Chabrier R, Steibel J, Poulet P. Sentinel lymph node detection by an optical method using scattered photons. Biomed Opt Express. 2010;1:902-10.
10. KleinJan GH, van den Berg NS, Brouwer OR, de Jong J, Acar C, Wit EM, et al. Optimisation of fluorescence guidance during robotassisted laparoscopic sentinel node biopsy for prostate cancer. Eur Urol. 2014;66:991-8.
11. van Leeuwen FWB, Hardwick JCH, van Erkel AR. Luminescencebased imaging approaches in the field of interventional (molecular) imaging. Radiology. 2015;276:12-29.
12. Valdes Olmos RA, Vidal-Sicart S, Giammarile F, Zaknun JJ, Van Leeuwen FW, Mariani G. The GOSTT concept and hybrid mixed/virtual/augmented reality environment radioguided surgery. Q J Nucl Med Mol Imaging. 2014;58:207-15.
13. Engelen T, Winkel BMF, Rietbergen DDD, KleinJan GH, Vidal- Sicart S, Valdés Olmos RA, van den Berg NS, van Leeuwen FWB. The next evolution in radioguided surgery: breast cancer related sentinel node localization using a freehandSPECT-mobile gamma camera combination. A J Nucl Med Mol Imaging. 2015;5:233-45.
14. Brouwer OR, Klop WM, Buckle T, Vermeeren L, van den Brekel MW, BalmAJ, et al. Feasibility of sentinel node biopsy in head and neck melanoma using a hybrid radioactive and fluorescent tracer. Ann Surg Oncol. 2012;19:1988-94.
15. Crane LM, Themelis G, Arts HJ, Buddingh KT, Brouwers AH, Ntziachristos V, et al. Intraoperative near-infrared fluorescence imaging for sentinel lymph node detection in vulvar cancer: first clinical results. Gynecol Oncol. 2011;120:291-5.
16. Mieog JS, Troyan SL, HuttemanM, Donohoe KJ, van der Vorst JR, Stockdale A, et al. Toward optimization of imaging system and lymphatic tracer for near-infrared fluorescent sentinel lymph node mapping in breast cancer. Ann Surg Oncol. 2011;18:2483-91.
17. Bjurlin MA, Gan M, McClintock TR, Volpe A, Borofsky MS, Mottrie A, et al. Near-infrared fluorescence imaging: emerging applications in robotic upper urinary tract surgery. Eur Urol. 2014;65:793-801.

18. Ishizawa T, Fukushima N, Shibahara J,Masuda K, Tamura S, Aoki T, et al. Real-time identification of liver cancers by using indocyanine green fluorescent imaging. Cancer. 2009;115:2491-504.
19. Zhou Y, Kim YS, Milenic DE, Baidoo KE, Brechbiel MW. In vitro and in vivo analysis of indocyanine green-labeled panitumumab for optical imaging-a cautionary tale. Bioconjug Chem. 2014;25:1801-10.
20. Choi HS, Nasr K, Alyabyev S, Feith D, Lee JH, Kim SH, et al. Synthesis and in vivo fate of zwitterionic near-infrared fluorophores. Angew Chem. 2011;50:6258-63.

OUTLOOK

CHAPTER 12

SENTINEL NODE BIOPSY FOR PROSTATE CANCER: A HYBRID APPROACH

Adapted from: van den Berg NS, Valdés-Olmos RA, van der Poel HG, van Leeuwen FWB. J Nucl Med. 2013;54:493-6.

ABSTRACT

To provide surgeons with optimal guidance during interventions, it is crucial that the molecular imaging data generated at the diagnostic departments finds its way to the operating room. Sentinel node (SN) biopsy provides a textbook example in which molecular imaging data acquired in the department of nuclear medicine guides the surgical management of patients. For prostate cancer, in which SNs are generally located deep in the pelvis, procedures are preferably performed via a (robot-assisted) laparoscopic approach. Unfortunately, in the laparoscopic setting the senses of the surgeon are reduced. This topical review discusses technologic innovations that can help improve surgical guidance during SN biopsy procedures.

INTRODUCTION

Metastasis in pelvic lymph nodes is considered an important prognostic factor in prostate cancer. Prostate-specific antigen levels, pathologic stage, and Gleason score are predictors for lymph nodes involvement; the higher these factors are, the greater is the chance of nodal involvement. Postoperative (histo-)pathologic examination of tissue samples obtained during (extended) pelvic lymphadenectomy is considered the gold standard in assessing metastatic spread. With an increasing lymph nodes dissection template, the prognosis of both N0 and N1 groups increases ("Will Rogers" phenomenon). Unfortunately, (extended) pelvic lymphadenectomy also increases the chance of postoperative complications such as lymphoceles, injuries to the obturator nerve or the ureter, and lymphedema of the lower extremity. Such complications can lead to a decrease in the patient's quality of life.

Sentinel node (SN) biopsy focuses on the identification, subsequent minimally invasive excision, and pathologic and histopathologic evaluation of the lymph nodes that drain directly from the primary tumor. Assuming the orderly spread of tumor cells through the lymphatic system, SN biopsy can be used for lymph nodes staging. After staging, therapeutic follow-up can be decided on.

The potential of SN biopsy for detecting lymph nodes metastasis has been validated in several studies. The Augsburg group validated the SN biopsy procedure in more than 2,000 patients with prostate cancer and reported a high sensitivity and an overall false-negative rate of 5.9% [1]. Moreover, SN biopsy allows the identification of SNs outside the pelvic lymphadenectomy field [2-4]. Recently, Joniau et al. showed that 44% of SNs were located outside the extended pelvic lymphadenectomy field; in 6% of patients, a positive lymph nodes was located exclusively in the presacral or para-aortic region [2].

Ideally, a surgeon is able to identify and excise the preoperatively identified SNs in a minimally invasive manner, with a high sensitivity and specificity. This topical review discusses technologic improvements that may help improve the different aspects involved in (robot-assisted) laparoscopic SN biopsy for prostate cancer; SN biopsy for the prostate is often performed in combination with laparoscopic radical prostatectomy. Potential improvements can be found in (hybrid) tracers that are radioactive and fluorescent, the injection procedure, preoperative SN identification and planning of the surgical procedure, translation of the preoperatively acquired imaging data to the operating room (e.g. via navigation), and intraoperative imaging for SN identification. A schematic overview of these points is given in Figure 1. Similar technologies are also expected to help improve guidance for other SN indications and in the future may even help enable tumor-specific resections.

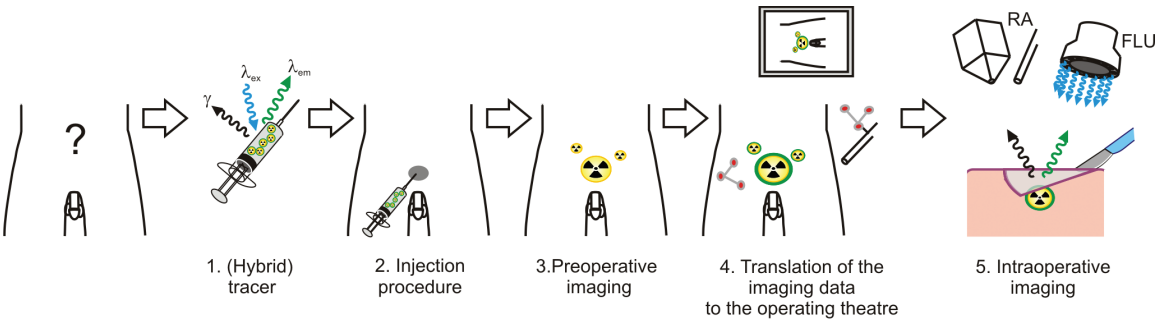

Figure 1. Schematic overview of the integrated hybrid sentinel node biopsy procedure. On presentation of the patient, a hybrid SN tracer (1) is injected into the prostate (2). Preoperative imaging is performed to identify the SNs (3). Preoperatively acquired images can be directly translated to operating room - for example, via augmented-reality-based navigation (4) - to provide both radio- and fluorescence-based surgical guidance toward SNs (5). SN = sentinel node; FLU = fluorescence imaging; λem = emission wavelength of the fluorophore; λex = excitation wavelength of the fluorophore; γ = gamma signal coming from the radioisotope; RA = radioactivity-based detection (i.e., gamma imaging or -tracing).

(HYBRID) TRACERS

Despite the success of radioguided surgery, to provide optical guidance blue dyes are often injected before the start of the operation. However, for prostate cancer, in which SNs are generally localized deep within the tissue, blue dye is of little value. An alternative optical detection technology can be found in near-infrared fluorescence imaging, which allows for real-time optical detection of lesions less than 10 mm deep [5]. The requirement of preoperative SN mapping data for surgical planning, however, dictates that fluorescence guidance has to be used in combination with the more common radioguided procedures.

Conventional SN mapping is performed using 20-600 nm radiocolloids. Because of their size, these exogenous compounds are recognized by the immune system, leading to accumulation in the SN [6]. We found that premixing of the clinically approved near-infrared dye indocyanine green (ICG) and an albumin-based radiocolloid (^{99m}Tc-nanocolloid) yields the non-covalent ICG-^{99m}Tc-nanocolloid complex. This complex has migratory properties similar to the parental ^{99m}Tc-nanocolloid [7]. Other hybrid nanoparticles also have the potential to guide SN biopsy [8]. A recent preclinical example of a hybrid SN tracer can be found in ^{99m}Tc-Tilmanocept labeled with the near-infrared dye Cy7 [9]. Alternatively, Cerenkov imaging of positron-emitting radionuclides has been proposed as a hybrid imaging technology; Thorek et al. demonstrated that lymph nodes could be detected after a subdermal injection of ^{18}F-FDG in the tail of a mouse [10].

Ideally, for more accurate lymph nodes staging, direct identification of nodal metastases would be preferred. Research is now focusing on the introduction of hybrid tracers that specifically target tumor tissue [11,12]: for example, by targeting prostate specific

biomarkers such as prostate specific membrane antigen or the gastrin-releasing peptide receptor. In this light, a hybrid prostate-specific membrane anti gentracer, labeled with indium-111 and the near-infrared dye CW800, was shown to facilitate radioactivity- and fluorescence-based detection of prostate specific membrane antigen-overexpressing tumors in mice [13].

INJECTION PROCEDURE

Before SN biopsy, transrectal ultrasound guidance is used to direct the tracer deposition toward the peripheral zone of the prostate (Figure 2A). Nevertheless, a recent study showed that in only 53% of patients was the tracer actually deposited in this area [14]. Interestingly, the same study also suggested that the location of tracer deposition influences the lymphatic drainage pattern. The main question is whether, in order to identify the true tumor-draining SNs, the tracer should be injected randomly in the peripheral zone of the prostate. It might be better to aim for peri- or intratumoral tracer deposition as is common in, for example, breast cancer and melanoma.

Multiparametric magnetic resonance (MR) imaging (T2-weighted, contrast-enhanced, and diffusion weighted) was shown to be promising in the identification of localized prostate cancer [15]. Integrating such MR imaging information with real-time acquired contrast-enhanced transrectal ultrasound may allow MR imaging-based navigation of injection needles toward the intraprostatic tumor foci.

PREOPERATIVE SENTINEL NODE IDENTIFICATION AND PLANNING OF THE SURGICAL PROCEDURE

After tracer injection, obtaining sequential anterior (Figure 2B) and posterior lymphoscintigraphic images is recommended in order to differentiate early draining SNs from higher-echelon nodes [16]. Via the introduction of single photon emission computed tomography imaging combined with computed tomography (SPECT/CT) imaging, the three-dimensional (3D) distribution of the radiocolloid can be directly placed in the anatomic context provided by the CT component (Figure 2C, D). Moreover, with SPECT/CT imaging, SNs not seen on lymphoscintigraphic images, such as those in the presacral region, can be identified [17]. As such, preoperative identification of the lymphatic drainage patterns allows surgeons to decide beforehand on the optimal and least invasive surgical approach.

Position emission tomography (PET)/CT, PET/MR imaging, or multiparametric MR imaging may, in the future, also be of value in planning surgical procedures. For example, lymph nodes mapping can be performed using radiocolloids suitable for PET imaging, via the direct identification of lymph nodes metastasis using targeted PET tracers or using ultrasmall superparamagnetic iron oxide particles or targeted dendrimers suitable for MR imaging.

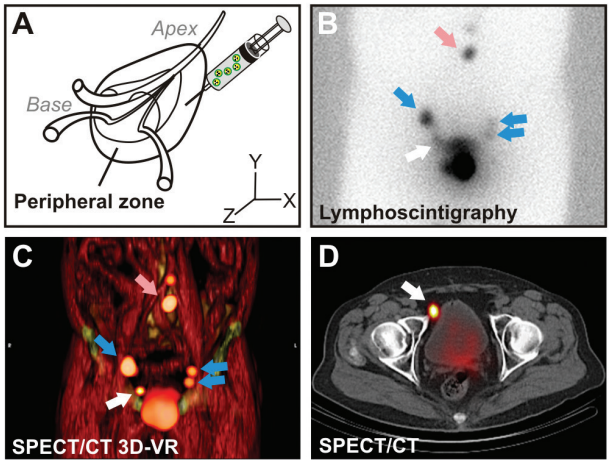

Figure 2. Preoperative Sentinel node mapping. After tracer injection in the peripheral zone of prostate (A), planar lymphoscintigraphic images are acquired to identify the SNs (B). SPECT/CT imaging allows identification of the anatomic location of the SNs and, in some cases, identification of SNs outside extended pelvic lymphadenectomy field; here, a paravesical SN (white arrow) not clearly detectable on the lymphoscintigraphic image was identified after SPECT/CT imaging (C-D). In this patient, five SNs were detected, with two being located outside extended pelvic lymphadenectomy field (white and pink arrows). SN = sentinel node; SPECT/CT = single photon emission computed tomography combined with computed tomography; 3D-VR = three-dimensional volume rendering.

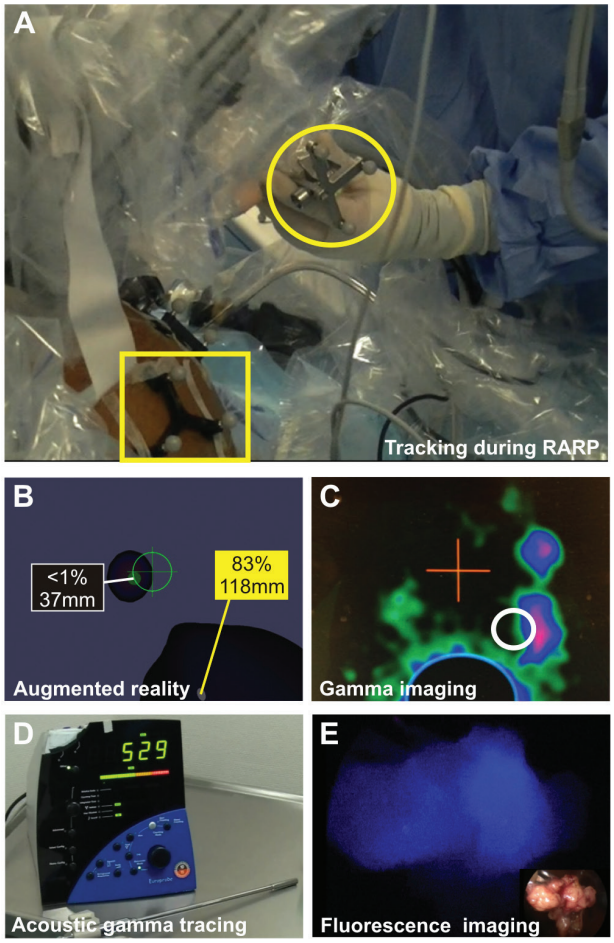

Figure 3. Intraoperative sentinel node identification. Via patient and tool tracking (yellow square and circle, respectively) (A), preoperatively acquired images can be translated into the operating room via 3D virtual reality navigation (B). A portable gamma camera allows visualization of the radioactive hot spots in 2D whereby a iodine-125 seed placed on the tip of the laparoscopic gamma probe (white circle) can be used for navigation (C). Hybrid tracers allow SNs to be acoustically traced using a gamma probe (D) and optically detected via fluorescence imaging (E). SN = sentinel node; 3D = three-dimentional; 2D = two-dimentional; RARP = robot-assisted radical prostatectomy.

TRANSLATION OF THE PREOPERATIVELY ACQUIRED IMAGING DATA TO THE OPERATION ROOM

Ideally, preoperatively acquired two-dimensional (2D) and 3D imaging data can be directly translated into the operating room to help navigate the surgeon to the areas of interest. Improvement is especially desired in localization of SNs near vital structures. Most straightforward is 2D navigation provided by a portable gamma camera [18]. By placing a iodine-125 seed on a laparoscopic gamma probe and performing dual-isotope gamma imaging, it is possible to surgically navigate a laparoscopic gamma probe toward the SNs (Figure 3C) [18].

The freehandSPECT technology, which is based on real-time tracking of both the patient and a gamma probe, enables the generation of intraoperative 3D SPECT data that can be viewed in augmented- or virtual-reality (i.e. mixed-reality) as an improvement over 2D imaging [19]. Alternatively, virtual-reality images can be generated using segmentation of SPECT scans (Figure 3B), CT scans [20] or using transrectal ultrasound images [21]. For robot-assisted procedures, one can load virtual-reality images and/or the preoperatively acquired 3D images into the TilePro function of the da Vinci robot (Intuitive Surgical Inc.). By attaching a 3D motion controller, it even becomes possible to manually manipulate these images [22].

For mixed-reality-based navigation in soft tissue, organ deformation and movement of organs or the cameras can be a serious problem. Hence, one must compensate for such movements by placing internal [20] or external [23] navigation aids (Figure 3A). A disadvantage of that approach is that it is difficult to correct for motion and organ deformation.

The fluorescence signature of a hybrid tracer, in combination with the tracking of a fluorescence laparoscope, can potentially be used to compensate for navigation errors of less than 10 mm [23].

INTRAOPERATIVE SENTINEL NODE IDENTIFICATION

Intraoperative SN identification is traditionally facilitated via acoustic gamma tracing (Figure 3D). With the introduction of robot-assisted laparoscopic procedures, not only are the senses of the surgeon reduced but also new challenges are faced for intraoperative gamma tracing. For example, the reduction in the movement of the gamma probe reduces the spatial accuracy of this technology even further. This is particularly problematic in areas near the injection site, where the high background signal hinders SN identification. With regard to a two dimensional protocol, the natural decay of the radioactive signal over time can reduce the detection sensitivity, which is already relatively low for the prostate.

Hybrid tracers such as ICG-^{99m}Tc-nanocolloid can be used to extend the conventional radioguided surgical procedure with the benefits that near-infrared fluorescence imaging

has to offer [24]. With this tracer, gamma tracing can be used to obtain a rough localization of the SN while the increased spatial resolution provided by the fluorescent signature enables accurate delineation of the SN (Figure 3E). An excellent example of the spatial information that fluorescence imaging provides during laparoscopic surgery was demonstrated by Jeschke et al., who showed lymphatic tracts draining from the prostate to the SN, as well as the SN itself [25].

PATIENT BENEFIT

We envision that symbiosis between the above-mentioned surgical guidance technologies may, in the future, provide patient benefit. Diagnostic images may help surgeons to select the least invasive surgical approach. Such planning should result in minimization of the exploration time. A one-to-one correlation between pre and intraoperatively generated images helps validate complete excision of lesions. Finally, more accurate surgical identification of diseased and anatomic structures may result in further reduction of complications associated with nodal dissection.

CONCLUSION

Optimal use of interventional molecular imaging techniques is expected to lead to new surgical treatment paradigms for indications such as the SN biopsy procedure for prostate cancer. One of the major challenges in the wide implementation of such technologies is their clinical translation. The first proof-of-concept studies, however, can provide a clinical basis for further improvements in this research field.

REFERENCES

1. Holl G, Dorn R, Wengenmair H, Weckermann D, Sciuk J. Validation of sentinel lymph node dissection in prostate cancer: experience in more than 2,000 patients. Eur J Nucl Med Mol Imaging. 2009;36:1377-1382.
2. Joniau S, Van den Bergh L, Lerut E, et al. Mapping of pelvic lymph node metastases in prostate cancer. Eur Urol. 2013;63:450-458.
3. Mattei A, Fuechsel FG, Bhatta Dhar N, et al. The template of the primary lymphatic landing sites of the prostate should be revisited: results of a multimodality mapping study. Eur Urol. 2008;53:118-125.
4. Meinhardt W, van der Poel HG, Valdes Olmos RA, Bex A, Brouwer OR, Horenblas S. Laparoscopic sentinel lymph node biopsy for prostate cancer: the relevance of locations outside the extended dissection area. Prostate Cancer. 2012;2012:751753.
5. van den Berg NS, van Leeuwen FW, van der Poel HG. Fluorescence guidance in urologic surgery. Curr Opin Urol. 2012;22:109-120.

6. Uren RF. Lymphatic drainage of the skin. Ann Surg Oncol. 2004;11:179S-185S.
7. Brouwer OR, Buckle T, Vermeeren L, et al. Comparing the hybrid fluorescentradioactive tracer indocyanine green-^{99m}Tc-nanocolloid with ^{99m}Tc-nanocolloid for sentinel node identification: a validation study using lymphoscintigraphy and SPECT/CT. J Nucl Med. 2012;53:1034-1040.
8. Buckle T, Chin PT, van Leeuwen FW. (Non-targeted) radioactive/fluorescent nanoparticles and their potential in combined pre- and intraoperative imaging during sentinel lymph node resection. Nanotechnology. 2010;21:482001.
9. Emerson DK, Limmer KK, Hall DJ, et al. A receptor-targeted fluorescent radiopharmaceutical for multireporter sentinel lymph node imaging. Radiology. 2012;265:186-193.
10. Thorek DL, Abou DS, Beattie BJ, et al. Positron lymphography: multimodal, high-resolution, dynamic mapping and resection of lymph nodes after intradermal injection of 18F-FDG. J Nucl Med. 2012;53:1438-1445.
11. Kuil J, Velders AH, van Leeuwen FW. Multimodal tumor-targeting peptides functionalized with both a radio- and a fluorescent label. Bioconjug Chem. 2010;21:1709-1719.
12. Azhdarinia A, Ghosh P, Ghosh S, Wilganowski N, Sevick-Muraca EM. Dual-labeling strategies for nuclear and fluorescence molecular imaging: a review and analysis. Mol Imaging Biol. 2012;14:261-276.
13. Banerjee SR, Pullambhatla M, Byun Y, et al. Sequential SPECT and optical imaging of experimental models of prostate cancer with a dual modality inhibitor of the prostate-specific membrane antigen. Angew Chem Int Ed Engl.2011;50:9167-9170.
14. Buckle T, Brouwer OR, Valdes Olmos RA, van der Poel HG, van Leeuwen FW. Relationship between intraprostatic tracer deposits and sentinel lymph node mapping in prostate cancer patients. J Nucl Med. 2012;53:1026-1033.
15. Fütterer JJ, Barentsz JO. MR imaging-guided and robotic-assisted prostate biopsy. Curr Opin Urol. 2012;22:316-319.
16. Valdés Olmos RA, Vidal-Sicart S. SPECT/CT image generation and criteria for sentinel node mapping. In: Mariani G, Manca G, Orsini P, Vidal-Sicart S, Valdes Olmos R, eds. Atlas of Lymphoscintigraphy and Sentinel Node Mapping. Milan, Italy: Springer; 2012:269-283.
17. Vermeeren L, Valdes Olmos RA, Meinhardt W, et al. Value of SPECT/CT for detection and anatomic localization of sentinel lymph nodes before laparoscopic sentinel node lymphadenectomy in prostate carcinoma. J Nucl Med. 2009;50:865-870.
18. Vermeeren L, Valdes Olmos RA, Meinhardt W, et al. Intraoperative radioguidance with a portable gamma camera: a novel technique for laparoscopic sentinel node localisation in urological malignancies. Eur J Nucl Med Mol Imaging. 2009;36:1029-1036.
19. Navab N, Blum T, Wang L, Okur A, Wendler T. First deployments of augmented reality in operating rooms. Computer. 2012;45:48-55.
20. Simpfendo¨rfer T, Baumhauer M, Muller M, et al. Augmented reality visualization during laparoscopic radical prostatectomy. J Endourol. 2011;25:1841-1845.

21. Ukimura O, Nakamoto M, Gill IS. Three-dimensional reconstruction of renovascular-tumor anatomy to facilitate zero-ischemia partial nephrectomy. Eur Urol. 2012;61:211-217.
22. Volonté F, Pugin F, Buchs NC, et al. Console-integrated stereoscopic osirix 3D volume-rendered images for da Vinci colorectal robotic surgery. Surg Innov. 2013;20:158-63.
23. Brouwer OR, Buckle T, Bunschoten A, et al. Image navigation as a means to expand the boundaries of fluorescence-guided surgery. Phys Med Biol. 2012;57:3123-3136.
24. van der Poel HG, Buckle T, Brouwer OR, Valdes Olmos RA, van Leeuwen FW. Intraoperative laparoscopic fluorescence guidance to the sentinel lymph node in prostate cancer patients: clinical proof of concept of an integrated functional imaging approach using a multimodal tracer. Eur Urol. 2011;60:826-833.
25. Jeschke S, Lusuardi L, Myatt A, Hruby S, Pirich C, Janetschek G. Visualisation of the lymph node pathway in real time by laparoscopic radioisotope- and fluorescence-guided sentinel lymph node dissection in prostate cancer staging. Urology. 2012;80:1080-1086.

SUMMARY

The work described in this thesis shows how intraoperative lesion identification can be improved via the introduction of (hybrid) tracers and optimized (hybrid) imaging modalities capable of detecting these tracers. In **part one** of this thesis, the reader is introduced to the concept of fluorescence image-guided surgery and the evolution thereof. Furthermore, the hybrid approach for image-guided surgical guidance is presented. **Part two** of this thesis describes the clinical evaluation of the hybrid approach using the hybrid indocyanine green (ICG)-technetium-99m (^{99m}Tc)-nanocolloid. To further refine the hybrid approach for surgical guidance, **part three** of this thesis describes the development and evaluation of different types of (hybrid) imaging modalities.

PART ONE

In chapter 2, the concept of fluorescence image guidance is introduced by describing the various fluorescence tracers and detection modalities used within the field of urology. Although both visible and near-infrared fluorescence tracers are commonly used for e.g. cancer diagnosis (e.g. protoporphyrin IX precursors 5-ALA or HAL), (lymph-)angiography (e.g. fluorescein or ICG), ureter visualization (fluorescein) and sentinel node mapping (ICG-^{99m}Tc-nanocolloid), the majority of (commercially) available fluorescence cameras can only detect the near-infrared fluorescence signal of ICG.

Chapter 3 provides an overview of the clinically available tracers for sentinel node biopsy, a routine clinical procedure in staging of patients with early stage cancer. Radiotracers (e.g. ^{99m}Tc-nanocolloid) have proven to be of great value in this setting as they allow for non-invasive preoperative sentinel node mapping, as well as providing intraoperative radioguidance. To allow for intraoperative optical detection of the sentinel node(s), generally blue dye(s) or the near-infrared fluorescence tracer (ICG) are used as a separate entity. With the introduction of hybrid tracers, e.g. ICG-^{99m}Tc-nanocolloid, integration of the pre- and the intraoperative approach was facilitated allowing direct translation of preoperative imaging information in the operation theatre. Furthermore in this chapter, using the hybrid tracer the hybrid approach for sentinel node biopsy is introduced and put into perspective with respect to the conventional radioguided and blue dye-based approach.

PART TWO

Part two of this thesis focuses on the evaluation of the hybrid tracer ICG-^{99m}Tc-nanocolloid for various indications of sentinel node biopsy as such to determine its clinical value. In chapter 4, the technology was evaluated in 14 patients with oral cavity carcinoma. In this setting the fluorescence signature of the hybrid tracer proved to be of particular value for the identification of near-injection site sentinel nodes. Chapter 5 evaluated the feasibility of the hybrid tracer-based sentinel node biopsy procedure in a large cohort of penile cancer patients (n=65; 119 groins). Here the fluorescent signature of the hybrid tracer allowed optical identification of 96.8% of the sentinel nodes, while using blue dye merely 55.7% of the sentinel nodes could be visualized ($p<0.0001$). Compared to blue dye,

fluorescence imaging provided improved tissue penetration resulting in the visualization of sentinel nodes through the intact skin in some patients. Ex vivo evaluation of four tumor-positive sentinel nodes also revealed that the hybrid tracer was mainly present in the unaffected lymphatic tissue of the sentinel node.

In chapter 6, the hybrid tracer approach was evaluated in 104 patients with melanoma (in the head-and-neck, on the trunk or on an extremity), with drainage to, amongst others, the neck, axilla and groin. Here radioguidance alone allowed the identification of 93.8% of the sentinel nodes, while the fluorescent signature of the same tracer gave an intraoperative detection rate of 96.7%. In contrast, with blue dye only 61.7% of the sentinel nodes could be visualized. Fluorescence imaging provided welcome guidance when no blue dye was used or when sentinel nodes failed to take up blue dye (n=12 patients), or in case the SNs could not be detected using gamma tracing (n=5 patients).

From **part two** it can be concluded that there is a definite value in using the hybrid tracer for sentinel node biopsy in comparison to the conventional radio- and blue dye-guidance. Moreover the results from the above-described studies illustrate that this value seems to be biggest when sentinel nodes reside in close proximity to the injection site and/or at a location of complex anatomy (e.g. the parotid gland).

PART THREE

To accommodate routine clinical embedment of the hybrid tracer, further improvements in the surgical imaging modalities are required. **Part three** of this thesis focuses on refining currently clinical grade imaging hardware, as well as on the introduction of a novel hybrid imaging modality. In chapter 7 a prototype handheld open surgery fluorescence camera that allows fluorescence guidance under ambient light conditions is presented. In seven patients, in a direct comparison to its predecessor, this prototype fluorescence camera identified a higher number of sentinel nodes intraoperatively (100% vs. 81.4%), more transcutaneous sentinel node visualization (40.7% vs. 22.2%) as well as lymphatic duct visualization (7.4% vs. 0%). In an additional 20 patients, the value of the technical improvements made was further underlined; in some patients real-time fluorescence-guided sentinel node excision was possible where previously fluorescence imaging was mainly used to confirm localization of the sentinel node(s) (**part two**). Chapter 8 is aimed at improving laparoscopic fluorescence imaging during sentinel node identification in patients with prostate cancer that were to undergo robot-assisted laparoscopic sentinel node biopsy (n=40). Here, optimization of the hybrid tracer formulation and injection resulted in an improvement of intraoperative sentinel node identification from 63.7% to 85.2%, which further increased to 93.5% after improving the fluorescence imaging laparoscope. Similarly as described in chapter 7, improvements eventually resulted in enabling real-time fluorescence guidance. In chapter 9 this same fluorescence laparoscope was further refined to allow for the intraoperative detection of two complementary fluorescence signatures (ICG-^{99m}Tc-nanocolloid and fluorescein) via a so-called multispectral fluorescence imaging approach. In a pilot study in ten patients the hybrid tracer could be

used for sentinel node visualization, whereas the visible dye fluorescein could be used as a lymphangiographic agent highlighting the ducts running to the hybrid tracer-stained sentinel node(s). Results from this study showed that intraoperative multispectral imaging is clinically feasible.

Alternative to optimization of the fluorescence imaging technologies, optimization of gamma imaging modalities can be explored. In chapter 10 the introduction of a navigation technology for surgical guidance is presented. With this navigation technology, using augmented- and virtual-reality, preoperative imaging information is made directly available to the surgeon in the operation theatre. Using this set-up, an average error of 8.0±2.1 and 8.5±5.4 mm in the coronal and saggital/axial plane was found when navigating the conventional gamma probe in 3D preoperative SPECT/CT images to the sentinel node in the groin (n=5 patients).

Hybrid imaging modalities capable of detecting both signatures may further enhance the clinical application of hybrid tracers. Chapter 11 describes the evaluation of a modality that allows combined radio- and fluorescence tracing. The feasibility of the prototype opto-nuclear probe for combined radio- and fluorescence-guided sentinel node identification was demonstrated ex vivo in clinical (non)sentinel node samples (n=150), and in a pilot study in patients with head-and-neck malignancies or penile cancer (n=9). Of the 20 sentinel nodes that were intraoperatively evaluated, the prototype opto-nuclear probe detected the radio- and fluorescence signal in all nodes. Fluorescence tracing could be performed under ambient light conditions.

The general conclusion from **part three** of this thesis is that the introduction of novel imaging modalities, or the improvement of current existing hardware, required for radio- and/or fluorescence-guided surgery has the potential to further refine currently existing surgical procedures. The above-described studies all present pilot studies though, of which the results will have to be validated in larger, preferably multicenter, studies.

OUTLOOK

In the **outlook,** chapter 12, we describe how we envision the hybrid approach for sentinel node biopsy of prostate cancer in the near future. Although this chapter is focused on sentinel node biopsy for prostate cancer, the same approach can easily be translated to other malignancies and targets, e.g. nerves. Via the introduction of navigation technologies, in the hybrid guidance concept the preoperative imaging information can be directly linked to the findings in the operation theatre. Additionally, the introduction of (novel) gamma and fluorescence imaging technologies can help to further optimize intraoperative sentinel node identification. When reaching beyond proof-of-principal studies, integrated use of the proposed technologies (**part three**) in combination with (hybrid) tracers (**part one** and **two**) can result in new surgical treatment paradigms.

SAMENVATTING

Dit proefschrift beschrijft hoe de identificatie van laesies tijdens een operatie verbeterd kan worden door de introductie van (hybride) speurstoffen en geoptimaliseerde (hybride) beeldvormingsmodaliteiten die deze speurstoffen kunnen detecteren. In **deel één** van dit proefschrift maakt de lezer kennis met het concept van fluorescentie-geleide chirurgie en de evolutie die daarin plaatsgevonden heeft. Tevens wordt de hybride benadering voor beeldgeleide chirurgie gepresenteerd. **Deel twee** beschrijft de klinische evaluatie van de hybride benadering gebruikmakend van de speurstof indocyanine groen (ICG)-technetium-99m (^{99m}Tc)-nanocolloid. In **deel drie** wordt de ontwikkeling en optimalisatie van verschillende (hybride) beeldvormingsmodaliteiten besproken teneinde de hybride benadering verder te vervolmaken.

DEEL ÉÉN

Hoofdstuk 2 introduceert het concept van fluorescentie-geleide chirurgie aan de hand van de verschillende klinisch gebruikte fluorescente speurstoffen en detectiesystemen binnen het terrein van de urologie. Waar zowel visuele als nabij-infrarode fluorescente speurstoffen gebruikt worden voor onder andere de diagnose van kanker (protoporfyrine IX voorlopers 5-ALA of HAL), (lymfe-)angiografie (fluoresceïne of ICG), visualisatie van de urineleiders (fluoresceïne) of de schildwachtklierbeeldvorming (ICG-^{99m}Tc-nanocolloid), zijn de meeste commercieel beschikbare fluorescentie camera's alleen geschikt voor de detectie van de nabij-infrarode fluorescente speurstof ICG.

In hoofdstuk 3 wordt een overzicht gegeven van de klinisch beschikbare speurstoffen voor de schildwachtklierprocedure, een routine procedure voor stadiëring van patiënten met een vroeg stadium kanker. Radioactieve speurstoffen (bijvoorbeeld ^{99m}Tc-nanocolloïd) zijn van grote waarde bij deze procedure omdat ze, na injectie rondom de tumor, de mogelijkheid bieden om op een niet-invasieve manier de schildwachtklieren op te laten lichten. Tijdens de operatie kunnen deze schildwachtklieren dan door middel van radiogeleiding geïdentificeerd worden. Om de schildwachtklieren zichtbaar te maken tijdens de operatie wordt vaak ook nog een blauwe kleurstof of een fluorescente speurstof rondom de tumor toegediend. Met de introductie van hybride speurstoffen, bijvoorbeeld ICG-^{99m}Tc-nanocolloid, kan integratie van de pre- en intraoperatieve benadering bereikt worden waarbij de preoperatief verkregen informatie direct naar de operatiekamer vertaald kan worden. De hybride benadering voor de schildwachtlierprocedure wordt in dit hoofdstuk geïntroduceerd en vergeleken met de conventionele radiogeleide en blauwe kleurstof-gebaseerde benadering.

DEEL TWEE

Deel twee richt zich op de evaluatie van ICG-^{99m}Tc-nanocolloid voor de schildwachtklierprocedure bij patiënten met verschillende soorten vroeg stadium kanker teneinde de klinische waarde te bepalen. Hoofdstuk 4 beschrijft de evaluatie van de hybride speurstof in 14 patiënten die de schildwachtklierprocedure ondergingen vanwege

mondholte kanker. De fluorescente handtekening was met name van belang voor de identificatie van schildwachtklieren die zich naast de injectieplaats bevonden. In hoofdstuk 5 wordt de hybride speurstof geëvalueerd in 65 patiënten met penis kanker (119 liezen). Visuele identificatie van de schildwachtklier met behulp van fluorescentie beeldvorming was aantoonbaar beter ten opzichte van de blauwe kleurstof-gebaseerde methode: 96,8% vs. 55,7% ($p<0,001$). In sommige patiënten werd met fluorescentie beeldvorming de schildwachtklier al door de intacte huid heen waargenomen terwijl dit met de blauwe kleurstof niet mogelijk was. Ex vivo evaluatie van tumor-positieve schildwachtklieren leerde ons ook dat de hybride speurstof zich met name in het gezonde lymfeklierweefsel bevond.

Het belang van de hybride benadering voor de schildwachtklierprocedure in patiënten met een melanoom wordt geëvalueerd in hoofdstuk 6. In 104 patiënten met een hoofd-hals melanoom, een melanoom op de romp of op een arm of been werd lymfatische drainage gezien naar schildwachtklieren in, onder andere, de hals, oksel en lies. Waar tijdens de operatie 93,8% van de schildwachtklieren opgespoord kon worden via radiogeleiding, kon door middel van fluorescentie beeldvorming 96,7% van de schildwachtklieren zichtbaar gemaakt worden. In vergelijking, met blauwe kleurstof werd slechts 61,7% van de schildwachtklieren gevisualiseerd. Fluorescentie beeldvorming was met name van waarde wanneer de blauwe kleurstof niet gebruikt werd, wanneer de schildwachtklieren geen blauwe kleurstof hadden opgenomen (22 patiënten), of wanneer de schildwachtklier niet gedetecteerd kon worden via radiogeleiding (5 patiënten).

Deel twee concludeert dat, in vergelijking met de conventionele radio- en blauwe kleurstof-geleide schildwachtklierprocedure er een duidelijk belang is voor het gebruik van de hybride speurstof voor deze procedure. De waarde van de hybride speurstof werd het grootste gevonden voor de identificatie van schildwachtklieren die zich vlakbij de injectieplek bevonden en op plaatsen met een lastige anatomie, bijvoorbeeld in het parotis gebied.

DEEL DRIE

Om de hybride speurstof in de klinische routine opgenomen te krijgen is verbetering van de huidige beeldvormingsmodaliteiten gewenst. **Deel drie** van dit proefschrift richt zich op het verbeteren van de huidige klinisch beschikbare fluorescentie beeldvormingsmodaliteiten en tevens op de introductie van een nieuwe hybride beeldvormingsmodaliteit. Hoofdstuk 7 beschrijft een prototype draagbare fluorescentie camera voor open chirurgie welke werkt onder normale licht omstandigheden. Deze camera werd vergeleken met zijn voorganger in zeven patiënten die een schildwachtklierprocedure ondergingen gebruikmakend van de hybride speurstof. De prototype camera visualiseerde meer schildwachtklieren en lymfebanen tijdens de operatie, respectievelijk 100% en 7,4% vs. 81,4% en 0%. Ook werden de schildwachtklieren vaker door de intacte huid heen gezien (40,7% vs. 22,2%). In 20 additioneel geïncludeerde patiënten werd het belang van deze technische verbeteringen verder versterkt. In sommige patiënten was real-time

fluorescentie-geleide schildwachtklier-identificatie en -excisie mogelijk waar de techniek eerder vooral werd gebruikt ter bevestiging van de lokalisatie van de schildwachtklier(en) (deel twee).

Hoofdstuk 8 beschrijft de optimalisatie van laparoscopische fluorescentiebeeldvorming in patiënten met prostaatkanker welke een robot-geassisteerde laparoscopische schildwachtklierprocedure ondergingen (40 patiënten). Optimalisatie van de samenstelling van de hybride speurstof leidde tot een verbetering in schildwachtklieridentificatie van 63,7% naar 85,2%. Dit verbeterde verder naar 93,5% na de introductie van een verbeterde laparoscopische fluorescentiecamera. Vergelijkbaar aan het uiteengezette in hoofdstuk 7, hebben deze verbeteringen er ook toe geleid dat real-time fluorescentiegeleide schildwachtklier-identificatie en -excisie mogelijk werd. Door deze fluorescentiecamera geschikt te maken voor de detectie van meerdere fluorescente signalen, werd intraoperatieve multispectrale fluorescentie beeldvorming mogelijk (beschreven in hoofdstuk 9). In een haalbaarheidsstudie in tien patiënten werd deze multispectrale fluorescentiebeeldvormingsbenadering geëvalueerd gebruikmakend van de lymfe-angiografische kleurstof fluoresceïne (visuele fluorescentie) en de hybride, nabij-infrarode, schildwachtklier speurstof ICG-^{99m}Tc-nancolloid. Waar de eerste de naar de schildwachtklieren lopende lymfebanen deed oplichten, konden met de hybride tracer ICG-^{99m}Tc-nanocolloïd de schildwachtklieren gevisualiseerd worden.

Alternatief aan de optimalisatie van fluorescentie beeldvormingsmodaliteiten, hebben we ook gekeken naar optimalisatie van gamma imaging modaliteiten. Hoofdstuk 10 beschrijft de introductie van een navigatie systeem voor intraoperatieve geleiding. Gebruikmakend van deze navigatie technologie hebben we in vijf patiënten aangetoond dat preoperatieve beeldvorming direct beschikbaar gemaakt kon worden voor de chirurg in de operatiekamer. Een afwijking van 8,5±2,1 en 8,0±5,4 mm in het coronale en saggitale/axiale vlak werd gevonden wanneer de conventionele gamma probe in augmented- en virtual-reality in 3D preoperatieve SPECT/CT beeldvorming genavigeerd werd in naar de schildwachtklier(en).

In hoofdstuk 11 wordt een hybride modaliteit beschreven die zowel radioactiviteit als fluorescentie kan detecteren. Na een ex vivo haalbaarheidsstudie waarin 150 schildwachtklierweefsels werden geëvalueerd werd een klinische pilot studie uitgevoerd in 9 patiënten die een schildwachtklierprocedure ondergingen gebruikmakend van de hybride speurstof. Tijdens de operatie werden 20 schildwachtklieren met de opto-nuclear probe gemeten waarbij in alle gevallen zowel het radioactieve, als het fluorescentie signaal in de klier gemeten kon worden. Fluorescentie geleiding was hierbij mogelijk onder normale licht omstandigheden.

Concluderend, chirurgische procedures kunnen mogelijk verbeterd worden door optimalisatie van de bestaande beeldvormingsmodaliteiten en/of de introductie van nieuwe hybride modaliteiten zoals beschreven in **deel drie**. Dit kan mogelijk leiden tot opname van deze technieken in de klinische routine. Echter, de hierboven beschreven

studies betreffen allemaal haalbaarheidsstudies waarvan de resultaten eerst nog verder gevalideerd moeten worden in grotere, bij voorkeur multicenter, studies.

PERSPECTIEF

In het **perspectief**, hoofdstuk 12, van dit proefschrift, beschrijven we hoe wij in de nabije toekomst de hybride benadering voor de schildwachtklierprocedure bij prostaatkanker voor ons zien. Ondanks het feit dat dit hoofdstuk zich richt op de schildwachtklierprocedure voor prostaatkanker kan deze benadering ook eenvoudig vertaald worden naar andere maligniteiten en anatomische structuren, bijvoorbeeld zenuwen. We laten zien dat, door gebruik te maken van navigatietechnieken, in combinatie met de hybride benadering, directe vertaling van preoperatieve beeldvormingsinformatie in de operatiekamer mogelijk wordt. De introductie van radio- en fluorescentie detectietechnieken kan hierbij gebruikt worden om schildwachtklier identificatie verder te verbeteren. Hierbij geldt, dat als we voorbij proof-of-principle studies komen, geïntegreerd gebruik van de hierboven beschreven beeldvormingstechnieken (**deel drie**) in combinatie met hybride speurstoffen (**deel één** en **twee**) mogelijk kan leiden tot (nieuwe) verbeterde chirurgische behandelingen.

RESUMEN

El trabajo descrito en esta tesis muestra cómo la identificación intraoperatoria de lesiones puede ser mejorada a través de la introducción de trazadores (híbridos) y de técnicas (híbridas) optimizadas de imagen capaces de detectarlos. En la **primera parte** de esta tesis, se introduce al lector en el concepto de la cirugía guiada por la fluorescencia y la evolución de la misma para efectuarla. Al mismo tiempo, se presenta el enfoque híbrido de la cirugía guiada por la imagen. En la **segunda parte** de esta tesis se describe la evaluación clínica del trazador híbrido verde de indocianina (ICG)-tecnecio-99m (^{99m}Tc)-nanocoloide. En la **tercera parte** de esta tesis se describe el desarrollo y la evaluación de diferentes tipos de modalidades de formación de imágenes híbridas para perfeccionar la cirugía radioguiada.

PRIMERA PARTE

En el capítulo 2, el concepto de guía por imágenes de fluorescencia se introduce mediante la descripción de los diferentes trazadores de fluorescencia y las modalidades de detección utilizadas en el campo de la urología. Aunque tanto los trazadores de fluorescencia visible como los de infrarrojo cercano se utilizan comúnmente para el diagnóstico de cáncer (por ejemplo, precursores de protoporfirina IX (5-ALA o HAL), la (linfa)angiografía (fluoresceína o ICG), la visualización del uréter (fluoresceína) y el mapeo del ganglio centinela (ICG-^{99m}Tc-nanocoloides), la mayoría de las cámaras de fluorescencia (comercialmente) disponibles sólo pueden detectar la señal de fluorescencia de infrarrojo cercano del ICG.

El capítulo 3 proporciona una panorámica general de los trazadores clínicamente disponibles para biopsia del ganglio centinela, un procedimiento clínico de rutina en la estadificación de los pacientes con cáncer en fase temprana. Los radiotrazadores (por ejemplo el ^{99m}Tc-nanocoloide) han demostrado ser de gran valor para permitir tanto el mapeo del ganglio centinela preoperatorio en forma no invasiva, así como la cirugía radioguiada. Para permitir la detección óptica intraoperatoria de los ganglio centinelas, en general, colorantes vitales como el azul o compuestos fluorescentes del infrarrojo cercano (ICG), se utilizan como entidades separadas. Con la introducción de trazadores híbridos, como por ejemplo el ICG-^{99m}Tc-nanocoloide, la integración de los componentes pre- e intraoperatorio ha sido facilitada permitiendo la transferencia directa de la información de las imágenes preoperatorias al teatro de operaciones. Además en este capítulo, sobre la base del ICG-^{99m}Tc-nanocoloide se introduce el procedimiento híbrido para la biopsia del ganglio centinela y se lo coloca en perspectiva con respecto a la cirugía radioguiada convencional basada en la utilización del azul.

SEGUDA PARTE

La **segunda parte** de esta tesis se centra en la evaluación del trazador híbrido ICG-^{99m}Tc-nanocoloide en la determinación de su valor clínico para varias indicaciones de la biopsia del ganglio centinela. En el capítulo 4, la tecnología se evalúa en 14 pacientes con carcinoma de cavidad oral. Para este objetivo el componente fluorescente del trazador híbrido

demostró ser de particular valor para la identificación de ganglios centinelas próximos al sitio de inyección. En el capítulo 5 se evalúa la factibilidad del procedimiento de la biopsia del ganglio centinela basado en el trazador híbrido en un gran cohorte de pacientes con cáncer de pene (n=65; 119 ingles). El componente fluorescente del trazador híbrido permitió intraoperatoriamente la identificación óptica del 96,8% de los ganglios centinela, mientras que con el colorante azul sólo un 55,7% de los ganglios centinela pudo ser visualizado (p <0,0001). En comparación con el azul la fluorescencia permitió en el pabellón de operaciones una mayor visualización de ganglios centinela a través de la piel intacta en algunos pacientes debido a su mejor penetración en el tejido. La evaluación ex vivo de cuatro ganglios centinela con infiltración tumoral positiva también reveló que el trazador híbrido estaba presente principalmente en la parte no afectada del tejido linfático del ganglio centinela.

En el capítulo 6 se evalúa el procedimiento con el trazador híbrido en 104 pacientes con melanoma (localizado en cabeza/cuello, tronco o extremidades), con drenaje cervical, axilar e inguinal. En el quirófano el componente radioguiado permitió solo la identificación de un 93,8% de los ganglios centinela, mientras que con la fluorescencia del mismo trazador se llegó a una tasa de detección del 96,7%. Contrastando con esto, el colorante azul solo pudo visualizar un 61,7% de los ganglios centinela. Las imágenes de fluorescencia pudieron proporcionar una orientación muy útil cuando no se utilizó colorante azul o cuando los ganglios centinela no se tiñeron de azul (n=12 pacientes), o en caso que los ganglios centinela no pudieron ser localizados utilizando la detección de rayos gamma (n=5 pacientes).

A partir de lo expuesto en la segunda parte, se puede concluir que existe un valor agregado concreto del trazador híbrido en la biopsia del ganglio centinela en comparación con la detección ya sea convencionalmente radioguiada o basada exclusivamente en el colorante azul. Además, los resultados de los estudios descritos anteriormente ilustran que este valor parece ser mayor cuando los ganglios centinela están ubicados en la proximidad de la zona de inyección y/o en lugares de anatomía compleja (como por ejemplo la región de la glándula parótida).

TERCERA PARTE

Para lograr la incorporación definitiva del trazador híbrido a la práctica clínica habitual se requiere mejorar su visualización en el pabellón quirúrgico. La **tercera parte** de esta tesis se centra en cómo refinar los equipos actuales de generación de imágenes clínicas intraoperatorias así como en la introducción de una nueva modalidad de imagen híbrida.
En el capítulo 7 se presenta el prototipo de una nueva cámara, para el uso manual en cirugía abierta, que permite visualizar la fluorescencia bajo condiciones de luz ambiental. En una comparación intraoperatoria directa con su predecesora en 7 pacientes este prototipo de cámara de fluorescencia logró identificar un mayor número de ganglios centinela (100% versus 81,4%), visualizar más ganglios centinela transcutáneamente

(40,7% vs. 22,2%), así como más ductos linfáticos (7,4% vs. 0%). En otros 20 pacientes, el valor de las mejoras técnicas realizadas se acentuó; en algunos pacientes la exéresis del ganglio centinela guiada por la fluorescencia fue posible en tiempo real cuando antes las imágenes de fluorescencia se utilizaban principalmente para confirmar la localización del ganglio centinela (ver segunda parte).

En el capítulo 8 se discute como la imagen de fluorescencia laparoscópica mejora la identificación del ganglio centinela en pacientes con cáncer de próstata planificados para la biopsia del ganglio centinela mediante laparoscopía asistida por robot (n = 40). En esto, la optimización de la formulación tanto del trazador híbrido como de su inyección resultó en un mejoramiento de la identificación del ganglio centinela intraoperatorio de 63,7% a 85,2%, aumentando al 93,5% cuando se mejoró el laparoscopio para las imágenes de fluorescencia. De manera similar a como se describe en el capítulo 7, estas mejoras dieron lugar a permitir la utilización de la fluorescencia para la escisión del ganglio centinela en tiempo real.

En el capítulo 9 este mismo laparoscopio fue perfeccionado para permitir la detección intraoperatoria de dos señales de fluorescencia complementarias (la de ICG del ICG-^{99m}Tc-nanocoloide y la de la fluoresceína) mediante un método de visualización multiespectral. En un estudio piloto incluyendo 10 pacientes el trazador híbrido pudo ser utilizado para visualizar el ganglio centinela, mientras que la fluoresceína fue utilizada para delinear los ductos linfáticos que afluyen hacia el ganglio centinela. Los resultados de este estudio mostraron que las imágenes multiespectrales intraoperatorias por fluorescencia son clínicamente factibles.

Como alternativa o complemento de la optimización de las tecnologías de imágenes de fluorescencia, el mejoramiento de las técnicas de imagen gamma también puede ser explorado. En el capítulo 10 se presenta la introducción de una tecnología de navegación como instrumento de guía quirúrgica. Con esta tecnología de navegación, utilizando un modelo de realidad virtual aumentada y mixta, la información de las imágenes tomográficas preoperatorias se coloca directamente a disposición del cirujano en el quirófano. Utilizando este método, errores promedios de 8,0±2,1 mm y 8,5±5,4 mm en el plano coronal y sagital/axial fueron encontrados al navegar con la sonda gamma convencional en un entorno 3D obtenido con la SPECT/CT preoperatoria en la búsqueda de ganglios centinela en la ingle (n=5 pacientes).

Las modalidades de imágenes híbridas capaces de detectar ambos componentes del ICG-^{99m}Tc-nanocoloide pueden mejorar aún más la aplicación clínica de los trazadores híbridos. El capítulo 11 describe la evaluación de una modalidad que permite el rastreo combinado de las señales radioactivas y fluorescentes. La factibilidad de un prototipo de sonda opto-nuclear para la identificación combinada del ganglio centinela tanto radioactivamente como guiada por fluorescencia fue demostrada ex vivo en muestras clínicas de ganglios linfáticos (no)centinela (n=150) y en un estudio piloto incluyendo pacientes con tumores malignos de cabeza y cuello o cáncer de pene (n=9). En este último

estudio, de los 20 ganglios centinela que fueron evaluados durante la operación, la sonda prototipo opto-nuclear detectó la señal de los componentes radioactivos y fluorescencentes en todos ellos. El rastreo de la fluorescencia pudo realizarse en condiciones de luz ambiental.

La conclusión general de la tercera parte de esta tesis es que tanto la introducción de nuevas modalidades de imagen como el mejoramiento de los equipos existentes en la actualidad requeridos para la cirugía radioguiada y/o guiada por fluorescencia tiene el potencial para perfeccionar los procedimientos quirúrgicos existentes en la actualidad. Los estudios anteriormente descritos representan muestras piloto por lo que los resultados tendrán que ser validados en estudios mayores preferentemente multicéntricos.

PERSPECTIVAS

En el capítulo 12 se entregan las **perspectivas** de esta tesis, describiéndose cómo visualizamos el enfoque híbrido para la biopsia del ganglio centinela en cáncer de próstata en un futuro próximo. Aunque este capítulo se centra en la biopsia del ganglio centinela para el cáncer de próstata, el mismo enfoque puede ser fácilmente extrapolado a otros tumores malignos y de aplicación con otros fines, como por ejemplo, nervios. A través de la introducción de las tecnologías de navegación en el concepto de orientación híbrida la información de las imágenes preoperatorias puede ser directamente relacionado con los hallazgos en la sala de operaciones. Adicionalmente, la introducción de nuevas tecnologías para generar imágenes gammagráficas y de fluorescencia puede ayudar a optimizar aún más la identificación intraoperatoria del ganglio centinela. Cuando se pase de los estudios de validación metodológica a los multicéntricos, el uso integrado de las tecnologías propuestas (**tercera parte**) en combinación con los trazadores híbridos (**parte uno** y **dos**) puede llevar a nuevos paradigmas de tratamiento quirúrgico.

GEARFETTING

Dit proefskrift beskriuwt hoe't de identifikaasje fan laesies ûnder in operaasje ferbettere wurde kin troch de ynfiering fan (hybride) speurmiddels en optimalisearre (hybride) byldfoarmingsmodaliteiten dy't dy speurmiddels opspoare kinne. Yn **diel ien** fan dit proefskrift komt de lêzer yn de kunde mei it konsept fan fluoressinsje-stjoerde sjirurgy en de evolúsje dêrfan binnen dy sjirurgy. Fierder wurdt it hybride oanpakken foar byldstjoerde sjirurgy presentearre. **Diel twa** fan dit proefskrift beskriuwt de klinyske evaluaasje fan de hybride oanpak mei help fan it speurmiddel indocyanine grien (ICG)-technetium-99m (^{99m}Tc) -nanocolloid. Om de hybride oanpak by sjirurgyske begelieding fierder te ferbetterjen, beskriuwt **diel trije** fan dit proefskrift de ûntwikkeling en optimalisaasje fan ferskillende soarten (hybride) byldfoarmingsmodaliteiten.

DIEL IEN

Haadstik 2 yntrodusearret it konsept fan fluoressinsje-stjoerde sjirurgy oan de hân fan de ferskate klinysk brûkte fluoressinte middels en de wizen fan opspoaren dy't brûkt wurde binnen it mêd fan urology. Wêr't likegoed fisuele as tichteby-ynfrareade fluoressinte middels brûkt wurde foar bygelyks de diagnoaze fan kanker (bygelyks protoporphyrin IX foarrinners 5-ALA of HAL), (lymph-)angiografy (bygelyks fluoresceine of ICG), fisualisaasje fan de urinelieders (fluoresceine) of de byldfoarming fan de skyldwachtklier (ICG-^{99m}Tc-nanocolloid), binne de measte fan de (kommersjeel) beskikbere fluoressinsje kamera's allinnich geskikt om it tichteby-ynfrareade fluoressinte middel ICG op te spoaren.

Haadstik 3 jout in oersjoch fan de klinysk beskikbere speurmiddels foar de skyldwachtklierproseduere, in rûtineproseduere foar it bepalen fan yn hokker fase pasjinten ferkeare yn in ier stadium fan kanker. Radioaktive speurmiddels (bygelyks ^{99m}Tc-nanocolloid) binne fan grutte wearde om't hja, nei ynjeksje om de tumor hinne, de mooglikheid biede om op in net ynvasive wize de skyldwachtklier opljochtsje te litten. Under de operaasje kinne dy skyldwachtklieren dan troch middel fan radiolieding identifisearre wurde. Om de skyldwachtklieren sichtber te meitsjen ûnder de operaasje wurdt fakentiid ek noch in blauwe kleurstof of in fluoressint middel jûn om de tumor hinne. Mei de yntroduksje fan hybride speurmiddels, bygelyks IGC-^{99m}Tc-nanocolloid, kin yntegraasje fan de pre- en ynteroperative oanpak berikt wurde, wêrby't de preoperatyf krigen ynformaasje fuortendaliks nei de operaasjekeamer oerset wurde kin. De hybride oanpak foar de skyldwachtklierproseduere wurdt in dit haadstik yntrodusearre en ferlike mei de konvensjonele radiolate en blauwe kleurstof-basearre oanpak.

DIE TWA

Diel twa fan dit proefskrift rjochtet him op de evaluaasje fan it hybride speurmiddel ICG-^{99m}Tc-nanocolloid foar de skyldwachtproseduere by pasjinten mei ferskate soarten fan kanker yn in betiid stadium, mei as doel de klinyske wearde te bepalen. Haadstik 4 beskriuwt de evaluaasje fan it hybride speurmiddel in 14 pasjinten dy't de skyldwachtklierproseduere ûndergongen fanwegen kanker yn de mûleholte. De

fluoressinte hantekening wie benammen fan belang foar de identifikaasje fan skyldwachtklieren dy't njonken it ynjeksjeplak sieten. Yn haadstik 5 wurdt it hybride speurmiddel evaluearre yn 65 pasjinten mei peniskanker (119 ljisken). Fisuele identifikaasje van de skyldwachtklier mei help fan fluoressinte byldfoarming wie oantoanber better dan de methoade fan de blauwe kleurstof: 96,8% vs. 55,7% (p <0,0001). Yn guon pasjinten waard mei de fluoressinte byldfoarming de skyldwachtklier al troch de yntakte hûd hinne waarnommen, wylst dat mei de blauwe kleurstof net mooglik wie. Ex vivo evaluaasje fan tumor-positive skyldwachtklieren learde ús ek dat it hybride speurmiddel benammen oanwêzich wie yn it sûne lymfeklierweefsel.

It belang fan de hybride oanpak foar de skyldwachtklierproseduere yn pasjinten mei in melanoom wurdt evaluearre yn haadstik 6. Yn 104 pasjinten mei in holle-halsmelanoom, in melanoom op de romp of op in earm of in foet waard lymfatyske ôfwettering sjoen nei skyldwachtklieren yn ûnder oare de hals, de earmsholte en de ljisk. Wêr't ûnder de operaasje 93,8% fan de skyldwachtklieren opspoard wurde koe fia radiolieding, koe mei fluoressinte byldfoarming 96,7% fan de skylwachtklieren sichtber makke wurde. Dêr neffens, mei blauwe kleurstof waard mar 61,7% fan de skyldwachtklieren sichtber. Fluoressinte byldfoarming wie benammen fan wearde as de blauwe kleurstof net brûkt waard, wannear't de skyldwachtklieren gjin blauwe kleurstof opnommen hiene (22 pasjinten) of yn it gefal dat de skyldwachtklier net fûn wurde koe fia radiolieding (5 pasjinten).

Diel twa konkludearret dat der neffens de konvinsjonele radio- en blauwe kleurstoflate skyldwachtklierproseduere in dúdlik belang is foar it brûken fan it hybride speurmiddel fan dy proseduere. De wearde fan it hybride speurmiddel waard it grutste fûn foar de identifikaasje fan skyldwachtklieren tichteby it ynjeksjeplak en op plakken mei in minne anatomy, bygelyks yn it parotis gebiet.

DIEL TRIJE

Om it hybride speurmiddel yn de klinyske rûtine opnommen te krijen is in ferbettering fan de hjoeddeiske byldfoarmingsmodaliteiten winsklik. **Diel trije** fan dit proefskrift rjochtet him op it ferbetterjen fan de hjoeddeiske klinysk beskikbere fluoressinsje byldfoarmingsmodaliteiten en ek op de yntroduksje fan in nije hybride byldfoarmingsmodaliteit. Haadstik 7 beskriuwt in prototype draagbere fluoressinsje kamera foar iepen sjirurgy, dy't wurket ûnder normale ljochtomstannichheden. Dy kamera waard ferliken mei syn foarrinner yn sân pasjinten dy't in skyldwachtklierproseduere ûndergongen dêr't it hybride speurmiddel by brûkt waard. De prototype kamera fisualisearre mear skyldwachtklieren en lymfebanen ûnder de operaasje, respektivelijk 100% en 7,4% vs. 81,4% en 0%). De skyldwachtklieren waarden ek faker troch de yntakte hûd hinne sjoen (40,7% vs. 22,2%). Yn 20 ekstra pasjinten waard it belang fan dy technyske ferbetterings fierder ûnderstreke. Yn guon pasjinten wie direkte fluoressinsjestjoerde skyldwachtklieridentifikaasje mooglik wêr't de technyk earder benammen brûkt waard om de lokalisaasje fan de skylwachtklier(en) te befêstigjen (**diel twa**).

Haadstik 8 beskriuwt it optimalisearjen fan laparoskopyske fluoressinsjebyldfoarming yn pasjinten mei prostaatkanker, dy't in robot-bystiene laparoskopyske skyldwachtklierproseduere ûndergongen (40 pasjinten). It optimalisearjen fan de gearstalling fan it hybride speurmiddel resultearre yn in ferbettering yn skyldwachtklieridentifikaasje fan 63,7% nei 85,2%. Dat ferbettere fierder nei 93.5% nei de yntroduksje fan in ferbettere laparoskopyske fluoressinsjekamera. Omtrint lykas beskreaun yn haadstik 7, ha dy ferbetterings der úteinlik ek yn resultearre dat direkte fluoressinsjestjoerde skyldwachtklieridentifikaasje mooglik waard. Troch dy fluoressinjekamera geschikt te meitsjen foar de deteksje fan meardere fluoressinte sinjalen, waard ynteroperative multispektrale fluoressinsje byldfoarming mooglik (beskreaun yn haadstik 9). Yn in helberheidsstúdzje yn tsien pasjinten waard dy multispektrale fluoressinsjebyldfoarmingsbeneiering evaluearre mei gebrûk fan de lymfe-angiografyske kleurstof fluoresceïne (fisuele fluoressinsje) en it hybride, tichteby-ynfrareade skyldwachtklier speurmiddel ICG-^{99m}Tc-nanocolloid. Dêr't de earste de nei de skyldwachtklieren rinnende lymfebanen opljochtsjen die, koene mei it hybride speurmiddel ICG-^{99m}Tc-nanocolloid de skyldwachtklieren sichtber makke wurde.

Alternatyf oan it optimalisearjen fan fluoressinsje byldfoarmingsmodaliteiten hawwe wy ek sjoen nei it optimalisearjen fan gamma byldfoarmingsmodaliteiten. Haadstik 10 beskriuwt de ynfiering fan in navigaasje systeem foar ynteroperative lieding. Mei dy navigaasje technology hawwe wy yn fiif pasjinten oantoand dat preoperative byldfoarming fuortendaliks beskikber makke wurde koe foar de sjirurg yn de operaasjekeamer. In ôfwiking fan 8,0 ± 2,1 en 8,5 ± 5,4 mm yn it koronale en saggitale/aksiale flak waard fûn wannear't de konvinsjonele gamma probe yn augmented- en virtual-reality yn 3D preoperative SPECT/CT byldfoarming navigearre waard nei de skyldwachtklier(en).

Yn haadstik 11 wurdt in hybride modaliteit beskreaun dy't likegoed radioaktiviteit as fluoressinsje opspoare kin. Nei in ex vivo helberensstúdzje dêr't 150 skyldwachtklierweefsels evaluearre waarden, waard in klinyske pilotstúdzje útfierd yn njoggen pasjinten dy't in skyldwachtklierproseduere ûndergongen mei gebrûk fan it hybride speurmiddel. Under de operaasje waarden 20 skyldwachtklieren mei de opto-nuclear probe mjitten, wêrby't yn alle gefallen likegoed it radioaktive as it fluoressinsje sinjaal yn de klier mjitten wurde koe. Fluoressinsje lieding wie dêrby mooglik ûnder normale ljochtomstannichheden.

Konkludearjend, sjirurgyske prosedueres kinne mooglik ferbettere wurde troch it optimalisearjen fan de besteande byldfoarmingsmodaliteiten en/of de yntroduksje fan nije hybride modaliteiten lykas beskreaun yn **diel trije**. Dat kin mooglik liede ta it opnimmen fan dy techniken yn de klinyske rûtine. Mar, de hjir boppe beskreaune stúdzjes binne allegear helberheidsstúdzjes wêrfan't de resultaten earst noch fierder validearre wurde moatte yn gruttere, by foarkar multicenter, stúdzjes.

FOARÚTSICHTEN

Yn haadstik 12, de **foarútsicht** fan dit proefskrift, beskriuwe wy hoe't wy de hybride oanpak foar de skyldwachtklierproseduere by prostaatkanker foar eagen ha yn de takomst deunby. Hoewol't dit haadstik rjochte is op de skyldwachtklierproseduere foar prostaatkanker, kin deselde oanpak ek maklik oerset wurde nei oare maligniteiten en anatomyske struktueren, bygelyks de senuwen. Wy litte sjen dat, troch gebrûk te meitsjen fan navigaasje techniken yn kombinaasje mei de hybride oanpak, direkte oersetting fan preoperative byldfoarmingsynformaasje yn de operaasjekeamer mooglik wurdt. De yntroduksje fan radio- en fluoressinsje opspoaringstechniken kin dêr by brûkt wurde om skyldwachtklieridentifikaasje fierder te ferbetterjen. Dêrby jildt, dat as we fierder komme as proof-of-principle stúdzjes, yntegrearre gebrûk fan de hjir boppe beskreaune byldfoarmingstechniken (**diel trije**) yn kombinaasje mei hybride speurmiddels (**diel ien** en **twa**) mooglik liede kin ta (nije) ferbettere sjirurgyske behannelingen.

CURRICULUM VITAE

Nynke Sjoerdtje van den Berg was born in Harlingen, the Netherlands on April 28th 1986. She graduated high school (VWO; Marne College, Bolsward, the Netherlands) in 2004. In 2009 she obtained her bachelor in Health and Life Sciences (Vrije Universiteit, Amsterdam, the Netherlands) after which she graduated from the master Oncology (Vrije Universiteit) in August 2011. During her master she explored the field of molecular imaging with her first master internship (April 2009-April 2010) conducted at the departments of Radiology and Nuclear Medicine (group of dr. Fijs W.B. van Leeuwen) at the Netherlands Cancer Institute-Antoni van Leeuwenhoek Hospital (NKI-AVL). Here she worked on the evaluation of imaging probes for the chemokine receptor 4 (CXCR4) in breast cancer models. For her second internship (June 2010-May 2011) she was invited to Massachusetts General Hospital-Harvard Medical School in Boston, United States, where she worked at the Center for Translational Nuclear Medicine and Molecular Imaging under the supervision of prof. dr. Umar Mahmood. Here her research focused on the effect of Metformin on tumor metabolism and -proliferation and the effects of this interaction on response prediction via ^{18}F-FDG and ^{18}F-FLT positron emission computed tomography imaging. In June 2011 she started her PhD at the Interventional Molecular Imaging Laboratory (group of dr. Fijs W.B. van Leeuwen) within the department of Radiology at the Leiden University Medical Center where, and in close collaboration with the departments of Urology and Head & Neck Surgery and Oncology at the Netherlands Cancer Institute-Antoni van Leeuwenhoek Hospital the work described in this thesis was conducted. In June 2015 she continued her research as a post-doctoral fellow.

PUBLICATION LIST, AWARDS/GRANTS

PUBLICATIONS

* = shared first authorship

1. Wit EMK, Acar C, Grivas N, Yuan C, Horenblas S, Liedberg F, Valdés Olmos RA, van Leeuwen FWB, **van den Berg NS**, Winter A, Wawroschek F, Hruby S, Janetschek G, Vidal-Sicart S, MacLennan S, Lam TB, van der Poel HG. Sentinel node procedure in prostate cancer: A systematic review to assess diagnostic accuracy. Eur Urol 2016. DOI: 10.1016/j.eururo.2016.09.007.
2. KleinJan GH, Hellingman D, **van den Berg NS**, van Oosterom MN, Hendricksen K, Horenblas K, Valdés-Olmos RA, van Leeuwen FWB. Hybrid surgical guidance: Does hardware integration of gamma- and fluorescence-imaging modalities make sense? J Nucl Med, 2016. In press.
3. van Oosterom MN, Engelen MA, **van den Berg NS**, KleinJan GH, van der Poel HG, Wendler T, van de Velde CJH, Navab N, van Leeuwen FWB. Navigation of a robot-integrated fluorescence laparoscope in preoperative SPECT/CT and intraoperative freehand SPECT imaging data. J Biomed Optical. 2016;21:86008.
4. Buckle T, KleinJan GH, Engelen T, **van den Berg NS**, DeRuiter MC, van der Heide U, Valdés-Olmos RA, Webb A, van Buchem MA, Balm AJM, van Leeuwen FWB. Diffusion-weighted-preparation (D-prep) MRI as a future extension of SPECT/CT based surgical planning for sentinel node procedures in the head and neck area? Oral Oncology. 2016;60:48-54.
5. **van den Berg NS**, Buckle T, KleinJan GH, van der Poel HG, van Leeuwen FWB. Multispectral fluorescence imaging during robot-assisted laparoscopic sentinel node biopsy, a first step towards a fluorescencebased anatomical roadmap. Eur Urol. 2016. DO1: 10.1016/j.eururo.2016.06.012
6. KleinJan GH, **van den Berg NS**, van Oosterom MN, Wendler T, Miwa M, Bex A, Hendricksen K, Horenblas S, van Leeuwen FWB. Towards (hybrid) navigation of a fluorescence camera in an open surgery setting. J Nucl Med. 2016. DOI: 10.2967/jnumed.115.171645
7. Bunschoten A, van Willigen DM, Buckle T, **van den Berg NS**, Welling MM, Spa SJ, van Leeuwen FWB. Tailoring fluorescent dyes in an attempt to optimize the biodistribution of hybrid RGD analogues. Bioconjugate Chem. 2016:18;27(5):1253-8.
8. KleinJan GH, Bunschoten A, **van den Berg NS**, Valdés-Olmos RA, Klop WMC, Horenblas S, van der Poel HG, Wester HJ, van Leeuwen FWB. Fluorescence guided surgery and tracer-dose, fact or fiction? Eur J Nucl Med Mol Imaging. 2016;43:1857-67.
9. **van den Berg NS**, Brouwer OR, Mathéron HM, Nieweg OE, Valdés Olmos RA, van Leeuwen FWB. Surgical navigation towards the sentinel node in patients with melanoma: a pilot study on expanding the intraoperative use of preoperative SPECT/CT images. Nucl Med Comm. 2016;37:812-7.
10. KleinJan GH, Brouwer OR, Mathéron HM, Rietbergen DDD, Valdés-Olmos RA, Wouters

MW, **van den Berg NS**, van Leeuwen FWB. Hybrid radioguided occult lesion localization (hROLL) of 18F-FDG-avid metastases using the hybrid tracer indocyanine green-^{99m}Tc-nanocolloid. Rev Esp Nucl Med Mol Imagen. 2016. DO1: 10.1016/j.remn.2016.04.001.

11. **van den Berg NS**, KleinJan GH, Miwa M, Sato T, Maeda Y, van Akkooi ACJ, Horenblas S, Karakullukcu B, van Leeuwen FBW. (Near-infrared) fluorescence guided surgery under ambient light conditions, a next step to embedment of the technology in clinical routine. Ann Surg Oncol. 2016;23:2586-95.
12. KleinJan GH, **van den Berg NS**, de Jong J, Wit EM, Thygessen H, Vegt E, van der Poel HG, van Leeuwen FWB. Multimodal hybrid imaging agents for sentinel node mapping as a means to (re)connect nuclear medicine to advances made in robot-assisted surgery. Eur J Nucl Med Mol Imaging. 2016;43:1278-87.
13. van Oosterom MN, Simon H, Welling MM, Mengus L, van der Poel HG, **van den Berg NS**, van Leeuwen FWB. Revolutionizing (robot-assisted) laparoscopic gamma tracing using a drop-in gamma probe technology. Am J Nucl Med Mol Imaging. 2016;6(1):1-17.
14. Fuerst B, Sprung J, Pinto F, Frisch B, Wendler T, Simon H, Mengus L, **van den Berg NS**, van der Poel HG, van Leeuwen FWB. Navab N. First robotic SPECT for minimally invasive sentinel lymph node mapping. IEEE Transactions on Medical Imaging. 2016;35:830-8.
15. Vidal-Sicart S, van Leeuwen FWB, **van den Berg NS**, Valdés Olmos RA. Fluorescent radiocolloids, are hybrid tracers the future for lymphatic mapping? Eur J Nucl Med Mol Imaging. 2015;42:1627-30.
16. **van den Berg NS**, Simon H, KleinJan GH, Engelen T, Bunschoten A, Welling MN, Tijink BM, Horenblas S, Chambron J, van Leeuwen FWB. First-in-human evaluation of a hybrid modality that allows combined radio- and (near-infrared) fluorescence tracing during surgery. Eur J Nucl Med Mol Imaging. 2015;42:1639-47.
17. Acar C, KleinJan GH, **van den Berg NS**, Wit EM, van Leeuwen FWB, van der Poel HG. The advances in sentinel node dissection in prostate cancer: from a technical perspective. Int J Urology. 2015;22:898-909.
18. Engelen T, Winkel, BMF, Rietbergen DDD, KleinJan GH, Vidal-Sicart S, Valdés Olmos RA, **van den Berg NS**, van Leeuwen FWB. The next evolution in radioguided surgery: Breast cancer related sentinel node localization using a freehandSPECT-mobile gamma camera combination. A J Nucl Med Mol Imaging. 2015;5:233-45.
19. Engelen T, KleinJan GH, van Leeuwen FWB, **van den Berg NS**. Virtual-reality in de operatiekamer: Kan intra-operatieve navigatie op basis van preoperatieve (nucleaire) beeldvorming worden gebruikt om de chirurgische opsporing van laesies te verbeteren?. Medisch Contact. 2015.
20. **van den Berg NS**, Brouwer OR, Schaafsma BE, Mathéron HM, Klop WMC, Balm AJM, van den Brekel MWM, van Tinteren H, Nieweg OE, van Leeuwen FWB, Valdés-Olmos RA. Multimodal surgical guidance during sentinel node biopsy for melanoma: Combined gamma tracing and fluorescence imaging of the sentinel node through use of the hybrid tracer indocyanine green-technetium-^{99m}-nanocolloid. Radiology. 2015:275(2);530-537.

21. van der Poel HG, **van den Berg NS**, KleinJan GH, van Leeuwen FWB. Removing nodes that count rather than counting nodes that don't. Reply from authors to: Francesco Montorsi, Giorgio Gandaglia. Sentinel node biopsy for prostate cancer: A useless surgical exercise? Eur Urol 2014;66:999-1000.
22. Chícharo de Freitas JR, KleinJan GH, van der Poel HG, **van den Berg NS**, Vegt E, Stokkel MP, Valdés Olmos RA. Utilidad de la SPECT-TC para la localización anatómica de los ganglios centinelas presacrales y pararrectales en el cáncer de prostate. Rev Esp Med Nucl Imagen Molecular. DOI: 10.1016/j.remn.2014.09.001
23. Kleinjan GH*, **van den Berg NS***, Brouwer OR, de Jong J, Acar C, Wit EM, Vegt E, van der Noort V, Valdés Olmos RA, van Leeuwen FW, van der Poel HG. Optimisation of fluorescence guidance during robot-assisted laparoscopic sentinel node biopsy for prostate cancer. Eur Urol. 2014:66(6);991-8.
24. Brouwer OR, **van den Berg NS**, Mathéron HM, Nieweg OE, Horenblas S, van der Poel HG, Valdés-Olmos, van Leeuwen FWB. Feasibility of intraoperative navigation to the sentinel node in the groin using preoperatively acquired single photon emission computed tomography data: Transferring functional imaging to the operating room. J Urol. 2014:192(6);1810-6.
25. Brouwer OR*, **van den Berg NS***, Mathéron HM, van der Poel HG, van Rhijn BW, Bex A, Valdés-Olmos RA, van Leeuwen FWB, Horenblas S. A hybrid radioactive and fluorescent tracer for SN biopsy in penile carcinoma as a potential replacement for blue dye. Eur Urol. 2014;65:600-609.
26. Borbón-Arce M, Brouwer OR, **van den Berg NS**, Mathéron H, Klop WMC, Balm AJM, van Leeuwen FWB, Valdés-Olmos RA. An innovative multimodality approach for sentinel node mapping and biopsy in head and neck malignancies. Rev Esp Med Nucl Imagen Mol. 2014:33(5):274-9.
27. van Leeuwen FWB, **van den Berg NS**, van der Poel HG. Fluorescence applications in robotic surgery. Eur Urol Today. February/March 2014.
28. **van den Berg NS**, Buckle T, KleinJan GH, Klop WMC, Horenblas S, van der Poel HG, Valdés Olmos RA, van Leeuwen FWB. Hybrid tracers for sentinel node biopsy. Q J Nucl Med Mol Imaging. 2014;58(2):193-206.
29. KleinJan GH, Bunschoten A, Brouwer OR, **van den Berg NS**, Valdés-Olmos RA, van Leeuwen FWB. Multimodal imaging in radioguided surgery. Clinical and Translational Imaging. 2013;1:433-444.
30. Mathéron HM*, **van den Berg NS***, Brouwer OR, KleinJan GH, van Driel WJ, Trum JH, Vegt E Kenter G, van Leeuwen FWB, Valdés Olmos RA. Multimodal surgical guidance towards the sentinel node in vulvar cancer. Gynecol Oncol. 2013;131(3):720-5.
31. Frontado ML, Brouwer OR, **van den Berg NS**, Mathéron HM, Vidal-Sicart S, van Leeuwen FW, Valdés Olmos RA. Added value of the hybrid tracer indocyanine green-^{99m}Tc-nanocolloid for sentinel node patients in a series of patients with different lymphatic drainage patterns. Rev Esp Med Nucl Imagen Mol. 2013;32(4):227-33.
32. **van den Berg NS**, Valdés-Olmos RA, van der Poel HG, van Leeuwen FW. Sentinel lymph

node biopsy for prostate cancer: A hybrid approach. J Nucl Med. 2013;54(4):493-6.
33. Rietbergen DDD, **van den Berg NS**, van Leeuwen FWB, Valdés Olmos RA. Hybrid techniques for intraoperative sentinel lymph node imaging: early experiences and future prospects. Imaging Med. 2014;5(2):147-159.
34. Habibollahi P*, **van den Berg NS***, Kuruppu D, Loda M, Mahmood U. Metformin--an adjunct antineoplastic therapy--divergently modulates tumor metabolism and proliferation, interfering with early response prediction by 18F-FDG PET imaging. J Nucl Med. 2013;54(2):252-8.
35. Buckle T, Kuil J, Bunschoten A, **van den Berg NS**, Yuan H, Josephson L, Jonkers J, Borowsky AD, van Leeuwen FWB. Target validation and staging in fresh tumor tissue suspensions; expanding the applicability of hybrid imaging agents. PLoS One. 2013;8(1):e48324.
36. **van den Berg NS***, Brouwer OR*, Klop WMC, Karkullukcu B, Zuur CL, Tan BI, Balm AJM, van den Brekel MWM, Valdés Olmos RA, van Leeuwen FWB. Concomitant radio- and fluorescence-guided sentinel lymph node biopsy in squamous cell carcinoma of the oral cavity using ICG-^{99m}Tc-nanocolloid. Eur J Nucl Med Mol Imaging. 2012;39(7):1128-36.
37. Buckle T, **van den Berg NS**, Kuil J, Bunschoten A, Oldenburg J, Borowsky AD, Wesseling J, Masada R, Oishi S, Fujii N, van Leeuwen FWB. Non-invasive longitudinal imaging of tumor progression using an 111Indium labeled CXCR4 peptide antagonist. Am J Nucl Med Mol Imaging. 2012;2(1):99-109.
38. **van den Berg NS**, van Leeuwen FWB, van der Poel HG. Fluorescence guidance in urologic surgery. Curr Opin Urol. 2012;22(2):109-20.
39. Steunenberg P, Ruggi A, **van den Berg NS**, Buckle T, Kuil J, van Leeuwen FWB, Velders AH. Phosphorescence imaging of living cells with amino acid-functionalized tris(phenylpyridine)iridium(III) complexes. Inorganic Chemistry. 2012;51:2105-2114.
40. van der Poel HG, Brouwer OR, **van den Berg NS**, Buckle T, van Leeuwen FW. Reply to K. Polom, D. Murawa, W. Polom's Letter to the Editor re: Henk G. van der Poel, Tessa Buckle, Oscar R. Brouwer, Renato A. Valdés Olmos, Fijs W.B. van Leeuwen. Intraoperative laparoscopic fluorescence guidance to the sentinel lymph node in prostate cancer patients: Clinical proof of concept of an integrated functional imaging approach using a multimodal tracer. Eur Urol. 2011;60:826-33.
41. **van den Berg NS***, Buckle T*, Kuil J, Wesseling J, Roos E, van Leeuwen FWB. Direct fluorescent detection of CXCR4 using a targeted peptide antagonist. Translational Oncology. 2011;4:234-40.
42. Kuil J, Buckle T, Yuan H, **van den Berg NS**, Oishi S, Fujii N, Josephson L, van Leeuwen FWB. Synthesis and evaluation of a bimodal CXCR4 antagonistic peptide. Bioconjug Chem. 2011; 18;22(5):859-64.
43. Buckle T, Chin PTK, **van den Berg NS**, Loo C, Koops W, Gilhuijs KAG, van Leeuwen FWB. Tumor bracketing and safety margin estimation using multimodal marker seeds; a proof of concept. J Biomed Opt. 2010;15(5):056021.

BOOK CHAPTERS

1. Bunschoten A, **van den Berg NS**, Valdés Olmos RA, Blokland JAK, van Leeuwen FWB. Tracers applied in radioguided surgery. In: Radioguided Surgery - Current Applications and Innovation Directions in Clinical Practice. Editors: K. Hermann K., Nieweg OE, and Povoski SP. 2015.
2. Waelkens P, van Oosterom MN, **van den Berg NS**, Navab N, van Leeuwen FWB. Surgical navigation - An overview of the state-of-the-art clinical applications. In: Radioguided Surgery - Current Applications and Innovation Directions in Clinical Practice. Editors: K. Hermann K., Nieweg OE, and Povoski SP. 2015.

AWARDS/GRANTS

1. Financial support from the Leiden University Fund / Den Dulk-Boermans to visit the 9th annual meeting of the AHNS (2016), Seattle, WA, United States.
2. Student travel award EMIM 2014, Antwerp, Belgium
3. Student travel award RSNA 2013, Chicago, Illinois, United States.
4. Student travel award WMIC 2013, Savannah, Georgia, United States.
5. Student travel award EMIM 2013, Torino, Italy.
6. Student travel award RSNA 2012, Chicago, Illinois, United States.
7. Best scientific poster award at the Dutch MicroNano Conference in 2012. Poster title: A hybrid tracer, ICG-^{99m}Tc-nanocolloid, for concomitant radio- and fluorescence guided sentinel node biopsy in oral cancer.
8. Student travel award RSNA 2011, Chicago, Illinois, United States.
9. KWF student grant (2011) to visit Harvard Medical School/Massachusetts General Hospital, Boston, MA, United States.
10. "Facultair Fonds VUmc" grant (2011) for master internship at Harvard Medical School/ Massachusetts General Hospital, Boston, MA, United States.
11. "VU Fondsendesk" grant (2011) for master internship at Harvard Medical School/ Massachusetts General Hospital, Boston, MA, United States.

DANKWOORD

Prof. dr. Hans Bloem, bedankt voor het aan elkaar knopen van de laatste promotie-eindjes. Tevens bedank ik mijn co-promotores, dr. Fijs van Leeuwen en dr. Renato Valdés Olmos. Fijs, ik bewonder jouw passie voor het onderzoek, je wil om het veld vooruit te brengen, en het altijd tot in de puntjes willen begrijpen van de (complexe) materie waarmee we in ons veld te maken krijgen. Dat stapje extra dat je altijd voor mij doet maken dat dit proefschrift er nu is. Bedankt! Renato, bedankt voor alles wat je me geleerd hebt over het wel en wee rondom jouw passie, de sentinel node. Marianne, bedankt voor de laatste waardevolle spellingscheck van dit proefschrift.

Prof. dr. Hans Tanke, prof. dr. Marion de Jong, prof. dr. Fons Balm, dr. Arian van Erkel, en dr. Henk van der Poel, bedankt voor jullie kritische blik op dit proefschrift.

Collega's en ex-collega's van het Interventional Molecular Imaging Laboratory op het LUMC, bedankt voor de mooie tijd die we (gehad) hebben, voor de prettige samenwerking en jullie tolerantie. Gijs, "mijn"-rechter-klinische-studies-hand, bedankt voor onze fijne samenwerking en je tomeloze inzet! "Mijn" studenten, bedankt voor jullie kritische vragen, en het mooie werk dat jullie hebben geleverd! Collega promovendi op het NKI-AVL bedankt voor de mooie tijd. Oscar en Hanna, jullie hebben een belangrijke rol gespeeld tijdens (de begintijd van) mijn promotieonderzoek. Bedankt, ook voor de bijzondere vriendschap die we hebben opgebouwd. Collega's van de OK, het KFI, medisch nucleair medewerkers en specialisten van de nucleaire geneeskunde, pathologie, radiologie, chirurgie, gynaecologie, hoofd-hals chirurgie en oncologie en urologie van het NKI-AVL, bedankt voor jullie inzet en (gemaakte) tijd om het onderzoek uit te voeren, voor jullie interesse, (kritische) feedback en bereidheid om een en ander toe te lichten. Dr. Klop, Martin, jouw kritische noot en scherpe blik heeft me al menigmaal gedwongen nog verder te denken dan ik al deed. Bedankt! Prof. Dr. Balm, Fons, ik bewonder je passie voor het vak hoofd-hals chirurgie en ik heb veel van je geleerd de afgelopen jaren. Bedankt, ook voor de fijne samenwerking. Dr. Van der Poel, Henk, bedankt voor de mooie samenwerking die ik met jou heb mogen opbouwen, jouw immer snelle reactie op (domme) vragen, en de workshops en presentaties die we samen hebben mogen geven. I also owe a big thank you to the industrial collaborators that always responded positively when I asked "Can I get…" or "How to…". Tevens bedank ik alle patiënten die belangeloos hebben meegewerkt aan de onderzoeken beschreven in dit proefschrift.

Vrienden en familie, het feit dat jullie achter me staan en altijd voor mij klaar staan maakt dat ik kan doen wat ik nu doe en kan zijn wie ik ben. Lucia, Anoek, Dian, Franka, Kim en Jessica bedankt dat jullie er altijd zijn wanneer dat nodig is. Елена, мне очень дорога наша межконтинентальная дружба всегда насыщенная содержательными беседами. Спасибо!

Leave heit en mem, ik kin net beskriuwe hoe wichtich jimme binne in myn libben. Ut en troch sa fier fuort, mar altyd sa tichteby. Fan jongs ôf hawwe jim ús foarholden dat asto eat yn't hier hast, dasto der dan nei stribje moast om dat te forwêzentlikje en ree wêze moast om dêr fûl foar te arbeidzjen. Jimme stipesunder bitingsten hat derby altyd hiel wichtich west. Jildau, Bauke en Femke, wannear't der wat is, dan binne wy der foar elkoar.

Sa hearlik! Ik mei myn hantsjes tichtknipe mei jimme! Ik bin ek grutsk en tige bliid dat jimme, Bauke en Femke, myn paranimfen wêze sille! Caroline, Thomas, Bart en Paul, fijn dat jullie de boel in toom houden! Stephan, “mijn” +1, bedankt dat je er altijd voor mij bent en dat je me hebt laten inzien dat er veel meer is dan werk alleen.